Study of double exchange phenomenon: from microscopic origins to collective properties

Vijay Gopal Chilkuri

THÈSE

En vue de l'obtention du

DOCTORAT DE L'UNIVERSITÉ DE TOULOUSE

Délivré par : *l'Université Toulouse 3 Paul Sabatier (UT3 Paul Sabatier)*

Présentée et soutenue le *16/10/2015* **par :**

Vijay Gopal CHILKURI

Etude du phénomène de double échange : de l'origine microscopique aux propriétés collectives

---

JURY

Sylvain CAPPONI	Professeur d'Université	Président du Jury
Coen DE GRAAF	Professeur d'Université	Membre du Jury
Vincent ROBERT	Professeur d'Université	Membre du Jury
Nathalie GUIHERY	Professeur d'Université	Membre du Jury
Nicolas SUAUD	Maître de conférence	Membre du Jury
Nicolas FERRE	Professeur d'Université	Membre du Jury

École doctorale et spécialité :
SDM : Physicochimie théorique - COP 01

Unité de Recherche :
Laboratoire de chimie et physique quantiques

Directeur(s) de Thèse :
Nathalie GUIHERY et *Nicolas SUAUD*

Rapporteurs :
Coen DE GRAAF et *Vincent ROBERT*

Contents

List of Figures

List of Tables

Introduction

Magnetic systems are becoming increasingly important in our daily lives. They may be found in data storage devices, energy storage, medical imaging and more recently in the Magnetic random access memories (MRAM's). With the miniaturization techniques, they are also expected to be of interest in quantum computing for instance and many other technological fields. Spintronics based devices are gaining popularity and are crucial in the conception of electronics of increasingly smaller dimensions. From a fundamental point of view, magnetic systems always motivate the interest of researchers as some of their properties are still unclear although they are already being used in technological devices. This is the case for instance in high critical temperature superconductors [1] or systems exhibiting colossal magnetoresistance (CMR) [2, 3]. Magnetism found its origin in the quantum behavior of the matter. As magnetic materials (or compounds) are highly correlated systems [4], the understanding of their electronic structure and of the collective effects present at the infinite scale is a rather difficult task for theoreticians. Such insights are however necessary if one wants to elucidate unexplained properties and to improve in a rational manner the existing systems and/or propose new systems with controlled properties.

Several strategies have been used to produce magnetic materials or compounds [5]. As ferromagnetic interactions are usually of weak magnitude, antiferromagnetic couplings between spin units of different spins (resulting in a ferrimagnet) happened to be an interesting alternative. Another strategy consists in exploiting the double exchange (DE) phenomenon. The DE mechanism rationalizes the appearance of a high spin ground state in antiferromagnetic systems under doping [6, 7, 8]. It is also at the origin of the magnetoresistive effects observed in manganites [9] and widely used in spintronics. The present work focuses on this mechanism. Several objectives are pursued:

- The design of double exchange organic compounds resulting in high spin conjugated organic system. While transition metal compounds may exhibit double exchange interactions, the scarcity of transition metals pushes the

scientific community to synthesize compounds having the same properties but only made of carbon atoms which are much more abundant.

- The *ab initio* study of these systems and the extraction of the double exchange model interactions in order to compare them to those observed in transition metal compounds. Such a study should also permit one to discuss the topology of the systems appropriate for exhibiting a DE phenomenon. The parameters extracted here will also aid in the conception of other organic double exchange systems.

- A study of linear chain double exchange model with open boundary conditions. The use of chains in magnetism is interesting by itself and can find applications in low dimensional electronic systems. For instance, introducing heavier elements at appropriate positions could lead to single chain magnets behavior provided that the whole system shows shows a ground state of spin-multiplicity of $S = 1$ and preferably higher. This study should allow us to determine the range of DE interactions for which a high spin molecule can be generated from a DE mechanism.

- From the study of increasing size chains, one hopes to be able to find some size-independent characteristics which would enable us to understand properties observed in bulk double exchange materials. A first aim is to find the number of spins which can be aligned by a single hole for physical values of the DE parameters. The properties of the chains will also be analyzed as functions of the number of holes (doping). Another objective is to quantify the effect of a magnetic field on the delocalization of the holes. This can be used as an indicator of the variation of electrical conductivity with magnetic field, of an infinite chain. Finally we will also seek to determine the nature (electronic structure) of the states which may be responsible for the magnetoresistive effects observed in double exchange materials.

The complexity of providing an accurate description of magnetic systems originates from the multireference character of the lowest spin states wavefunctions combined with the large size (infinite for materials) of the systems. Two alternative approaches are currently used. The first one consists in a density functional theory description (which is intrinsically single reference) but usually permits the treatment of the whole system. It is applicable to large size systems and can also be used with periodic boundary conditions for materials. Another approach consists in a multiscale procedure. In a first place, the electronic structure of the lowest spin states of fragments of the system is calculated using ab initio calculations. From both the lowest spectrum and the corresponding wavefunctions, simple models, working on a small model space, can be extracted. As these models

may be used to study the properties of larger systems, systems of larger sizes can then studied. This second part of the work allows us to introduce collective effects which are important for highly correlated materials. The present work combines both approaches. DFT calculations are performed on organic molecules and model calculations are performed on model DE chains of different sizes and for various dopings.

The thesis is organized as follows. In a first chapter, organic polyradicals are conceived and studied using density functional theory. Their low-energy spectrum is reconstructed from the energies of various broken symmetry solutions. Two different methods of extraction of the DE parameters are proposed and applied to quantify the ability of these systems to exhibit a double exchange phenomenon. A second chapter is devoted to the study of the spatial extent of the ferromagnetic cloud in a doped linear chain of spins $S = 1$, i.e. one aims to answer the question: how many spins can be aligned by the presence of a single hole? The dependence of the results on the presence of a second hole is also studied for physical values of double exchange parameters. Finally in the third chapter we will characterize the property of chains of various sizes in presence of several holes. The electronic structure of both the ground and the lowest excited states will be studied. As we use an unusual tool to analyze the delocalization of the holes, the Total Position Spread (TPS), the physical meaning of this object will first be analyzed and then used to characterize the chains. Finally, the response to an applied magnetic field will be presented.

At the end of the thesis, I have introduced a recently submitted article on a mononuclear compound exhibiting a single molecule magnet behavior. As this subject is quite far from the study of DE systems and for sake of homogeneity, I have not commented my contribution to this work in the present manuscript. I was in charge of the calculations of the magnetic couplings between the molecule and the atoms of the surface on which it is deposited. I also have computed the magnetic anisotropy parameters using the spin orbit state interaction method implemented in MOLCAS.

Chapter 1

Double Exchange in Organic systems

1.1 Introduction

High-spin molecular systems have wide ranging applications, for e.g. the conception of single molecule magnets [10] and spintronic devices [11]. Nature makes it difficult to synthesize high spin molecular systems because organic radicals are facile. Conjugated organic radicals tend to exist as in closed shell states due to the diffuse character of the frontier orbitals. Therefore, the traditional route towards the synthesis of high-spin systems have relied on organometallic systems where the organic radicals are linked to transition metal atoms which exist as high spin centers. These organometallic molecules are difficult to synthesize, hard to manipulate and prohibitively expensive. Recently, progress has been made towards the use of double exchange mechanism in the synthesis of high-spin molecules [5]. The use of double exchange based organic systems for spintronics has also been achieved [7]. Keeping this is mind, our objective for this chapter is to propose high-spin conjugated organic systems based on the double exchange mechanism. We will also propose a methodology to study the origin of such properties, with the goal of facilitating the conception of high-spin organic molecules based on the double exchange mechanism.

The drastic difference between metal atom based systems and organic molecules is the ease of obtaining high spin subunits with unpaired electrons such as metal complexes and crystals composed of Ni or Mn which are formed of $S = 1$ up to $S = \frac{5}{2}$ spin subunits [12, 13, 14, 15, 16]. As the magnetic electrons are hosted by the transition metals, the highest spin of the magnetic unit is restricted to $S = \frac{5}{2}$ (or $S = \frac{7}{2}$ for Lanthanides). One advantage of organic systems is the possibility to build magnetic units of any spin. Numerous attempts by experimentalists have

lead to the synthesis of giant spin organic molecules [17, 18, 19, 20, 21]. There have also been attempts to synthesize two dimensional organic cavities which would have a highly polyradical character [22, 23]. Theoretical studies on such systems have also shown that it is now possible to have organic systems which are poly-radicals and can show interesting magneto electric properties [24, 25]. Triangulenes, one candidate high spin system which was first studied by Clar [26, 27] in the 1950's, have interesting polyradical characteristics [28] such as ferromagnetic behavior on electron reduction [29]. At present, there is sufficient expertize, in the domain of organic chemistry, in synthesis and characterization of complicated two dimensional conjugated structures. This encourages us to study organic molecules which may have interesting applications in the domain of spintronics.

As conjugated organic molecules are generally large, containing several carbon atoms which contribute to the magnetization via the pi-conjugate cloud, it is not easy to perform calculations for their analysis. One option that has gained success in the study of conjugated organic systems is the Density Functional Theory (DFT) which makes it possible to study large molecular systems. The errors introduced in DFT due to the single reference character (among other problems) can be corrected by various spin decontamination and post-treatment schemes. The first of which was proposed by Yamaguchi [30], who demonstrated a simple method using the $\langle S^2 \rangle$ values to decontaminate the spectrum. A more sophisticated post-treatment based method proposed by C. Boilleau [31] (for metallic systems) aims at obtaining accurate spectrum from DFT broken symmetry energies. The accuracy of various decontamination methods will eventually be system dependent and would have to be adapted accordingly.

In this chapter we will show how one might conceive such molecules and also present a methodology to study their properties. This section is organized as follows. Firstly, we introduce the Double Exchange (DE) model. Secondly, we shall introduce model organic molecules which are susceptible to show DE phenomenon. Finally, we present our results and discussions followed by a proposal of one and two dimensional organic lattices that could exhibit magneto-resistive effects.

1.2 Theory

The present chapter will only be concerned with **two site** systems containing two magnetic orbitals each (similar to $S = 1$ Ni complexes).

Let us start with a simple analysis of two magnetic ($S = 1$) units interacting through a bridge. The ionized system will be made up of two sites containing

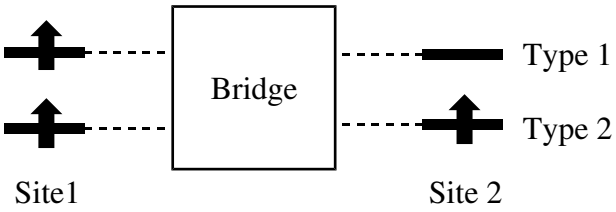

Figure 1.1: Schema of a general two site DE system linked by a bridging unit.

four magnetic orbitals and three electrons, Fig: 1.1. The two magnetic orbitals, will interact with each other via the paramagnetic bridging unit. The Type 1 orbitals are the ones that interact strongly with the bridge and the Type 2 orbitals interact weakly. Depending on the strength of this interaction between the two units (Fig: 1.2), we will either see a system with a quartet spin state or a closed shell doublet state based on the following situations:

- Case 1: The Type 1 orbitals of the two units interact strongly via the bridge giving rise to a large gap between the delocalized orbitals and the non-interacting Type 2 orbitals as shown on the left in Fig: 1.2. This favors a 1-OS electronic configuration and the ground state becomes a 1-OS doublet state. Note that in scenario I, the electronic configuration leads to maximal kinetic energy for the electrons occupying the Type 1 molecular orbitals (MO). Whereas, the unpaired electron occupies the localized Type 2 orbital. This corresponds to a strong covalent interaction between the two magnetic units.

- Case 2: The two units are weakly interacting. This maintains a small gap between the Type 1 MO and the Type 2 MO leading to the stabilization of the open shell configuration as shown in Fig: 1.2 on the right. The hole, in the Type 1 orbital, is strongly delocalized. The quartet, which is stabilized by hopping term among strong overlapping orbitals (t_1), is the ground state.

- For the doublet states, there is a competition between the two configurations with three open shells and with one open shell. The 3-OS configurations are stabilized by the antiferromagnetic exchange J_1 whereas the 1-OS determinants are stabilized via the kinetic energy term t_1.

- **The DE phenomenon is observed in Case II, when the overlap between the Type 1 orbitals of the two magnetic unit and the bridge is sufficiently small (but not zero).**

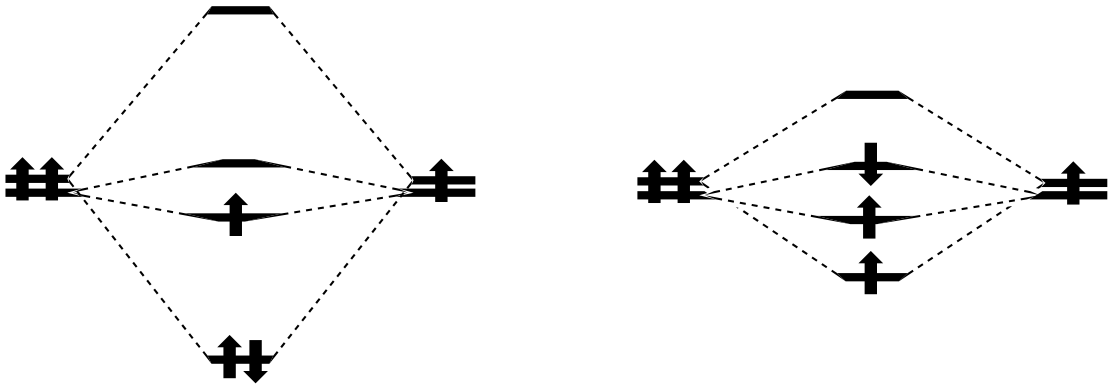

(a) Case I (b) Case II

Figure 1.2: A schematic of the two scenarios that of strong (left) and weak (right) interaction with the bridge. There are four frontier molecular orbitals formed primarily of the two magnetic orbitals of the two TMM's each.

Therefore, for systems that follow DE mechanism, there are two types of electrons: The electron occupying Type 1 orbital is responsible for the transport properties while the electron occupying the Type 2 (localized) orbitals is responsible for the magnetic properties. *The determinants where the hole occupies the strongly overlapping orbitals (Type 1) will be referred to as* ***Fam 1*** *and the determinants where the hole occupies the weakly overlapping orbitals will be referred to as* ***Fam 2****.*

The Double Exchange model is applicable to a three open-shell (3-OS) systems for a well defined range of parameters. However, in some cases, the low energy spectrum will also contain determinants made up of a single open-shell doublets (1-OS doublets). The lowest energy states of transition metal double exchange systems are almost always constituted of 3 open-shells determinants, because of the large intra-site electron repulsion U, the 1 open shell determinants are higher in energy. On the contrary, in organic molecules due to the diffuse character of magnetic orbitals (spread out over several atoms), U is small the 1-OS doublet states can be low in energy.

Generally, in the case of transition metal atoms, the two orbitals (usually d_{z^2},$d_{x^2-y^2}$) are strongly localized on a single center (atom). Consequently, the on-site exchange integral K is large. Things become more complicated in the case of magnetic orbitals made up of organic units. These organic orbitals are spread over multiple centers (3 for the case of TMM and 19 for Triangulene for instance). *This leads to a decrease in the exchange integral K and the non-Hund states interact strongly with the low energy spectrum.*

Concerning the 1-OS determinants, there are of two types depending on the electronic configuration. *Firstly, the "Ionic" determinant are those where all three electrons occupy the same site and for the case when the single unpaired electron occupies a site different than the one with the electron pair, the determinant will be referred to as the "pseudo-Ionic" determinant.*

1.2.1 Double Exchange model

In original double exchange model proposed by Zener [32] the energy of the non-Hund determinants was taken to be very large. Further refinements on the model by the inclusion of the ionic determinants by Girerd and Papaefthymiou (GP) [33, 34, 35] also assume the Hund term to be very large $K >> |t|$ (t being the kinetic energy integral.) Later, Anderson and Hasegawa (AH) have showed that the inclusion of the local low spin states via K qualitatively changes the nature of the ground states [36]. Since we study systems where K plays a significant role, in this thesis we have used the combined effects of the anti-ferromagnetic exchange interaction J_1 (Zener, Girerd and Papaefthymiou) and the non-Hund states (Anderson and Hasegawa) via $K \approx t_1$. This double exchange model has been previously proposed by Guihéry *et al* [37, 38]. The model is shown schematically in Fig: 1.3. Since the overlap between the Type 2 orbitals is small, the J_1 is expected to be small and the kinetic energy term t_1 is expected to be large due to the large overlap between the Type 1 orbitals.

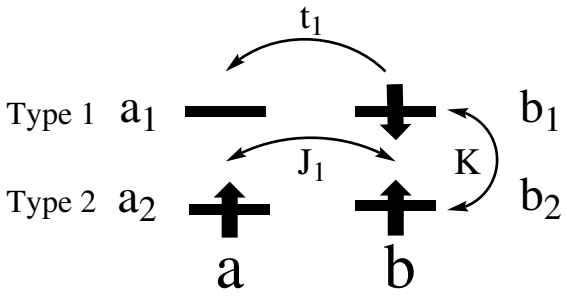

Figure 1.3: A schema of the Hamiltonian, showing all the interactions taken into account. The two types of orbitals of a single site are a_1 and a_2, the hole occupies the strongly delocalized orbitals of type 1. Note that the hopping integral t_1 is much larger than t_2.

Note that the **Fam 1** does not interact with the second family if the hopping

term (t_3) between orbitals a_1 and b_2 is zero for symmetry reasons. The presence of the intra-site exchange term K implies that there are two types of local states taken into consideration, the triplet represented by T_+, T_0, T_{-1} corresponding to the $m_s = 1, m_s = 0$ and $m_s = -1$ and singlet S_0 spin states. The local triplet states (called the Hund states) are $2K$ below the local singlet states (i.e. the non-Hund states).

The energy of the DE Hamiltonian for two sites (shown in Fig: 1.3) is know exactly. The analytical expression for the energies of the quartet states is given by:

$$^4E^{(AH/GP)}_{\mp,1} = \pm t_1 \tag{1.2.1}$$

and that of the doublet states is given by:

$$^2E^{(AH/GP)}_{\mp,1} = K - \sqrt{K^2 + t_1(t_1 \pm K)} + \frac{3J_1}{2} \tag{1.2.2}$$

where $\pm$ denotes the *gerade* or the *ungerade* combinations. Therefore, knowing the energies of the quartet and doublet states, would be enough to extract the parameters of the DE model, i.e. K and J_1.

1.3 Model systems, Extraction and Results

Please refer to the articles that follow for details on the methodology used for the design and analysis of the DE Organic systems. An updated version of the present manuscript will contain a complete chapter with detailed explanations on the various methods employed and the results obtained.

JCTC Journal of Chemical Theory and Computation

Article

pubs.acs.org/JCTC

In Search of Organic Compounds Presenting a Double Exchange Phenomenon

Vijay Gopal Chilkuri, Georges Trinquier, Nadia Ben Amor, Jean-Paul Malrieu, and Nathalie Guihéry*

Laboratoire de Chimie et de Physique Quantiques, IRSAMC/UMR5626, Université de Toulouse 3, 118 route de Narbonne, F-31062 Toulouse Cédex 4, France

Supporting Information

ABSTRACT: The objective of this paper is to design a consistent series of organic molecules that may present a double exchange mechanism and study their low energy spectrum using spin unrestricted Density Functional Theory. For this purpose, organic tetra-methylene methane units having an $S = 1$ spin ground state and diamagnetic organic bridges are taken as building blocks for constructing molecules having two or more magnetic units. When biunit systems are ionized, the ground state of the resulting molecular ions may be either a quartet, if the spectrum is ruled by a double exchange mechanism, or a doublet, if it obeys the logic of a monoelectronic picture. A strategy based on the physical analysis of the leading interactions is followed in order to energetically favor a high-spin ground state. It is shown that the most promising compounds involve bridges that have both a large gap between the highest occupied and the lowest unoccupied molecular orbitals and small coefficients on the atoms to which the magnetic units are connected. While the followed strategy enables one to conceive organic compounds exhibiting a double exchange phenomenon, it is shown that the electronic mechanism ruling the spectrum of such organic double exchange compounds is different from that of their inorganic homologues. A new method to reconstruct the spectrum of low energy from various spin unrestricted DFT solutions is proposed and applied. Finally monodimensional and bidimensional periodic lattices based on the most promising organic architecture are suggested.

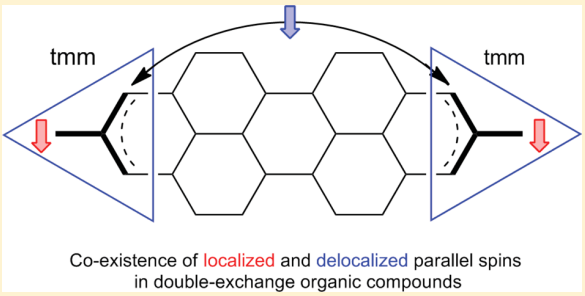

I. INTRODUCTION

Owing to the Hund's rule, monometallic complexes having several unpaired electrons exhibit a nonzero spin ground state. Connecting these magnetic units through diamagnetic bridges leads to fascinating inorganic materials presenting remarkable properties such as ferro-, antiferro-, ferri-magnetism,[1] spin crossover,[2] superconductivity,[3] magnetoresistive effects,[4] etc. Recent interest in organic materials, including hydrocarbons, as an intriguing alternative to silicon and transition metals used currently in electronic devices, has grown considerably since they are easier and cheaper to produce. While magnetic properties in organic compounds are less commonly encountered, they have been the subject of a constant research.[5] Organic chemists have synthesized and characterized organic single radicals such as nitroxides[6] or verdazyl[7] and also polyradicalar hydrocarbons such as assemblies of meta-xylylene.[8] Spectacular architectures with spin up to $S = 80$ were even obtained by Rajca et al., though in a context of dendritic structures that cannot lead as such to periodic lattices.[9] Playing with the donor and acceptor character of some molecules, it has also been possible to conceive conducting salts and even superconductive materials.[10]

Recently, a family of organic polyradicalar units presenting a nonzero spin ground state have been proposed.[11] They are based on fused poly benzenic hydrocarbons and may present a high-spin ground state ($S = 5/2$ for instance) when certain specific carbons are saturated. Connecting these units using appropriate bridges can lead to ferro-, antiferro-, and ferrimagnetic materials.[12] In the present work, we study the possibility to assemble such magnetic units in order to conceive organic systems presenting double exchange phenomenon under doping. The first double exchange model had been proposed by Zener[13] in order to rationalize the giant magnetoresistive effects observed in manganites. The underlying mechanism involves two populations of unpaired electrons: strongly localized electrons responsible for magnetic properties and delocalized electrons inducing conduction. It therefore represents interesting means to combine transport and magnetic properties, which can hardly be encountered simultaneously although their association is of prime interest in spintronics.[14] Finally, it also appears a very promising means to prepare high-spin molecules.[15] While the study of this phenomenon in inorganic systems has received a lot of attention from both chemists and physicists, examples of purely organic double exchange compounds are extremely rare. One should quote for instance a mixed-valence bis(semiquinone) biradical anion resulting from an electron reduction of an

Received: July 4, 2013
Published: September 26, 2013

dx.doi.org/10.1021/ct4005855 | J. Chem. Theory Comput. 2013, 9, 4805−4815

antiferromagnetically coupled triradical, reported by Shultz and co-workers.[16]

The double exchange mechanism happens in mixed valence compounds involving magnetic units having more than one unpaired electron. The mechanism implies three kinds of interactions, the on-site exchange integral K between the local magnetic orbitals of each magnetic unit, hopping integrals t of a hole (or an extra electron) between the magnetic units and intersite exchange interactions J between localized spin momenta, as illustrated in Figure 1. While the magnetic couplings J are usually antiferromagnetic, the hopping integrals favor a ferromagnetic arrangement of all the spins. Since the itinerant electron or hole is usually delocalized between the most interacting orbitals of the units, the hopping integral between these orbitals dominates the physics of low energy and a high-spin ground state is obtained. In order to get organic compounds with such a property, several conditions should be fulfilled: (i) in the first place, the molecular frame should be seen as involving spin $S = 1$ magnetic units (before doping, i.e. ionization) such that two populations of electrons, itinerant and localized, can be obtained under doping, (ii) the organic bridges should not affect the magnetism of the units in the resulting doped architecture, (iii) the interactions through the bridges should be large enough in order to have a magnetic ordering of the spins at room temperature but not too large in order to keep a magnetic behavior, and (iv) finally, it is desirable that the pattern formed by the unit and the bridge be repeatable so that a periodic network can be formed.

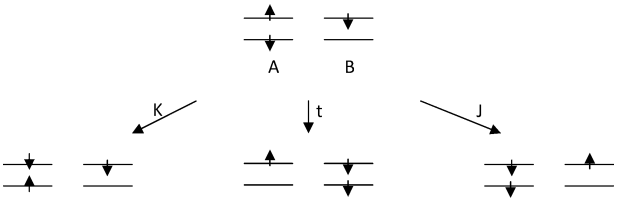

Figure 1. Illustration of the leading electronic interactions in double exchange phenomenon taking place between two magnetic units A and B.

The extraction of the double exchange interactions is straightforward from wave function methods calculations of the lowest energy states.[17] Due to the multideterminantal character of some of these states, it is much more complicate to determine these interactions from spin unrestricted DFT calculations. Recently, a procedure of extraction of double exchange interactions has been proposed.[18] It consists of determining the interactions of a generalized Hubbard model from various DFT solutions and then expressing the interactions of the double exchange model as functions of the Hubbard ones. Unfortunately, this procedure is not accurate enough here due to the important covalence effects inherent to organic compounds. A refined method is therefore proposed that enables one to reconstruct the spectrum of the multiconfigurational states and then to extract rigorously the double exchange interactions.

This paper is organized as follows. The next section recalls the theory of the double exchange model, the method of reconstruction of all the states of low energy and the procedure of extraction of the double exchange interactions from the energies of various spin unrestricted DFT solutions. Section III analyses and discusses the results obtained for a consistent series of designed compounds. The possibility to design promising hydrocarbons likely to present double exchange interaction from the simple calculations of the molecular orbitals diagrams at the Hückel level is presented in Supporting Information. From the knowledge acquired during the analysis of the studied compounds, new architectures likely to present improved features are proposed in section IV. Mono- and bidimensional periodic lattices based on the most promising molecular architecture are designed.

II. THEORETICAL INFORMATION

II.1. Studied Molecular Compounds and Computational Information. A consistent series of organic molecules likely to exhibit a double exchange phenomenon is represented in Figure 2. These molecules may be seen as constituted of two magnetic units, namely, the trimethylene methane (TMM) molecules, which have a triplet ground state in the isolated state and various diamagnetic bridges. The considered bridges have different lengths and different shapes. It is possible to anticipate the nature of the magnetic coupling between the two magnetic units using the Ovchinnikov's rule,[19] which states that the spin of the ground state is given by the M_s component of the most alternant spin distribution of the π electrons. In all considered

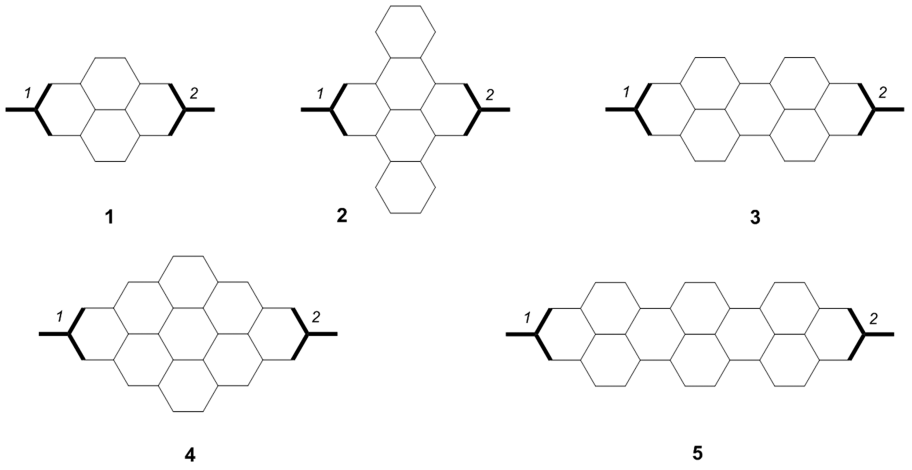

Figure 2. Schematic representation of the studied compounds.

dx.doi.org/10.1021/ct4005855 | J. Chem. Theory Comput. 2013, 9, 4805−4815

cases, the connection ensures an antiferromagnetic coupling. As a consequence, before oxidation, the ground state of these compounds is expected to be a singlet. In the cation, the spin of the ground state is a result of the competition between the various double exchange interactions and might be either a doublet or a quartet.

The geometries of the designed compounds have been optimized for various electronic solutions, namely $M_s = 0$ and $M_s = 1$ for neutral molecules and $M_s = 1/2$ and $M_s = 3/2$ for cationic molecules, using the B3LYP functional of the GAUSSIAN package.[20] To optimize the singlet state geometry a recently proposed method[21] of spin decontamination has been used. 6-311G** basis sets have been used for all atoms. Expectation values of S^2 have been computed for all solutions and are reported and discussed in the following.

II.2. Monoelectronic Picture versus Double Exchange Mechanism: Theory. Let us consider an organic molecular cation containing three unpaired electrons localized on two magnetic units A and B connected through a diamagnetic organic bridge. The local magnetic orbitals are called a_1, a_2 on site A and b_1, b_2 on site B. For a sake of simplicity, we shall first assume that the orbitals 1 and 2 belong to different irreducible representations; hence, there is no interaction between orbitals a_1 (a_2) and b_2 (b_1). For a symmetric cation (we will use the irreducible representation of the D_{2h} symmetry point group to which the studied molecules belong), the hole is completely delocalized between the units. One may expect that the interaction will be larger between the orbitals a_1 and b_1 than between the orbitals a_2 and b_2. From the resulting molecular orbital diagram represented in Figure 3, one may also expect

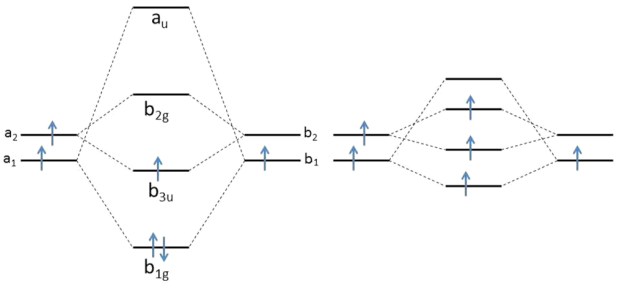

Figure 3. Molecular orbital diagrams obtained in case of strong (left) and weak (right) interactions for D_{2h} molecules such as **1**, **2**, **3**, **4**, and **5**. A doublet ground state can be anticipated in the left diagram while a quartet ground state is expected in the right diagram, that is, when the MOs are quasi-degenerate.

that the ground state is a doublet state with a single open shell, namely the bonding MO b_{3u} built from a_2 and b_2. The first excited doublet state would result from an excitation from this MO to the corresponding antibonding MO b_{2g}. In both states, the hole is delocalized between the a_2 and b_2 orbitals. The quartet state, which would be obtained from the excitation of an electron from the b_{1g} bonding MO between a_1 and b_1 to the antibonding a_u MO and a spin change, usually lies much higher in energy than the two previously mentioned doublet states. This simple monoelectronic picture reproduces qualitatively well the spectrum of most organic cations even though they are constituted of units that are magnetic when considered separately, such as the trimethylene methane TMM molecule, which has a triplet ground state. In order to reach a magnetic regime in which the spectrum of low energy would exhibit a quartet ground state, these four MOs should be quasi degenerate.

Another formulation of the problem is provided by the double exchange mechanism. The simpler double exchange model proposed by Zener[13] is based on the idea that the spectrum of the biunits can be reproduced by considering the magnetic units in their atomic ground states. In the considered case, the magnetic units have either a triplet or a doublet ground state depending on the position of the hole. Two families of states can be generated according to the symmetry of the orbitals in which the hole is delocalized. The family (called 1 here after) to which the high-spin ground state belongs is such that the hole is delocalized between the most interacting orbitals, a_1 and b_1, for instance. The dominant electronic interaction is the corresponding hopping integral t_1 of the hole between these orbitals. In double exchange systems, this delocalization generates two quartet states Q^1_+ and Q^1_- and two doublet states D^1_+ and D^1_-. As shown by Girerd and Papaefthymiou,[22] the interaction between the electrons occupying the less interacting orbitals a_2 and b_2 is a magnetic coupling J_1 (contribution of Heisenberg type) that rules the relative energies of the doublet spin states in comparison to the quartet ones in family 1. Similar states, noted Q^2_+, Q^2_-, D^2_+, and D^2_- constitute family 2, in which the hole is delocalized between the orbitals a_2 and b_2 and the localized electrons occupy the a_1 and b_1 orbitals. In the particular case of a symmetric biunit system, the eigenenergies of the usual double exchange model (here noted the ZGP model in reference to Zener, Girerd, and Papaefthymiou) are analytically known. Energies $E(S, \pm)$ of the different states of total spin S are given by the expression:

$$E_i^{(ZGP)}(S, \pm) = \Delta\varepsilon(1 - \delta_{2i}) \pm \frac{t_i}{S_{max} + 1/2}\left(S + \frac{1}{2}\right) - \frac{J_i}{2}(S(S+1) - S_{max}(S_{max}+1)) \quad (1)$$

where S_{max} is the highest total spin of the double exchange model (here $S = 3/2$), δ is the Krönecker symbol, and the zero of energy is taken as the energy centroid of the highest-spin states of family 2, here the quartet states. The index i (1 or 2) indicates the family of states. The energy difference between the energy centroids of the two families of states is essentially given by the energy difference $\Delta\varepsilon = \varepsilon(a_1) - \varepsilon(a_2)$ between the orbitals a_1 (b_1) and a_2 (b_2). The first term of eq 1 is generally dominant and accounts for the appearance of a high-spin ground state, that is, a ferromagnetic order in family 1. Due to the presence of a bridging ligand, the t_1 integral is expected to be dominated by the through-ligand contribution. The second family of states (higher in energy) is generated by the delocalization t_2 of the hole in the less interacting orbitals a_2 and b_2 and a magnetic coupling J_2 between the electrons localized in the most interacting orbitals a_1 and b_1. The hopping integral t_2 between a_2 and b_2 may be very small while the magnetic coupling J_2, which is proportional to t_1, is usually antiferromagnetic and large, so that one usually observes that the doublet states are lower in energy than the quartets in that family.

When the local excited singlet state (called the non-Hund state in inorganic compounds) of the units is low in energy, as expected in organic compounds, it may affect the energy spacing between the various states. The Anderson Hasegawa model[23] takes only into account the non-Hund states.

dx.doi.org/10.1021/ct4005855 | J. Chem. Theory Comput. 2013, 9, 4805−4815

Combining both contributions leads to the more appropriate following expressions:[17]

$$
\begin{aligned}
{}^{4}E_i^{(\mathrm{AH/GP})}(S_{\max}, \pm) &= \Delta\varepsilon(1 - \delta_{2i}) \pm t_i \\
{}^{2}E_i^{(\mathrm{AH/GP})}(S \neq S_{\max}, \pm) &= \Delta\varepsilon(1 - \delta_{2i}) + K - \sqrt{K^2 + t_i(t_i \pm K)} \\
&\quad - \frac{J_i}{2}(S(S+1) - S_{\max}(S_{\max}+1))
\end{aligned}
\tag{2}
$$

where AH stands for Anderson Hasegawa. In inorganic compounds the non-Hund states are quite high in energy; however, due to the delocalized character of magnetic orbitals in organic compounds, one may expect that these states can be quite low in energy and may be dominant in the wave function of some of the doublet states.

Figure 4 represents schematically the two families of states (including only the two lowest doublet states) as functions of the various interactions in organic (or covalent systems). It should be noticed that while t_1 is the dominant interaction in the first family of states, J_2 is the most important interaction of the second family. For covalent compounds such as organic molecules, J_2 can be so large that the lowest doublet of family 2 can be lower in energy than the quartet state of family 1. In such a case, the double exchange model would predict the same ground state as the simple monoelectronic picture, but in such a case, one should be careful about the applicability of the double exchange model for the analysis of the spectra.

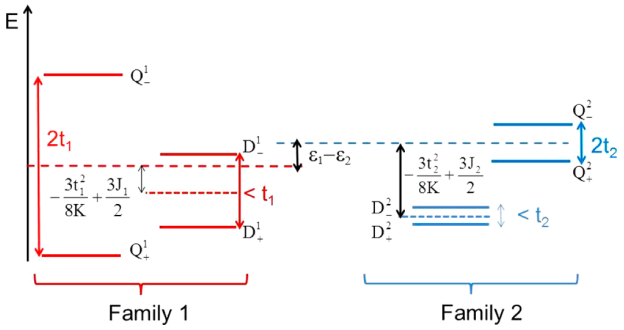

Figure 4. Schematic representation of the spectrum of the two families of states of a double exchange compound. The expression of the energy differences between the energy centroids of the quartet and doublet states is derived from perturbation expansion.

II.3. Reconstruction of the Spectrum of Low Energy and Extraction of the Double Exchange Interactions from DFT Calculations. The real difficulty in getting the low energy spectrum of double exchange compounds from spin unrestricted DFT calculations comes from the determination of accurate energies of the doublet states. Indeed, these doublet states are usually multiconfigurational while the spin unrestricted calculated DFT solutions are single determinants and quite certainly not eigenfunctions of S^2. While techniques of spin decontamination in the case of magnetic undoped systems are fairly simple, the situation is highly complex for the case of double exchange. For both the doublets with a single open shell and the quartets, the deviations of the expectation value of S^2 from the expected values, 3/4 and 15/4, respectively, are relatively small. Nevertheless, it is no longer true for three-open-shell $M_s = 1/2$ solutions. In order to get reliable estimates of the energies of such doublet states, we will use a method that slightly differs from the one proposed by some of the authors in a previous work;[18] this refined proposed method is more rigorous and more appropriate for organic compounds. It consists of determining the crucial interactions that are ruling the spectrum of low energy and then reconstructing the spectrum from these interactions. For this purpose, the various DFT solutions that are needed to extract all the interactions of a generalized Hubbard model are calculated. This Hamiltonian differs from the usual Hubbard model, which only considers intersite hopping integrals t_1, t_2 and on-site repulsion U_1, U_2, by the introduction of the on-site exchange integral $K = K_{a1a2} = K_{b1b2}$. This model is then numerically solved to get the energies of all doublet states, and the spectrum is reconstructed. The interactions of the double exchange model are consequently extracted from the reconstructed spectrum. This last extraction only makes sense for the states, which are ruled by a double exchange model, that is, the states of family 1 for systems for which the quartet is the ground state.

All needed interactions can be calculated from the seven DFT solutions represented in Figure 5.

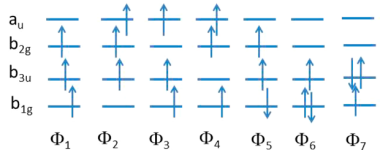

Figure 5. DFT solutions, which are used to extract the interactions of the Hubbard model (D_{2h} symmetry).

Their Hubbard energies are given by the following expressions:

$$
\begin{aligned}
E(\Phi_1) &= \Delta\varepsilon - |t_1| \\
E(\Phi_2) &= \Delta\varepsilon + |t_1| \\
E(\Phi_3) &= -|t_2| \\
E(\Phi_4) &= +|t_2| \\
E(\Phi_5) &= \Delta\varepsilon + K - |t_1| \\
E(\Phi_6) &= -2|t_1| - |t_2| + \left(\frac{4K + U_1}{4}\right) \\
E(\Phi_7) &= \Delta\varepsilon - 2|t_2| - |t_1| + \left(\frac{4K + U_2}{4}\right)
\end{aligned}
\tag{3}
$$

Solving this system of equations enables one to assess values to the interactions, K, t_1, t_2, U_1, and U_2. Due to strong covalence effects expected in organic compounds, it is not possible to get reliable values of the exchange integrals of the double exchange model from their perturbative expressions, as done in ref 18. The procedure proposed by the authors consists in determining variationally the energies of the doublet states. The neutral doublet (N) functions of the double exchange model are coupled with the ionic (I of energy U), the pseudo-ionic (pseudo I, of energy $3K$) and the non-Hund functions (NH of energy $2K$). Left-right combination of these functions furnishes a symmetric basis of gerade and ungerade functions for the doublet state of family 2:

dx.doi.org/10.1021/ct4005855 | J. Chem. Theory Comput. 2013, 9, 4805−4815

$$
{}^2\Psi_1^N = \left| \frac{1}{\sqrt{6}} \left[\sqrt{2}\,(|a_1 a_2 \overline{b}_1| - |\overline{a}_1 b_1 b_2|) + \left(\frac{|a_1 b_1 \overline{b}_2| + |a_1 \overline{b}_1 b_2|}{\sqrt{2}} - \frac{|a_1 \overline{a}_2 b_1| + |\overline{a}_1 a_2 b_1|}{\sqrt{2}} \right) \right] \right\rangle
$$

$$
{}^2\Psi_2^{NH} = \left| \frac{1}{\sqrt{2}} \left(\frac{|a_1 \overline{a}_2 b_1| - |\overline{a}_1 a_2 b_1|}{\sqrt{2}} - \frac{|a_1 b_1 \overline{b}_2| - |a_1 \overline{b}_1 b_2|}{\sqrt{2}} \right) \right\rangle
$$

$$
{}^2\Psi_3^{\mathrm{Pseudo}I} = \left| \frac{1}{\sqrt{2}} (|a_2 b_1 \overline{b}_1| - |a_1 \overline{a}_1 b_2|) \right\rangle
$$

$$
{}^2\Psi_4^{\mathrm{I}} = \left| \frac{1}{\sqrt{2}} (|a_1 \overline{a}_1 a_2| - |b_1 \overline{b}_1 b_2|) \right\rangle \tag{4}
$$

The 4 × 4 matrix of the Hubbard Hamiltonian working in this basis is

$$
\hat{H}_{D_+^2}^{\mathrm{Hubbard}} = \begin{pmatrix} -\frac{t_2}{2} & -\frac{\sqrt{3}\,t_2}{2} & -\sqrt{\frac{3}{2}}\,t_1 & -\sqrt{\frac{3}{2}}\,t_1 \\ -\frac{\sqrt{3}\,t_2}{2} & 2K + \frac{t_2}{2} & -\frac{t_1}{\sqrt{2}} & -\frac{t_1}{\sqrt{2}} \\ -\sqrt{\frac{3}{2}}\,t_1 & -\frac{t_1}{\sqrt{2}} & 3K & -t_2 \\ -\sqrt{\frac{3}{2}}\,t_1 & -\frac{t_1}{\sqrt{2}} & -t_2 & U_1 \end{pmatrix} \tag{5}
$$

Similar matrices can be calculated for the doublet states of family 1 and for the second doublet state of family 2. The following matrix describes the energy of the lowest doublet state of family 1:

$$
\hat{H}_{D_+^1}^{\mathrm{Hubbard}} = \begin{pmatrix} -\frac{t_1}{2} + \Delta\varepsilon & -\frac{\sqrt{3}\,t_1}{2} & -\sqrt{\frac{3}{2}}\,t_2 & -\sqrt{\frac{3}{2}}\,t_2 \\ -\frac{\sqrt{3}\,t_1}{2} & 2K + \frac{t_1}{2} + \Delta\varepsilon & -\frac{t_2}{\sqrt{2}} & -\frac{t_2}{\sqrt{2}} \\ -\sqrt{\frac{3}{2}}\,t_2 & -\frac{t_2}{\sqrt{2}} & 3K + \Delta\varepsilon & -t_1 \\ -\sqrt{\frac{3}{2}}\,t_2 & -\frac{t_2}{\sqrt{2}} & -t_1 & U_2 + \Delta\varepsilon \end{pmatrix} \tag{6}
$$

Using the numerical values of all the interactions determined from eqs 3, one may diagonalize all these matrices. The energy of the four doublet states of interest is given by the lowest eigenvalue of each matrix. Finally, when the system is ruled by a double exchange mechanism one may extract values of the effective magnetic couplings J^{eff} and local exchange K^{eff} interactions using the energies of the various states and the expression given in eq 2. Effective interactions incorporate correlation effects, which do not appear in the model space but which are accounted for in the numerical DFT calculations.

III. RESULTS AND DISCUSSION

III.1. Analysis of the DFT Results and Extraction of the Leading Interactions. The Singly Occupied Molecular Orbitals (SOMOs) of an isolated TMM unit are represented in Figure 6. It can be seen that connecting such a unit by two of its carbon atoms will lead to a stronger interaction between the bridge and the unit for orbital a_1 than for orbital a_2. The opposite result would be obtained in the case of a connection via a single carbon atom. As a consequence one may expect larger values for t_1 than for t_2 in the studied compounds.

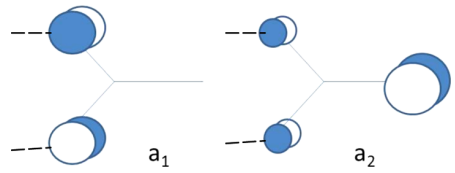

Figure 6. Magnetic orbitals of the TMM magnetic unit. Dotted lines indicate the connection to the bridge.

Both neutral and cationic molecules have been studied. Let us first concentrate on the results obtained for the neutral molecules. The energies and $\langle S^2 \rangle$ values of the $M_s = 0$ and $M_s = 1$ solutions computed for the optimized geometries of both the triplet and the spin decontaminated singlet are reported in Table 1. From the various solutions, vertical and adiabatic energy differences between the lowest singlet (spin decontaminated) and triplet states of the five molecules have been computed and are also reported in Table 1. The vertical energy difference between the real singlet and the triplet is equal to the effective exchange interaction of the Heisenberg Hamiltonian when the system is magnetic.

The various spin unrestricted DFT solutions needed for the reconstruction of the spectra of the cations have been computed. The geometries of the lowest in energy $M_s = 3/2$ and $M_s = 1/2$ solutions have been optimized and the corresponding values of their energies and of $\langle S^2 \rangle$ are reported in Table 2. The energies of the $M_s = 1/2$ solutions having three open shells at the geometries of the $M_s = 3/2$ solutions are also reported in Table 2. Table 3 collects all the values of the interactions of the Hubbard model for all systems and those of the double exchange one when the spectrum is ruled by a double exchange mechanism, that is, for family 1 of compounds **4** and **5**. The spectra reconstructed using the method presented in section II.3 are represented in Figure 7.

The t_1 and t_2 parameters, which have been extracted from the cations energies would be slightly different for the neutral molecules. One may, however, expect that the observed trends for the extracted parameters in this consistent series of molecules would be identical for both the neutral and cationic systems, and their relative values will be used to rationalize the observed trends in both neutral and cationic molecules.

The molecular orbitals have been optimized for the ground state of the cations. These orbitals are very similar for both neutral and cationic molecules. Those optimized for compounds **1** and **4** are represented in Figures 8 and 9. All the trends observed in the series can be correlated with the shape of these four MOs. These orbitals can be seen as resulting from bonding and antibonding combinations of the local orbitals (a_1, a_2, b_1, and b_2) of the TMM units with delocalization tails on the bridging ligand. The SOMO (b_{3u}) shows large components on the extracyclic carbons of both TMM. It can be seen as a

dx.doi.org/10.1021/ct4005855 | J. Chem. Theory Comput. 2013, 9, 4805−4815

Table 1. Neutral Molecules[a,b]

		$\langle S^2\rangle$	E (au or *eV*)
1	triplet (vert.)	2.03	−693.253712
	triplet	2.03	−693.256048
	BS M_s = 0 ("vert.")	0.92	−693.265296
	BS M_s = 0	0.80	−693.266979
	ΔE_{ST} (vertical)		*0.616*
	ΔE_{ST} (adiabatic)		*0.532*
2	triplet (vert.)	2.04	−1000.604739
	triplet	2.04	−1000.608011
	BS M_s = 0 ("vert.")	0.88	−1000.617184
	BS M_s = 0	0.71	−1000.619331
	ΔE_{ST} (vertical)		*0.614*
	ΔE_{ST} (adiabatic)		*0.520*
3	triplet (vert.)	2.05	−1076.854431
	triplet	2.05	−1076.854547
	BS M_s = 0 ("vert.")	1.09	−1076.857159
	BS M_s = 0	1.09	−1076.857267
	ΔE_{ST} (vertical)		*0.183*
	ΔE_{ST} (adiabatic)		*0.167*
4	triplet (vert.)	2.05	−1229.338761
	triplet	2.04	−1229.339042
	BS M_s = 0 ("vert.")	1.27	−1229.343328
	BS M_s = 0 ("vert.")	1.27	−1229.343328
	ΔE_{ST} (vertical)[c]		*0.302*
	ΔE_{ST} (adiabatic)[c]		*0.264*
5	triplet (vert.)	2.07	−1460.451337
	triplet	2.07	−1460.451356
	BS M_s = 0 ("vert.")	1.13	−1460.449958
	BS M_s = 0	1.14	−1460.452359
	ΔE_{ST} (vertical)		*0.062*
	ΔE_{ST} (adiabatic)		*0.061*

[a]UDFT-calculated energies for **1** to **5**, with corresponding singlet-triplet energy differences after spin decontamination. vert (resp. "vert") refers to the geometry of the ground state (resp. excited state). [b]The spin-decontaminated values are obtained from the UDFT energies and $\langle S^2\rangle$ values, assuming an harmonic geometry dependency of the energy and a linear geometry dependency of the spin decontamination factor λ. [c]In this case, the $\langle S^2\rangle$ values for the M_s = 0 solution compel to use a spin-decontamination factor λ = 2.

Table 2. Cationic Molecules[a]

		$\langle S^2\rangle$	energy (au)
1	quartet (vert.)	3.81	−692.993238
	quartet	3.81	−693.003177
	BS M_s = 1/2 ("vert.")	0.82	−693.027045
	BS M_s = 1/2	0.81	−693.036818
2	quartet (vert.)	3.81	−1000.345431
	quartet	3.82	−1000.354809
	BS M_s = 1/2 ("vert.")	0.85	−1000.385054
	BS M_s = 1/2	0.83	−1000.394285
3	quartet (vert.)	3.84	−1076.620122
	quartet	3.85	−1076.627585
	BS M_s = 1/2 ("vert.")	0.83	−1076.627146
	BS M_s = 1/2	0.83	−1076.634478
4	BS M_s = 1/2 ("vert.") 3 open-shell (ϕ_5)	1.77	−1229.110294
	BS M_s = 1/2 ("vert.")	0.84	−1229.113133
	BS M_s = 1/2	0.83	−1229.119439
	quartet (vert.)	3.85	−1229.118140
	quartet	3.85	−1229.123853
5	BS M_s = 1/2 ("vert.") 3 open-shells (ϕ_5)	1.78	−1460.229159
	BS M_s = 1/2 ("vert.")	0.85	−1460.225720
	BS M_s = 1/2	0.85	−1460.231719
	quartet (vert.)	3.86	−1460.232461
	quartet	3.87	−1460.238495

[a]UDFT-calculated energies of the lowest M_s = 1/2 and M_s = 3/2 solution for **1** to **5**. $\langle S^2\rangle$ values are also reported. vert (resp. "vert") refers to the geometry of the ground state (resp. excited state).

Table 3. Values of the Interactions of the Hubbard and Double Exchange Models[a]

	t_1	t_2	u_1	u_2 (eV)	K (eV)	K_{DE}	J_1
1	1.677	0.612	1.504	3.332	0.419	1.175	
2	1.831	0.653	1.171	3.546	0.345	1.149	
3	1.186	0.291	1.058	3.664	0.317	0.512	
4	0.802	0.234	1.554	4.066	0.369	0.509	−0.092
5	0.793	0.082	1.031	4.159	0.254	0.272	−0.014

[a]t_1, t_2, U_1, U_2, and K are the interactions of the Hubbard model while $\Delta\varepsilon$, t_1, J_1, and K^{DE} are the interactions of the double exchange model for family 1.

bonding combination between the outermost and hence less interacting orbitals of the TMM (a_2 and b_2). The b_{1g} MO, which results from a bonding combination between the most interacting orbitals of the TMM (a_1 and b_1, which have large components on the cyclic carbons), is delocalized inside the bridge, revealing a stronger covalence between the local orbitals of the magnetic units and the orbitals of the bridge. These observations are true for all compounds. However, comparing the orbitals of compounds **1** and **4**, one may easily see that the covalence, evidenced by the importance of the tails inside the bridge, decreases from compound **1** to compound **4**.

Looking at the results obtained for the **neutral** molecules several conclusions can be drawn:

(i) The spin multiplicity of the ground state of the five molecules is a singlet confirming the antiferromagnetic nature of the interactions between the two TMMs. As expected the values of ΔE_{ST} decrease with the length of the bridge.

(ii) The expectation value of S^2 in the lowest M_s = 0 solution shows that there is mainly a single open shell per TMM units, revealing that these units cannot be considered as a unit of spin S = 1 (for which $\langle S^2\rangle$ = 3) in the neutral compounds. As a consequence, the M_s = 2 solution which of course involves four open-shells is very high in energy (17138 cm^{-1} = 49 kcal·mol^{-1} higher than the M_s = 0 solution in compound **1** and 22 kcal·mol^{-1} in compound **5**). Comparing the values of $\langle S^2\rangle$, one may notice that even if they always support a diradicalar character in compounds **4** and **5** the values are slightly larger than 1. The spin polarization due to the contributions of four-open-shells determinants $|b_{1b}\bar{b}_{3u}\bar{b}_{2g}a_u|$ and $|\bar{b}_{1b}b_{3u}b_{2g}\bar{a}_u|$ introduces quintet components in the M_s = 0 solution resulting in $\langle S^2\rangle$ values larger than 1. Actually, since these contributions are larger for systems for which the b_{1g} and a_u orbitals are close in energy, that is, for small values of t_1, one may easily correlate the increase of the $\langle S^2\rangle$ values with the decrease of t_1 (Tables 1 and 3).

(iii) Another confirmation of the diradicalar character of these compounds is brought by the comparison between the t_2 hopping integrals and the energy difference between the singlet and the triplet states in the series. The decrease of

dx.doi.org/10.1021/ct4005855 | J. Chem. Theory Comput. 2013, 9, 4805−4815

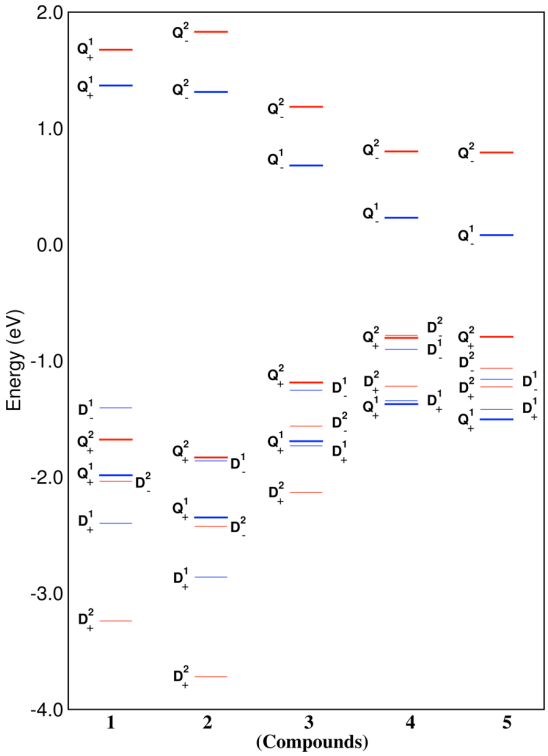

Figure 7. Reconstructed spectra of the cationic compounds **1**, **2**, **3**, **4**, and **5** indicated in abscissa. Energy levels of quartet states are represented with thick lines while that of the doublet state are represented with thin lines. Family 1 appears in blue and family 2 in red.

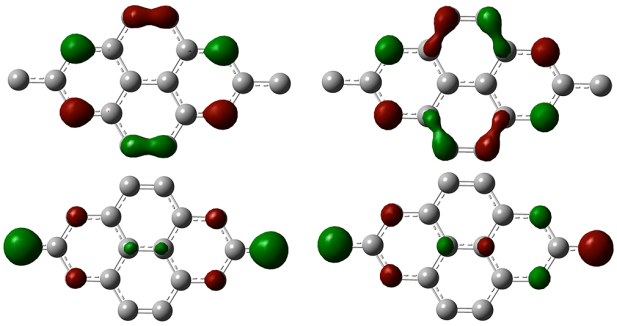

Figure 8. DFT molecular orbitals b_{1g} (top left), a_u (top right), b_{3u} (bottom left) b_{2g} (bottom right) optimized for the doublet ground state ($b_{1g}^2 b_{3u}^1$) of compound **1**.

ΔE_{ST} (Table 1) is actually correlated with the decrease of t_2 integrals (Table 3). The single open shells localized on the TMM are mainly the a_2 and b_2 orbitals while the b_{1g} MO obtained from the local a_1 and b_1 orbitals which undergo strong covalent interactions via the bridge is finally doubly occupied. This result is consistent with the strong values of the t_1 integrals in all compounds. One may also notice that while compound **4** has the smallest value of t_1, its value of t_2 is quite large rationalizing the obtaining of a large ΔE_{ST}.

The comparison of the results obtained for the **cations** deserves the following comments:

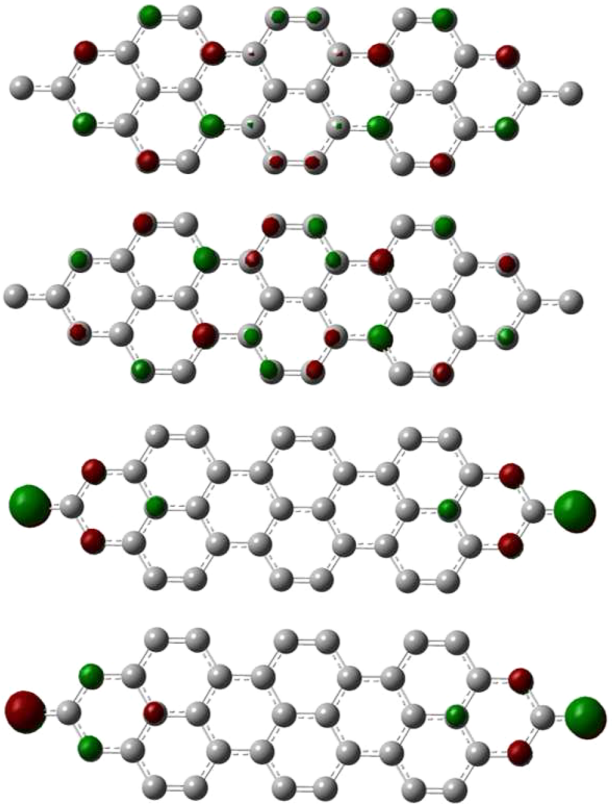

Figure 9. DFT molecular orbitals optimized for the lowest $M_s = 3/2$ solution ($b_{1g}^1 b_{3u}^1 b_{2g}^1$) of compound **5**: from top to bottom b_{1g}, a_u, b_{3u}, and b_{2g}.

(i) Looking at the reconstructed spectra (Figure 7), one may see that for compounds **1**, **2**, and **3** the ground state is the lowest doublet of family 2. For compounds **4** and **5**, the ground state is the quartet state of family 1, demonstrating that one may conceive hydrocarbons exhibiting a double exchange phenomenon. This result shows that while the magnetic units must be considered as a spin $S = 1/2$ unit in the neutral molecules, it may behave as a spin $S = 1$ in cationic molecules.

(ii) The analysis of the occupation numbers of the orbitals of the ground state and of the $\langle S^2 \rangle$ values in compounds **1**, **2**, and **3** (table 2) reveals that the lowest $M_s = 1/2$ DFT solution essentially has a single open shell, for both the lowest doublet and quartet optimized geometries. This result is in agreement with the occurrence of two open-shells only in the lowest solutions of the corresponding neutral molecules. The spectrum of these cations obeys the logic of the monoelectronic picture, which predicts that the ground state is the lowest doublet state of family **2**. A simple building block logic consisting in bridging magnetic unit by any diamagnetic bridge and then ionizing the system does not necessary succeed to generate a double exchange phenomenon.

(iii) In order to favor the occurrence of a high-spin ground state, the b_{1g} MO (Figure 3) should be destabilized; that is, the value of the hopping integral t_1 must be weak. The here-followed logic consists in extending the π system in order to decrease the energy differences between the orbitals at the Fermi level. Comparing the energies of the

dx.doi.org/10.1021/ct4005855 | J. Chem. Theory Comput. 2013, 9, 4805−4815

lowest doublet of family 2 and of the lowest quartet of family 1 (Table 2) in the series of compounds, one can notice the correlation between the decrease of t_1 and the relative stability of the quartet state, showing the crucial role of the magnitude of t_1 (Table 3) in the occurrence of a double exchange phenomenon. Looking more precisely at the consistent series **1**, **3**, and **5** (which have similar bridges that only differ by their length) shows the correlation of the decrease of t_1 with the length of the bridge. Interestingly enough, comparing t_1 in the full series, that is, including compounds **2** and **4**, which have slightly different bridges, leads to the conclusion that the t_1 values also depend on the shape of the bridge and may significantly decrease for some specific thickenings, as it occurs in compound **4**.

(iv) The correlation of the decrease of t_1 with the stabilization of the quartet state is meaningful for all compounds. However, from this quantity only, one may not anticipate the relative stability of the lowest quartet and doublet states of family 1. Actually in compounds **1**, **2**, and **3** this doublet is lower in energy than the quartet state, showing that it may be not sufficient to focus on the value of t_1 in order to reach a double exchange regime. In order to get more insight on the factors governing the relative stability of this doublet state, we have analyzed the physical content of its wave function, that is, of the eigenstate of the 4*4 matrices (see eq 6). In the first place, it is interesting to note that the weight of the non-Hund state in this doublet is large but constant in the series (for instance it is 0.15 in compound **1** and 0.13 in compound **5**). The main difference comes from the weight of the pseudoionic and ionic functions, which are respectively 0.13 and 0.06 for compound **1** and 0.05 and 0.01 in compound **5**. While the values of U_2 and K are rather similar from one compound to another, the t_2 values which determine the coupling between the neutral Hund's function and the pseudoionic and ionic functions dramatically decrease in the series, rationalizing the strong stabilizing contributions of these excited functions in the doublet state wave functions of compound **1**, **2**, and **3**. As a conclusion, one may say that the relative stability of the quartet and doublet states of family 1 is essentially determined by the value of the hopping integral t_2 between the weakly interacting orbitals.

(v) The analysis of the wave functions of the doublet states also reveals that the excited doublet states are slightly dominated by the non-Hund function in family 1. For instance, the relative weights of the Hund and non-Hund functions are 0.62 and 0.38 in the second doublet state of family 1 of compound **1**. This result will always be true as long as $t_1 > 2K$.

(vi) Finally, the parameters K^{DE} and J_1 of the double exchange model have been extracted for the family 1 of compounds **4** and **5** (see Table 3). One may notice that the values of K^{DE} differ from the Hubbard K values. One should recall that in eq 2, the Non-Hund functions are treated variationally while the ionic and pseudo ionic functions are treated perturbatively through the J parameter. As a consequence, the exchange parameter of the double exchange model described using eq 2 should be seen as an effective parameter and may be slightly different from the *ab initio* calculated one (expected to be very close to the Hubbard one). Finally one may note that the intersite exchange integral J_1 decreases between compounds **4** and **5** in agreement with the decrease of t_2.

As shown in Supporting Information, the extension of the π system of the bridge cannot rationalize by itself the observed trend: the shape of the bridge should be accounted for. Using the topological Hückel method combined with the fragment theory in terms of two TMM and the closed-shell bridge, one may rationalize the magnitude of the hopping integrals in the various studied compounds. It is interesting to note that such a simple method enables one to anticipate and therefore conceive molecular architectures susceptible to exhibit a double exchange phenomenon.

IV. OTHER POSSIBLE ARCHITECTURES AND LOW-DIMENSIONAL PERIODIC LATTICES LIKELY TO PRESENT A DOUBLE EXCHANGE PHENOMENON

One way to decrease the covalent interaction between the bridge and the TMM, would be to connect the TMM through only one of its carbon atoms. In such a case, the orbitals, which would generate the most important interactions, would be the a_1 (b_1) orbital. Saturating one of the orbitals of the bridge should diminish the interactions through the bridge and distinguish one of the carbon atoms of the TMM. Such a molecule is represented in Figure 10 (compound **6**). Another

6 7

Figure 10. Schematic representation of compounds **6** and **7**.

possibility consists in considering a nonsymmetric compound such as compound **7** also represented in Figure 10. In both compounds, the dissymmetry introduced in the molecule changes the nature of the most interacting orbital and one may expect that the proposed compounds would have smaller hopping integrals and therefore exhibits a double exchange mechanism. Due to the lack of symmetry, the two families interact and it is no more possible to make any extractions of the parameters from DFT calculations. Table 4 shows the energies of the $M_s = 3/2$ and $M_s = 1/2$ solutions having only

Table 4. UDFT-Calculated Energies of the Lowest $M_s = 1/2$ and $M_s = 3/2$ Solution for 6 and 7[a]

		$\langle S^2 \rangle$	energy (au)
6	BS $M_s = 1/2$ ("vert.")	1.50	−617.914525
	BS $M_s = 1/2$	1.35	−617.917603
	quartet (vert.)	3.84	−617.922641
	quartet	3.84	−617.926125
7	BS $M_s = 1/2$ ("vert.")	1.59	−1000.361133
	BS $M_s = 1/2$	1.50	−1000.362330
	quartet (vert.)	3.85	−1000.366575
	quartet	3.85	−1000.367770

[a] $\langle S^2 \rangle$ values are also reported.

dx.doi.org/10.1021/ct4005855 | J. Chem. Theory Comput. 2013, 9, 4805−4815

one unpaired electron. In both cases, the $M_s = 3/2$ solution is the lowest solution, which is quite encouraging.

From one of the most promising architectures (compound **4**), it is possible to conceive monodimensional and bidimensional periodic lattices. Fragments of the two proposed low dimensional lattices are represented in Figures 11 and 12.

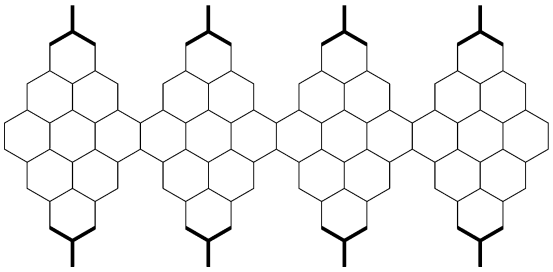

Figure 11. Example of 1D lattice constituted of compound **4** units.

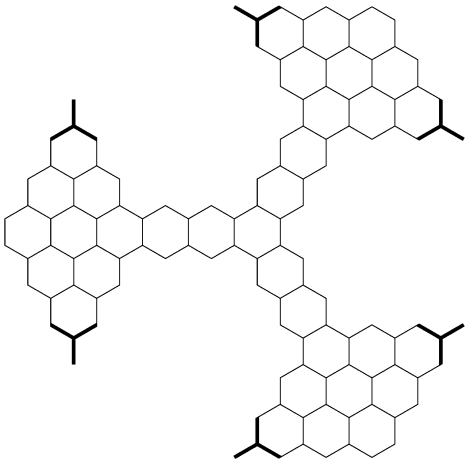

Figure 12. Example of 2D lattice constituted of compound **4** units.

V. CONCLUSION

Magnetism and double exchange phenomenon are more likely to occur in inorganic compounds, for which the hopping integrals between magnetic centers are often weak due to the strong localization of the magnetic orbitals. The spectrum of magnetic inorganic compounds hence usually obeys simple physical models as the Heisenberg or double exchange ones. In contrast, organic systems for which the magnetic orbitals are delocalized over several centers are more sensitive to chemical factors, such as the geometrical features of the bridge and the strength of covalent interactions. As a consequence, their spectrum of low energy may or may not be well reproduced by simple physical models. This paper discusses the possible occurrence of a double exchange phenomenon in a consistent series of organic molecules. Both neutral and cationic molecules have been studied. While for neutral magnetic systems well-known spin decontamination techniques can be used to determine the energy difference between the lowest magnetic states, the determination of the energies of the doublet states of double exchange compounds is more complicate. A method that consists in determining the leading interactions of the Hubbard model from series of UDFT calculations and then uses the numerical values of these interactions in order to reconstruct the spectra has been proposed and applied here. The mains conclusions of this work are the following:

(i) While these molecules may be seen as involving TMM units that have a triplet ground state (when isolated), these units cannot be considered as $S = 1$ magnetic units when they are bridged by the here-considered diamagnetic bridges in the resulting neutral compounds. The energy difference between the singlet and triplet lowest states results from an antiferromagnetic coupling between $S = 1/2$ momenta strongly localized on the extracyclic carbon atoms.

(ii) In contrast, two of the corresponding cations exhibit a quartet ground state showing that the TMM of such molecules may behave as a $S = 1$ unit **under doping**.

(iii) The comparison of the spectra reveals that the real challenge in order to get a double exchange phenomenon is to control the factors governing the relative stability of the quartet ground state of family 1 and the lowest doublet state of family 2. We have shown that the main factor is the hopping integral t_1 between the most interacting orbitals between the TMMs, the magnitude of which is determined by the strength of the covalence between the TMM and the bridge. The other leading factor is the hopping integral t_2 between the weakly interacting orbitals which is decisive for the relative stability of the lowest quartet and doublet states of a same family.

(iv) While the magnitude of the t_2 integral essentially depends on the length of the bridge, t_1 is also sensitive to the shape of the bridge, in the studied compounds. Both the relative stability of the magnetic orbitals and the impact of the shape of the bridge on the leading interactions can be easily anticipated using the Hückel method (see Supporting Information). This simple model combined with a deep analysis of the leading interactions of the double exchange model can be a predictive tool in order to anticipate organic systems likely to present a double exchange phenomenon.

(v) Finally, it is interesting to note that the lowest local excited state of the TMM, that is, the non-Hund state, is particularly low in energy and plays an important role in the physics of these systems. The weight of these local states is important in the wave functions of the lowest doublets states of both families and it is dominant in the wave functions of the second doublets states. As a consequence, the model of Girerd and Papaefthymiou[22] cannot be used to describe the physics of the double exchange mechanism in these organic compounds. Due to the delocalized character of magnetic orbitals, one may expect that the role of non-Hund states will generally be more important in organic compounds than in inorganic ones. In order to account for both the non-Hund and the ionic and pseudo ionic functions which all may have a large coefficient in the wave functions of the lowest states, the relevant double exchange model should account for both the Anderson−Hazegawa and Girerd−Papaefthymiou contributions. Moreover, in order to extract all the parameters of the model, it is necessary to use also the expression describing the energy of the non-Hund states (which are discarded in the usual model since they are expected to be highly excited).

dx.doi.org/10.1021/ct4005855 | J. Chem. Theory Comput. 2013, 9, 4805−4815

Other architectures in which the interactions go through a single carbon atom of the TMM have been proposed in section IV. The comparison between the energies of the lowest $M_s = 3/2$ and $M_s = 1/2$ spin unrestricted DFT solutions indicate that these molecules are likely to exhibit a double exchange phenomenon. Unfortunately, due to the lack of symmetry, the energies of the real doublets could not be determined using the proposed method.

Finally, one- and two-dimensional periodic lattices have been designed from the most promising compounds **4** and **5**. One may expect that under doping such lattices could present both magnetic and conductive properties of potential interest in spintronics. A forthcoming work will be devoted to the study of spin polarized current in such systems.

■ ASSOCIATED CONTENT

Supporting Information

A Hückel based rationalization. This material is available free of charge via the Internet at http://pubs.acs.org.

■ AUTHOR INFORMATION

Corresponding Author

*E-mail: nathalie.guihery@irsamc.ups-tlse.fr.

Notes

The authors declare no competing financial interest.

■ REFERENCES

(1) (a) *Magnetic Molecular Materials*; Gatteschi, D.; Kahn, O.; Miller, J.S.; Palacio, F., Eds.; Kluwer: Dordrecht, Netherlands, 1991; (b) Kahn, O. *Molecular Magnetism*; VCH: Weinheim, 1993; (c) Gatteschi, D. *Adv. Mater.* **1994**, *6*, 635. (d) Miller, J. S.; Epstein, A. J. *Angew. Chem., Int. Ed. Engl.* **1994**, *33*, 385. (e) *Molecule-Based Magnetic Materials*, ACS Symposium Series; American Chemical Society: Washington, DC, 1996; Vol. *644*; (f) *Molecular Magnetism*; Itoh, K., Kinoshita, M., Eds.; Gordon and Breach: Tokyo, 2000; (g) Long, J. In *Chemistry of Nanostructured Materials*, Yang, P., Ed.; World Scientific Publishing: Hong Kong, 2003; (h) *Coord. Chem. Rev.* **2005**, *249*, Special Issue *"Molecular Magnetism"*; (i) Gatteschi, D.; Bogani, L.; Cornia, A.; Mannini, M.; Sorace, L.; Sessoli, R. *Solid State Sci.* **2008**, *10*, 1701. (j) Kahn, O. *Acc. Chem. Res.* **2000**, *33*, 647. (k) Georges, R.; J. J. Borrás-Almenar, Coronado, E.; J. Curély, Drillon, M. In *Magnetism: Molecules to Materials*; Miller, J. S.; Drillon, M., Eds.; Wiley-VCH: Weinheim, 2001; Vol. *1*, Chapter 1, p 1; (l) Verdaguer, M. *Polyhedron* **2004**, *20*, 1115. (m) Souletie, J.; Rabu, P.; Drillon, M. In *Magnetism: Molecules to Materials*; Miller, J. S., Drillon, M., Eds.; Wiley-VCH: Weinheim, 2005; Vol. *5*, Chapter 10, p 347.

(2) (a) Gütlich, P.; Hauser, A.; Spiering, H. *Angew. Chem., Int. Ed. Engl.* **1994**, *33*, 2024. (b) *Spin Crossover in Transition Metal Compounds (Vol. I–III). In Topics in Current Chemistry*; P. Gütlich, Goodwin, H.A., Eds.; Springer: New York, 2004; Vol. *233, 234, 235*; (c) Gaspar, A. B.; Seredyuk, M.; Villain, F.; et al. *Eur. J. Inorg. Chem.* **2007**, 4181–4191.

(3) (a) Dingh, H.-Q. *J. Phys. Condens. Matter* **1990**, *2*, 7979. (b) Barnes, T. *Int. J. Mod. Phys.* **1991**, *2*, 659. (c) Ueda, K.; Moriya, T.; Takahashi, Y. *J. Phys. Chem. Solids* **1992**, *53*, 1515. (d) Allega, A. M.; Matsumoto, H.; Odashima, S. *J. Phys. Condens. Matter* **1996**, *8*, 4411. (e) Yanase, Y.; Jujo, T.; Nomura, T.; Ikeda, H.; Hotta, T.; Yamada, K. *Phys. Rep.* **2003**, *387*, 1.

(4) (a) Nagaev, E. L. *Phys. Rep.* **2001**, 387. (b) *Colossal Magneto-resistive Oxydes*; Tokura, Y., Ed.; Gordon and Breach: Amsterdam, 2000; (c) Kimura, T.; Tokura, Y. *Lectures Notes in Physics* **2002**, *259*, 361.

(5) (a) *Stable Radicals: Fundamentals and Applied Aspects of Odd-Electron Compounds*; Hicks, R., Ed.; Wiley-Blackwell: New York, 2010; (b) Bally, T.; Borden, W. T. In *Reviews in Computational Chemistry*; Lipkowitz, K. B.; Boyd, D. B., Eds.; Wiley: New York, 1999; Vol. *13*, p 1; (c) *Carbon Based Magnetism: An Overview of the Magnetism of Metal Free Carbon-Based Compounds and Materials*; Makarova, T.L., Palacio, F., Eds.; Elsevier: Amsterdam, 2006; (d) Train, C.; Norel, L.; Baumgarten, M. *Coord. Chem. Rev.* **2009**, *253*, 2342. (e) Lineberger, W. C.; Borden, W. T. *Phys. Chem. Chem. Phys.* **2011**, *12*, 11792.

(6) (a) *Landolt-Börnstein, 'Magnetic Properties of Free Radicals', Group II 'Molecules and Radicals'*; Springer-Verlag: Heidelberg-Berlin, 2005; Vol. *26*, Supplement D: Nitroxide Radicals and Nitroxide Based High-Spin Systems.

(7) Rota, J.-B.; Le Guennic, B.; Robert, V. *Inorg. Chem.* **2010**, *49*, 1230.

(8) (a) Lahti, P. M.; Ichimura, A. S. *J. Org. Chem.* **1991**, *56*, 3030. (b) Wenthold, P. G.; Kim, J. B.; Lineberger, W. C. *J. Am. Chem. Soc.* **1997**, *119*, 1354. (c) Wang, T.; Krylov, A. I. *J. Chem. Phys.* **2005**, *123*, 104304. (d) Ma, H.; Liu, C.; Zhang, C.; Jiang, Y. *J. Phys. Chem. A* **2007**, *111*, 9471. (e) Hatanaka, M.; Shiba, R. *Bull. Chem. Soc. Jpn.* **2007**, *81*, 460. (c) Hatanaka, N. *Chem. Phys. Lett.* **2010**, *488*, 187.

(9) (a) Rajca, A. *Chem. Rev.* **1994**, *94*, 871. (b) Rajca, A.; Wongsriratanakul, J.; Rajca, S. *J. Am. Chem. Soc.* **1997**, *119*, 11674. (c) Rajca, A.; Rajca, S.; Wongsriratanakul, J. *J. Am. Chem. Soc.* **1999**, *121*, 6308. (d) Rajca, A.; Wongsriratanakul, J.; Rajca, S. *Science* **2001**, *294*, 1503. (e) Rajca, A.; Wongsriratanakul, J.; Rajca, S.; Cerny, R. L. *Chem.—Eur. J.* **2004**, *10*, 3144. (f) Rajca, A.; Wongsriratanakul, J.; Rajca, S. *J. Am. Chem. Soc.* **2004**, *126*, 6608. (g) Rajca, S.; Rajca, A.; Wongsriratanakul, J.; Butler, P.; Choi, S.-M. *J. Am. Chem. Soc.* **2004**, *126*, 6972.

(10) (a) *The Physics of Organic Superconductors and Conductors*, Series in Materials Science; Lebed, A.G. Ed.; Springer: New York, 2008; Vol. *110*; (b) Jérôme, D.; Mazaud, A.; Ribault, M.; Bechgaard, K. *J. Phys. Lett.* **1980**, *41* (4), L95–98. (c) Bechgaard, K.; Carneiro, K.; Olsen, M.; Rasmussen, F.; Jacobsen, C. S. *Phys. Rev. Lett.* **1981**, *46*, 852. (d) Little, W. A. *Phys. Rev.* **1964**, *134*, A1416.

(11) Trinquier, G.; Suaud, N.; Malrieu, J.-P. *Chem.—Eur. J.* **2010**, *16*, 8762.

(12) Trinquier, G.; Suaud, N.; Guihéry, N.; Malrieu, J.-P. *Chem. Phys. Chem.* **2011**, *12*, 3020.

(13) (a) Zener, C. *Phys. Rev.* **1951**, *81*, 440. (b) Zener, C. *Phys. Rev.* **1951**, *82*, 403.

(14) (a) Wolf, S. A.; Awschalom, D. D.; Buhrman, R. A.; Daughton, J. M.; von Molnár, S.; Roukes, M. L.; Chtchelkanova, A. Y.; Treger, D. M. *Science* **2001**, *294*, 1488. (b) Žutic, I.; Fabian, J.; Das Sarma, S. *Rev. Mod. Phys.* **2004**, *76*, 323. (c) Johnson, M. *J. Phys. Chem. B* **2005**, *109*, 14278. (d) Rocha, A. C.; García-Suárez, V. M.; Bailey, S. W.; Lambert, C. J.; Ferrer, J.; Sanvito, S. *Nat. Mater.* **2005**, *4*, 335. (e) Bogani, L.; Wernsdorfer, W. *Nat. Mater.* **2008**, *7*, 179. (f) Kim, W. Y.; Kim, K. S. *Acc. Chem. Res.* **2010**, *43*, 111. (g) Soncini, A.; Mallah, T.; Chibotaru, L. *J. Am. Chem. Soc.* **2010**, *132*, 8106. (h) Soriano, D.; Muñoz-Rojas, F.; Fernández-Rossier, J.; Palacio, J. J. *Phys. Rev. B* **2010**, *81*, 165409. (i) Sanvito, S. *Chem. Soc. Rev.* **2011**, *40*, 3336. (j) Clemente-Juan, J.-M.; Coronado, E.; Gaita-Ariño, A. *Chem. Soc. Rev.* **2012**, *41*, 7464. (k) Mas-Torrent, M.; Crivillers, N.; Rovira, C.; Veciana, J. *Chem. Rev.* **2012**, *112*, 2506. (l) Pesin, D.; MacDonald, A. H. *Nat. Mater.* **2012**, *11*, 409.

(15) Lemaire, M. T. *Pure Appl. Chem.* **2011**, *83*, 141.

(16) Shultz, D. A.; Kumar, R. K.; K., R. *J. Am. Chem. Soc.* **2001**, *123*, 6431.

(17) (a) Guihéry, N.; Malrieu, J. P. *J. Chem. Phys.* **2003**, *119*, 8956. (b) Taratiel, D.; Guihéry, N. *J. Chem. Phys.* **2004**, *121*, 7127. (c) Carissan, Y.; Heully, J. L.; Guihéry, N.; Alary, F. *J. Chem. Phys.* **2004**, *121*, 9453. (d) Guihéry, N. *Theor. Chem. Acc.* **2006**, *116*, 576. (d) Bastardis, R.; Guihéry, N.; Suaud, N.; de Graaf, C. *J. Chem. Phys.* **2006**, *125*, 194708. (e) Bastardis, R.; Guihéry, N.; de Graaf, C. *Phys. Rev. B* **2008**, *39*, 054426.

(18) Boilleau, C.; Suaud, N.; Bastardis, R.; et al. *Theor. Chem. Acc.* **2010**, *126*, 231–241.

(19) Ovchinnikov, A. A. *Theor. Chim. Acta* **1978**, *47*, 297.

(20) Frisch, M. J. et al. *Gaussian 03*, Revision B.05; Gaussian, Inc.: Wallingford, CT, 2004; geometry optimizations are carried on up to energy gradients of 10 to 10 according to the cases.

(21) Malrieu, J.-P.; Trinquier, G. *J. Phys. Chem. A* **2012**, *116*, 8226−8237.
(22) (a) Girerd, J.-J. *J. Chem. Phys.* **1983**, *79*, 1766. (b) Papaefthymiou, V.; Girerd, J.-J.; Moura, I.; J.J.G. Moura, I.; Münck, E. *J. Am. Chem. Soc.* **1987**, *109*, 4703. (c) Girerd, J.-J.; Papaefthymiou, V.; Surerus, K. K.; Münck, E. *Pure Appl. Chem.* **1989**, *61*, 805.
(23) Anderson, P. W.; Hasegawa, H., H. *Phys. Rev.* **1955**, *100*, 675.

THE JOURNAL OF CHEMICAL PHYSICS **140**, 204113 (2014)

When a single hole aligns several spins: Double exchange in organic systems

Georges Trinquier, Vijay Gopal Chilkuri, and Jean-Paul Malrieu
Laboratoire de Chimie et Physique Quantiques, CNRS, UMR 5626, IRSAMC, Université Paul-Sabatier, 118 Rte de Narbonne, 31062 Toulouse Cedex, France

(Received 11 February 2014; accepted 1 May 2014; published online 29 May 2014)

The double exchange is a well-known and technically important phenomenon in solid state physics. Ionizing a system composed of two antiferromagnetically coupled high-spin units, the ground state of which is a singlet state, may actually produce a high-spin ground state. This work illustrates the possible occurrence of such a phenomenon in organic chemistry. The here-considered high-spin units are triangulenes, the ground state of which is a triplet. Bridging two of them through a benzene ring produces a molecular architecture of singlet ground state. A careful exploitation of a series of unrestricted density functional calculations enables one to avoid spin contamination in the treatment of the doublet states and shows that under ionization the system becomes of quartet multiplicity in its ground state. The possibility to align more than three spins from conjugated hydrocarbon polyradicals is explored, considering partially hydrogenated triangulenes. A dramatic example shows that ionization of a singlet ground state molecule may generate a decuplet. © *2014 AIP Publishing LLC*. [http://dx.doi.org/10.1063/1.4878498]

I. INTRODUCTION

The double exchange phenomenon attracted the attention of solid-state physicists from the early 1950s.[1] One may schematize it as the possibility to transform a low-spin system into a high-spin system under ionization. A system involving two magnetic units of spin larger than 1/2, with n unpaired electrons in each unit, will have a singlet ground state when the coupling between these units is antiferromagnetic. The surprising phenomenon is the spin multiplicity of the ionized state of such systems, which will be a $(2n-1)$-uplet (a quartet if $n = 2$), while in closed-shell systems ionizing a singlet state only generates a doublet state. Several rationalizations and modelizations of this phenomenon have been proposed, the first one by Zener,[2] a second one by Anderson and Hazegawa.[3] Girerd and Papaefthymiou[4] have sophisticated the Zener's model and the most refined model[5] combines the mechanisms invoked in the two basic models. Hereafter, the reconstruction of the low-energy spectrum will be quite straightforward, but refers to the refined model.

The double exchange phenomenon is very important both as a fundamental physical problem, and as a possible source of technological applications. Let us recall, for instance, that it is responsible for the so-called colossal magnetoresistivity in manganites.[6] Up to now the systems exhibiting the phenomenon essentially involve magnetic transition-metal ions, bearing several unpaired electrons in a high-spin ground state, such as Ni^{2+} (d^8), or Mn (d^7). They can be periodic metal-oxide lattices or coordination complexes, for which experiments confirm the high spin multiplicity of the ground state.[7] It may be interesting to analyze the alternative possibility through the conception of organic molecular architectures exhibiting this property. A previous paper has succeeded to show, from density functional theory (DFT) calculations, that one might conceive branched polycyclic aromatic systems which have a singlet ground state when neutral, and which have a quartet ground state after ionization.[8] This work has confirmed that in organic chemistry too a single hole may align three spins.[9,10] The suggested systems, based on Chichibabin type branched poly-aromatic chains, slightly deviate from the double-exchange canonical models since in their neutral ground state they only involve *two* unpaired electrons. From a chemist point of view, they are essentially diradicals. It is only after ionization that one may see them as involving triplet state units (in this case, trimethylenemethane, TMM). In some sense, obtaining three unpaired electrons of parallel spins by ionizing a system with two unpaired electrons is even more challenging than staying in the strict orthodoxy of double exchange, which goes from four to three unpaired electrons. The price to pay is in the complexity of the spectrum and of its modelization. In such a case, there is competition and mixing between states with three unpaired electrons and states with one unpaired electron only, while the low-energy states of the typical double exchange systems only involve states with three unpaired electrons.[8]

In this context, we found it useful to look for molecular organic systems which would remain closer to the orthodox double-exchange situation, starting from magnetic units which are doubtlessly of high-spin multiplicity. We have selected fused polycyclic molecules since we have recently shown that it is possible to conceive systems with several delocalized unpaired electrons of parallel spins.[11] Connecting these high-spin units through conjugated bridges enables one to conceive, in a rational and controlled manner, ferro- or antiferromagnetic couplings.[12] In the proposed molecular architectures, the antiferromagnetic coupling, while producing a singlet ground state, does not reduce the number of unpaired electrons in each unit, and the system remains polyradicalar. For instance, coupling two magnetic units of spin one maintains four unpaired electrons, analogously to the coupling of

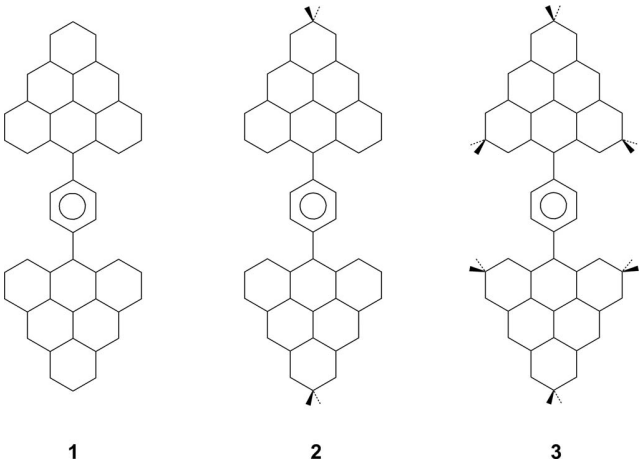

FIG. 1. The three open-shell dimer skeletons addressed in the present study. Hydrogen labels of the perpendicular methylene groups are omitted for clarity.

two Ni (d^8) ions in coordination chemistry. They might therefore be good candidates as organic counterparts of the coordination chemistry complexes exhibiting double exchange.

The units chosen hereafter are among the simplest ones, namely, triangulene molecules,[13] the ground state of which is a triplet. We first recall the properties of this molecule, its triplet-singlet gap, and introduce the qualitative picture of the unpaired singly occupied molecular orbitals (MOs) which is relevant for the understanding of the coupling between two such molecules. Provided that a spin decontamination technique is applied, the results of unrestricted density functional (UDFT) calculations, performed with a B3LYP parametrization of the exchange correlation potential and a 6-311G** basis set,[11] are in good agreement with those of the correlated wave-function based methods.[14,15] We therefore shall hereafter exploit the UDFT calculations, trying to reach the energies of spin eigenfunctions from the available set of single determinantal solutions. Introducing a simple *p*-benzene symmetrical bridge between two triangulenes as in compound **1** (Figure 1) is enough to produce a strong antiferromagnetic coupling between the two $S = 1$ units, and the physical content of the ensuing singlet ground state is analyzed.

Going then to the ionized molecule, we show that the ground state is a quartet state, indeed. The energy spacings between the quartets are rationalized. While some of the lowest doublet states have three unpaired electrons, as in the canonical double exchange systems, the lowest doublet state has only one unpaired electron. In three-openshell systems, as the $m_s = 1/2$ broken-symmetry UDFT (BS-UDFT) solutions are not eigenfunctions of the S^2 spin operator, a direct mapping onto doublet states is in principle forbidden.[16] However, exploiting the multiplicity of the BS-UDFT solutions makes it possible to reach the energies of pure doublet states. Several works have exploited these BS solutions to return to a valence-bond picture of the wavefunction, or to build an extended Hubbard Hamiltonian, with diagonalization of this model Hamiltonian as a final step.[8,17] In the present paper, an alternative formalism is proposed to treat the interaction between the 3-unpaired electron and the 1-unpaired electron configurations, which happen to be in competition for the low spin-multiplicity states.

Section IV explores dimers of higher spin multiplicity, obtained from partially saturated triangulenes. Two types of units with ground states $S = 3/2$ and $S = 5/2$ have been considered, with the same bridge as before, leading to compounds **2** and **3**, respectively. They both have a singlet ground state, with non-negligible excitation energy to the lowest triplet state. Ionizing these compounds produces sextet and decuplet ground states, respectively. These examples show that a single hole may align up to nine spins in properly chosen organic architectures.

II. RECALL: TRIANGULENES AND THEIR COUPLING

The triangulene molecule has been studied previously by both wave-function based and UDFT methods.[13] The ground state is a triplet, the geometry of which is easily optimized with UDFT. The vertical excitation energy to the singlet state has been accurately estimated to be 0.59 eV in DFT, 0.76 eV from a difference-dedicated configuration interaction calculation (DDCI). The two unpaired electrons are delocalized on the π skeleton. As in all alternant hydrocarbons (free from odd-membered rings), one may attach one of two colors to each of the carbon atoms in such a manner that two adjacent atoms do not have the same color. In triangulene, 12 atoms have one color, ten the other one, and according to the Ovchinnikov's rule[18] the ground state is a triplet, the unpaired electrons occupying two non-bonding MOs. It is well known that in the Hückel model the singly occupied molecular orbitals (SOMOs) present amplitudes on the carbons of "major color," and zeros on the "minor color" atoms. The wavefunction is invariant under rotations of the two non-bonding MOs, but since the bridge considered hereafter will keep an axial symmetry passing through an apex and through the central atom of the opposite side, it is important to define these two MOs according to this symmetry.

Figure 2 gives the amplitudes of the SOMOs in the Hückel model, which may be obtained directly as rational numbers, on the back of an envelope, applying the eigenequation $(h - E)\varphi = 0$ for $E = 0$. UDFT spin densities, which roughly follow the sum of the square of the coefficients of these two SOMOs, are also reported in this figure. The largest spin density is on the central side atoms (0.24 in Hückel, 0.39 in UDFT, 0.27 in DDCI) followed by the other side atoms (0.20 in Hückel, 0.34 in UDFT, 0.23 in DDCI). Of course, the UDFT or extended CI calculations introduce some spin polarization of both π and σ systems, and thus negative spin densities on the atoms of minor color. As a crucial feature, one will notice that the symmetrical SOMO, which we shall label *a*, presents an important amplitude on the atom to which the bridge will be attached, while the antisymmetric SOMO, hereafter labeled *b*, has a zero amplitude on this atom. The *a* orbital has zero amplitudes on the upper part of the triangulene, while the *b* orbital has larger amplitudes in this region (Figure 2).

We now suggest connecting the two triangulenes from one of their central side-atom through a benzene ring in *para* position. To avoid steric hindrance between hydrogen

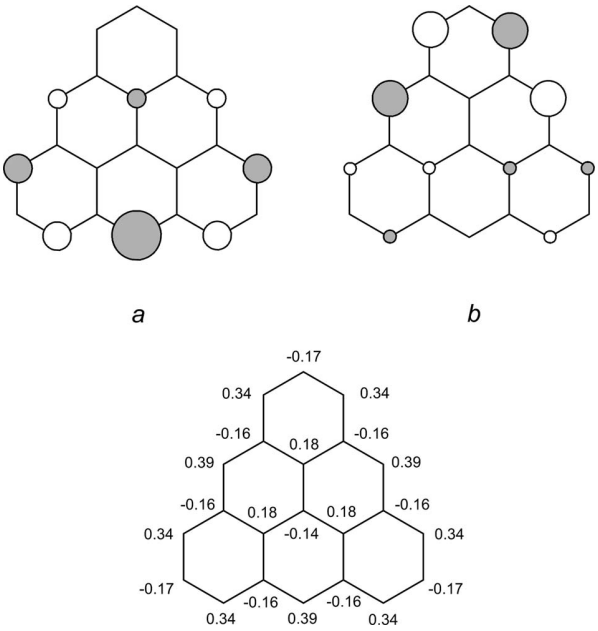

FIG. 2. The two SOMOs of triangulene, as obtained from HMO treatment, and UDFT-calculated spin densities in the triplet ground-state.

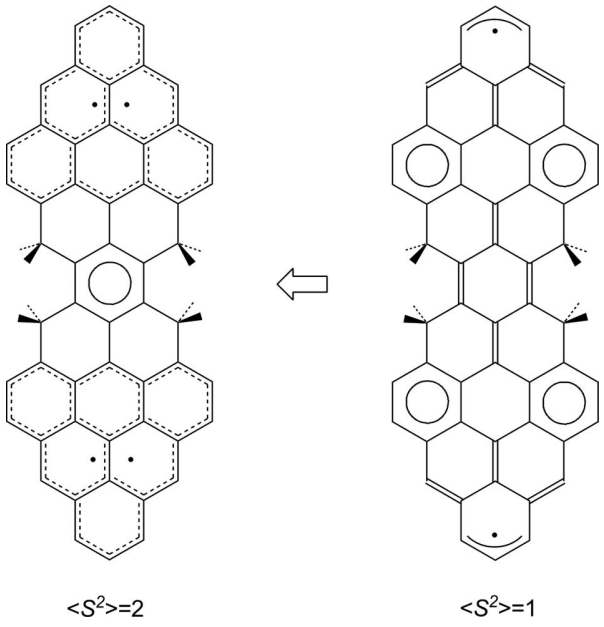

FIG. 4. Alternative configurations for the broken-symmetry $m_s = 0$ solution of compound **1**.

atoms and to maintain the planarity of the molecule, we have added four CH_2 groups, forming 6-membered rings (Figure 3). These saturated carbon atoms should not participate significantly to the communication of the π electrons of the magnetic units and of the bridge. From now on, the labels **1**, **2**, and **3** will refer to these "stapled" versions of our dimers. Dimer **1** has been studied previously.[12] The lowest optimized UDFT solution is obtained for $m_s = 0$, same number of α and β spin electrons, which indicates a singlet ground state, but the mean value of the S^2 operator ($\langle S^2 \rangle = 1.89$) clearly suggests that the ground state is of open-shell character, with the number of unpaired electrons close to 4. Each triangulene bears 1.73 spin densities. The closed-shell restricted DFT solution is much higher in energy. It is worth noticing that a quinonization of the bridge may in principle suppress two unpaired electrons, which would result in a diradicalar moiety (Figure 4). In broken-symmetry approaches, this would correspond to a $\langle S^2 \rangle = 1$ value, which is much below the calculated one. The optimized bond lengths in the bridge remain close to the ideal aromatic structure of the benzene ring (1.44 Å for C–Ar, and 1.42 Å and 1.39 Å for C–C intra-aromatic).[19] One may definitely say that the system can be seen as maintaining two unpaired electrons per triangulene.

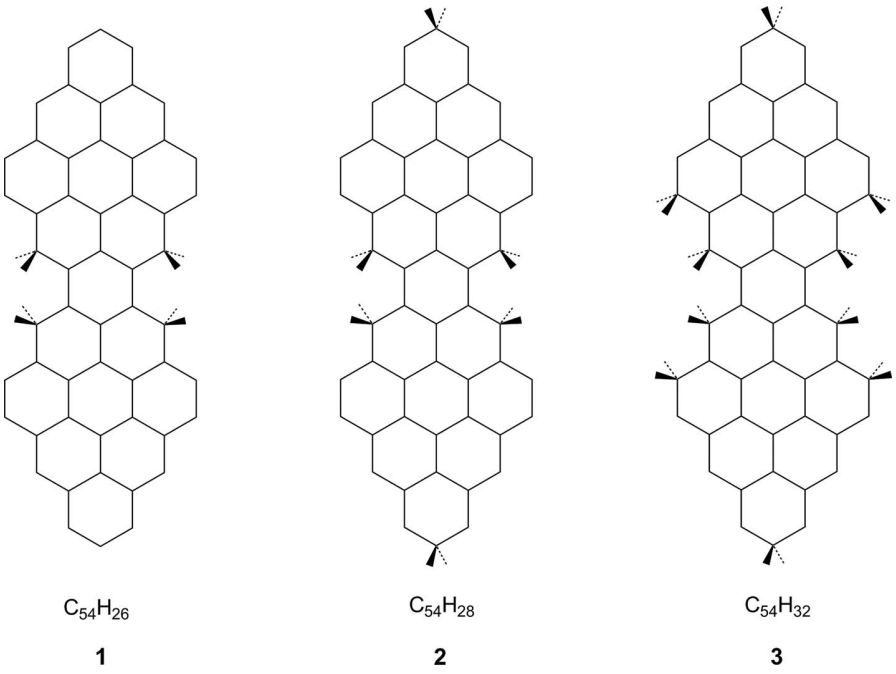

FIG. 3. The three open-shell hydrocarbons actually studied in the present study. Hydrogen labels of the perpendicular methylene groups are omitted for clarity.

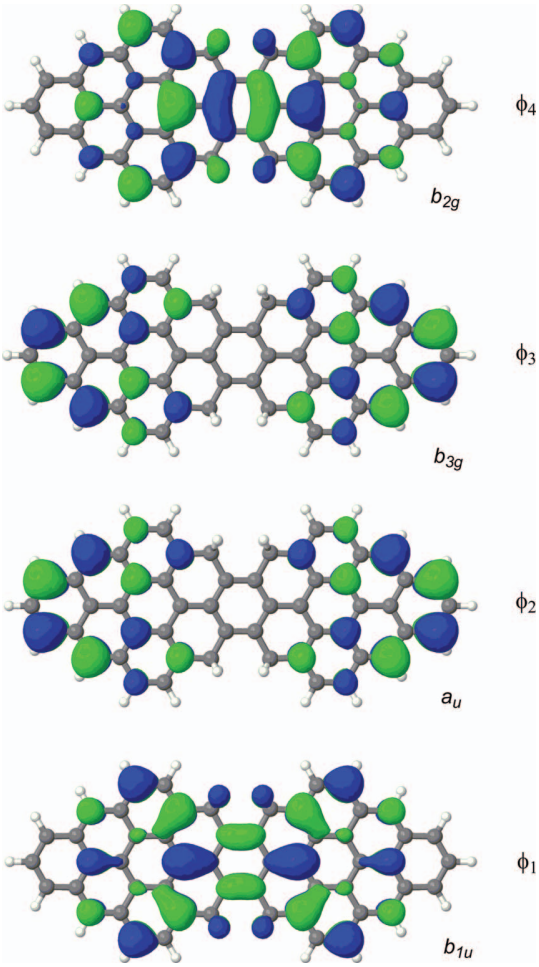

FIG. 5. The four singly occupied orbitals of neutral dimer **1** in its quintet ground state.

We have also calculated the $m_s = 1$ and the $m_s = 2$ UDFT solutions. The last one is a quintet state, lying 3.9 kcal/mol above the $m_s = 0$ solution. A spin decontamination of the singlet state using simple factor 3/2 suggests an adiabatic excitation energy of $\Delta E_{SQ} = 5.9$ kcal/mol to the quintet, and thus a value of $J = 1/3\Delta E_{SQ} \approx 2.0$ kcal/mol for the magnetic-coupling term. In the quintet, four open shells of different symmetries are singly occupied. Assigning labels 1 and 2 to the upper and lower triangulenes, respectively, the lowest energy MO, of symmetry b_{1u}, results from an in-phase combination of the two a-type MOs,

$$\varphi_1 = (a_1 + a_2)/\sqrt{2} = b_{1u},$$

with important tails on the bridge. The corresponding out-of-phase combination

$$\varphi_4 = (a_1 - a_2)/\sqrt{2} = b_{2g},$$

appears as the highest singly occupied MO, of b_{2g} symmetry. In between, two MOs, nearly degenerate in energy, are constructed from the in-phase and out-of-phase combinations of the b-type orbitals

$$\varphi_2 = (b_1 + b_2)/\sqrt{2} = a_u,$$
$$\varphi_3 = (b_1 - b_2)/\sqrt{2} = b_{3g}.$$

Since these last two orbitals have near-zero amplitudes on the connecting carbons of the triangulenes, they have vanishingly small interaction, which explains their near-degeneracy.[20] These four orbitals are plotted in Figure 5.

III. THE IONIZED DIMER OF TRIANGULENES: A RIGOROUS EXPLOITATION OF UDFT SOLUTIONS

A. Three-openshell solutions

In a qualitative picture, one may say that before ionization the two spins of the unpaired electrons are parallel but that they have opposite orientations on units A and B (antiferromagnetic coupling between the units). After ionization, an electron (or a hole) will be delocalized between the two equivalent units

$$|\varphi_1\varphi_2\varphi_3| = |\varphi_1 b_1 b_2| = (|a_1 b_1 b_2| + |a_2 b_1 b_2|)/\sqrt{2}$$

and one sees that the delocalization of the φ_1 MO provides delocalization energy. Note that when the delocalized electron is on site A (or B), the neutral site is in its triplet ground state. One also understands that this would no longer be the case if the delocalized electron had an opposite spin

$$|\overline{\varphi_1}\varphi_2\varphi_3| = |\overline{\varphi_1} b_1 b_2| = (|\overline{a_1} b_1 b_2| + |\overline{a_2} b_1 b_2|)/\sqrt{2}.$$

One must also keep in mind that another type of doublet configuration $|\varphi_1\overline{\varphi_1}\varphi_2|$ may be rather low in energy. It ignores the preference of the units for high spin multiplicity but takes full benefit of the possible delocalization between the a-type orbitals. To simplify, the order of the low energy states is ruled by a competition between the delocalization of the electrons in the a-type orbitals and the triplet-singlet energy difference of the magnetic units.

The results of various UDFT solutions relative to the ion are reported in Table I. One may first discuss the $m_s = 3/2$ solutions. They definitely correspond to quartet states with three unpaired electrons since the corresponding $\langle S^2 \rangle$ values range between 3.85 and 3.90, slightly above the expected value (3.75) for pure quartet states of this type. The small deviation comes from the spin polarization of the closed shells. All these solutions imply single occupancies of the site-centered orbitals. The lowest solution is of $^4B_{2g}$ symmetry, the singly occupied MOs are the three lowest ones, b_{1u} b_{3g} a_u, $|\varphi_1\varphi_2\varphi_3|$. Changing the symmetry of the occupied SOMOs one obtains 3 other quartet states. Two of them, which occupy both the b_{1u} and b_{2g} MOs, and empty either the b_{3g} $|\varphi_1\varphi_2\varphi_4| = |a_1 a_2 (b_1 + b_2)/\sqrt{2}|$ or the a_u MO, $|\varphi_1\varphi_3\varphi_4| = |a_1 a_2 (b_1 - b_2)/\sqrt{2}|$, are nearly degenerate, at 13.3 and 14.0 kcal/mol above the lowest quartet. This near degeneracy reflects that of these two MOs, built from b-type orbitals of the triangulenes. Their weak splitting suggests that the hopping integral between the orbitals b_1 and b_2 is very small (0.4 kcal/mol). Finally, in the upper quartet, of $^4B_{1u}$ symmetry, the empty SOMO is the bonding b_{1u} MO, $|\varphi_2\varphi_3\varphi_4| = |b_1 b_2 (a_1 - a_2)/\sqrt{2}|$. It lies 17.3 kcal/mol above the lowest quartet, suggesting a large effective hopping integral (8.6 kcal/mol) between the orbitals a_1 and a_2, through their delocalization tails on the benzene ring.

TABLE I. UDFT-calculated energies differences for **1** at the D_{2h} geometry of $^4B_{2g}$ cation ground state.

Species	Spin multiplicities	States	Spinorbital occupations	$\langle S^2\rangle$ Ising	$\langle S^2\rangle_{\text{calc.}}$	ΔE (kcal/mol)
Neutral	Quintet	^5A_g	$b_{1u}\ b_{3g}\ a_u\ b_{2g}\ (\alpha)$	6.00	6.18	
Cation	Quartet	$^4B_{1u}$	$b_{3g}\ a_u\ b_{2g}\ (\alpha)$	3.75	3.87	17.3
	Quartet	$^4B_{3g}$	$b_{1u}\ a_u\ b_{2g}\ (\alpha)$	3.75	3.85	14.0
	Quartet	^4A_u	$b_{1u}\ b_{3g}\ b_{2g}\ (\alpha)$	3.75	3.85	13.3
	Quartet	$^4B_{2g}$	$b_{1u}\ b_{3g}\ a_u\ (\alpha)$	3.75	3.90	0
	Doublet	$^2B_{1u}$	$b_{1u}\ b_{2g}\ (\alpha)\ b_{2g}\ (\beta)$	0.75	0.78	44.4
	Doublet	$^2B_{1u}$	$b_{1u}\ a_u\ (\alpha)\ a_u\ (\beta)$	0.75	0.77	21.1
	Doublet	$^2B_{1u}$	$b_{1u}\ b_{3g}\ (\alpha)\ b_{3g}\ (\beta)$	0.75	0.77	19.4
	"Doublet"[a]	B_{1u}	$b_{2g}\ b_{3g}\ (\alpha)\ a_u\ (\beta)$	1.75	1.77	37.3
	"Doublet"[a]	B_{1u}	$b_{2g}\ a_u\ (\alpha)\ b_{3g}\ (\beta)$	1.75	1.77	37.1
	"Doublet"[a]	B_{1u}	$b_{3g}\ a_u\ (\alpha)\ b_{2g}\ (\beta)$	1.75	1.83	22.6
	Doublet	^2A_u	$b_{2g}\ a_u\ (\alpha)\ b_{2g}\ (\beta)$	0.75	0.78	45.4
	Doublet	^2A_u	$b_{3g}\ a_u\ (\alpha)\ b_{3g}\ (\beta)$	0.75	0.78	32.7
	Doublet	^2A_u	$b_{1u}\ a_u\ (\alpha)\ b_{1u}\ (\beta)$	0.75	0.78	11.4
	"Doublet"[a]	A_u	$b_{3g}\ b_{2g}\ (\alpha)\ b_{1u}\ (\beta)$	1.75	1.78	27.4
	"Doublet"[a]	A_u	$b_{1u}\ b_{3g}\ (\alpha)\ b_{2g}\ (\beta)$	1.75	1.78	27.3
	"Doublet"[a]	A_u	$b_{1u}\ b_{2g}\ (\alpha)\ b_{3g}\ (\beta)$	1.75	1.81	18.8
	Doublet	$^2B_{3g}$	$b_{3g}\ b_{2g}\ (\alpha)\ b_{2g}\ (\beta)$	0.75	0.78	44.8
	Doublet	$^2B_{3g}$	$b_{3g}\ a_u\ (\alpha)\ a_u\ (\beta)$	0.75	0.78	33.6
	Doublet	$^2B_{3g}$	$b_{3g}\ b_{1u}\ (\alpha)\ b_{1u}\ (\beta)$	0.75	0.79	10.5
	"Doublet"[a]	B_{3g}	$b_{1u}\ a_u\ (\alpha)\ b_{2g}\ (\beta)$	1.75	1.78	28.1
	"Doublet"[a]	B_{3g}	$a_u\ b_{2g}\ (\alpha)\ b_{1u}\ (\beta)$	1.75	1.78	27.9
	"Doublet"[a]	B_{3g}	$b_{1u}\ b_{2g}\ (\alpha)\ a_u\ (\beta)$	1.75	1.81	19.5
	Doublet	$^2B_{2g}$	$b_{2g}\ a_u\ (\alpha)\ a_u\ (\beta)$	0.75	0.77	37.9
	Doublet	$^2B_{2g}$	$b_{2g}\ b_{3g}\ (\alpha)\ b_{3g}\ (\beta)$	0.75	0.77	36.5
	Doublet	$^2B_{2g}$	$b_{1u}\ b_{2g}\ (\alpha)\ b_{1u}\ (\beta)$	0.75	0.77	28.1
	"Doublet"[a]	B_{2g}	$b_{1u}\ a_u\ (\alpha)\ b_{3g}\ (\beta)$	1.75	1.77	20.3
	"Doublet"[a]	B_{2g}	$b_{1u}\ b_{3g}\ (\alpha)\ a_u\ (\beta)$	1.75	1.77	20.2
	"Doublet"[a]	B_{2g}	$b_{3g}\ a_u\ (\alpha)\ b_{1u}\ (\beta)$	1.75	1.81	5.8

[a]These determinants are combinations of doublet and quartet states.

Regarding the doublet states, the single-determinant solutions provided by the $m_s = 1/2$ UDFT calculations have to be analyzed and carefully exploited. There are two types of solutions. One set of solutions present three singly occupied orbitals. The corresponding values of $\langle S^2\rangle$ (1.81–1.83) are close to the expected value for a 3-openshell determinant (1.75). The other set exhibits a single open shell, as visible from the $\langle S^2\rangle$ values which are close to the expected value for a pure doublet (0.75). For each space-symmetry, we have three 3-openshell solutions and three 1-openshell solutions. Notice immediately that all the $m_s = 1/2$ UDFT solutions have energies higher than the lowest quartet state, which suggests that the spectrum is ruled by the double exchange phenomenon, but this must be confirmed by a correct description of the doublet states.

Such a description requires to take into account the interactions between the six determinants of a given space symmetry and the same $m_s = 1/2$ value. The analysis will proceed by first considering the interaction taking place between the 3-openshell determinants, which have the same orbital occupancy as in the corresponding quartet, then by considering the interaction between the 1-openshell determinants, and last by establishing the interactions between the two subclasses. We shall concentrate first on the space-symmetry B_{2g} of the lowest quartet state. Notice that the lowest energy $m_s = 1/2$ determinant belongs to this symmetry, being only 5.8 kcal/mol above the lowest quartet state.

In this $|\overline{b_{1u}} b_{3g} a_u| = |\overline{\varphi_1}\varphi_2\varphi_3|$ determinant, the down spin occupies the $\varphi_1 = b_{1u}$ orbital. However, this single determinant is not a pure spin doublet, it has a component on the $m_s = 1/2$ quartet, and one must reconstruct the doublet state. To do so, one calculates the energy of the two other spin distributions of the same space configuration, the energies of which appear in Table I. Taking the energy of the corresponding quartet as zero of energy, the CI matrix relative to this space configuration is

$$\begin{array}{llll} |\overline{\varphi}_1\varphi_2\varphi_3| & K_{12}+K_{13} & & \\ |\varphi_1\overline{\varphi}_2\varphi_3| & -K_{12} & K_{12}+K_{23} & \\ |\varphi_1\varphi_2\overline{\varphi}_3| & -K_{13} & -K_{23} & K_{13}+K_{23} \end{array}.$$

Hereafter, these three determinants will be labeled Φ_1, Φ_2, and Φ_3.

From the knowledge of the energies of the single determinants, the matrix elements of this matrix are known. Notice that the energies of $\Phi_1 = |\varphi_1\overline{\varphi}_2\varphi_3|$ and $\Phi_2 = |\varphi_1\varphi_2\overline{\varphi}_3|$ are practically the same, which implies that $K_{12} = K_{13} = 2.9$ kcal/mol, and $K_{23} = 17.9$ kcal/mol, while $\Phi_3 = |\overline{\varphi_1}\varphi_2\varphi_3|$ only interacts with the combination $(|\varphi_1\bar{\varphi}_2\varphi_3| + |\varphi_1\varphi_2\bar{\varphi}_3|)/\sqrt{2}$. The

lowest doublet eigenvector is

$$\Psi_D = (2|\overline{\varphi_1}\varphi_2\varphi_3| - |\varphi_1\overline{\varphi}_2\varphi_3| - |\varphi_1\varphi_2\overline{\varphi}_3|)/\sqrt{6}$$
$$= (2\Phi_1 - \Phi_2 - \Phi_3)/\sqrt{6}.$$

When expressed in terms of site-centered orbitals, this doublet state is purely VB neutral. The other doublet state is VB ionic and lies at much higher energy. It is easy to rationalize the difference between the values of the exchange integrals, returning to the physical content of the dimer MOs in terms of singly occupied orbitals a and b of triangulenes

$$K_{12} = ((b_1 + b_2)(a_1 + a_2), (b_1 + b_2)(a_1 + a_2))/4 = K_{a_1b_1}/2.$$

The calculated value is slightly lower than the value $1/4\Delta E_{TS}$ (3.5 kcal/mol) of the isolated triangulene, the lowering coming from a slight delocalization of the a-type orbitals in the bridge. On the contrary, the K_{23} integral is large, since a similar development gives

$$K_{23} = ((b_1 + b_2)(b_1 - b_2), (b_1 + b_2)(b_1 - b_2))/4$$
$$= (J_{b_1b_1} - J_{b_1b_2})/2.$$

This is the difference between intra- and inter-dimer electron repulsions, which is of course large and positive. The main point is that the 3-openshell doublet lies 8.7 kcal/mol above the quartet state. This quartet ground state is therefore well separated from the doublet states of the same space part, as shown in the left part of Figure 6.

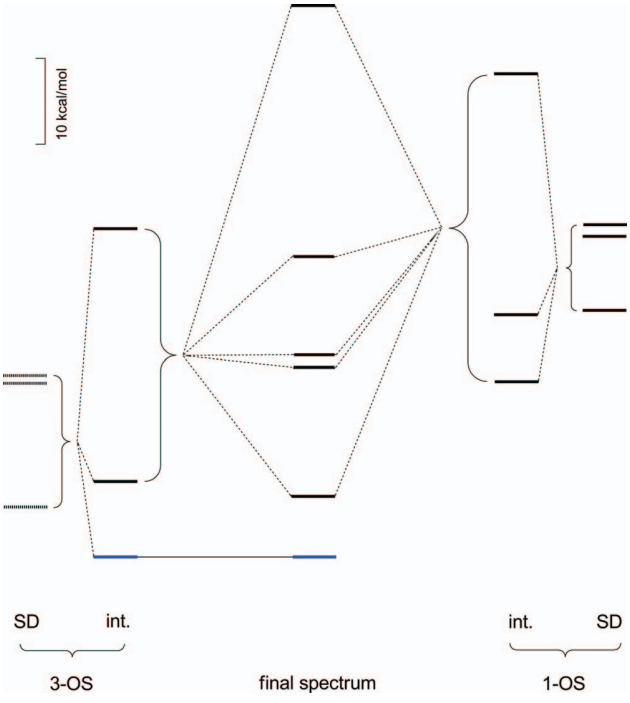

FIG. 6. Interaction scheme within B_{2g} symmetry. Horizontal lines: blue: quartet; black: doublets; dashed (left): doublet/quartet mixtures; 3-OS: three openshell determinants; 1-OS: one openshell determinants; SD: single determinants; *int.*: after their interaction.

B. One-openshell doublets

One may of course verify the position of the doublet single determinants with a single open shell. The calculated energies of these solutions are reported in Table I. The singly occupied MO is the $\varphi_4 = b_{2g}$ orbital, each of the three other orbitals being doubly occupied in one of the three determinants of this type. Double occupancy of molecular orbitals introduces double occupancies of the orbitals a or b. The CI matrix between $\Phi_4 = |\varphi_1\bar{\varphi}_1\varphi_4|$, $\Phi_5 = |\varphi_2\bar{\varphi}_2\varphi_4|$, and $\Phi_6 = |\varphi_3\bar{\varphi}_3\varphi_4|$ is

$$\begin{array}{llll} |\varphi_1\bar{\varphi}_1\varphi_4| & H_{44} & & \\ |\varphi_2\bar{\varphi}_2\varphi_4| & K_{12} & H_{55} & \\ |\varphi_3\bar{\varphi}_3\varphi_4| & K_{13} & K_{23} & H_{66} \end{array}.$$

In the first determinant, there are two electrons in a-type orbitals, which have half and half neutral and ionic VB content. The last two determinants have two electrons in b-type orbitals, and their out-of-phase combination is now purely neutral. Notice that the extradiagonal matrix elements of this matrix are the same exchange integrals which appear in the interaction between the 3-openshell determinants. The diagonal matrix elements are given in the table, and the lowest energy determinant is Φ_4 in which the three active electrons occupy a-type orbitals. As a result of these interactions, summarized in the right part of Figure 6, the lowest doublet state generated by 1-openshell determinants remains at 20 kcal/mol above the quartet.

C. Interactions between 1- and 3-openshell doublets

One must now establish the interactions between the two blocks of determinants. The two lowest determinants of this type occupy twice the low energy φ_1 MO and singly occupy either the φ_2 or φ_3 MO. They are about 11 kcal/mol above the lowest quartet, and split by a quantity 0.9 kcal/mol, close to the energy difference between the $^4B_{3g}$ and ^4A_u states. The single determinant of B_{2g} symmetry is much higher, at 28 kcal/mol above the quartet state. It is possible to calculate its interaction with the 3-openshell doublet of the same symmetry. Writing bielectronic integrals in terms of electronic distributions as

$$(\varphi_1\varphi_2, \varphi_3\varphi_4) = \langle\varphi_1(1)\varphi_3(2)|r_{12}^{-1}|\varphi_2(1)\varphi_4(2)\rangle,$$

one finds

$$\langle\Phi_1|H|\Phi_4\rangle = \langle|\overline{\varphi_1}\varphi_2\varphi_3||H||\varphi_1\overline{\varphi}_1\varphi_4|\rangle$$
$$= -(\varphi_1\varphi_2, \varphi_3\varphi_4) + (\varphi_1\varphi_3, \varphi_2\varphi_4),$$
$$\langle\Phi_1|H|\Phi_5\rangle = \langle|\overline{\varphi_1}\varphi_2\varphi_3||H||\varphi_2\overline{\varphi}_2\varphi_4|\rangle = -(\varphi_1\varphi_2, \varphi_3\varphi_4),$$
$$\langle\Phi_1|H|\Phi_6\rangle = \langle|\overline{\varphi_1}\varphi_2\varphi_3||H||\varphi_3\overline{\varphi}_3\varphi_4|\rangle = (\varphi_1\varphi_3, \varphi_2\varphi_4),$$
$$\langle\Phi_2|H|\Phi_4\rangle = \langle|\varphi_1\overline{\varphi_2}\varphi_3||H||\varphi_1\overline{\varphi}_1\varphi_4|\rangle = (\varphi_1\varphi_2, \varphi_3\varphi_4),$$
$$\langle\Phi_2|H|\Phi_5\rangle = \langle|\varphi_1\overline{\varphi_2}\varphi_3||H||\varphi_2\overline{\varphi}_2\varphi_4|\rangle$$
$$= (\varphi_1\varphi_2, \varphi_3\varphi_4) - (\varphi_1\varphi_4, \varphi_3\varphi_2),$$
$$\langle\Phi_2|H|\Phi_6\rangle = \langle|\varphi_1\overline{\varphi_2}\varphi_3||H||\varphi_3\overline{\varphi}_3\varphi_4|\rangle = -(\varphi_1\varphi_4, \varphi_3\varphi_2),$$
$$\langle\Phi_3|H|\Phi_4\rangle = \langle|\varphi_1\varphi_2\overline{\varphi_3}||H||\varphi_1\overline{\varphi}_1\varphi_4|\rangle = -(\varphi_1\varphi_3, \varphi_2\varphi_4),$$
$$\langle\Phi_3|H|\Phi_5\rangle = \langle|\varphi_1\varphi_2\overline{\varphi_3}||H||\varphi_2\overline{\varphi}_2\varphi_4|\rangle = (\varphi_1\varphi_4, \varphi_3\varphi_2),$$
$$\langle\Phi_3|H|\Phi_6\rangle = \langle|\varphi_1\varphi_2\overline{\varphi_3}||H||\varphi_3\overline{\varphi}_3\varphi_4|\rangle$$
$$= (\varphi_1\varphi_4, \varphi_3\varphi_2) - (\varphi_1\varphi_3, \varphi_4\varphi_2).$$

The corresponding bielectronic integrals are easily evaluated by expressing the MOs in terms of site-centered orbitals, and keeping only on-site electronic distributions, which gives, for instance,

$$(\varphi_1\varphi_2, \varphi_3\varphi_4) = ((a_1 + a_2)(b_1 + b_2), (b_1 - b_2)(a_1 - a_2))/4$$
$$= (K_{a_1b_1} + K_{a_2b_2})/4 = K_{a_1b_1}/2.$$

All the integrals involving products of a-type (φ_1, φ_4) orbitals by b-type (φ_2, φ_3) orbitals are identical in this approximation and reduce to

$$(\varphi_1\varphi_2, \varphi_3\varphi_4) = (\varphi_1\varphi_3, \varphi_2\varphi_4) = K_{12} = K_{13} = K_{42}$$
$$= K_{43} = K_{a_1b_1}/2 = 2.9\,\text{kcal/mol}.$$

One may also evaluate the integral

$$(\varphi_1\varphi_4, \varphi_2\varphi_3) = ((a_1 + a_2)(a_1 - a_2), (b_1 + b_2), (b_1 - b_2))/4$$
$$= (J_{a_1b_1} - J_{a_1b_2})/2.$$

Remembering that

$$(\varphi_1\varphi_4, \varphi_1\varphi_4) = K_{14} = ((a_1+a_2)(a_1-a_2), (a_1+a_2)(a_1-a_2))/4$$
$$= (J_{a_1a_1} - J_{a_1a_2})/2,$$

and that $J_{a_1a_1} = J_{a_1b_1} + 2K_{a_1b_1}$, neglecting the difference between $J_{a_1a_2}$ and $J_{a_1b_2}$, one may write

$$(\varphi_1\varphi_4, \varphi_2\varphi_3) = K_{14} - K_{a_1b_1}.$$

The value of K_{14} is easily obtained from the solutions of other symmetries, for instance, B_{3g}, as we did for K_{23}. One gets $K_{14} = 11.3$ kcal/mol, significantly less than K_{23}. This smaller value is due to the fact that the orbitals a_1 and a_2 are closer than the orbitals b_1 and b_2. Finally, $(\varphi_1\varphi_4, \varphi_2\varphi_3) = 5.1$ kcal/mol.

D. Final spectrum

Knowing all the elements of the 6 × 6 CI matrix, its diagonalization leads to the levels plotted in the middle of Figure 6, the eigenenergy of the lowest doublet of B_{2g} symmetry being

$$E(^2B_{2g}) - E(^4B_{2g}) = 6.8\,\text{kcal/mol}.$$

The corresponding eigenvector is essentially spanned by the three 3-openshell determinants, with coefficients close to $2/\sqrt{6}$, $-1/\sqrt{6}$, $-1/\sqrt{6}$. The 1-openshell determinants only act as weak perturbers, with weights below 5%. The lowest doublet dominated by a 1-openshell determinant lies 21.8 kcal/mol above the lowest quartet.

Transposing to B_{3g} symmetry the derivation performed for B_{2g} symmetry, the lowest $m_s = 1/2$ UDFT solution has now a single open shell (as evident from it $\langle S^2\rangle$ value at 0.79). It may be written $|\varphi_1\overline{\varphi}_1\varphi_2|$ and lies at 10.5 kcal/mol above the lowest quartet state. The 3-openshell determinants of the same symmetry, the space part of which is $\varphi_1\varphi_3\varphi_4$, are much higher in energy, by 9–18 kcal/mol. The lowest doublet issued from the 3-openshell configuration is 16.7 kcal/mol above the lowest quartet state. As noticed, the $|\varphi_1\overline{\varphi}_1\varphi_2|$ determinant is half and half neutral and ionic,

$$|\varphi_1\overline{\varphi}_1\varphi_2| = |(a_1\overline{a}_2 + a_2\overline{a}_1 + a_1\overline{a}_1 + a_2\overline{a}_2)\varphi_2|/2$$

but there is a strong interaction, through the integral K_{14}, (11.3 kcal/mol), between this determinant and the determinant $|\varphi_4\overline{\varphi}_4\varphi_2|$, which lies 34.2 kcal/mole (i.e., $4t$) above. This interaction, which reduces the weight of the ionic components, results in an energy lowering of 3.3 kcal/mol, so that the lowest doublet state of B_{3g} symmetry built from the 1-openshell determinants is only 7.2 kcal/mol above the lowest quartet state. One may then take into account the interaction between the 1-openshell and the 3-openshell determinants. The numerical results give

$$E(^2B_{3g}) - E(^4B_{2g}) = 4.4\,\text{kcal/mol},$$

and the eigenvector is dominated by the $|\varphi_1\overline{\varphi}_1\varphi_2|$ determinant, the coefficient of which is 0.924. The second doublet state of this symmetry is at 18.3 kcal/mol above the lowest quartet. It is a strong mixture of 1-openshell and 3-openshell determinants. Thus, the lowest doublet state of this symmetry belongs to the second family of states; it possesses 2 electrons in the a-type orbitals and 1 in the b-type orbitals, in contrast with the lowest state, which is a quartet and puts only one electron in the a-type orbitals and 2 in the b-type orbitals. This situation is similar to that observed in the diradicalar hydrocarbons studied in Ref. 8. Figure 7 summarizes the relative energies of these lowest states.

The physics of the A_u states is quite similar to that of the B_{3g} symmetry. The lowest doublet, essentially of closed-shell character, lies at 3.6 kcal/mol above the quartet ground state, and the spacing between the two lowest doublet states is approximately the same as that between the quartet states.

Going to the B_{1u} symmetry, which the highest quartet belongs to, the lowest doublet state is of 1-openshell character, with two leading determinants, $|\varphi_1\overline{\varphi}_2\varphi_2|$ and $|\varphi_1\overline{\varphi}_3\varphi_3|$ in an out-of-phase combination with nearly equal and opposite coefficients. The function can be read as well as $(|\varphi_1\overline{b_2}b_1|$ $+ |\varphi_1\overline{b_1}b_2|)/\sqrt{2}$. Its energy is the lowest one of all doublets, at 2.1 kcal/mol above the lowest quartet state. This is finally the lowest doublet state. The second doublet state is at a much higher energy, at 26.1 kcal/mol above the lowest quartet state, and it is an essentially 3-openshell state. All these relative energies are summarized in Table II and Figure 7.

E. Discussion

To summarize this section, one may say that:

- the lowest eigenstate of the ionized molecule is a quartet. Therefore, the neutral molecule, which results from antiferromagnetic coupling between triplet diradicals ($S = 1$ units), exhibits a double exchange phenomenon under ionization;
- we have proposed a model and a derivation which works with space symmetry-adapted determinants having either three open shells or one open shell, and exploited their energies;
- from the energies of these six determinants, it is possible to construct in a rational manner the CI matrix

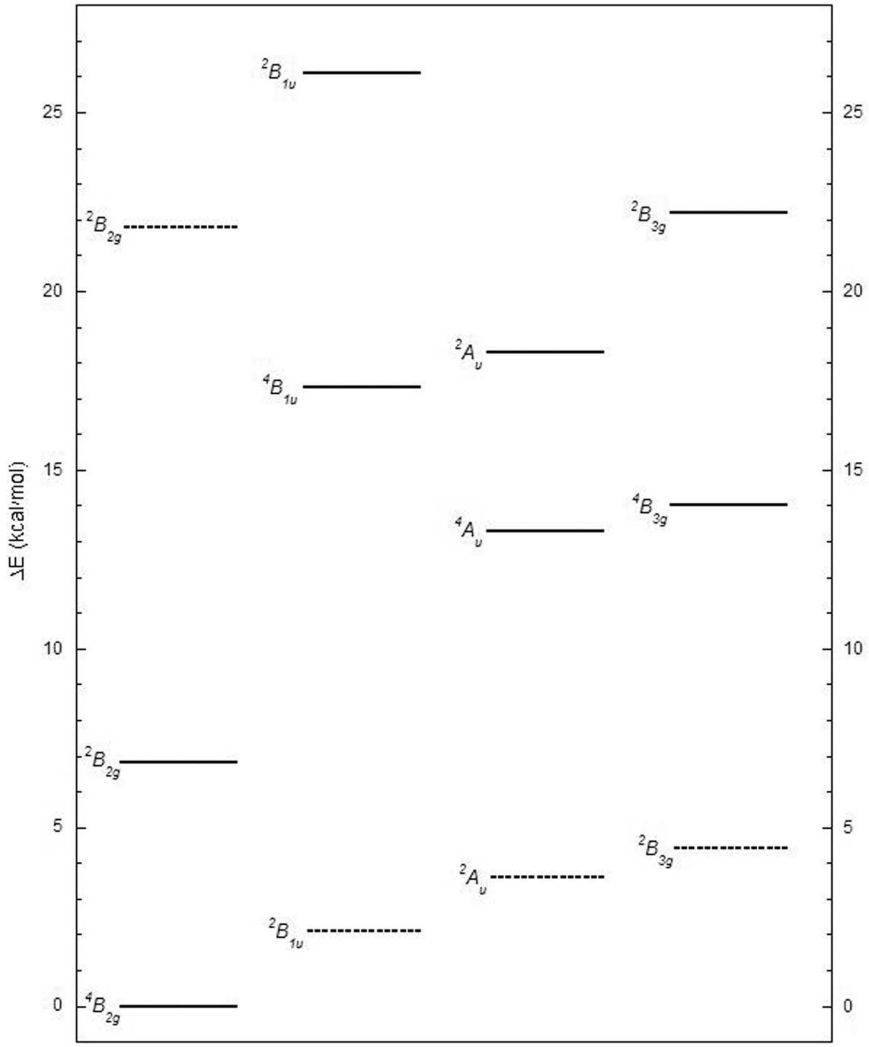

FIG. 7. Final estimates of vertical relative energies for low-lying states of cationic **1**. Dashed lines correspond to doublet states with a single open shell.

between them, and to obtain eigenvectors which mix, without prejudice, the 3-openshell and 1-openshell determinants;

- the present modelization contains the same physics as the one proposed in the previous work,[8] but it does not introduce space symmetry-broken determinants nor an intermediate Hubbard-type Hamiltonian;
- the traditional modelizations of double exchange systems work within the set of 3-openshell determinants.[2–5] It is shown here that the lowest doublet may be of 1-openshell character, as already observed in a previous work.[8] However, the 3-openshell doublet handled by the traditional model here belongs to the low-lying states;
- most of the usual modelizations of the double exchange spectrum assume that the lowest states can be considered as essentially obeying the intra-site Hund's rule, or that the model space can be built from products of on-site triplet states.[2,4,5,8] The here-obtained wavefunctions for the doublet states do not satisfy this hypothesis. As a consequence, we have not tried to produce an analytical effective Hamiltonian.

TABLE II. Final estimates of the low-lying state energies for cationic dimer **1**.

	Open shells	ΔE (kcal/mol)
$^2B_{1u}$	3	26.1
$^2B_{3g}$	3	22.2
$^2B_{2g}$	1	21.8
^2A_u	3	18.3
$^4B_{1u}$	3	17.3
$^4B_{3g}$	3	14.1
^4A_u	3	13.3
$^2B_{2g}$	3	6.8
$^2B_{3g}$	1	4.4
^2A_u	1	3.6
$^2B_{1u}$	1	2.1
$^4B_{2g}$	3	0

Finally, one may address the problem of the geometry relaxation of the doublet state, since up to now all the reported energies have been calculated at the equilibrium geometry of the lowest quartet state. The geometry of the lowest 3-openshell $m_s = 1/2$ solution, of B_{2g} symmetry, has been

optimized, first keeping D_{2h} symmetry. The energy stabilization is small (0.1 kcal/mol), but becomes more important when removing this symmetry constraint. The lowest energy solution adopts a C_{2v} symmetry, which weakly breaks the symmetry between the two triangulene groups. The energy lowering is significant, and this determinant is now 2.6 kcal/mol above the lowest quartet state $^4B_{2g}$. At this geometry, the energy of the quartet is almost unchanged (energy loss of only 0.1 kcal/mol). One should remember that the spin decontamination will increase the energy difference between the quartet and the 3-openshell doublet by a factor 3/2, and the lowest $^2B_{2g}$ doublet state should be at about 3.8 kcal/mol above the lowest quartet state. We have also looked at the lowest 1-openshell doublet determinant of $^2B_{3g}$ symmetry. The energy relaxation is 1.5 kcal/mol, diminishing the energy difference to $E(^2B_{3g}) - E(^4B_{2g}) = 2.9$ kcal/mol.

This study confirms that the lowest eigenstate remains a quartet state, even when looking at the adiabatic energy differences between the lowest quartet and doublet states. The geometry relaxation of the lowest doublet state of B_{1u} symmetry is more difficult to perform since it is an equal mixture of two determinants but its energy relaxation should remain small.

IV. IONIZING ANTIFERROMAGNETICALLY COUPLED UNITS OF SPINS HIGHER THAN 1

It may be interesting to consider systems of magnetic units bearing spins larger than 1. Staying close to the previous problem, one can replace plain triangulenes by hydrogenated triangulenes, which have higher spin ground states,[11] while keeping unchanged the *para*-benzene bridge, thus maintaining the D_{2h} symmetry. In such systems, apex CH_2 groups actually behave as steric-hindrance releaser or planarity helper, as do bridging methylene groups introduced in Sec. II.

Saturating an apex carbon atom of the triangulene generates a molecule with a quartet ground state. In the building unit of **2**, this carbon belongs to the longitudinal axis of symmetry of the dimer (Figure 3). The $m_s = 3/2$ quartet of this monomer unit, the π skeleton of which is explicated in Figure 8, middle, may be written from its three SOMOS a, a', and b, as $|aa'b|$. The a and a' SOMOs, are symmetrical with respect to the symmetry plane perpendicular to the molecular plane, while b is antisymmetrical, as in the previous triangulene case. The latter orbital has zero amplitude on the bridging carbon atom, and it is possible to obtain the same property for a', by performing a rotation among a and a'. These two symmetrical SOMOs are illustrated in Figure 9.

Moving to dimer **2**, let us assign, again, labels 1 and 2 to the upper and lower units, respectively. Since the orbitals a'_1 and a'_2 have very small amplitudes on the bridging carbon atom, they will not participate in the inter-site delocalization, and will essentially behave as b_1 and b_2. The three SOMOs will generate six MOs in the dimer, decomposing into three couples:

- The bonding b_{1u} MO built from the a set:

$$\varphi_1 = (a_1 + a_2)/\sqrt{2},$$

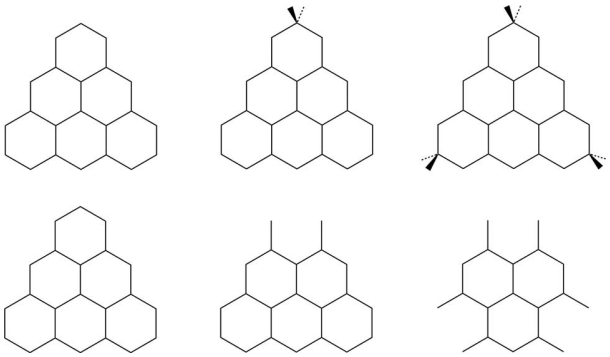

FIG. 8. Constitutive units of dimers **1**, **2**, and **3**, with corresponding π frameworks.

with its corresponding b_{2g} out-of-phase combination

$$\varphi_6 = (a_1 - a_2)/\sqrt{2}.$$

These two orbitals have significant tails on the bridge, and are well separated in energy.

- A same b_{1u}/b_{2g} duo, built from the a' set:

$$\varphi_2 = (a'_1 + a'_2)/\sqrt{2},$$
$$\varphi_5 = (a'_1 - a'_2)/\sqrt{2}.$$

These orbitals have little contribution on the bridge, and remain close in energy.

- A b_{3g}/a_u pair, built from the b set:

$$\varphi_3 = (b_1 + b_2)/\sqrt{2},$$
$$\varphi_4 = (b_1 + b_2)/\sqrt{2}.$$

Again, these orbitals are close in energy. The full set of the six SOMOs of dimer **2** is plotted in Figure 10, in the UDFT ordering of the cation ground state. Notice that the orbital ordering, as it comes up from the UDFT calculations on neutral or cationic species, is not as clear-cut as discussed above (see Table III). In particular, bonding $\varphi_1(b_{1u})$ is lying above nonbonding $\varphi_3(b_{3g})$, probably due to the significant involvement in the former of π orbitals of the top CH_2 groups, in antibonding phase, as conspicuously appearing in the bottom of Figure 10.

The high-spin state of neutral **2** is a $^7B_{3u}$ state. As in the preceding case, the optimized lowest UDFT solution is obtained for $m_s = 0$, suggesting a singlet ground state with clear open-shell character ($\langle S^2 \rangle = 2.96$), associated with a singlet-septet gap of about 8 kcal/mol, after correction by the

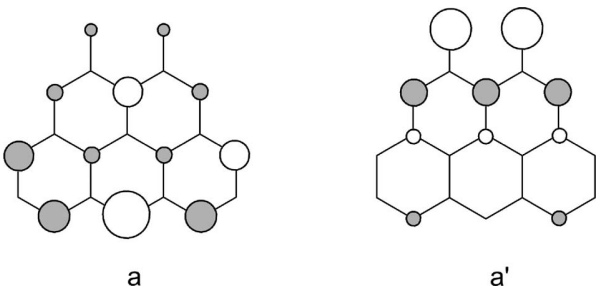

FIG. 9. The two symmetrical SOMOs of single apex-saturated triangulene.

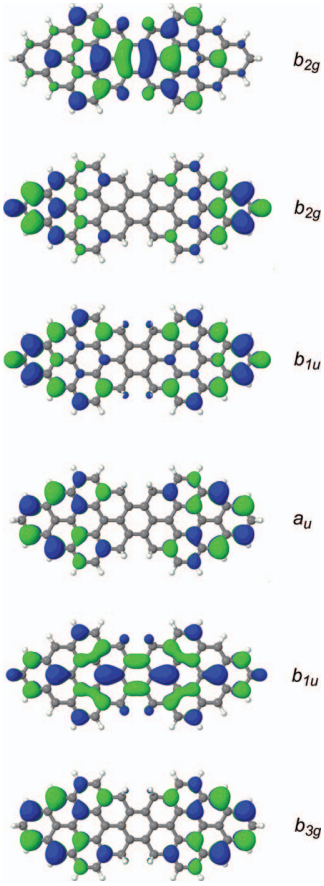

FIG. 10. Singly occupied orbitals in dimer **2**, in the ordering they arise in cationic ground state. In this sextet state, the top orbital is therefore virtual.

decontamination factor of 4/3. In cationic **2**, φ_6 has been emptied and the $m_s = 5/2$ lowest sextet state is of $^6B_{1u}$ symmetry

$$|\varphi_1\varphi_2\varphi_3\varphi_4\varphi_5| = |\varphi_1 a_1' a_2' b_1 b_2| = (|a_1 a_1' a_2' b_1 b_2| + |a_2 a_1' a_2' b_1 b_2|)/\sqrt{2},$$

while other sextet determinants are higher in energy. Their energy differences enable to evaluate the exchange integrals between the singly occupied MOs. However, it is difficult to converge on the second state of the same symmetry and we shall not proceed here to the same explicit derivation of the energies of the quartet states, which would be rather tedious. We have simply optimized the energy of a $m_s = 3/2$ determinant, without imposing any constraint in the filling of the MOs of various symmetries. In the geometry of the lowest sextet state, we have obtained a solution which exhibits five open shells ($\langle S^2\rangle = 4.81$, close to the expected value of 4.75) and may be read as

$$|\overline{\varphi_1}\varphi_2\varphi_3\varphi_4\varphi_5| = |\overline{\varphi_1} a_1' a_2' b_1 b_2| = (|a_1 a_1' a_2' b_1 b_2| + |\overline{a_2} a_1' a_2' b_1 b_2|)/\sqrt{2}$$

and which lies 7.5 kcal/mol above the lowest sextet state. Relaxing the geometry diminishes the energy of this determinant to 7.3 kcal/mol in the D_{2h} symmetry, while leaving any symmetry constraint one gets a C_{2v} geometry and a significant energy lowering. The minimum energy of this single determinantal function is now 2.8 kcal/mol above the sextet state minimum, but the spin decontamination factor of 5/4 will push the lowest 5-openshell quartet to 3.5 kcal/mol above the sextet. The 3-openshell $m_s = 3/2$ solutions, of B_{2g} symmetry, are

TABLE III. Summary of UDFT-calculated energy differences for compounds **1**–**3**.[a]

	Species	Spin multiplicities	States	Spinorbital occupations	$\langle S^2\rangle_{\text{Ising}}$	$\langle S^2\rangle_{\text{calc.}}$	ΔE (kcal/mol)
1	Neutral	Quintet	^5A_g	$b_{1u}\ b_{3g}\ a_u\ b_{2g}\ (\alpha)$	6.00	6.18	
	Cation	Quartet	$^4B_{2g}$	$b_{1u}\ b_{3g}\ a_u\ (\alpha)$	3.75	3.90	0
		Quartet ("vert." C_{2v})[b]	$^4B_1$	$b_1\ a_2\ a_2\ (\alpha)$	3.75	3.90	0.1
		"Doublet"[c] (vert.)	B_{2g}	$b_{3g}\ a_u\ (\alpha)\ b_{1u}\ (\beta)$	1.75	1.81	5.8
		"Doublet"[c]	B_{2g}	$b_{3g}\ a_u\ (\alpha)\ b_{1u}\ (\beta)$	1.75	1.81	5.7
		"Doublet"[c] (C_{2v})	B_1	$a_2\ a_2\ (\alpha)\ b_1\ (\beta)$	1.75	1.86	2.6
		Doublet (vert.)	$^2B_{3g}$	$b_{1u}\ b_{3g}\ (\alpha)\ b_{1u}\ (\beta)$	0.75	0.79	10.5
		Doublet	$^2B_{3g}$	$b_{1u}\ b_{3g}\ (\alpha)\ b_{1u}\ (\beta)$	0.75	0.79	9.0
2	Neutral	Septet	$^7B_{3u}$	$b_{3g}\ b_{1u}\ a_u\ b_{2g}\ b_{1u}\ b_{2g}\ (\alpha)$	12.00	12.25	
	Cation	Sextet	$^6B_{1u}$	$b_{3g}\ b_{1u}\ a_u\ b_{1u}\ b_{2g}\ (\alpha)$	8.75	8.96	0.
		"Quartet"[d] (vert.)	B_{1u}	$b_{3g}\ a_u\ b_{1u}\ b_{2g}\ (\alpha)\ b_{1u}\ (\beta)$	4.75	4.81	7.5
		"Quartet"[d]	B_{1u}	$b_{3g}\ a_u\ b_{1u}\ b_{2g}\ (\alpha)\ b_{1u}\ (\beta)$	4.75	4.80	7.3
		"Quartet"[d] (C_{2v})	B_1	$a_2\ a_2\ b_1\ b_1\ (\alpha)\ b_1\ (\beta)$	4.75	4.89	2.8
		Quartet (vert.)	$^4B_{2g}$	$b_{3g}\ a_u\ b_{1u}\ b_{1u}\ (\alpha)\ b_{1u}\ (\beta)$	3.75	3.88	16.8
		Quartet	$^4B_{2g}$	$b_{3g}\ a_u\ b_{1u}\ b_{1u}\ (\alpha)\ b_{1u}\ (\beta)$	3.75	3.88	14.7
3	Neutral	Undecuplet	$^{11}B_{3u}$	$a_u\ b_{3g}\ b_{1u}\ b_{2g}\ b_{1u}\ b_{1u}\ b_{3g}\ b_{2g}\ a_u\ b_{2g}\ (\alpha)$	30.00	30.33	
	Cation	Decuplet	$^{10}B_{1u}$	$b_{1u}\ a_u\ b_{3g}\ b_{3g}\ b_{2g}\ b_{1u}\ a_u\ b_{1u}\ b_{2g}\ (\alpha)$	24.75	25.09	0
		Octuplet (vert.)	$^8B_{1u}$	$a_u\ b_{3g}\ b_{1u}\ b_{2g}\ b_{3g}\ b_{1u}\ a_u\ b_{2g}\ (\alpha)\ b_{1u}\ (\beta)$	15.75	16.75	8.7
		Octuplet	$^8B_{1u}$	$a_u\ b_{3g}\ b_{1u}\ b_{2g}\ b_{3g}\ b_{1u}\ a_u\ b_{2g}\ (\alpha)\ b_{1u}\ (\beta)$	15.75	16.69	7.8

[a]All species in D_{2h} symmetry, unless otherwise specified; vert. understands as vertical from the high-spin cation geometry.
[b]Here, "vert." refers to the optimized geometry of the doublet state.
[c]These determinants are combinations of doublet and quartet states.
[d]These determinants are combinations of quartet and sextet states.

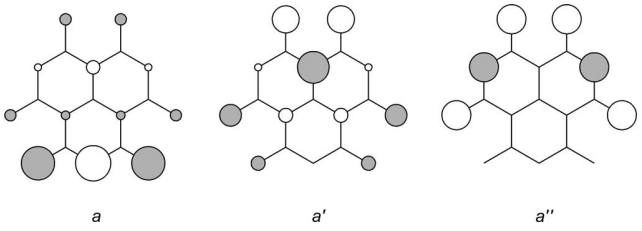

FIG. 11. The three symmetrical SOMOs of all apex-saturated triangulene.

much higher in energy (16.8 kcal/mol for vertical energy from the sextet state minimum, 14.7 kcal/mol for the adiabatic energy difference). These energies are collected in Table III, and the existence of a sextet ground state for this cation therefore seems certain.

If one now considers triply apex-saturated triangulenes, their ground state is a sextet. The excitation energy to the quartet state has been calculated to be around 0.6 eV from UDFT calculation, and around 0.5 eV from post-CAS CI calculations.[11] As documented in Ref. 11, among the five singly occupied MOs, three of them may be seen as located on *peripheral* pentadienyl entities, the two other ones having the largest amplitudes on the four *internal* atoms forming a TMM frame (see Figure 8, bottom right).

Like **1** and **2**, dimer **3** possesses a plane of symmetry perpendicular to the plane of the molecule. Among the 5-SOMO set of each hydrogenated triangulene building block, two of them are antisymmetrical with respect to this plane. As such, these orbitals have zero amplitudes on the connecting carbon atom, and cannot partake to bridge interaction. The three remaining SOMOs are symmetrical with respect to this plane of symmetry. Among them, returning again to the Hückel Hamiltonian and applying a proper rotation, it is possible to define two SOMOs having a zero amplitude on the connecting carbon (a' and a'', see Figure 11), and one having a large coefficient on this atom (a), identified as the strongly interacting one. A significant hopping integral between these latter in upper and lower triangulenes, will insure the double exchange

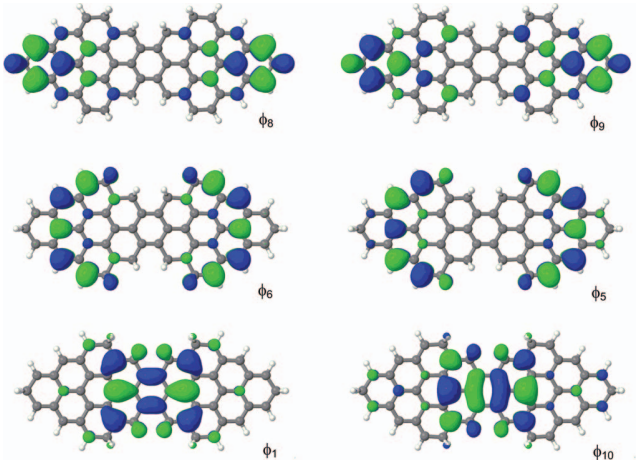

FIG. 12. Subset of six singly occupied orbitals in dimer **3**, built from the three symmetrical SOMOS of each building block. Left: b_{1u} in-phase combinations; right: b_{2g} out-of-phase combinations. Labelling reflects the ordering of the ten SOMOS in cationic **3**, where ϕ_{10} is therefore virtual.

mechanism to take place. As illustrated in Figure 12, six of the ten SOMOs of **3** can be built as b_{1u} in-phase and b_{2g} out-of-phase combinations of orbitals from this subset (a, a', a''). With labels 1 and 2 still referring to the upper and lower units, respectively, the extreme orbitals φ_1 and φ_{10} are clearly constructed from a-type orbitals,

$$\varphi_1 = (a_1 + a_2)/\sqrt{2},$$
$$\varphi_{10} = (a_1 - a_2)/\sqrt{2},$$

as are φ_8 and φ_9 from a'-type ones,

$$\varphi_8 = (a'_1 + a'_2)/\sqrt{2},$$
$$\varphi_9 = (a'_1 - a'_2)/\sqrt{2},$$

and – less conspicuously though – φ_6 and φ_5 from a''-type ones,

$$\varphi_6 = (a''_1 + a''_2)/\sqrt{2},$$
$$\varphi_5 = (a''_1 - a''_2)/\sqrt{2}.$$

TABLE IV. UDFT-calculated low-lying states energies (ΔE, kcal/mol) and ionization energies (IE, eV) for neutral systems.

	Species	States		$\langle S^2\rangle_{\text{Ising}}$	$\langle S^2\rangle_{\text{calc.}}$	ΔE (kcal/mol) [a]		IE (eV)
1	Cation	Quartet vert.	$^4B_{2g}$	3.75	3.90			5.19
	Cation	Quartet	$^4B_{2g}$	3.75	3.90			5.18
	Neutral	Quintet vert.	^5A_g	6.00	6.18	5.4	8.1	
	Neutral	Quintet	^5A_g	6.00	6.18	3.9	5.9	
	Neutral	"Singlet" BS $M_s = 0$	$^1A_1$	2.00	1.89	0	0	
2	Cation	Sextet vert.	$^6B_{1u}$	8.75	8.97			5.13
	Cation	Sextet	$^6B_{1u}$	8.75	8.96			5.12
	Neutral	Septet vert.	$^7B_{3u}$	12.00	12.25	6.0	8.0	
	Neutral	Septet	$^7B_{3u}$	12.00	12.25	5.9	7.9	
	Neutral	"Singlet" BS $M_s = 0$	$^1A_1$	3.00	2.96	0	0	
3	Cation	Decuplet vert.	$^{10}B_{1u}$	24.75	25.09			5.25
	Cation	Decuplet	$^{10}B_{1u}$	24.75	25.09			5.24
	Neutral	Undecuplet vert.	$^{11}B_{3u}$	30.00	30.34	7.1	8.6	
	Neutral	Undecuplet	$^{11}B_{3u}$	30.00	30.34	5.9	7.1	
	Neutral	"Singlet" BS $M_s = 0$	$^1A_1$	5.00	5.08	0	0	

[a]The second column applies the correcting factors of 3/2, 4/3, and 6/5 for **1**, **2**, and **3**, respectively.

The high-spin state of neutral **3** is a $^{11}B_{3u}$ state. Again, the optimized lowest UDFT solution is obtained for $m_s = 0$, suggesting a singlet ground state with clear open-shell character ($\langle S^2 \rangle = 5.08$), associated with a singlet-undecuplet gap around 8 kcal/mol, after correction by the decontamination factor of 6/5. The low-spin/high-spin energy gaps for neutral dimers **1**, **2**, and **3** are gathered in Table IV, together with their ionization energies, calculated around 5.2 eV in all cases, at this level of description. In cationic **3**, φ_{10} has been emptied and the $m_s = 9/2$ lowest decuplet state is of $^{10}B_{1u}$ symmetry. It is actually found to be the lowest state of the cation, with an energy gap to the $m_s = 7/2$ lowest energy 9-openshell determinant of 8.7 kcal/mol for the vertical energy, and 7.8 kcal/mol for the adiabatic energy (see Table III). The spin decontamination would only increase slightly these quantities. We did not find solutions with lower $\langle S^2 \rangle$ values, i.e., with 7 open shells.

V. CONCLUSION

The present work first confirms the possible occurrence of double exchange phenomena in organic systems where two high-spin multiplicity units are antiferromagnetically coupled. If each unit bears n unpaired electrons, the dimer brings $2n$ unpaired electrons but the ground state of the neutral system is a singlet state. In such systems, the ground state of the cation is not a doublet but a state of $2n$ spin multiplicity. One may say that the hole aligns the remaining $2n - 1$ unpaired electrons. The cations of compounds **1**, **2**, and **3** have, respectively, 3, 5, and 9 unpaired electrons of parallel spins.

A previous work had evidenced the existence of quartet ground state in the cation of diradicalar conjugated polycyclic hydrocarbons.[8] This result was somewhat unexpected since the units were of low spin multiplicity, while canonical double exchange is expected when the units are at least of triplet spin multiplicity, as it is the case in the present series of compounds. In Ref. 8, the lowest doublet states had only one open shell, while canonical double exchange models assume them to have the same number of unpaired electrons as the state of highest spin multiplicity.

In the present work, we have proposed a procedure exploiting the large variety of UDFT solutions obtained by changing the occupation number and spins of the magnetic orbitals. In the case of the interaction between two $S = 1$ units, we have shown that one may treat in a rigorous manner the interaction between 3-openshell and 1-openshell determinants. The off-diagonal matrix elements of the corresponding CI-type matrix can be deduced from the differences between the diagonal matrix elements. One obtains spin-decontaminated doublet functions. In the case of compound **1**, four doublets coexist, a few kcal/mol above the quartet ground state, one being dominated by a 3-openshell configuration, the other ones being essentially supported by 1-openshell symmetry-adapted determinants. The former is compatible with the usual modelization of double-exchange systems, while the latter are not, which do not respect intra-site Hund's rule. Note that were the lowest doublet state slightly below the quartet state, the molecules could become spin-crossover systems – an interesting property, quite as well.

Finally, we would like to stress on the potentialities of such polybenzenic architectures. They actually combine magnetism and conductivity, delocalized and localized electrons, the former ones insuring conductivity, the second one potentially fixing the magnetic orientation. This combination would here take place within a same molecular unit, but most promising developments in this domain imply electronic delocalization – i.e., conduction – between magnetic units, frequently involving hetero-organic radicals.[21–24] Both approaches certainly deserve attention in the context of spintronic development.

[1] G. H. Jonker and J. H. Van Staten, Physica **16**, 337 (1950).
[2] C. Zener, Phys. Rev. **81**, 440 (1951); **82**, 403 (1951).
[3] P. W. Anderson and H. H. Hazegawa, Phys. Rev. **100**, 675 (1955).
[4] J. J. Girerd, J. Chem. Phys. **79**, 1766 (1983); V. Papaefthymiou, J. J. Girerd, I. Moura, and E. Münck, J. Am. Chem. Soc. **109**, 4703 (1987); J. J. Girerd, V. Papaefthymiou, K. K. Surerus, and E. Münck, Pure Appl. Chem. **61**, 805 (1989).
[5] N. Guihéry and J. P. Malrieu, J. Chem. Phys. **119**, 8956 (2003); N. Guihéry and D. Taratiel, *ibid.* **121**, 7127 (2004); N. Guihéry, Theor. Chem. Acc. **116**, 576 (2006); R. Bastardis, N. Guihéry, N. Suaud, and C. de Graaf, J. Chem. Phys. **125**, 194708 (2006); R. Bastardis, N. Guihéry, and C. de Graaf, Phys. Rev. B **77**, 054426 (2008).
[6] R. von Helmot, J. Wecker, B. Holzapfel, L. Schultz, and K. Samwer, Phys. Rev. Lett. **71**, 2331 (1993); S. Jin, T. H. Tiefel, M. McCormack, R. A. Fastnacht, R. Ramesh, and L. H. Chen, Science **264**, 413 (1994).
[7] See, for example, for Ni ions: D. Gatteschi, C. Mealli, and L. Sacconi, J. Am. Chem. Soc. **95**, 2736 (1973); L. Sacconi, C. Mealli, and D. Gatteschi, Inorg. Chem. **13**, 1985 (1974); A. Bencini, D. Gatteschi, and L. Sacconi, *ibid.* **17**, 2670 (1978); for Fe ions: S. Drüeke, P. Chaudhuri, K. Pohl, K. Wieghardt, X.-Q. Ding, E. Bill, A. Sawaryn, A. X. Trautwein, H. Winkler, and S. J. Gurman, J. Chem. Soc., Chem. Commun. **1989**, 59; X.-Q. Ding, E. L. Bominaar, E. Bill, H. Winkler, A. X. Trautwein, S. Drüecke, P. Chaudhuri, and K. Wieghardt, J. Chem. Phys. **92**, 178 (1990); for Re ions: T. Lis and B. Jezowska-Trzebiatowska, Acta Cryst. **B32**, 867 (1976).
[8] V. G. Chilkuri, G. Trinquier, N. Ben Amor, J. P. Malrieu, and N. Guihéry, J. Comput. Theor. Chem. **9**, 4805 (2013).
[9] As previously suggested: M. T. Lemaire, Pure Appl. Chem. **83**, 141 (2011).
[10] For double exchange in oxygen-containing organic systems, see, for instance, D. A. Shultz and R. K. Kumar, J. Am. Chem. Soc. **123**, 6431 (2001).
[11] G. Trinquier, N. Suaud, and J. P. Malrieu, Chem.-Eur. J. **16**, 8762 (2010).
[12] G. Trinquier, N. Suaud, N. Guihéry, and J. P. Malrieu, Chem. Phys. Chem. **12**, 3020 (2011).
[13] On triangulene and its derivatives, see: E. Clar and G. Stewart, J. Am. Chem. Soc. **75**, 2667 (1953); **76**, 3504 (1954); M. Lofthagen, R. Vernon Clark, K. K. Baldridge, and J. S. Siegel, J. Org. Chem. **57**, 61 (1992); B. W. Laursen, C. Krebs, M. F. Nielsen, K. Bechgaard, J. B. Christensen, and N. Harrit, J. Am. Chem. Soc. **120**, 12255 (1998); J. Inoue, K. Fukui, T. Kubo, S. Nakazawa, K. Sato, D. Shiomi, Y. Morita, K. Yamamoto, T. Takui, and K. Nakasuji, *ibid.* **123**, 12702 (2001); J. E. Field and D. Venkataraman, Chem. Mater. **14**, 962 (2002); M. J. Bearpark, F. Ogliaro, T. Vreven, M. Boggio-Pasqua, M. J. Frisch, S. M. Larkin, M. Morrison, and M. A. Robb, J. Photochem. Photobiol. A **190**, 207 (2007); M. R. Philpott, F. Cimpoesu, and Y. Kawazoe, Chem. Phys. **354**, 1 (2008); A. Ueda, H. Wasa, S. Nishida, Y. Kanzaki, K. Sato, D. Shiomi, T. Takui, and Y. Morita, Chem.-Eur. J. **18**, 16272 (2012); O. A. Gapurenko, R. M. Minyaev, A. G. Starikov, and V. I. Minkin, Dokl. Chem. **448**(1), 23 (2013); see also http://www.chemexplore.net/triangulene.htm for further discussion around the triangulene family.
[14] The UDFT calculations were performed with the *Gaussian 09* quantum chemistry package, M. J. Frisch, G. W. Trucks, H. B. Schlegel *et al.*, Gaussian 09, Revision A.02, Gaussian, Inc., Wallingford, CT, 2009.
[15] Other exchange-correlation potentials do not change the here-studied properties, and the lack of dispersive interactions should not have significant impact in the present problem. The LC-BLYP version, for instance, induces minor changes in excitation energies of the neutral dimers, while introducing larger spin-polarization effects, i.e., larger deviations of $\langle S^2 \rangle$ values from those expected from Ising.
[16] V. Barone, A. Bencini, I. Ciofini, C. A. Daul, and F. Totti, J. Am. Chem. Soc. **120**, 8357 (1998); A. Bencini, F. Berti, A. Caneschi, D. Gatteschi, E. Giannasi, and I. Inverni, Chem.-Eur. J. **8**, 3660 (2002); Y. Carissan,

J.-L. Heully, F. Alary, and J.-P. Daudey, Inorg. Chem. **43**, 1411 (2004); Y. Carissan, J.-L. Heully, N. Guihéry, and F. Alary, J. Chem. Phys. **121**, 9453 (2004).
[17]C. Boileau, N. Suaud, R. Bastardis, J. P. Malrieu, and N. Guihéry, Theor. Chem. Acc. **126**, 231 (2010).
[18]A. A. Ovchinnikov, Theor. Chim. Acta **47**, 297 (1978).
[19]Full geometry optimizations were carried out up to energy gradients lower than 10^{-6} a.u. Cartesian coordinates of optimized geometries of all presently addressed species are available upon request.
[20]The actual UDFT-calculated energy ordering is $b_{3g} < a_u$, a somewhat counterintuitive result, which could originate from the partaking of methylene bridges.
[21]R. G. Hicks, Nat. Chem. **3**, 189 (2011); C. W. Johnston, S. D. J. McKinnon, B. O. Patrick, and R. G. Hicks, Dalton Trans. **42**, 16829 (2013); S. D. J. McKinnon, B. O. Patrick, A. B. P. Lever, and R. G. Hicks, Inorg. Chem. **52**, 8053 (2013).
[22]J. W. L. Wong, A. Mailman, S. M. Winter, R. M. Robertson, R. J. Holmberg, M. Murugesu, P. A. Dube, and R. T. Oakley, Chem. Commun. **50**, 785 (2014); J. W. L. Wong, A. Mailman, K. Lekin, S. M. Winter, W. Yong, J. Zhao, S. V. Garimella, J. S. Tse, R. A. Secco, S. Desgreniers, Y. Ohishi, F. Borondics, and R. T. Oakley, J. Am. Chem. Soc. **136**, 1070 (2014); S. M. Winter, A. R. Balo, R. J. Roberts, K. Lekin, A. Assoud, P. A. Dube, and R. T. Oakley, Chem. Commun. **49**, 1603 (2013); A. Mailman, S. M. Winter, X. Yu, C. M. Robertson, W. Yong, J. S. Tse, R. A. Secco, Z. Liu, P. A. Dube, J. A. K. Howard, and R. T. Oakley, J. Am. Chem. Soc. **134**, 9886 (2012).
[23]K. Awaga, K. Nomura, H. Kishida, W. Fujita, H. Yoshikawa, M. Matsushita, L. Hu, Y. Shuku, and R. Suizu, Bull. Chem. Soc. Jpn. **87**, 234 (2014); Y. Shuku, R. Suizu, A. Domingo, C. J. Calzado, V. Robert, and K. Agawa, Inorg. Chem. **52**, 9921 (2013).
[24]M. Vérot, J.-B. Rota, M. Kepenekian, B. Le Guennic, and V. Robert, Phys. Chem. Chem. Phys. **13**, 6657 (2011).

Chapter 2

Collective effects I

2.1 Introduction

Exotic properties observed in doped manganites like the colossal magneto resistance (CMR) result from the critical nature of the interactions at work in such doped transition metal oxides (TMO) and to collective effects. This leads to an important sensitivity of the macroscopic properties to the amount of doping, the temperature, the presence of a magnetic field and other external perturbations. In doped transition metal oxides like manganites and nickelates, Double Exchange (DE) and Super Exchange (SE) interactions compete giving rise to remarkable electromagnetic properties.

The previous chapter dealt with the DE model with a minimal system of two magnetic centers. In that case, since there was only a single electron occupying the two delocalized orbitals, therefore there was no exchange term J between the electrons occupying delocalized orbitals. The presence of three sites or more and at least two electrons in the delocalized orbitals, introduces the effect of the inter-site effective exchange term J. The parameters K and t favor a ferromagnetic alignment, as shown in the previous chapter, whereas J favors antiferromagnetic alignment. Thus there is a competition between the antiferromagnetic and ferromagnetic ground states. We believe that it is this competition that gives rise to the anomalous properties of doped transition metal oxides. The following two chapters consist of a study of this competition by numerically solving the Double Exchange model for systems larger than two sites.

In this first chapter on collective effects, we will study the influence of a single hole. Through this analysis, we will determine the number of spins aligned by a single hole in the parameter range of interest, i.e. the values typically observed in TMO.

Following this, we will study the influence of two and more holes on the number of spins aligned. In the next chapter, we will analyze the electron delocalization and the effect of a magnetic field.

2.2 Background and objectives

In the present section, we will review the various experimental and theoretical studies on finite and crystalline high-spin systems showing DE phenomenon. Then we will present our objectives and the position of the present work in the context of the available literature.

2.2.1 Experimental results

2.2.1.1 Applications: Finite systems

Traditionally, high-spin clusters are based on ferromagnetic or ferrimagnetic interactions. Recently, focus has been turned to the double exchange mechanism for the design of high-spin metallic clusters. A large number of studies can now be seen, that target high-spin systems based on the double exchange mechanism [5]. A very nice and clear demonstration of a high-spin molecule based on the di-vanadium ($S = \frac{5}{2}$) complex originating from the DE mechanism have been developed and studied by Belchars *et al* [6]. Large clusters based on mixed valence Iron ($Fe^{II}Fe^{III}_7$) centers that show DE phenomenon have also been synthesized quite recently (2014) that show a high-spin ground state of up to $S = \frac{39}{2}$ [8]. These advances on the synthesis of finite clusters with high-spin centers shows great potential for applications in spintronics. In fact there have already been a few studies on the application of these clusters for electronic devices. Linear clusters of mixed valance Mn centers showing controllable DE phenomenon have been successfully demonstrated [39]. Spin valves based on the DE mechanism have been proposed by Dul *et al* [7] and Soncini *et al* [11]. The theoretical study of these systems mostly use Density functional theory methods to characterize the energy gap for the low lying states. Although these methods are useful for a qualitative analysis of the clusters, a more accurate analysis is desirable. The objective of the present work is also to target finite size systems. We would like to give predictions on the values of the DE parameters J, K and t that would lead to high-spin linear chain clusters.

2.2.1.2 Applications: Bulk materials

There has been a renewed interest in the study of doped transition metal oxides [40, 41] since the discovery of colossal magneto resistance (CMR) in manganites [9]. The linear nickel oxide Y_2BaNiO_5 has been identified as being well

modeled by a 1D $S = 1$ model system in the early 1990's by Darriet *et.al.* [42, 43]. Doping Y_2BaNiO_5 with holes (Ca) would therefore correspond to a one dimensional system with two valence orbitals on each site. A possible application of the present study to bulk systems is the one dimensional doped transition metal oxide of nickel Y_2BaNiO_5 and by extension, it can also be generalized towards an understanding of 2D bulk systems such as manganese $La_{1-x}Ca_xMnO_3$ Perovskites. (YBCO). In the following few paragraphs, we present some experimental results on YBCO in order to gain perspective on the numerical analysis that follows.

The electronic configuration of binuclear nickel oxide has previously been studied by *ab initio* methods [44]. Such studies show the presence of two localized open shell d orbitals (d_{z^2} and $d_{x^2-y^2}$) on each nickel atom. As the NiO_6 system forms a distorted octahedron, the two valence electrons of the Ni atom reside on the d_{z^2} and $d_{x^2-y^2}$ orbitals. The doped system composed of mixed valence $Ni(III)/Ni(II)$ sites, made up of two orbitals each with one or two electrons, as shown in the Fig: 2.1, will give rise to double-exchange like interactions. The z axis is oriented along the axis of the chain as shown in the Fig: 2.1. Therefore, the overlap between the d_{z^2} orbitals is larger than the $d_{x^2-y^2}$ orbitals. Consequently, the holes preferentially reside on the d_{z^2} orbitals as confirmed by experiment [45]. This implies that there are primarily two kinds of electrons on each Ni center. Firstly, the electron, residing on the d_{z^2} orbital and delocalized along the neighbouring atoms, is responsible for the transport properties. Secondly, the electron occupying the $d_{x^2-y^2}$ is strongly localized and weakly couples with the other site ($J_2 \approx 0$).

Although 1D nickelates do not show CMR effects, an important change in resistivity with magnetic field has been observed [46]. The experimental studies in 1D nickelates and 2D manganites aim to understand the origin of these anomalous dependence of the transport on the magnetic field. Experimental studies can be classified by means of the methods used to probe the various properties. Optical spectroscopy measurements by Tsutsui *et al* [47] show that the transport in one and two dimensions are not the same due to the presence of the Zener polaron [48, 49] in 2D manganites which introduces lattice distortions. Ito and Yamaguchi [45] have also performed optical spectroscopy measurements, concluding that on doping, there is a general tendency of forming a ferromagnetic polaron surrounding the holes which increases with the application of magnetic field. Another work using optical spectroscopy by Fagot-Revurat *et al* shows a significant decrease in the $Ni-O$ distance resulting in the increasing p character for the delocalized orbitals. Their study shows the importance of the electron-phonon effects in such systems. The X-Ray absorption spectroscopy studies on YBCO [50] essentially verify the one dimensionality of the YBCO system. The transport and magnetic suscepti-

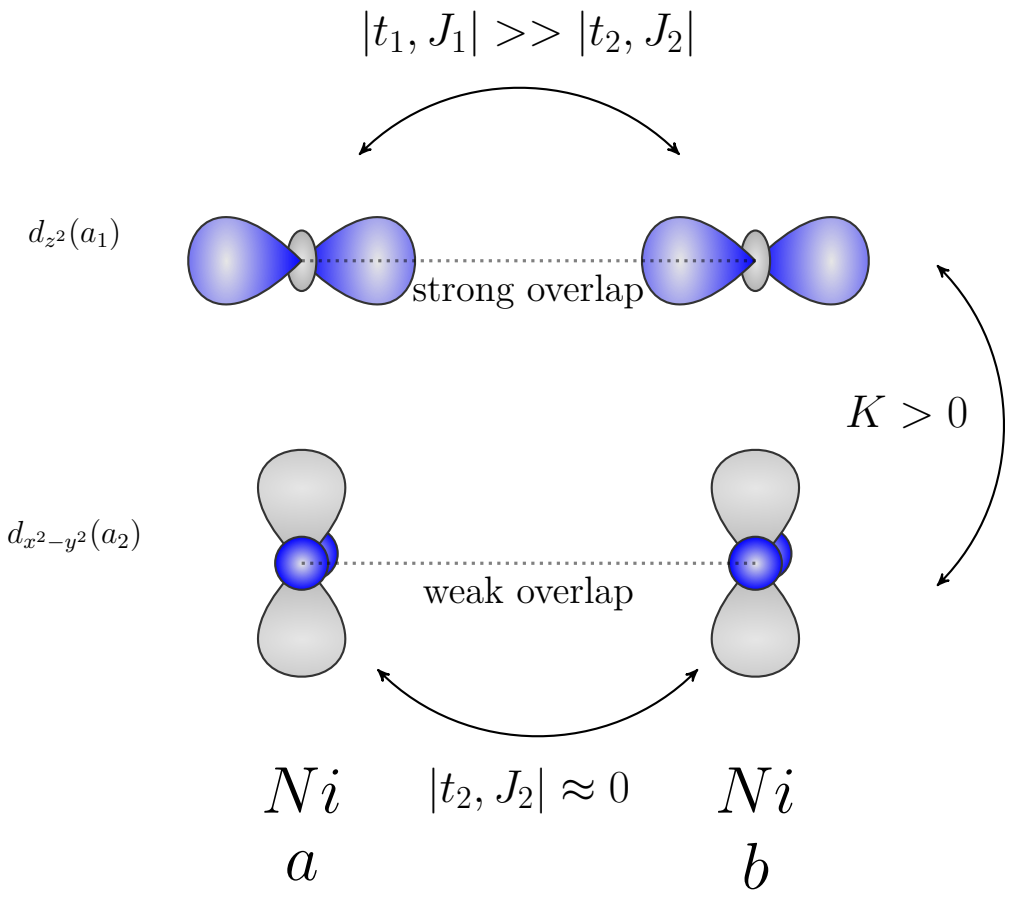

Figure 2.1: A schematic representation of two sites showing the two orbitals on each Ni site in YBCO and their orientation along the axis of the chain taken as the z axis.

bility measurements on YBCO have been carried out by many groups [51, 52, 53]. An important experimental study of transport in 1D YBCO by Ito *et al* [45] shows the variation of resistivity as a function of doping ratio. They conclude that for the 1D nickelates, the introduction of holes introduces only local distortions resulting in a ferromagnetic region surrounding the hole. Neutron scattering measurements show the presence of spin and charge stripes [54, 55] only for 2D nickelates. The 2D nickelates show stripe ordering and spin incommensurability in the doping range $0.289 \leq x \leq 0.5$, this is reminiscent of a similar stripe order observed in manganites. Other studies on 2D nickelates by Mizokawa *et al* [56] report the charge density waves (CDW) and spin density waves (SDW) and the extent of the domain walls containing the stripes. They also postulate an effective coupling between the

different domains separating the CDW and SDW regions. Moreover, work by Xu *et.al.* [57] has shown the existence of spin incommensurabilities which arise when the parent compound Y_2BaNiO_5 is doped with Ca holes confirming the presence of local spin distortions. In conclusion, we find that the experimental results show the following important points:

- Presence of local distortions (polarons) for 1D nickelates on doping with holes.
- The size of the polarons increases with an increase in the strength of the magnetic field.
- The doping ration for which we see an important modulation in conductivity is between 0.3 to 0.5 for nickelates.

2.2.2 Theoretical studies

This section presents in brief, the progress in the understanding of the role of collective effects of the DE Hamiltonian. There have been numerous studies on the double exchange model in the context of doped transition metal oxides with methods ranging from full diagonalization and Monte Carlo techniques [58] to more advanced methods like the density matrix renormalization group (DMRG) calculations and DMFT [59]. Since in the double exchange model even with only two orbitals per site the configuration space grows very fast, numerical studies simplify the DE model in order to treat larger systems. The studies can be grouped into two general sections (i) effective one band models and (ii) effective two band models.

The one band models [60, 59, 61, 62] are derived from the generalized Hubbard Hamiltonian containing two orbitals (d_{z^2} and $d_{x^2-y^2}$) per site including all usual parameters along with the Coulomb repulsion between the electrons (on-site U and the inter site V). Low energy spectrum of the dimer studied with this generalized Hamiltonian is used to extract the parameters of an effective one band $t-J$ Hamiltonian (J_{eff} and t_{eff}) which reproduce the low energy spectrum. These effective parameters are then used to model the collective properties for large 1D chain of sites. Dagotto *et al* [3] have studied the influence of a single hole for the one and two dimensional lattices, they used the one band $t-J$ model Hamiltonian not including the local singlet S_0 states. An important work by Malvezzi *et al* [63] on collective effects of the DE model showed the presence of a ferromagnetic polaron surrounding the hole that forms small "islands" immersed in an antiferromagnetic spin liquid and that the extension of such "islands" is affected neither by U nor V repulsion. They do not perform a detailed study of the extension of

this polaron with varying J and K. A recent study by Navarro *et al* [64] on a one-band magnetic field dependent DE Hamiltonian ($K \to \infty$) presents the effect of the magnetic field on the mobility of the electrons via the magnetic susceptibility curves. They were able to show that there is a dependence of the Curie constant on the spin impurities near the Curie temperature.

The two orbital models [65, 66, 67] consider two antiferromagnetic $t-J$ chains ferromagnetically coupled by a very large Hund's rule coupling ($K \geq 10|t|$). D. J. Garcia *et al* [68] have modeled the full two band $t-J$ Hamiltonian while neglecting the double occupancies ($U \to \infty$) and taking very large values of Hund interaction $K = 20|t|$. In this work, they found the existence of an "island phase" which separates the ferromagnetic (metallic) phase (FM) from the antiferromagnetic (AF) phase, it is in this phase that the competition between DE and super exchange (SE) is at its peak. A study including the double occupancies and a two band model was done by Malvezzi *et al* [69], they used DMRG to study the effect of hole doping on the phase diagram of the Hubbard model. They reported also that a sufficiently large hole doping will always lead to a ferromagnetic region surrounding the holes due to the DE mechanism. Costamagna *et al* have studied the $J \to 0$ limit with one [70] and two impurities [71]. While they used a two band model, their model is what is called the Ferromagnetic Kondo Lattice Model (FKLM) in which the impurity is essentially fixed at the center of the chain. They present a study of the spin-spin correlation of close to the hole and between two holes. Their study is important in the sense that it gives a first idea of the extension of the correlation due to a single hole and between two holes. There also has been an analytical study of the single hole doped DE Hamiltonian, using the series expansion method to the ninth order, which was carried out by Koga *et al* [72].

Summarizing the conclusions from all the above studies. The first case is when $J = 0$, i.e. no antiferromagnetic coupling, and $K > 0$ the system is ferromagnetic for a 1D open-chain with more than one hole, this exact result has been demonstrated by Kubo [73]. Riera *et al* effectively verify Kubo's analysis showing that the result is valid also for periodic boundary conditions for an odd number of holes. For the one hole case, Nagoka [74] and Tasaki [75] have shown that a ferromagnetic phase would not be observed for a single hole case in a 1D open chain system at the vanishing J limit. Switching on J one starts to observe ferromagnetic polarons surrounding the holes, these ferromagnetic polarons are coupled antiferromagnetically. Most of the previous studies mentioned above have taken a value of $K \approx 10|t|$ in the calculation of the various spin-spin correlations. There is no explicit detailed study of the number of spins aligned by a single hole. Nevertheless, we can conclude from the works of Costamagna *et al* that the extension of

the influence of the hole is between three to four sites and the interaction between two holes survives from 15 to 20 sites. The size of the polarons depends on the relative strength of the various parameters (K, J and t) and survive the inclusion of the electron repulsion U and V. A possible mechanism of how the magnetic field could induce a change in the transport properties is only hinted at by Batista *et al* [67] without numerical results. Riera *et al* [76] have studied an effective two band model formulated in terms of spin like operators for large values of Hund term K using exact diagonalization (ED) and DMRG. They reported the presence of a ferromagnetic region for the DE Hamiltonian for doped spin $S = 1$ chains as well as spin $S = 2$ chains, it is not clear though how one would extrapolate these results to understand the delocalization in the system. There have been no detailed studies on the transport properties of the DE Hamiltonian specifically taking into account the local exchange term K.

2.2.3 Our objectives

The present study concerns the Double Exchange in systems which have a small value of the Hund term $K < |t|$, i.e. nickelates and Organic DE systems. The objective of this work is to extend the understanding of the collective properties of the DE model taking into account the low lying local non-Hund states ($S = 0$). This would allow a more realistic understanding of the DE phenomenon in Organic as well as TMO systems where K plays an important role in the low energy physics. In summary, the aim of the present work is to tackle two problems:

- The problem of finite size high-spin systems, with the scope of application in spintronics. Our methods can also be used to aid in the design of single molecule magnets or open chain organometallic complexes composed of several magnetic centers.

- The problem of the electromagnetic properties of doped transition metal oxides, i.e. nickelates and manganites. The results of the present work may be generalized to very large 1D and 2D systems.

We also aim to develop tools of analysis which help in a theoretical analysis of finite high-spin systems. In the context of TMO systems, we have aimed to develop analytical methods that would facilitate the extrapolation to very large systems. Therefore, as the title of this manuscript, we aim an understanding of microscopic and macroscopic properties resulting from the collective effects of the DE mechanism.

2.3 Hamiltonian: Three sites

The DE Hamiltonian for two sites has been presented in the previous chapter. In this section, we proceed with the analysis of the three site Hamiltonian. The aim of this section is a detailed study of the Hamiltonian in order to understand the effect of the various competing interactions on the low energy spectrum of a three site system with a single hole.

The form of the Hamiltonian for three and more sites is:

$$\hat{H}^{AH/GP} = \sum_{i,\sigma}^{N-1} -t_1 \mathscr{P}\left(\hat{c}^{\dagger}_{i,\sigma}\hat{c}_{i+1,\sigma} + \hat{c}^{\dagger}_{i+1,\sigma}\hat{c}_{i,\sigma}\right)\mathscr{P}^T \\ - 2K\sum_{i}^{N}\left(\hat{S}_{i,1}\hat{S}_{i,2} - \frac{1}{4}\right) + 2J\sum_{i}^{N-1}\left(\hat{S}_{i,1}\hat{S}_{i+1,1} - \frac{1}{4}\right) \quad (2.3.1)$$

where we have neglected the hopping between the localized orbitals $t_2 = 0$ and the antiferromagnetic exchange between localized orbitals has been taken to be zero ($J_2 = 0$). $t_1 = t$ and J concern the hopping and exchange term for the delocalized orbitals respectively, whereas the K represents the intra site Hund term.

The two site system did not involve the antiferromagnetic (between the strongly interacting orbitals) parameter J and thus the ground state was a quartet state. Whereas, in the case of three or more sites, there is a competition between the super-exchange effect (SE) due to J which favors an antiferromagnetic ordering and the double exchange (DE) effect due to t and K which favors ferromagnetic ordering. The low spin states are now stabilized by the presence of J, whereas the high-spin states are unaffected by J. We have projected out those determinants where the hole occupies the localized orbitals ($d_{x^2-y^2}$) since they are very high in energy.

In order to find the nature of the ground state, one needs to carry out an analytical study of the Hamiltonian involving the three parameters t, K, J. As it is difficult to do an analytic determination of the spectrum and wavefunction for matrices larger than three, instead one needs to carry out numerical diagonalizations to obtain the ground state for t, K, J values that are reasonable for the nickelates. In this section we present a study of the Hamiltonian with three sites and one hole in order to illustrate this.

We shall use the notation n_1h in order to denote a system with n sites and one hole and n_2h for two holes throughout the following chapters.

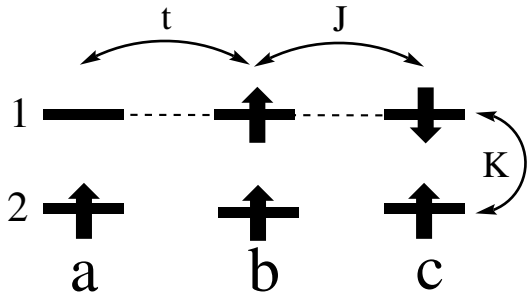

Figure 2.2: A schema showing all the interactions taken into account. The effective exchange interaction and the hopping term between the non overlapping orbitals (t_2) is neglected.

The Fig: 2.2 shows the three dominant interactions t, K and J. The 3_1h Hilbert space is made up of three sextets, twelve quartet states and fifteen doublet states. Once the basis has been spin symmetrized using the appropriate Clebsch-Gordan coefficients [77, 78] (CGC), the Hamiltonian matrix would therefore be of rank 30 and would have three blocks of sizes 3, 12 and 15. The analytic form of the Hamiltonian matrices for the various spin-sub-spaces is shown in Tables 2.1, 2.2 and 2.3. From the above Hamiltonian matrices we see clearly that the influence of the intra-site exchange term K is only on the diagonal. This is not surprising since K effects only the local triplet T_+, T_0, T_- and the local singlet states S_0 and does not contribute to interaction between sites. Although, once the full spin sub-space is diagonalized, the ground states would of course contain contributions from the local Hund T_+, T_0, T_- configurations for the Sextets and local Hund and non-Hund (S_0) configurations for quartet and doublet states due to coupling by t. The relative weights of the local singlet and triplet states would depend on K. Looking at the three matrices individually, the three sextets are coupled only by t and are not effected either by K or by J, this is because the energy of the sextets has been taken as the energy origin. In other words the energy of the local triplet states T_+, T_-, T_0 has been taken as 0 and that of the local singlet states S_0 as $2K$. The other two matrices depend on all the three parameters. The effect of the local non-Hund states is to lower the energy of the states (dominated by Hund configurations) through interactions via t and J. Since the non-Hund states are at an energy of $2K$ and $4K$ compared to the Hund, the strength of this interaction of the non-Hund state depend on the relative value of K and t. It is interesting to note that if we took an infinitely large K, i.e. ignoring the effect of the local non-Hund states, the low energy spectrum would be dominated by the sextet states for the

small J limit. This is clear once we look at the relative coupling terms for the sextet (t), quartet ($\frac{3t}{4}$) and doublets ($\frac{t}{\sqrt{2}}$) spin sub-spaces. Thus, the local non-Hund configurations indirectly play a significant role in determining the ground state for the small J regime. Finally, it is very difficult to predict the nature of the ground state analytically. Since the dominant coupling terms within the various sextets, quartets and doublets sub-spaces are t (which is of the same magnitude as K), a perturbative treatment is not possible. Thus, in order to obtain the energies of the doublet states of 3_1h system one needs to carry out numerical diagonalizations of matrices of dimensions larger than three.

$\hat{H}_{sext}$	$\|S_1\rangle$	$\|S_2\rangle$	$\|S_3\rangle$
$\langle S_1\|$	0	$-t$	0
$\langle S_2\|$	$-t$	0	$-t$
$\langle S_3\|$	0	$-t$	0

Table 2.1: The sextet spin Hamiltonian matrix for the 3_1h system.

$\hat{H}_{quart}$	$\|Q_1\rangle$	$\|Q_2\rangle$	$\|Q_3\rangle$	$\|Q_4\rangle$	$\|Q_5\rangle$	$\|Q_6\rangle$	$\|Q_7\rangle$	$\|Q_8\rangle$	$\|Q_9\rangle$	$\|Q_{10}\rangle$	$\|Q_{11}\rangle$	$\|Q_{12}\rangle$
$\langle Q_1\|$	0	$\frac{t}{4}$	0	0	$\sqrt{\frac{t^2}{3.2}}$	0	0	$\sqrt{\frac{t^2}{1.6}}$	0	0	0	0
$\langle Q_2\|$	$\frac{t}{4}$	0	$\frac{t}{4}$	$\sqrt{\frac{t^2}{3.2}}$	0	$-\sqrt{\frac{t^2}{3.2}}$	$-\sqrt{\frac{t^2}{1.6}}$	0	0	0	0	$\sqrt{\frac{t^2}{1.6}}$
$\langle Q_3\|$	0	$\frac{t}{4}$	0	0	$-\sqrt{\frac{t^2}{3.2}}$	0	0	0	0	0	$\sqrt{\frac{t^2}{1.6}}$	0
$\langle Q_4\|$	0	$\sqrt{\frac{t^2}{3.2}}$	0	$-J$	$-\frac{3t}{4}$	0	$-\frac{J}{\sqrt{2}}$	$\sqrt{\frac{t^2}{8}}$	0	$-\frac{J}{\sqrt{2}}$	0	0
$\langle Q_5\|$	$\sqrt{\frac{t^2}{3.2}}$	0	$-\sqrt{\frac{t^2}{3.2}}$	$-\frac{3t}{4}$	0	$-\frac{3t}{4}$	$-\sqrt{\frac{t^2}{8}}$	0	0	0	0	$-\sqrt{\frac{t^2}{8}}$
$\langle Q_6\|$	0	$-\sqrt{\frac{t^2}{3.2}}$	0	0	$-\frac{3t}{4}$	$-J$	0	0	$\frac{J}{\sqrt{2}}$	0	$-\sqrt{\frac{t^2}{8}}$	$-\frac{J}{\sqrt{2}}$
$\langle Q_7\|$	0	$-\sqrt{\frac{t^2}{1.6}}$	0	$-\frac{J}{\sqrt{2}}$	$-\sqrt{\frac{t^2}{8}}$	0	$-\frac{J}{2}+2k$	$\frac{t}{2}$	0	$-\frac{J}{2}$	0	0
$\langle Q_8\|$	$\sqrt{\frac{t^2}{1.6}}$	0	0	$\sqrt{\frac{t^2}{8}}$	0	0	$\frac{t}{2}$	$2k$	$-t$	0	0	0
$\langle Q_9\|$	0	0	0	0	0	$\frac{J}{\sqrt{2}}$	0	$-t$	$-\frac{J}{2}+2k$	0	0	$\frac{J}{2}$
$\langle Q_{10}\|$	0	0	0	$-\frac{J}{\sqrt{2}}$	0	0	$-\frac{J}{2}$	0	0	$-\frac{J}{2}+2k$	$-t$	0
$\langle Q_{11}\|$	0	0	$\sqrt{\frac{t^2}{1.6}}$	0	0	$-\sqrt{\frac{t^2}{8}}$	0	0	0	$-t$	$2k$	$-\frac{t}{2}$
$\langle Q_{12}\|$	0	$\sqrt{\frac{t^2}{1.6}}$	0	0	$-\sqrt{\frac{t^2}{8}}$	$-\frac{J}{\sqrt{2}}$	0	0	$\frac{J}{2}$	0	$-\frac{t}{2}$	$-\frac{J}{2}+2k$

Table 2.2: The quartet spin Hamiltonian matrix containing the 12 quartet states Q_1 to Q_{12}

$\hat{H}_{doub}$	$\lvert D_1\rangle$	$\lvert D_2\rangle$	$\lvert D_3\rangle$	$\lvert D_4\rangle$	$\lvert D_5\rangle$	$\lvert D_6\rangle$	$\lvert D_7\rangle$	$\lvert D_8\rangle$	$\lvert D_9\rangle$	$\lvert D_{10}\rangle$	$\lvert D_{11}\rangle$	$\lvert D_{12}\rangle$	$\lvert D_{13}\rangle$	$\lvert D_{14}\rangle$	$\lvert D_{15}\rangle$
$\langle D_1\rvert$	$-J$	$\frac{t}{\sqrt{2}}$	0	$-\frac{J}{\sqrt{2}}$	$-\frac{t}{\sqrt{2}}$	0	$\frac{J}{\sqrt{2}}$	0	0	0	0	0	0	0	0
$\langle D_2\rvert$	$\frac{t}{\sqrt{2}}$	0	$-\frac{t}{\sqrt{2}}$	$\frac{t}{2}$	0	0	0	0	$\frac{t}{2}$	0	0	0	$-\frac{t}{2}$	0	$-\frac{t}{2}$
$\langle D_3\rvert$	0	$-\frac{t}{\sqrt{2}}$	$-J$	0	0	$-\frac{J}{\sqrt{2}}$	0	$-\frac{t}{\sqrt{2}}$	$\frac{J}{\sqrt{2}}$	0	0	0	0	0	0
$\langle D_4\rvert$	$-\frac{J}{\sqrt{2}}$	$\frac{t}{2}$	0	$-\frac{J}{2}+2k$	$\frac{t}{2}$	0	$\frac{J}{2}$	0	0	0	0	0	0	$\frac{t}{\sqrt{2}}$	0
$\langle D_5\rvert$	$-\frac{t}{\sqrt{2}}$	0	0	$\frac{t}{2}$	$2k$	$\frac{t}{2}$	0	0	0	0	0	$-\sqrt{\frac{4t^2}{3}}$	$-\frac{t}{2}$	0	0
$\langle D_6\rvert$	0	0	$\frac{J}{\sqrt{2}}$	0	$\frac{t}{2}$	$-\frac{J}{2}+2k$	0	0	$-\frac{J}{2}$	0	$-\sqrt{\frac{4t^2}{3}}$	0	0	0	0
$\langle D_7\rvert$	$\frac{J}{\sqrt{2}}$	0	0	$\frac{J}{2}$	0	0	$-\frac{J}{2}+2k$	$\frac{t}{2}$	0	0	$\sqrt{\frac{4t^2}{3}}$	0	0	0	0
$\langle D_8\rvert$	0	0	$-\frac{t}{\sqrt{2}}$	0	0	0	$\frac{t}{2}$	$2k$	$-\frac{t}{2}$	$-\sqrt{\frac{4t^2}{3}}$	0	0	0	0	$\frac{t}{2}$
$\langle D_9\rvert$	0	$\frac{t}{2}$	$\frac{J}{\sqrt{2}}$	0	0	$-\frac{J}{2}$	0	$-\frac{t}{2}$	$-\frac{J}{2}+2k$	0	0	0	0	$-\frac{t}{\sqrt{2}}$	0
$\langle D_{10}\rvert$	0	0	0	0	0	0	0	$-\sqrt{\frac{4t^2}{3}}$	0	$-\frac{J}{2}+4k$	$\frac{t}{2}$	0	$-\sqrt{\frac{4J^2}{3}}$	0	0
$\langle D_{11}\rvert$	0	0	0	0	0	$-\sqrt{\frac{4t^2}{3}}$	$\sqrt{\frac{4t^2}{3}}$	0	0	$\frac{t}{2}$	$4k$	$-\frac{t}{2}$	0	0	0
$\langle D_{12}\rvert$	0	0	0	0	$-\sqrt{\frac{4t^2}{3}}$	0	0	0	0	0	$-\frac{t}{2}$	$-\frac{J}{2}+4k$	0	0	$\sqrt{\frac{4J^2}{3}}$
$\langle D_{13}\rvert$	0	$-\frac{t}{2}$	0	0	$-\frac{t}{2}$	0	0	0	0	$-\sqrt{\frac{4J^2}{3}}$	0	0	$-\frac{3J}{2}$	$\frac{t}{\sqrt{2}}$	0
$\langle D_{14}\rvert$	0	0	0	$\frac{t}{\sqrt{2}}$	0	0	0	0	$-\frac{t}{\sqrt{2}}$	0	0	0	$\frac{t}{\sqrt{2}}$	0	$-\frac{t}{\sqrt{2}}$
$\langle D_{15}\rvert$	0	$-\frac{t}{2}$	0	0	0	0	0	$\frac{t}{2}$	0	0	0	$\sqrt{\frac{4J^2}{3}}$	0	$-\frac{t}{\sqrt{2}}$	$-\frac{3J}{2}$

Table 2.3: The doublet spin Hamiltonian matrix containing the 15 doublet states D_1 to D_{15}

2.4 Computational details

In the present study, the modified DE Hamiltonian has been studied for the parameter range corresponding to real TMO's for which there is a strong competition between the DE and the SE mechanisms. The phase which results from such a competition has been called as the "island phase" by various authors [79, 68]. The island phase separates the Ferromagnetic Phase (FM) resulting from the dominant DE interaction from the AFM phase arising due to the SE interaction. There is a critical interplay between the parameters of the model Hamiltonian which leads to a dense low energy spectrum. Thus, one needs accurate methods like exact diagonalization in order to get clear energy differences and "clean" states. In this study we use sophisticated exact diagonalization (ED) techniques to overcome the convergence problems due to the intricate nature of the low lying states.

2.4.1 Deterministic methods

The advantage of deterministic diagonalization methods is not only the high accuracy of the eigenvalues(10^{-9}), but also the possibility of obtaining highly accurate (10^{-4}) coefficients for the ground state eigenvector. This accuracy in the eigenvectors would make it possible to reliably obtain expectation values for any observable which could be cumbersome or even impossible for other methods like the DMRG, DMFT and QMC.

The first choice for solving an eigensystem equation is to use the heavily optimized Mathematics Kernel Libraries (MKL) made accessible by Intel [80]. Although, we have used directly these libraries for smaller systems like 7_1h and 6_2h, they cannot be scaled for larger systems. The reason is the exponentially growing size of the nonzero elements of the Hamiltonian and the eigenvectors. The MKL implementations depend on two basic algorithms to get the eigenvalues and eigenvectors of the matrix. They first use the Householders tridiagonalization [81] to render the symmetric matrix tridiagonal followed by the QL algorithm to get full eigenvalues and eigenvectors [82]. These algorithms are adapted for obtaining the complete eigensystem and require the storage of the intermediate vectors in memory. Thus one would not only have to store the non-zero elements of the matrix but also the eigenvector matrices which in our case are extremely dense. The other option being writing the vectors on disc, which is prohibitively long. It is therefore not practical to use these libraries for large systems.

2.4.1.1 Exact diagonalization: low energy spectrum

The solution to the problem stated above of the storage of the vectors in the RAM which would require $N^2 * 8$ bytes of memory, is to obtain only a few eigenvectors corresponding to the low energy spectrum of the system. This is adequate for our purpose because we are interested mainly in low temperature behavior of the system. The first such algorithms was published by Nesbet [83] for the diagonalization of large CI matrices in mid 1960's. His algorithm was based on an iterative procedure to correct the error made by a trial guess vector adding on each iteration the component in the orthogonal direction to the trial vector. The basic idea is to use the Rayleigh quotient as the closest estimate using the current trial vector. Although Nesbet was successful in obtaining the lowest few eigenvalues, the method suffered from showing a very slow convergence. In the mid 1970's this idea of using the Rayleigh quotient was extended by Shavitt *et al* [84] and then Davidson [85] developing on the method of optimal-relaxations (MOR). The latter was able not only to find multiple eigenvalues at once and accelerate convergence, but also to reduce the amount of memory required to store the intermediate $\sum_{ij} A_{ij}C_j$, where A_{ij} represents the matrix and C_j the vectors. The algorithm proposed by Davidson would give similar performance to that proposed by Lanczos [86, 87] in the 1950's which is still widely used in the resolutions of model Hamiltonians.The most expensive step in all the above methods is the matrix vector step which scales as N^2 and requires the storage of at least two vectors of length N. Thus, the strength of such methods will depend not only on the hardware available but also the exploitation of the parallel architecture for speeding up the large matrix vector operations.

2.4.1.2 Krylov-Schür

Through experience, the method of choice seems to invariably involve some variant of the Krylov space method. There are a number of methods which use the idea of the orthogonal Krylov space like the Arnoldi algorithm [88] and the Lanczos one. The main issues under consideration while selecting methods adapted for application to specific problems can be stated as follows:

- The Hermiticity of the Hamiltonian matrix
- The type of hardware used and the amount of memory available
- The number of eigenstates required

Based on the above factors, the method of choice in our case is the so called Krylov-Schür method. The Krylov-Schür algorithm was proposed by Stewart [89, 90] in 2001. Although the algorithm bears similarity to the implicitly restarted Arnoldi

algorithm, the motivation for the Krylov-Schür decomposition is its invariance towards the application of similarity and translational transformations which renders the algorithm much more manageable and amenable towards a massively parallel implementation. For these reasons we have used the Krylov-Schür method available in the massively parallel eigensolver SLEPc [91, 92, 93].

2.4.2 Large sparse diagonalization

All the above algorithms focus on the problem of reducing the memory requirements for the solution of large eigenvalue problems. Such methods make it possible to solve very large systems consisting of about a million determinants ($N = 1,000,000$). In order to be able to study larger systems and go beyond the billion determinant mark, one needs to adapt the algorithms to state of the art architectures used in modern clusters. The largest diagonalization done up until the writing of this manuscript was by the Japanese group of Yamada. S. *et al* [94] in 2005, they used the Earth Simulator and algorithms adapted for high flop computation to diagonalize a 159-billion dimensional Trapped-Fermion Hubbard model. In the present work, we have similarly used algorithms and computer code adapted for distributed memory low latency clusters. The EOS cluster located in the intensive computation society of Midi-Pyrénées (CALMIP) was used. The program was written in C++ and the template library provided by PETSc [95, 96, 97] was used not only to set up the Hamiltonian but also to do the analysis. The template library provided by PETSc has been optimized for usage in multi node architecture and is adapted for a combined MPI and OpenMP parallelization. The PETSc library not only makes it easy to write parallel code but also provides objects and tools which distribute memory across multiple CPU nodes and manage the communication and exchange of memory objects. In order to gain efficiency, a homemade code [98] code in Fortran used to efficiently generate matrix elements was interfaced with the PETSc library and the final diagonalization was done using the Krylov-Schür algorithm available in the SLEPc library. The eigenvectors for low lying states were obtained and stored on disk for the following analysis. The analysis was done using a parallel homemade code [98]. It is important to note that in some cases the analysis of the ground state eigenvectors takes more CPU time than the actual diagonalization because of the complicated operators involved e.g. the two body density matrix (d_{PQRS}) and the S^2_{box} operators.

2.4.3 Approximate methods

The problem with using exact methods is the exponential scaling of the Hilbert space. This problem is overcome by using either renormalization group meth-

ods (DMRG), mean field methods (DMFT) or stochastic methods like Quantum Monte Carlo (QMC) which rely on an approximate resolution of the Hamiltonian. Stochastic methods work under the assumption that the ground state of a large correlated system is essentially described by a few ($< 1\%$) determinants which contain the physics of the model. This assumption appears to break down in our modified DE Hamiltonian where for the given parameter range there appears to be an increase of the spread of the ground state along a large number of determinants ($\approx 10\%$). Then there is the problem of statistical averaging which is amplified by the presence of a large density of states.

2.4.3.1 DMRG

Previous studies based on the Density matrix renormalization group (DMRG) [66, 79, 99, 100, 101, 68] have revealed the existence of island phases which separate the FM and AFM regions.The method of choice must satisfy the constraints of working with a large density of states where there might be hundreds of states in a few meVs of energy.

The density matrix renormalization group (DMRG) method is an approximate method for the calculation of energies and observables which works well at the least for finite one dimensional systems. The DMRG method is encompassed by a broader more general methods to solve infinite one dimensional systems like the matrix product states (MPS), projected entangled pare states (PEPS) and other more general renormalization group theories [102]. Since the DMRG is not an exact method, there are limits beyond which it fails. This is the case for our systems where the low energy spectrum is dense and there are hundreds of states in a gap of a few meV. Thus, in the region of interest for the parameters J, K and t, for which we would observe the Island phase of the Hamiltonian, DMRG is insufficient. A few tests have been done using the DMRG program implemented in the Algorithms and Libraries for Physics simulations [103] (ALPS) package Therefore, although the DMRG method would be effective to provide tendencies and a qualitative description of the system, in order to understand the nuances one needs to used exact methods wherever possible.

2.4.3.2 Stochastic methods

There have also been studies based on stochastic methods based on Quantum Monte Carlo [104, 105, 106] (QMC) which suffer from numerical instabilities. There have been studies where QMC is used along with more accurate meth-

ods like ED [107, 108]. The variational MC version have also been used but only to replace more exact methods like ED and DMRG which become too expensive for large 1D and 2D systems [109].

2.5 Single hole case

In this first part we undertake a detailed analysis of systems of various sizes containing a single hole in order to study the extension of the polaron as a function of J and K. The first problem is the characterization of the ground state spin phase diagram for systems from 3_1h to 7_1h. The second part would concern the study of the ferromagnetic polaron. Previous theoretical and experimental studies concluded that there is a ferromagnetic polaron surrounding the holes as presented in sec 2.2.1.2. Experimental evidence for 1D nickelates, although not conclusive, stated the size of the polaron to be between seven to eight sites [45]. The accurate knowledge of the size of the polaron will be crucial for the understanding of the doping ratio observed in YBCO and LCMO transition metal oxides. These results would also help us to understand the nature of the ground state in the presence of two or more holes.

2.5.1 Twisted boundary conditions

We have carried out a preliminary comparison of results obtained using open as well as twisted boundary conditions on small systems (3_1h to 6_1h). The results show that the spectrum of small systems is greatly influenced by the presence of $4n$ and $4n+2$ sites in the cyclic system, these effects are well known in the Hückel model. This makes it difficult to separate DE physics from the topological effects amplified by the small size of the system. Therefore, we have concentrated only on 1D open chain systems.

In the following sections, a systematic analysis of the ground state of systems with various number of sites and a single hole is presented. The open boundary conditions (OBC) have been used throughout unless where mentioned otherwise. The first section consists of an analysis of the spin phase diagram which is followed by the polaron extension plots.

2.5.2 Phase diagrams

In all the following results, the numbers are given in units of t. Hence J and K are represented in terms of t. As $t \approx 1eV$ in many real systems this would give the following parameter range:

$$0.01eV \leq J \leq 0.15eV \tag{2.5.1}$$

$$0.3eV \leq K \leq 1.8eV \tag{2.5.2}$$

$$t = 1eV \tag{2.5.3}$$

Very large (0.15) and small (0.01) values of J have been considered. This will help the generalization to the results of this paper to any real transition metal oxide system, given the full extent of the parameter range chosen.

Phase diagrams for the 3_1h to 7_1h systems have been obtained for the full parameter range J and K. The procedure for the calculation of the diagrams is as follows. About 200 points in the phase space constituted of 20 values of J and 10 values of K have been used. The Hamiltonian matrix was diagonalized and the full spectrum obtained for all the 200 points for each of the systems. These energies were used to form the surface of the spin subspace of a given system as a function of J and K. The surface is formed of 200 data points, this alone is insufficient to obtain good curves of intersection between the surfaces of the different states. Thus, a C++ interpolation library [110] was used to get a bi-cubic spline function for the surface. The interpolated surface was then used to obtain the curves of intersection between the various spin states. The curves of intersection are used to plot the regions corresponding to a different spin ground state as functions of J and K.

2.5.2.1 Three sites

The simplest case is that of the 3_1h system presented in Sec 2.3. The system consists of five electrons and one hole along three sites each containing two orbitals. Since the hole motion is restricted only on the a_1, b_1 orbitals i.e. only on one type of orbitals per site, there are only three positions for the hole on each of the three sites. **The configurations where the hole occupies the other type of orbitals a_2, b_2 occurs for unphysical large values of J and therefore have not been considered in the CI space.** Thus, the Hilbert space consists of $\binom{3}{1} \cdot \binom{5}{3} = 30$ determinants in the lowest $M_s = \frac{1}{2}$ subspace.

The phase diagram is shown in Fig: 2.3, as can be seen from the figure there are three zones constituted by the three different spin spaces. **The orange square represents physical values of J and K observed in transition metal oxides.** The dominant determinants (i.e. having the largest coefficient in the wavefunction) for the $S = \frac{1}{2}$ and $S = \frac{5}{2}$ states of lower energy are shown on the right hand side. The following few points are worth mentioning for the 3_1h system:

- The characteristic ferromagnetic alignment of spins is obtained for low values of J where the hole is located at the center (this configuration is optimal in terms of kinetic energy.)

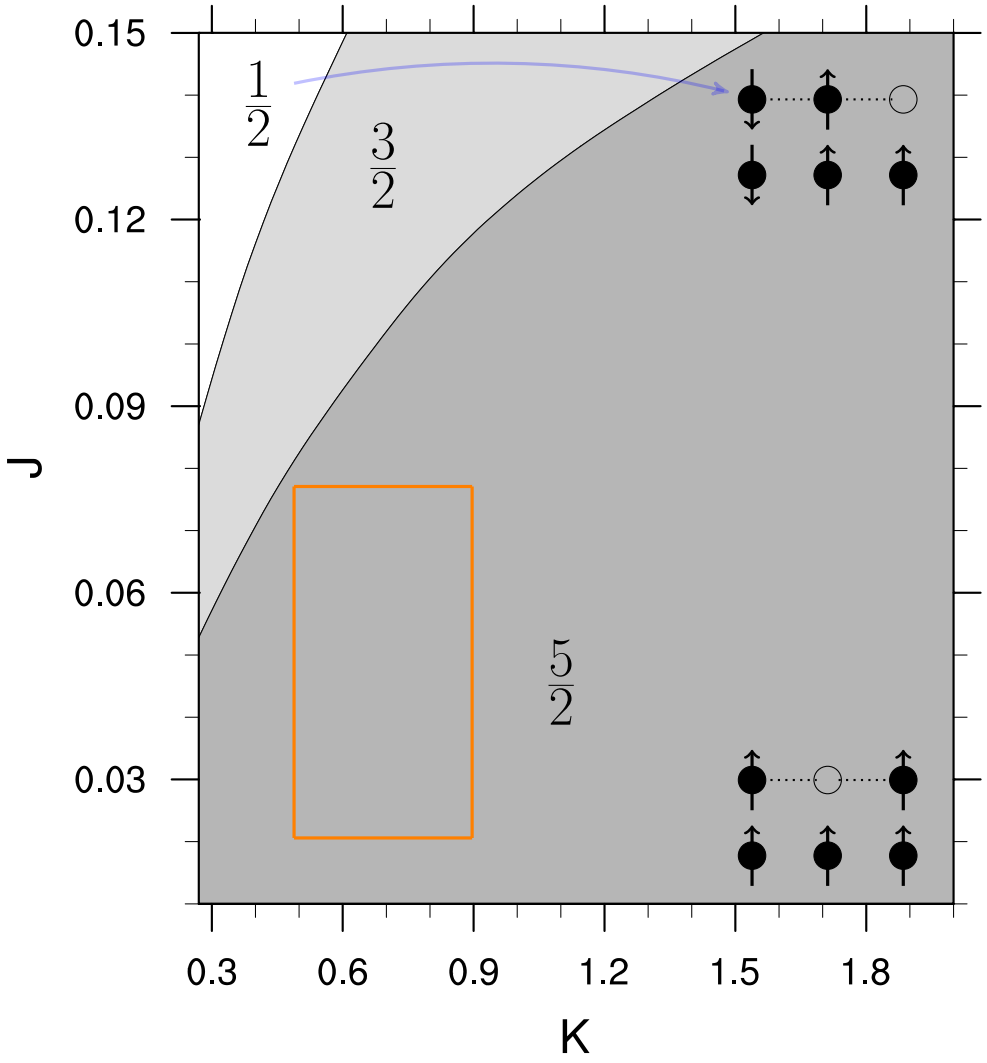

Figure 2.3: Phase diagram of the 3_1h system for various values of J and K. The nature of the ground state is shown by the determinants with the largest coefficient in the ground state.

- Large values of J force the hole at the edges in order to gain antiferromagnetic interaction J between adjacent sites.
- There is a large effect of the local Hund term K for all values of J. In fact the asymptotic values for $K \to \infty$ of the intersection of $S = \frac{5}{2}$ and $S = \frac{3}{2}$ state is for $J > 0.17$ which is too large. Therefore, at least for finite systems one cannot neglect the influence of the low lying non-Hund states (i.e. small value of K).
- Finally, we notice that for the 3_1h system, just by the spin ground state of

the 3_1h system, one can easily find out the nature of the physics at play. Although, as we shall see later, such a direct analysis is not possible for larger systems.

- At least for the 3_1h system, for physical values of J and K, a single hole has aligned the five spins (or three sites.)

An important conclusion from the analysis of the smallest system is the role of K. The effect of K is to stabilize the local triplet states, but one must not forget that in physical systems (for e.x. nickelates) the non-Hund states are low in energy and do effect the low energy spectrum.

2.5.2.2 Four and more sites

In this section, we will study larger systems up to 7_1h in order to verify the above analysis. We would like to point out that an analysis such as the present one would also serve as a starting point for the synthesis of finite chain high-spin systems.

Let us continue with the next larger systems, i.e. 4_1h and 7_1h systems. The phase diagrams of four to seven site system is shown in Fig: 2.4, 2.5, 2.5 and Fig: 2.7 below. For four and five site systems, all the spin values can be obtained as ground states whereas for the 6_1h and 7_1h system this is not the case. The topology of the 6_1h and 7_1h system causes the $S = \frac{1}{2}$ state to be favorable only in the range of unphysical large values of J. It can be seen that some of the states (e.g. the $S = \frac{7}{2}$ state for the 5_1h system) are observed for a smaller range of values of J and K than other this is due to the finite size of the system.

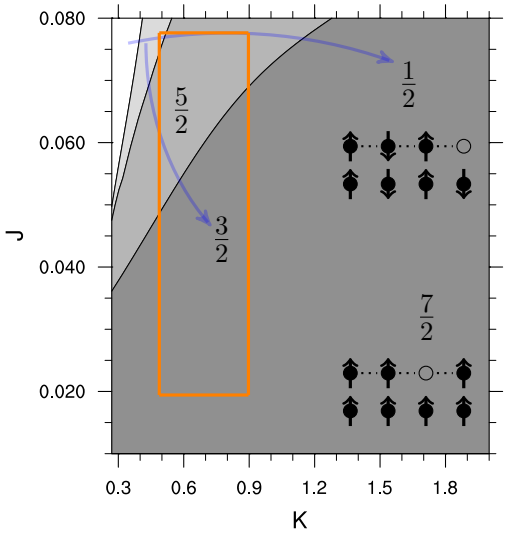

Figure 2.4: Phase diagram of the 4_1h system as a function of J and K. There are regions which are not favorable due to the topology of the system and occupy a very small portion of the phase space.

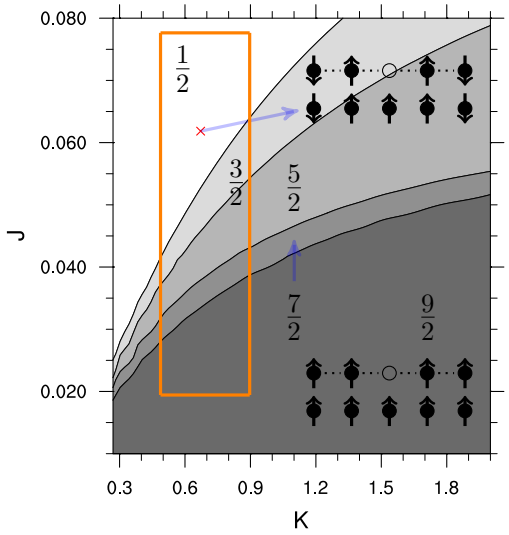

Figure 2.5: The Phase diagraom for the 5_1h system. The 5_1h system has five spin phases in total from $S = \frac{1}{2}$ to $S = \frac{9}{2}$, all the phases show clearly in the plot.

We observe also that, as in the previous case, K plays an important role in determining the spin ground state for 4_1h to 7_1h systems. In fact we have also shown the asymptotic values ($K \to \infty$) of intersection of states for the two systems 6_1h and 7_1h with dashed red lines. These asymptotic values represent the intersection at the $K \to \infty$ limit. Therefore, we conclude that at least for the systems studied here, the role of K is crucial in the determination of the spin ground state.

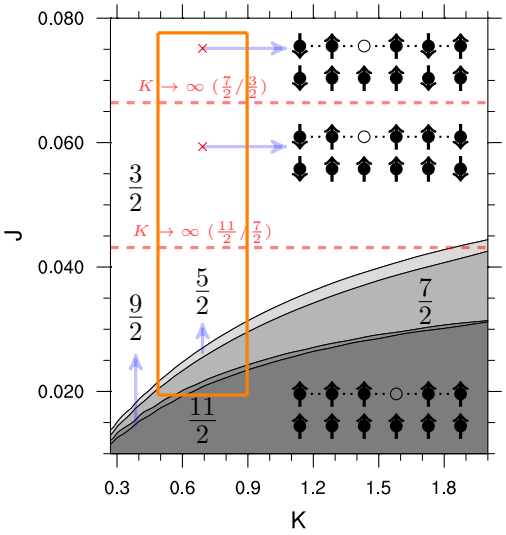

Figure 2.6: The phase diagram of six sites, similar to the 4_1h system, shows regions of space not favourable due to the topology of the 6_1h system.

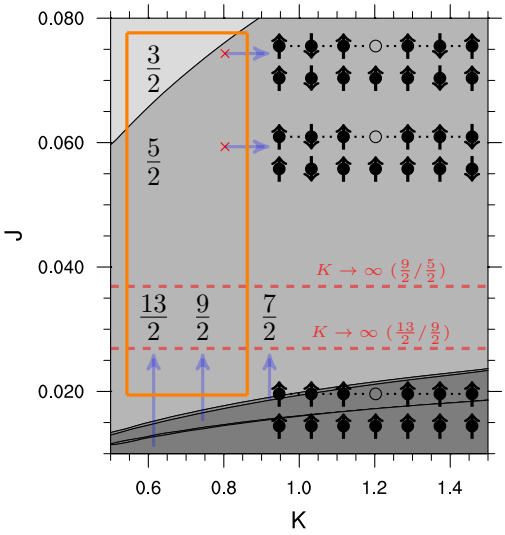

Figure 2.7: The diagram plot of seven sites is shown. There are six spin phases, two of which are very small.

Focusing at the physical values of J and K, i.e. inside the orange box. It is interesting to note that for the parameter region of interest, the spin space varies for all the four systems 4_1h to 7_1h systems and is not the S_{max} value as it was the case for the previous system (3_1h). This is of course because the total spin would depend on the size of the system although locally, the hole would individually align a fixed number of spins. Therefore, contrary to the previous case, **looking at the spin of the ground state, or the determinant with the largest coefficient will not conclusively give the number of spins aligned by a single hole.**

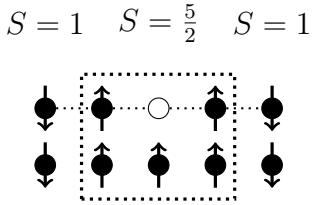

Figure 2.8: Expected spin configuration in the region inside the rectangle when the hole aligns five spins around it for the 5_1h system.

The nature of the system in the region of interest can be analyzed for the four systems by a closer inspection of the wavefunction for the values inside the rectangle. In the following we try to understand the nature of the ground state for 5_1h and

7_1h system as an example.

- Case 5_1h: The dominant determinants consist of the hole in the middle surrounded by five parallel spins (the ferromagnetic polaron), this situation is shown in Fig: 2.8. The ferromagnetic polaron of $S = \frac{5}{2}$ will interact with the border $S = 1$ spins leading to a total $\frac{1}{2} \leq S \leq \frac{9}{2}$ state. This is what we see inside the rectangle for the 5_1h phase diagram.

- Case 7_1h: For the seven site system with a single hole, the phase diagram (Fig: 2.7) does not show much variation in the spin of the ground state for a large range of K and J. A study of the dominating determinants in the parameter space in question, is shown in the Fig: 2.9 below. The figure shows the determinant ($m_s = \frac{5}{2}$) with the largest coefficient for various values of $0.04 \geq J \geq 0.07$ and the total spin at each value. From the figure it appears that there is a drastic change in the size of the polaron surrounding the hole with increasing J, although the total spin remains the same.

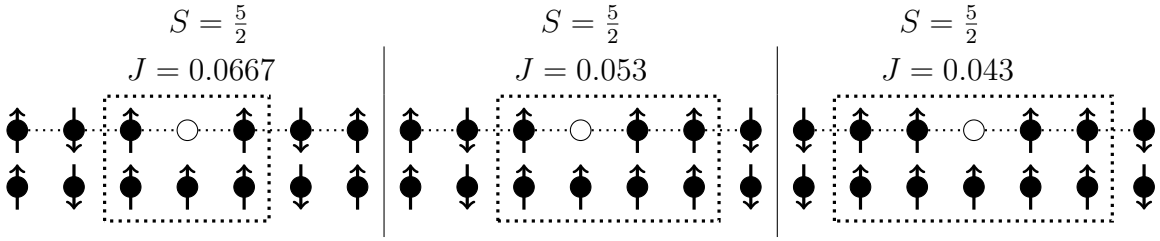

Figure 2.9: The dominant determinants for three different values of J at $K = 0.8$ are shown along with the total spin of the ground state.

Of course the value of the ground state spin multiplicity is not sufficient to determine the extent of the spin polaron. More importantly, we realize that this is not only due to topological effects (due to the OBC). Even for sufficiently large systems, it would become practically impossible to predict the number of spins aligned by a single hole by looking at the dominant determinant due to the sheer number of determinants. Therefore, we conclude that one needs a more refined and practical tool to quantify the size of the ferromagnetic polaron.

2.5.2.3 Conclusion for phase diagrams

The above study on finite size systems can be valuable in itself from the perspective of the conception of finite chains of high-spin multiplicities as mentioned in

the introduction. One can use directly the values of J and K provided here in order to conclude whether the finite sized chain will show a high-spin ground state or not. In order to give some quantitative conclusions the nature of the spin polaron for larger systems, one needs to perform a different analysis. In the section that follows, we will present a novel tool to quantify the size of the ferromagnetic polaron.

2.5.3 Spin polaron

The spin polaron is a region of high-spin state S_{max} formed by the hole due to the DE mechanism. What we require is a tool that would give an accurate value of the spin in a small region surrounding the hole, using this we would then be able to estimate the size of the polaron. In order to estimate the amount of spin in a small region (box), we have calculated the spin density, using the truncated spin density operator $\hat{S}^2_{box}$, inside a box, **while fixing the hole at the center.** The $\hat{S}^2_{box}$ operator, shown in Eq 2.5.4, calculated in this manner by fixing the hole, will give a lower bound to the amount of spin aligned by the hole. The spin density can then be used to calculate the effective spin inside the box (S_{box}). We will give precise definitions in the section that follows.

2.5.3.1 S_{box}

The spins are aligned by the hole due to the DE mechanism. Therefore, these spins are on the neighbouring and next-neighbouring sites of the hole, i.e. the sites surrounding the hole. Thus, it appears logical to calculate the spin in a region with the hole at the center if we want an estimate of the number of spins aligned by a single hole. This is the idea behind the use of the S_{box} operator which will be defined and explained in this section.

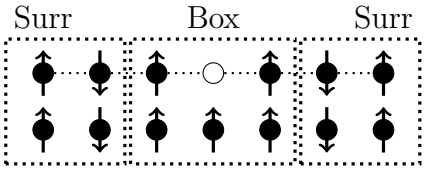

Figure 2.10: Seven sites with one hole and the S_{box} region.

Consider the case of the 7_1h system with values of J and K for which a single hole has aligned five spins Fig: 2.10. The system is composed of the polaron (box

region) bordered by the antiferromagnetic surrounding (surr). The box region is of course not in a pure state and would exist in general as a mixture of all possible spins states $S = \frac{1}{2}, \frac{3}{2}$ and $\frac{5}{2}$. In fact what we would like to calculate is the weight of each of the states for various box sizes and use it to get the size of the "real box" region. In order to do that, we can proceed as follows. We know that the wavefunction of the system can be written as:

$$|\psi_{sys}\rangle = \sum_i c_i \, |\psi_{box,i}\rangle \otimes |\psi_{surr,i}\rangle$$

where the states of the box are represented by ψ_{box} and the surrounding by ψ_{surr}. We are interested in the dominant ψ_{box} states. With the above notation, the density matrix of the states inside the box can be written as:

$$\begin{aligned}
\hat{\rho}_{sys} &= |\psi_{sys}\rangle \langle\psi_{sys}| \\
\hat{\rho}_{box} &= \sum_i \rho_i \, |\psi_{box,i}\rangle \langle\psi_{box,i}| \\
\hat{\rho}_{box} &= \mathrm{Tr}_{surr} \left[\rho_{sys}\right]
\end{aligned}$$

where $\rho_i = c_i^2$ is the weight of the i^{th} box state $\psi_{box,i}$, this is what we need. In order to estimate the weight of each of the spin states, we can use the $\hat{S}^2_{box}$ operator defined as:

$$\hat{S}^2_{box} = \hat{\rho}_{box} \cdot \hat{S}^2 \tag{2.5.4}$$

Once we know the form of the operator, we can calculate the expectation values as follows:

$$\begin{aligned}
\left\langle S^2_{box} \right\rangle &= \langle\psi| \, \hat{S}^2_{box} \, |\psi\rangle = \mathrm{Tr}\left[\rho_{box} \hat{S}^2\right] \\
\left\langle S^2_{box} \right\rangle &= S_{box} \left(S_{box} + 1\right) \\
\left\langle S^2_{box} \right\rangle &= \sum_i \rho_i S_i (S_i + 1)
\end{aligned}$$

the S_i represent the various spin states possible inside the box. Since the box with three sites contains five spins, there will be a total of 10 states: 1 sextet ($S = \frac{5}{2}$), 4 quartet ($S = \frac{3}{2}$) and 5 doublet ($S = \frac{1}{2}$) states. For example, when the ferromagnetic polaron will occupy three sites, the box will be dominated by the sextet

state and consequently we will have an S_{box} value close to $\frac{5}{2}$. Therefore, the S_{box} is expected to be a good measure of the size of the polaron.

$$\begin{aligned} \left[\hat{H}_{sys}, S^2_{box}\right] &\neq 0 \\ \left[\hat{H}_{box}, S^2_{box}\right] &= 0 \end{aligned} \tag{2.5.5}$$

Since the wavefunction of the box ψ_{box} will in general be a mixture of all the spin states, the resulting S_{box} value will be a mixture of the three spins $\frac{5}{2}, \frac{3}{2}$ and $\frac{1}{2}$. When the box wavefunction ψ_{box} is made up of only a single spin state (e.g. $S = \frac{5}{2}$), only then the S_{box} will be close to the $\frac{5}{2}$ value and we can say that the hole has aligned five spins. Note that this will always be true for the S_{max} states for all systems always. The advantage of using $\hat{S}^2_{box}$ operators is two fold. Firstly, we can probe directly the size of the FM domain and secondly, it allows us to compare two systems irrespective of finite size effects as we shall see below. Since the wavefunction ψ_{box} will be a mixture of all the states of the Hamiltonian of the box system $\hat{H}_{box}$, the operator S^2_{box} no longer commutes will the full Hamiltonian, as shown in Eq: 2.5.5.

Finally, in order to simplify the analysis of S_{box}, **we have fixed the hole at the center of the box in order to remove effects of additional mixing due to hole motion.** Once the S_{box} value is calculated with the hole fixed, we renormalise the S_{box} in order to get comparable values. We state that, although we fix the position of the hole at the center of the box, this does not effect **drastically** the weight of S_{box}. **A numerical verification of the relevance of this approximation will be presented in the sec: 2.6.1.**

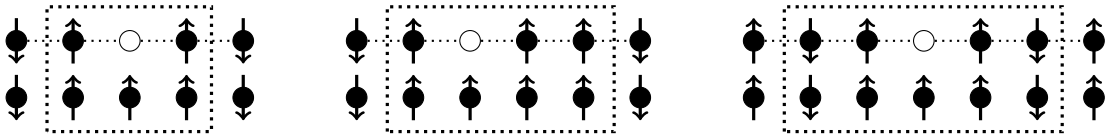

Figure 2.11: Topological dependence of the truncated spin density operator on the size of the system. Odd numbered systems are adapted to calculate S_{box} with odd number of sites.

In the following sections, we will present the S_{box} values for the various systems shown in Fig: 2.11 below. Through this analysis we would be able to quantitatively state the number of spins aligned by a single hole for physical values of J and K. Due to topology, odd numbered systems are adapted to calculate S_{box} values for

odd number of sites in the box this is illustrated in Table: 2.11 and vice-versa. For the symmetric cases i.e. for odd number of sites (5_1h and 7_1h), the hole will be fixed at the center of the box, whereas for the 6_1h system, the hole will be fixed at one of the two symmetric central positions. **The size of the box is varied (from 2 to 5) on all systems and for all values of J and K such that we can accurately determine the size of the polaron for the full range of parameters.** The box size of 6 and more sites is not considered because we have checked that for the parameter range of interest, the polaron extension never exceeds six sites.

2.5.3.2 S_{box} five sites

The spin plots (S_{box}) vs J and K for a box with three and four sites in a 5_1h system is shown in Fig: 2.12. The physical region of the parameter space is delineated in all the plots with an orange rectangle just as for the phase diagrams. The S_{box} was calculated by fixing the box with three sites at the center of the 5_1h system. The hole was also fixed at the center of the box and hence at the center of the 5_1h system and the final expectation value was renormalized. Note that although the S_{box} calculations have been carried out by fixing the hole at the most favorable position, the actual diagonalization considers the full space.

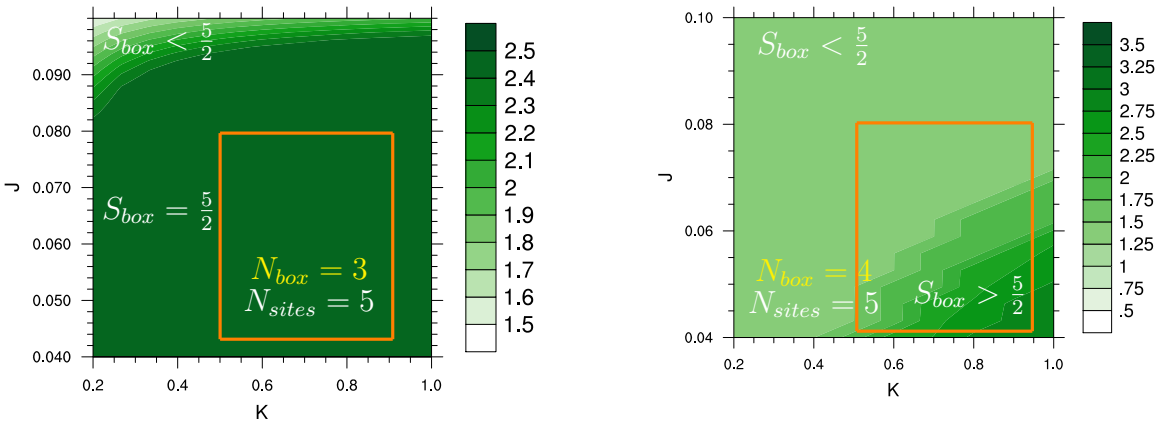

(a) S_{box} values with three sites in the box.

(b) S_{box} values with four sites in the box.

Figure 2.12: The system 5_1h is adapted to calculate the spin alignment in a box with three sites and one hole. The (a) shows the S_{box} value for 5_1h system with 3 sites in the box. (b) shows the S_{box} of the 5_1h system with four sites in the box.

The Fig: 2.12a shows for which values of J and K, five spins (3 sites) have been aligned and the Fig: 2.12b shows the values of S_{box} with four sites in the box. We see that for almost all the values in the rectangle, the S_{box} remains close to $\frac{5}{2}$ therefore for these values, the hole has aligned at least five spins (3 sites). The hole starts to align seven spins for relatively small values of $J \approx 0.04$ as shown in Fig: 2.12b. Therefore, we conclude that for the 5_1h system, for physical values of J and K a single hole aligns five spins (i.e. 3 sites.) Note that a box with four sites would not be symmetrically placed in the system and would thus result in unphysical topological artifacts.

2.5.3.3 S_{box} six sites

Similar analysis has been carried out for the S_{box} on a system of 6_1h with a box of four sites as shown in Fig: 2.13. The choice of a box with four sites was made in this case due to the topology of the system. In this case, there are two symmetrically equivalent positions for the hole inside the box, since the two positions would give exactly the same value of S_{box} due to symmetry reasons, the S_{box} value is reported for only one position.

The figure shows an S_{box} value close to $\frac{5}{2}$. Comparing the phase diagram of 6_1h system with the S_{box} values of $\frac{5}{2}$, one can clearly rationalize the results. In the phase diagram shown in Fig: 2.6, we see that the 6_1h system is in spin $S = \frac{3}{2}$ state for the region considered here. The dominant spin configurations are shown in Fig: 2.14 below.

In conclusion, we find that for a system with six sites and one hole, for physical values of J and K a single hole aligns five spins. This is in complete agreement with the 5_1h system.

2.5.3.4 S_{box} seven sites

The Fig: 2.15 shows the plots of S_{box} with the box containing five sites ($N_{box} = 5$) in a 7_1h system. The 7_1h system is symmetrically adapted for the calculation of S_{box} with $N_{box} = 3$ and $N_{box} = 5$.

The comparison of the phase plots for this case is much more complicated due to the presence of a significant number of spin states inside the box with seven spins (5 sites). Nevertheless, the S_{box} values show the same trend. Almost for all values of J, the S_{box} value corresponds to the case where a single hole has aligned five

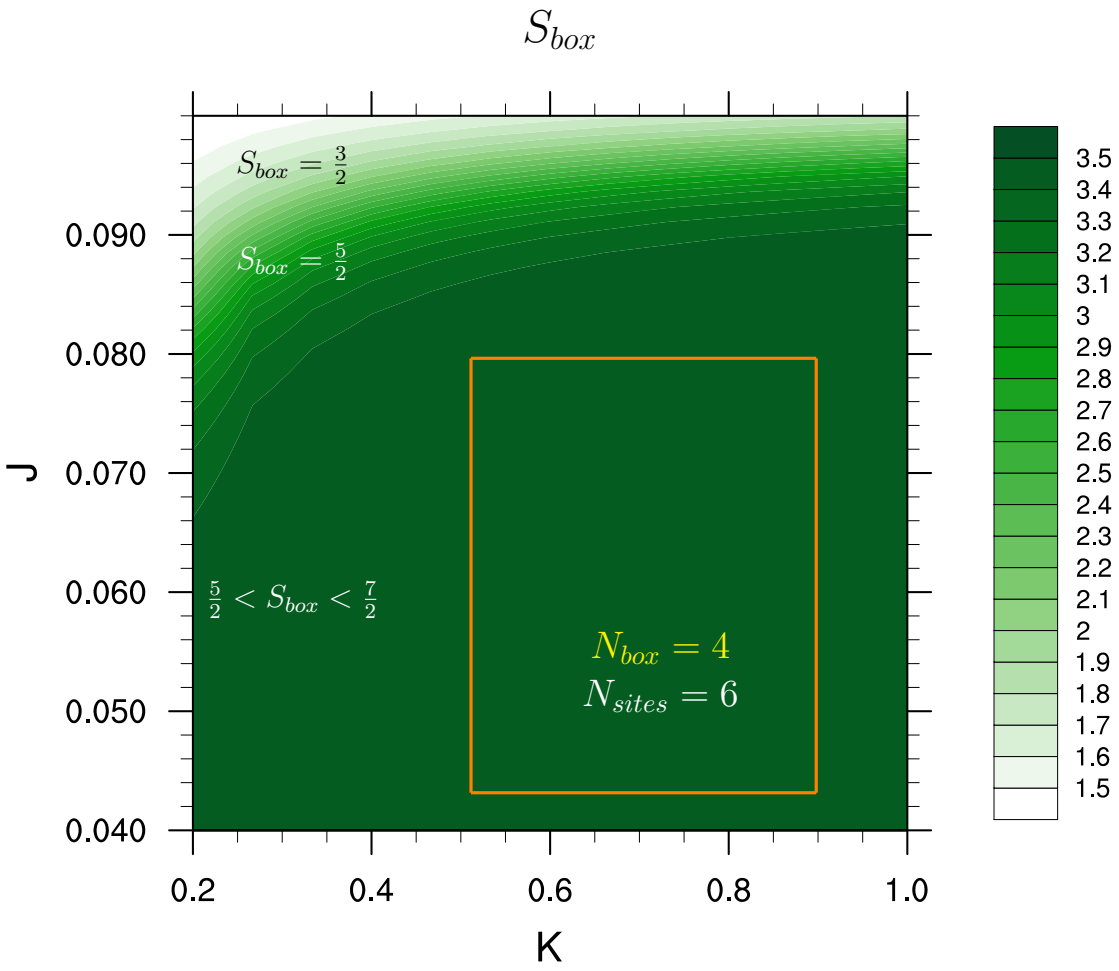

Figure 2.13: The dark green shows a spin $\frac{5}{2} < S < \frac{7}{2}$ indicating that a total of five to seven spins have been aligned in a box of four sites containing the hole. The system consists of six sites in total.

spins (3 sites).

In order to see the utility of the S_{box} value, let us compare the phase diagram of the 7_1h system Fig: 2.7 with the S_{box} values, inside the orange rectangle, the phase diagram shows no change in the nature of the ground state, whereas the spin plots for the same system shown in Fig: 2.15 clearly show the changing nature of the ground state for the same parameter space. A remarkable observation is the similarity of the spin plots of 5_1h and 7_1h systems for the box with three and five sites respectively. This tends to indicate that the extent of the ferromagnetic polaron is independent of the size of the system and the size of the box (N_{box}).

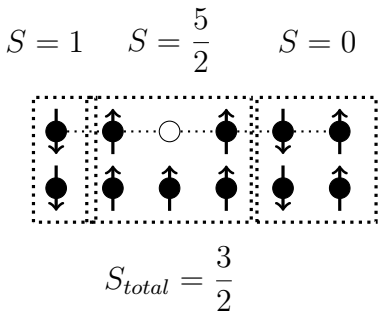

Figure 2.14: The dominant configuration of 6_1h system for physical values of J and K.

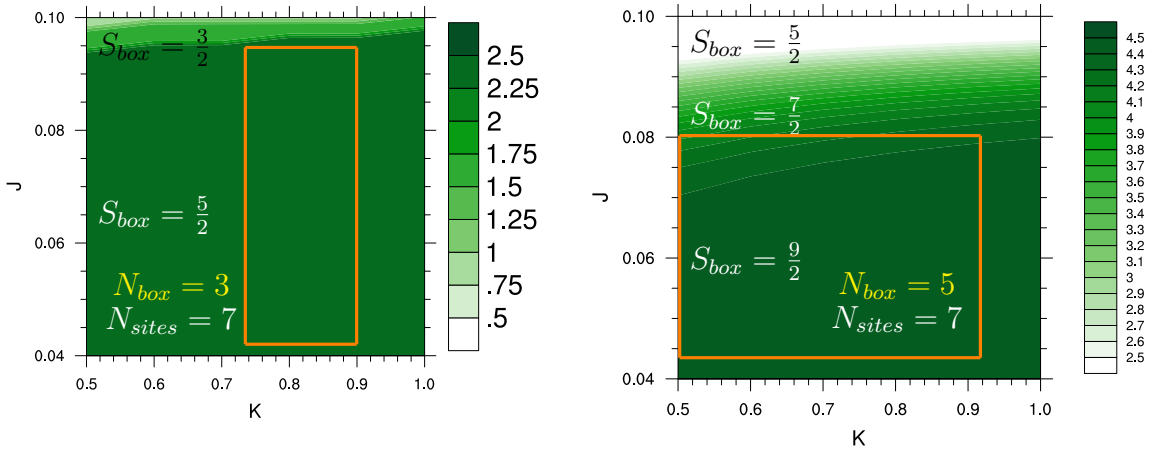

(a) S_{box} values with three sites in the box.

(b) S_{box} values with five sites in the box.

Figure 2.15: The plot of the spin in a box of three (a) sites and five sites (b) is plotted as a function of J and K. The system (7_1h) is made up of seven sites.

This observation will be analyzed in detail in the following sections.

2.5.3.5 Spins aligned: 1 hole

In order to avoid Friedel oscillations [111, 112, 113, 114] from interfering with the results, we have carried out calculations with increasing system size. The Fig: 2.16 shows the values of J for which five, seven and nine spins have been aligned as a function of the number of sites N_{sites}. The Friedel oscillations can be seen quite clearly and the values of J converge with increasing system size.

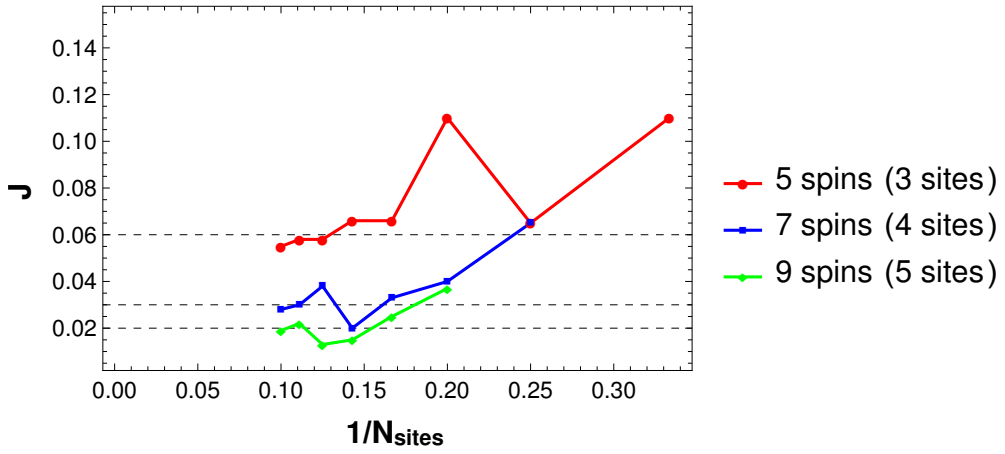

Figure 2.16: The values of J for which five, seven and nine spins have been aligned as a function of system size N_{sites}.

As mentioned in previous sections, the parameter space concerned for nickel oxides is shown in Table: 2.4. Thus, given the range of physical values of J and K, using the above plots of S_{box}, we can quantitatively find how many sites are aligned by the hole for finite systems. In the Table: 2.4, we compile the range of values of J and K for which three, four and five sites are aligned. Although this analysis was done for a finite size 1D chain of spin $S = 1$ (and $S = 1/2$) sites, in the following sections we attempt to demonstrate that these properties might carry over to infinite systems or for larger dimensions for different doping ratios.

$J(eV)$		$N_{spins}(N_{sites})$
min	max	*number of spins aligned*
$6.0{\cdot}10^{-2}$	$12{\cdot}10^{-2}$	5(3)
$3.0{\cdot}10^{-2}$	$8{\cdot}10^{-2}$	7(4)
$1.0{\cdot}10^{-2}$	$6{\cdot}10^{-2}$	9(5)
nickelates and manganites		
$0.8 \leq \|t\| \leq 1.2$		
$0.07 \leq J \leq 0.14$		$5 \leq N_{spins} \leq 7$
$0.07 \leq K \leq 0.10$		

Table 2.4: This table shows the range of values of J for which different number of spins are aligned for a given value of $K = 0.8eV$. The second part of the table shows the physical values of t,J and K for nickelates and Manganites and the resulting predicted N_{spins} aligned by a single hole.

2.5.4 Dependence on finite size: Edge effects

In this section we show whether the finite size results on small systems can be extrapolated to the very large 1D spin chains. Since the Double Exchange phenomenon is essentially local, the edge effects should diminish as the size of the system increases. The size of the polarons S_{box} has been studied with varying system size for a give fixed value of J, as shown in Fig: 2.17. Box with three, four and five sites have been studied for systems ranging from three to thirteen sites. The hole has been fixed at the central position. In order to avoid further topological problems, the box with three and five sites have been studied only in systems with an odd number of sites (3,5,7,9,11,13) and a box with four sites has been studied in system with even sites (4,6,8,10,12). As shown in Sec: 2.5.3.5, the Friedel oscillations can also be seen here and occur purely due to topological reasons. The S_{box} values for three and four sites can already be seen to converge at $\frac{5}{2}$ and $\frac{7}{2}$ for the respective values of J. One needs to carry out calculations on larger systems in order to verify whether the S_{box} with five sites converges, although we see no reason it will not. In conclusion, for systems with a single hole, we have found upper bounds of J (at $K = 0.8$) for aligning three ($J \approx 0.06$), four($J \approx 0.05$) and five spins ($J \approx 0.03$).

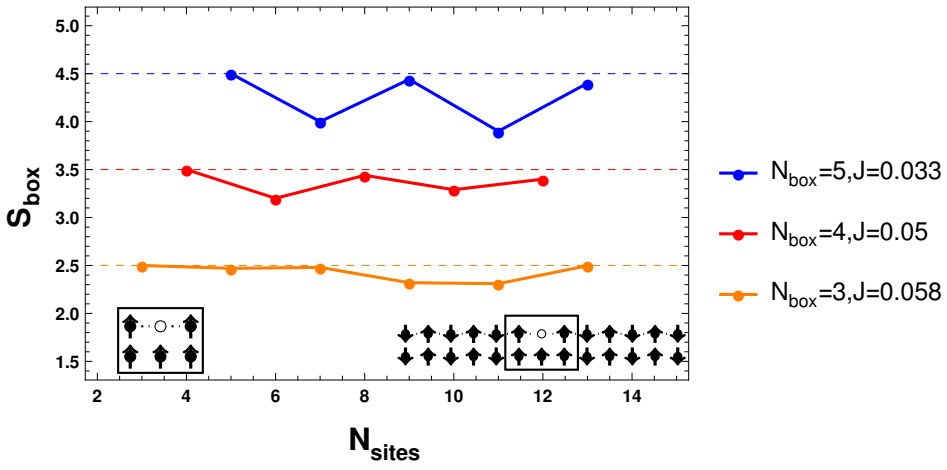

Figure 2.17: S_{box} as a function of number of sites N_{sites} for a box with three, four and five sites. $J = 0.058$ for $N_{box} = 3$, $J = 0.5$ for $N_{box} = 4$ and $J = 0.033$ for $N_{box} = 5$. The value of $K = 0.8$ for all the above calculations.

2.6 Interaction: 2 or more holes

2.6.1 S_{box} vs Exact weights

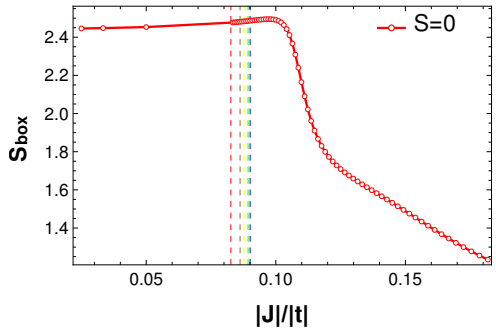

(a) S_{box} with three sites in the box for the 6_2h system.

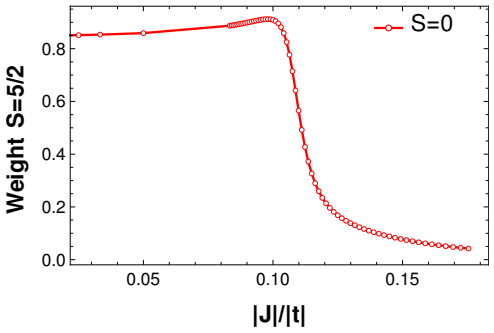

(b) Weight of the $S = \frac{5}{2}$ state for the 6_2h system.

Figure 2.18: A comparison of the S_{box} values with that of the exact weight of the $S = \frac{5}{2}$ states. The vertical lines represent the change of state from $S = 0$ to $S = 5$ for the 6_2h system.

The aim of this section is to show the relevance of the S_{box} as a tool for the analysis of the polaron extension. The S_{box} tool is used in order to simplify the analysis of the nature of the wavefunction. Take the case of two holes in six sites, for values of $J \approx 0.1$ and $K \approx 0.8$ for which a single hole aligns five spins. The wavefunction will then be composed of a low spin state which is dominated by determinants where each hole has aligned five spins. The wavefunction can then be written as a combination of the spin states in each box $S = \frac{1}{2}$ to $\frac{5}{2}$ giving rise to the spin state for the whole system (e.g. $S = 1$ spin state), Eq: 2.6.1.

$$(S=1) \equiv \underbrace{\left(\frac{5}{2} \otimes \frac{5}{2}\right)}_{\text{two } \frac{5}{2} \text{ spins}} \oplus \underbrace{\left(\frac{5}{2} \otimes \frac{3}{2}\right)}_{\text{mixed spin term}} \oplus \underbrace{\left(\frac{3}{2} \otimes \frac{3}{2}\right)}_{\text{two } \frac{3}{2} \text{ spins}} \oplus \underbrace{\left(\frac{3}{2} \otimes \frac{1}{2}\right)}_{\text{mixed spin term}} \oplus \underbrace{\left(\frac{1}{2} \otimes \frac{1}{2}\right)}_{\text{two } \frac{1}{2} \text{ spins}} \quad (2.6.1)$$

where each $\frac{5}{2}, \frac{3}{2} \cdots$ represent spin configurations due to the five spins in the box. The wavefunction will be dominated by the above configurations for values of J, K at which each hole aligns five spins.

Note that although only a single $S = \frac{3}{2}$ state was shown in the above breakdown of the wavefunction, there will be four $S = \frac{3}{2}$ generated by the coupling of the five electrons in the box and will simultaneously be contributing to the ground state of

the wavefunction as shown in Eq: 2.6.2 below. The equations below show explicit form of the wavefunction ($m_s = 0$) in terms of the configurations originating from the five spins of the box.

$$
\begin{aligned}
|\Psi\rangle^g = \Sigma_{jtrou}^{N_{trou}} \Big[C_{\frac{5}{2}}^{\frac{5}{2},\frac{5}{2}} \left(\left| \frac{5}{2}, -\frac{5}{2} \right\rangle + \left| -\frac{5}{2}, \frac{5}{2} \right\rangle \right) \Big] + \\
\Big[C_{\frac{3}{2}}^{\frac{5}{2},\frac{5}{2}} \left(\left| \frac{3}{2}, -\frac{3}{2} \right\rangle + \left| -\frac{3}{2}, \frac{3}{2} \right\rangle \right) + C'^{\frac{5}{2},\frac{3}{2}}_{\frac{3}{2}} \left(\left| \frac{3}{2}, -\frac{3}{2} \right\rangle + \left| -\frac{3}{2}, \frac{3}{2} \right\rangle \right) + \cdots \Big] + \\
\Big[C_{\frac{1}{2}}^{\frac{5}{2},\frac{5}{2}} \left(\left| \frac{1}{2}, -\frac{1}{2} \right\rangle + \left| -\frac{1}{2}, \frac{1}{2} \right\rangle \right) + C'^{\frac{5}{2},\frac{3}{2}}_{\frac{1}{2}} \left(\left| \frac{1}{2}, -\frac{1}{2} \right\rangle + \left| -\frac{1}{2}, \frac{1}{2} \right\rangle \right) + \cdots \Big]
\end{aligned} \tag{2.6.2}
$$

The notation is as follows, consider $C_{\frac{3}{2}}^{\frac{5}{2},\frac{3}{2}}$ for example, the superscript $\frac{5}{2}, \frac{3}{2}$ represent the spin in each box and the subscript represents the m_s component of the spin states. The primed coefficients C' represents the contributions resulting from the different $S = \frac{3}{2}$ configurations present inside the box. This makes the decontamination of the various contributions due to mixed $S = \frac{5}{2}$,$S = \frac{3}{2}$ and $S = \frac{1}{2}$ in the box difficult. We have used the Clebsch-Gordan Coefficients (CGC) in order to find an analytic expression for the total contribution from the $S = \frac{5}{2}$ determinant inside the box. Knowledge of the CGC's allows one to get the weight of the full $S = \frac{5}{2}$ simply from the weight of the $m_s = \frac{5}{2}$ configuration. The formulas for the weight of the $m_s = \frac{5}{2}$ determinant in the CGC's for the different spin states are shown in Table: 2.5. These allow us to extract the full weight of the $S = \frac{5}{2}$ configuration in the ground state wavefunction.

Spin state	Weight($S = \frac{5}{2}$)
0	$3 \cdot C_{\frac{5}{2}}^{\frac{5}{2},\frac{5}{2}} \cdot C_{\frac{5}{2}}^{\frac{5}{2},\frac{5}{2}}$
1	$\frac{35}{25} \cdot C_{\frac{5}{2}}^{\frac{5}{2},\frac{5}{2}} \cdot C_{\frac{5}{2}}^{\frac{5}{2},\frac{5}{2}}$
2	$\frac{42}{25} \cdot C_{\frac{5}{2}}^{\frac{5}{2},\frac{5}{2}} \cdot C_{\frac{5}{2}}^{\frac{5}{2},\frac{5}{2}}$
3	$\frac{90}{25} \cdot C_{\frac{5}{2}}^{\frac{5}{2},\frac{5}{2}} \cdot C_{\frac{5}{2}}^{\frac{5}{2},\frac{5}{2}}$
4	$14 \cdot C_{\frac{5}{2}}^{\frac{5}{2},\frac{5}{2}} \cdot C_{\frac{5}{2}}^{\frac{5}{2},\frac{5}{2}}$
5	$126 \cdot C_{\frac{5}{2}}^{\frac{5}{2},\frac{5}{2}} \cdot C_{\frac{5}{2}}^{\frac{5}{2},\frac{5}{2}}$

Table 2.5: The weights of the $S = \frac{5}{2}$ for each state in terms of the weight of the $m_s = \frac{5}{2}$ determinants.

The values obtained for S_{box} using the S^2_{box} operator and the above method to get the weight of the local $S = \frac{5}{2}$ are shown in Fig: 2.18a and 2.18b. The fact that the two plots show perfect agreement points to the fact that S_{box} is adequate to judge the nature of the lowest lying states.

Similar analysis has been carried out for the case of the coupling of three $S = \frac{5}{2}$ spins. Contrary to the previous case where each state resulting from the coupling of two spin $S = \frac{5}{2}$ was unique, the coupling of three $S = \frac{5}{2}$ spins would generate state with multiplicities more than one. This is illustrated in Eq: 2.6.3.

$$(0 \oplus 1 \oplus 2 \oplus 3 \oplus 4 \oplus 5) \otimes \frac{5}{2} = \frac{15}{2} \oplus \underbrace{\frac{13}{2}}_{2} \oplus \underbrace{\frac{11}{2}}_{3} \oplus \underbrace{\frac{9}{2}}_{4} \oplus \underbrace{\frac{7}{2}}_{5} \oplus \underbrace{\frac{5}{2}}_{6} \oplus \underbrace{\frac{3}{2}}_{4} \oplus \underbrace{\frac{1}{2}}_{2} \quad (2.6.3)$$

The coupling between three spins $S = \frac{5}{2}$ would then give their corresponding CGC which can then be used to get the weights of $S = \frac{5}{2}$ states in the ground state. Note that contrary to the previous case, there are no unique CGC, and they would depend on the topology of the system. The second problem in the case of three $S = \frac{5}{2}$ is that all states with the exception of $S = \frac{15}{2}$, have a multiplicity greater than one. Finally, we also find that contrary to the previous case, the coefficients will not be the same for different spin states. Take for example the first excited state $S = \frac{3}{2}$. This state will not show up in the $m_s = \frac{5}{2}$ subspace which contains the three important $m_s = \frac{5}{2}$ determinants. Thus, the complexity of the problem is significantly increased with respect to the previous case. We have used the S^2_{box} operator to simplify the analysis for 9_3h and larger systems.

2.6.2 6 sites vs 8 sites

In this section we will show a comparison of the S_{box} values for 6_2h and 8_2h systems. This is important in order to show that the value for which a single hole aligns five spins is independent of the size of the system and also its dependence on the presence of a second hole. The Fig: 2.19 and Fig: 2.20 compare the S_{box} values for the two systems.

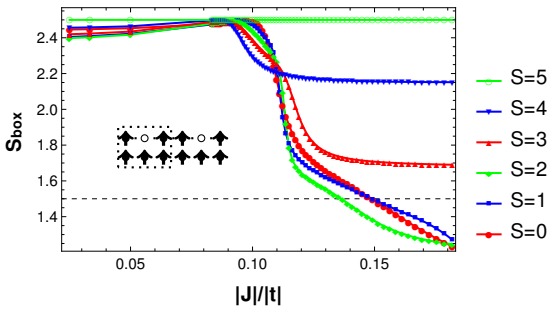

Figure 2.19: The 6_2h system as compared to the 8_2h system, concerning the S_{box} values.

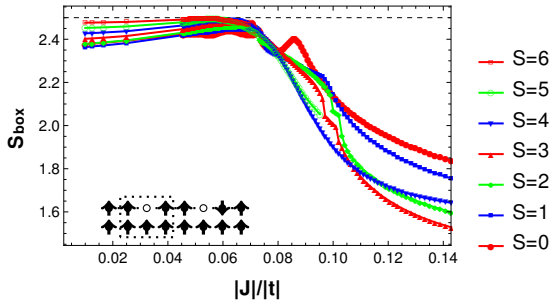

Figure 2.20: The S_{box} values for the 8_2h system.

The figures show the S_{box} values for a box with three sites in the two systems (6_2h, 8_2h). The value of J for which a single hole aligns all five spins in the box remains between 0.07 and 0.1. We argue the slight difference is due to the difference in the topology of the two systems. The 6_2h system is more adapted topologically for calculating the S_{box} value with three sites in the box and the 8_2h system is more adapted for calculating S_{box} with four sites in the box. The above analysis shows that the hole alignment is independent of the size of the system, as we see that although the hole has four available sites, it aligns only five spins (three sites) for given values of J. Therefore, the analysis done for small systems would be appropriate for extrapolation to larger systems.

2.6.3 1hole vs 2holes

Another question that must be answered is the interaction of the holes between each other. Does the presence of another hole affects the number of spins aligned ? The present section tries to answer this question on comparing the S_{box} value for three sites and four sites in the box in a 10_1h and 10_2h system. If the two holes do not interact, the value of J for which the hole/holes align five spins should be the same. It is clear from the Fig: 2.21 that the two holes interact. Although the interaction is quite small, it appears that two holes each will align five spins faster than a single hole. As a consequence, the size of the polaron, for a given value of the parameters increases with the doping.

Another manner to compare the influence of the second hole is to look at the two systems with the same effective number of sites per hole. This can be done with a comparison of the 5_1h and the 10_2h system. A plot of S_{box} values with three sites in the box is shown in Fig 2.22. In this case, there seems to be little influence of the second hole and the value of J for which five spins (3 sites) have been aligned seem to be almost the same $J \approx 0.06$ for the two systems.

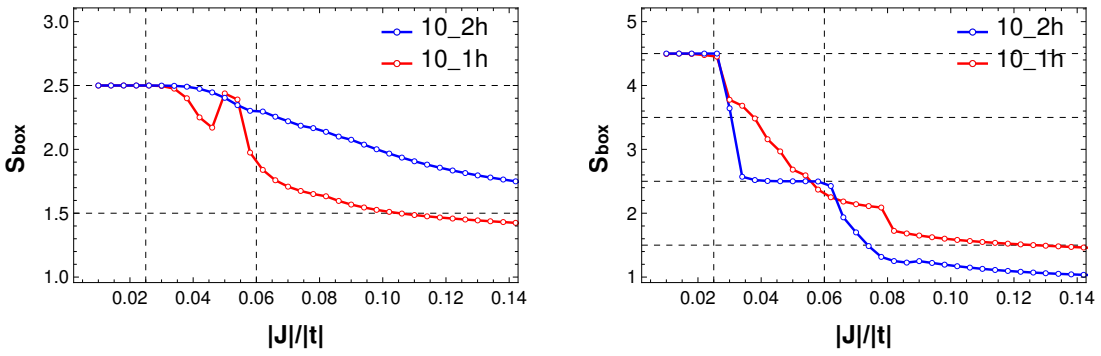

(a) Box of three sites.

(b) Box of five sites.

Figure 2.21: The comparison of the number of spins aligned in a box with three and five sites for various values of J for the one-hole 10_1h and two-hole 10_2h system.

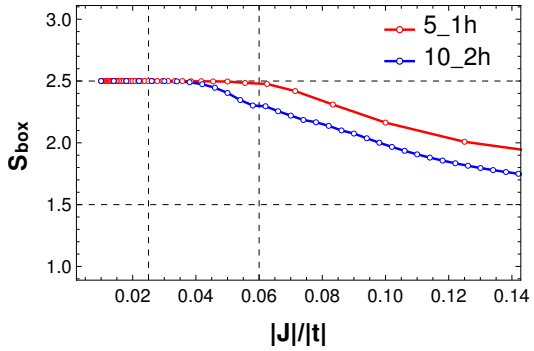

Figure 2.22: The comparison of the S_{box} values for the 5_1h and 10_2h systems. We consider only three sites in the box for the two cases..

2.6.4 DE vs SE

The DE mechanism creates a ferromagnetic polaron surrounding the hole, as we saw above. In this section we attempt to answer two questions. Firstly, does the polaron persist when there is another hole. Secondly, we would like to find the nature of the interaction, i.e. ferromagnetic or antiferromagnetic, between the two polarons surrounding the holes. In Fig: 2.23 we show a comparison of the ground state and S_{box} values for four representative values of J and K. It appears that, at least for small systems, there are two ferromagnetic polarons surrounding the two holes. Thus, the ferromagnetic polaron survives and hole pairing is minimal as expected. The coupling between the two ferromagnetic regions seems to be antiferromagnetic in character resulting in a low spin state. Thus, even though

each hole has aligned five spins around it, the ground state is a low spin state resulting from an antiferromagnetic coupling between the two $S_{box} = \frac{5}{2}$ regions. The Fig: 2.23 represents the basic idea of this thesis. Each hole has aligned five spins due to the double exchange mechanism but it is the super exchange coupling which leads to an antiferromagnetic coupling between the polarons and a low spin ground state.

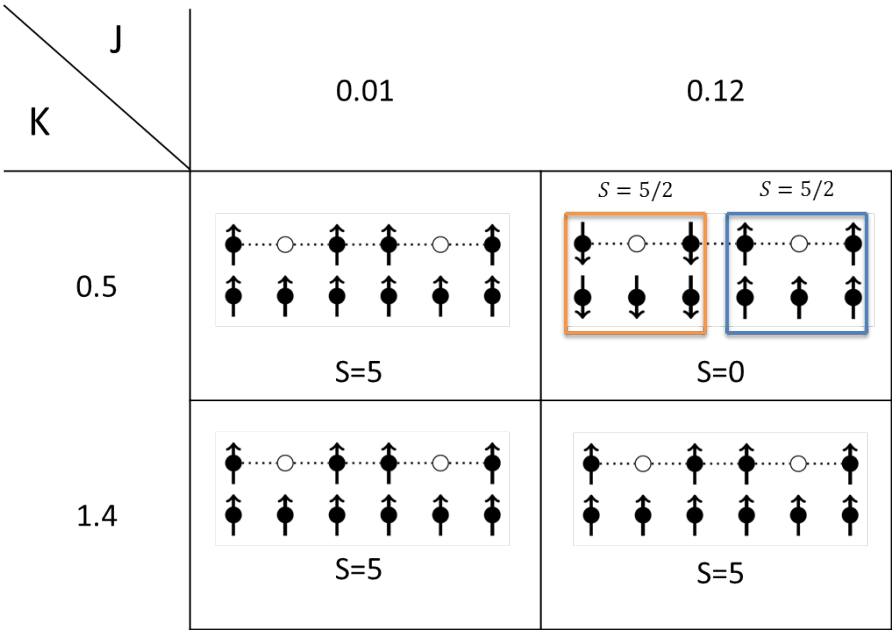

Figure 2.23: The interaction between two ferromagnetic polarons for four representative values of J and K

2.6.5 Effect of Doping ratio

Previous theoretical studies of the effect of doping ratio on the $t-J$ Hamiltonian have concluded that with an increase in hole concentration, the ferromagnetic character of the system should increase [69]. The impurities locally favor a ferromagnetic ground state. Increase in the doping ratio would therefore make the system more ferromagnetic. The question, however, concerns the interaction between the impurities, does it favor ferromagnetism also in the DE model? In order to compare the spin alignment S_{box} by a single hole in the presence of multiple impurities, we present in Fig: 2.24 a comparison of the S_{box} vs doping ratio. In order to eliminate topological effects in the comparison we have kept the size of the system constant ($N_{sites} = 9$) as well as the interaction parameters J and K constant. It is clearly seen that there is an increase in the amount of spin aligned by a single hole with an increase in the doping ratio. This seems to indicate that although there is no explicit interaction between the holes, they communicate indirectly via the hopping term t and the effective exchange term J. For very large values of doping ratio, the ferromagnetic domains of holes overlap resulting in a FM phase with mobile holes. Whereas, for low doping, the holes tend to stay localized inside their own FM domains with an antiferromagnetic interaction between adjacent FM polarons which facilitate the motion of the polaron in an AF spin chain.

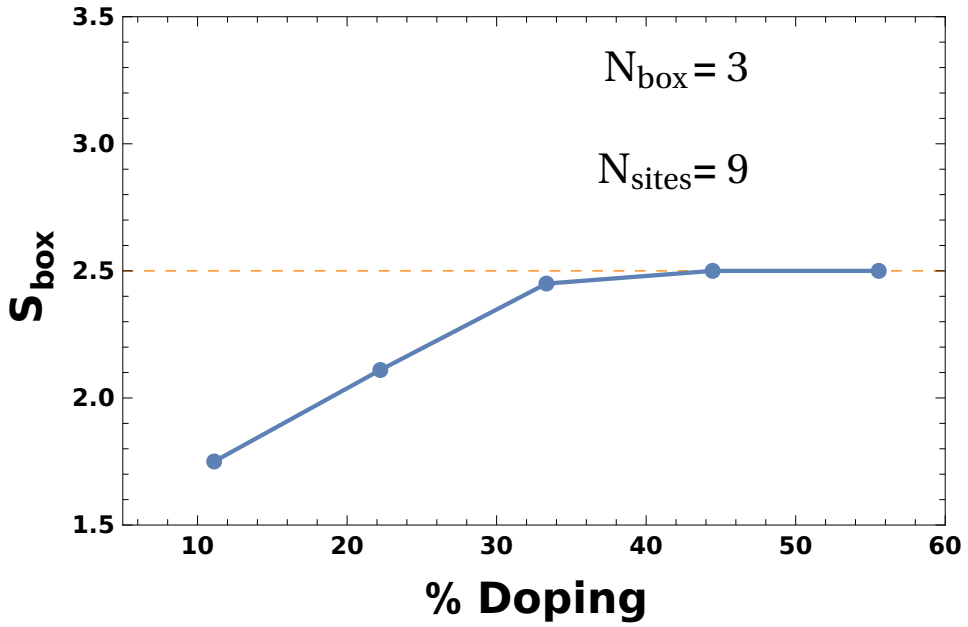

Figure 2.24: A comparison of S_{box} for various doping ratios in a system where J and K are kept constant at $K = 0.8$ and $J = 0.1$ for $N_{box} = 3$.

2.7 Conclusion

In this study we have used the truncated spin density operator to analyze quantitatively the size of the ferromagnetic polaron surrounding a hole. Firstly, we have shown that for values of J and K, t corresponding to real materials, a single hole aligns three to four sites. The extent of this ferromagnetic cloud decreases with increasing J, whereas increasing the value of K increases the size. We emphasize that in usual calculations on the DE model, the value of the Hund interaction is taken to be very large $K \approx 20|t|$, whereas in the present study, we have shown that K plays a crucial rule on the low energy physics of the DE system. Our important contribution is the rationalization of role played by the Hund term K.

The approximations resulting from using a finite number of sites and open boundary conditions were also tested by showing that the extension of the ferromagnetic polaron does not qualitatively change with the size of the system. Lastly, we have shown that on increasing the doping ratio, there is not much effect on the number of spins aligned per hole although there is a slight preference to align more spins. This shows that even in the absence any explicit interaction between the holes, there is a natural tendency of the holes to communicate indirectly. The CMR effect in manganites is observed for doping rations between 25 to 30 percent [3]. In our analysis, we find that for physical values of J and K, a single hole would align from three to four sites. It is therefore postulated that the systems which show CMR are governed by a similar physics. In the following chapter, we show how the influence of magnetic field on the electronic delocalization can be rationalized by the above picture.

Chapter 3

Collective effects II

The objective of this chapter is to study the electronic delocalization in 1D systems and the effect of the magnetic field. Models containing two or more holes are studied close to values of J and K for which each hole has aligned five or seven spins. Finally, we will try to understand the nature of the conducting and insulating states in the context of DE.

3.1 Electron delocalization

3.1.1 Literature review

The question of a measure of the metallic nature of a substance in the context of quantum mechanics, was first tackled by Kohn in his seminal paper from 1964 [115]. There he introduced the notion of electron localization in the framework of quantum mechanics. A more tangible description of the localization in a quantum mechanical wavefunction was given by Resta and Sorella [116](RS). Their paper introduces the notion of the localization spread of the electronic distribution in the ground state wavefunction as a measure of the insulating or metallic character of the state. Using the definitions of localization given by RS, the works of G. Bendazzoli *et al* [117, 118, 119, 120, 121] have demonstrated the usefulness of a Total Position Spread (TPS) tensor (**Eq: 3.1.2**) in the determination of the delocalization present in the system. We have used this quantity in our analysis in order to distinguish the conducting states from the localized ones. The fundamental problem that we must overcome is that the notion of current (and therefore conduction) cannot be strictly defined for an open (non-cyclic) finite system.

3.1.2 Formalism

The formalism given by RS consists of the definition of a localization λ as follows:

$$\lambda^2 = \left\langle x^2 \right\rangle - \langle x \rangle^2 \tag{3.1.1}$$

where $\langle\rangle$ denotes the usual expectation value. This quantity has been called the Total Position Spread (TPS) by G. Bendazzoli *et al* as it also corresponds to the second cumulant of the electron position (variance of the position.) **Note that this formulation makes the TPS invariant under translation (or rotation) of the coordinate system.** It is also important to note that the value of TPS is independent of the M_s subspace used for the calculation and **does not change upon the change of the M_s for a given spin state.** Since our Hamiltonian does not involve doubly occupied determinants, an alternative definition of the TPS (Eq: 3.1.3) can be given in terms of the motion of the hole. In this case, we can say that the **TPS also satisfies hole particle symmetry** on the condition of changing the original operator accordingly. This is not to say that the TPS is independent of the spin correlation, of course the hole mobility is strongly affected by the spin correlation in the system as will be shown in the following sections.

$$\text{TPS} = \left\langle x^2 \right\rangle_c = \langle\psi| \sum_{ij} \hat{x}_i \hat{x}_j |\psi\rangle - \left(\langle\psi| \sum_i \hat{x}_i |\psi\rangle \right)^2 \tag{3.1.2}$$

$$\text{TPS} = \left\langle x^2_{hole} \right\rangle_c = \langle\psi| \sum_{ij} \hat{x}_{i,hole} \hat{x}_{j,hole} |\psi\rangle - \left(\langle\psi| \sum_i \hat{x}_{i,hole} |\psi\rangle \right)^2 \tag{3.1.3}$$

where $\hat{x}_i$ is the operator $(x_i \cdot \hat{n}_i)$, $\hat{n}_i$ being the occupation number operator and x_i, the position of the i^{th} electron. Similarly, $\hat{x}_{i,hole}$ is $(x_{i,hole} \cdot (1 - \hat{n}_i))$, where $x_{i,hole}$ gives the position of the i^{th} hole. The summation carries over the number of particles (electrons, holes). Let us take for instance the $\hat{x}_i$ operators that give the position of the i^{th} electron from the origin. In the general case the two operators $\hat{x}$ and $\hat{x}^2$ would be written as:

$$
\begin{aligned}
\hat{x} &= \sum_i \hat{x}_i \\
\hat{x}^2 &= \sum_{ij} \hat{x}_i \hat{x}_j \\
\text{where; } x_i &= \sum_j \langle i|x|j\rangle \, a_i^\dagger a_j \\
\text{therefore; } \hat{x} &= \sum_{ij} \langle i|x|j\rangle \, a_i^\dagger a_j \\
\hat{x} &= \sum_i \langle i|x|i\rangle \, a_i^\dagger a_i + \sum_{i\neq j} \langle i|x|j\rangle \, a_i^\dagger a_j \\
\hat{x}^2 &= \sum_{ij} \langle i|x|i\rangle \, \langle j|x|j\rangle \, a_i^\dagger a_j^\dagger a_j a_i + \sum_{ij,kl} \langle i|x|k\rangle \, \langle j|x|l\rangle \, a_i^\dagger a_j^\dagger a_l a_k
\end{aligned}
$$

where i, j are the atomic orbitals constituting the determinants. Since in our model we have replaced atomic orbitals with delta functions (δ_i) which have the following property:

$$
\langle \delta_i|\delta_j\rangle = \begin{cases} 1, & \text{if } i = j \\ 0, & \text{otherwise} \end{cases}
$$

and

$$
\langle \delta_i|x|\delta_j\rangle = \begin{cases} x_i, & \text{if } i = j \\ 0, & \text{otherwise} \end{cases}
$$

Therefore, only the diagonal terms of the two operators survive. Note that this would not be so in *ab initio* calculations.

$$
\begin{aligned}
\hat{x} &= \sum_i (x_i)\hat{n}_i + 0 \\
\hat{x}^2 &= \sum_{ij} (x_i x_j)\hat{n}_i \hat{n}_j + 0
\end{aligned}
$$

where $\hat{n}_i$ is the occupation number operator for atomic orbital i.
Following the $D_{\infty h}$ symmetry of the system, the origin in all our calculations has been fixed at the center of the system as shown in Fig: 3.1. This leads to the vanishing of the second term in Eq: 3.1.2, i.e. the average position of the electrons $\langle x\rangle$. Therefore, in this case, we only need to calculate the $\langle x^2\rangle$ value. In order to demonstrate that $\langle x\rangle$ is strictly zero, one can proceed as follows. On integrating over the spin coordinates, the wavefunction given by $|\psi\rangle = \sum_j^n C_j \, |\phi_j\rangle$, where the indices run over the determinants that differ only by the position of the electrons. The one-body operator can be simplified as:

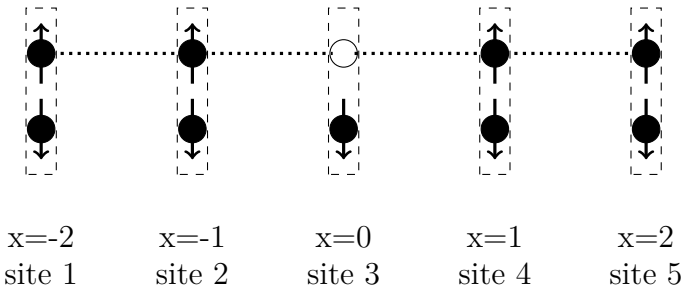

Figure 3.1: Definition of the position for a system of 5 sites.

$$\begin{aligned}
\langle x \rangle &= \langle \psi | \sum_{i}^{nelec} \hat{x}_i | \psi \rangle \\
\langle x \rangle &= \left(\sum_{k}^{ndet} C_k^\dagger \langle \phi_k | \right) \sum_{i}^{nelec} \hat{x}_i \left(\sum_{j}^{ndet} C_j | \phi_j \rangle \right) \\
\langle x \rangle &= \sum_{j}^{ndet} C_j^\dagger C_j \left(\sum_{i}^{nelec} \langle \phi_j | \hat{x}_i | \phi_j \rangle \right) \\
\langle x \rangle &= \sum_{j}^{ndet} X_j C_j^2
\end{aligned} \tag{3.1.4}$$

Here and in the equations that follow, N represents the number of sites. Since the system is symmetric with respect to inversion of coordinate x due to the $D_{\infty h}$ point group symmetry, C_j will be equal to C_{N-j} and $X_j = -X_{N-j}$, where $N - j$ is the index of the symmetric counterpart of determinant j. Using this symmetry one can see why the one-body term vanishes.

$$\begin{aligned}
\langle x \rangle &= \sum_{j}^{N/2} X_j C_j + \sum_{j}^{N/2} X_{N-j} C_{N-j} \\
C_j &= C_{N-j} \; \forall \; (j) \\
X_j &= -X_{N-j} \; \forall \; (j) \\
\langle x \rangle &= 0
\end{aligned} \tag{3.1.5}$$

The only term left is the two body operator $\hat{x}^2$. There are two ways to simplify the expression of the TPS. We can write the TPS in terms of the position of the electrons or the holes. In terms of electron operators, the TPS can be separated into contributions from α and β electrons as follows:

$$
\begin{aligned}
TPS &= \sum_i C_i^2 (\sum_{kl} \langle \psi_i | \hat{x}_k \hat{x}_l | \psi_i \rangle) \\
TPS &= \sum_i C_i^2 (TPS_i) \\
TPS_i &= \left(x_1^\alpha + x_2^\alpha + \cdots + x_1^\beta + x_2^\beta + \cdots \right)_i^2 \\
TPS_i &= TPS_{\alpha,i} + TPS_{\beta,i} + TPS_{\alpha\beta,i} \\
\text{where; } TPS_{\alpha,i} &= (x_1^\alpha + x_2^\alpha + \cdots)_i^2 \\
TPS_{\beta,i} &= \left(x_1^\beta + x_2^\beta + \cdots \right)_i^2 \\
TPS_{\alpha\beta,i} &= 2(x_1^\alpha + x_2^\alpha + \cdots)_i (x_1^\beta + x_2^\beta + \cdots)_i
\end{aligned}
\tag{3.1.6}
$$

where x_i^α and x_k^β are the position of the i^{th} and k^{th} α and β electrons respectively. Note that the sum $\left(x_1^\alpha + x_2^\alpha + \cdots + x_1^\beta + x_2^\beta + \cdots \right)$ can be related to the dipole moment of the determinant. This simplified form of the TPS is applicable also in the presence of doubly occupied determinants. The only problem with this form is its dependence on the electron coordinates which makes the analysis difficult. An alternative form of the TPS in terms of the position of the hole will be presented below.

Taking now the TPS in terms of the hole operators. We remind the readers that the indices of the wavefunction run over the determinants with different position of the particles since we have integrated over the spin components. The two-electron term can be separated into two parts. One consisting of purely a one-body term and a second, the off diagonal term, as shown below. Here x_i represents the position of the holes. For the one-body part we have:

$$
\begin{aligned}
\left\langle x^2 \right\rangle &= \langle \psi | \sum_{i,j} \hat{x}_i \hat{x}_j | \psi \rangle \\
\sum_{i,j} \hat{x}_i \hat{x}_j &= \sum_i \hat{x}_i \hat{x}_i + \sum_{i \neq j} \hat{x}_i \hat{x}_j \\
\sum_i \hat{x}_i \hat{x}_i | \psi \rangle &= \sum_j \left(\sum_i \hat{x}_i \hat{x}_i C_j | \phi_j \rangle \right) \\
\sum_j C_j^\dagger \langle \phi_j | \left(\sum_i \hat{x}_i \hat{x}_i \right) C_j | \phi_j \rangle &= \sum_j Y_j C_j^2
\end{aligned}
\tag{3.1.7}
$$

where C_j is the coefficients of the corresponding determinant ϕ_j and Y_j is the expectation value of the $\langle x^2 \rangle$ operator on ϕ_j. For the bi-electronic part we have:

$$\sum_{i\neq j} \hat{x}_i \hat{x}_j \left|\psi\right\rangle = \sum_k \left(\sum_{i\neq j} \hat{x}_i \hat{x}_j C_k \left|\phi_k\right\rangle \right)$$
$$\sum_{i\neq j} \hat{x}_i \hat{x}_j \left|\psi\right\rangle = \sum_k Z_k C_k \left|\phi_k\right\rangle$$
$$\left\langle\psi\right| \left(\sum_{i\neq j} \hat{x}_i \hat{x}_j \right) \left|\psi\right\rangle = \sum_k Z_k C_k^2 \tag{3.1.8}$$

The two integrals Y_k and Z_k represent the mono and the bi-electronic integrals corresponding to the mono and bi-electronic parts of the $\langle x^2 \rangle$ operator. In our case since we model the atomic orbitals as delta functions, the integrals give directly the distances of the atomic orbitals from the origin. The above expressions Eq: 3.1.7 and Eq: 3.1.8 can be further simplified for the **one hole** case as follows. Note that in the one hole case, the indices would then indicate the position of the holes:

$$\begin{aligned}
Y_k &= \sum_i \hat{x}_i \hat{x}_i \left|\phi_k\right\rangle \\
&= \left[\frac{m(m+1)(2m+1)}{3} - (m-k-1)^2 \right] \\
m &= \begin{cases} \dfrac{(n-1)}{2}, & \text{if } n \text{ is odd} \\ \dfrac{n}{2}, & \text{otherwise} \end{cases} \\
Z_k &= \sum_{i\neq j} \hat{x}_i \hat{x}_j \left|\phi_k\right\rangle \\
&= -Y_k + (m-k-1)^2
\end{aligned}$$

where k represents the position of the hole in ϕ_k. Thus, for the **one hole** case, we have an analytic expression for the TPS in terms of the hole position k, as shown in Eq: 3.1.9. Where we have taken the inter site distance to be of one units of length, i.e. $|x_i - x_{i+1}| = 1$.

$$\begin{aligned}
\left\langle\psi\right| \hat{x}^2 \left|\psi\right\rangle &= \sum_k \left(Y_k + Z_k\right) C_k^2 \\
&= \sum_k \left(m-k-1\right)^2 C_k^2
\end{aligned} \tag{3.1.9}$$

Thus, we can see that the TPS measures the delocalization in the system. Take the example of the case of strong J where the ground state wavefunction ($\left|\psi\right\rangle$) is

dominated only by two determinants, one consisting of the hole at site 1 and the other at site n. In this case, the TPS would be:

$$\begin{aligned} C_1^2 = C_n^2 &= \frac{1}{2} \\ C_k &= 0 \ \forall (k \neq 1, k \neq n) \\ TPS_{Smin} &\leq \frac{1}{2}\left(\frac{n-1}{2} - 2\right)^2 + \frac{1}{2}\left(\frac{n-1}{2} - n - 1\right)^2 \\ TPS_{Smin} &\leq \frac{1}{8}\left[(n-5)^2 + (n-1)^2\right] \end{aligned}$$

A complete analytic expression can be given for the maximal spin state S_{max}. The ground state wave vector of the maximal spin state with **one hole** would be a Hückel state, the analytic form of which is known. Thus, for the S_{max} state with a single hole we have:

$$\begin{aligned} TPS_{Smax} &= \langle \psi_{smax} | \, \hat{x}^2 \, | \psi_{smax} \rangle = \sum_j (m - j - 1)^2 \, C_j^2 \\ TPS_{Smax} &= \frac{n^3 + 3n^2 + \mathcal{O}(n)}{12(n+1)} \end{aligned} \tag{3.1.10}$$

As we see from Eq: 3.1.10, the TPS diverges quadratically with the number of sites n for the maximal spin state S_{max}. This would indicate that the S_{max} state is more metallic in nature compared to the S_{min} ground state at the $J \to \infty$ limit. This is not surprising since the high spin states are the ones which allow for the metallic character of the system.

Similarly, for the **two-hole** case, one can find analytic expressions for the TPS as a function of the ground state coefficients. In this case the wavefunction, after summing over the spin indices, will be represented in terms of two indices k, l which represent the position of the two-holes $\left(\sum_{k,l} C_{k,l} \psi_{k,l}\right)$. The expression for the mono-electronic term Y is:

$$\begin{aligned} Y_{k,l} &= C_{k,l}^2 \, \langle \phi_{k,l} | \sum_i \hat{x}_i \hat{x}_i \, | \phi_{k,l} \rangle \\ Y_{k,l} &= \left[\frac{n^3 - n}{12} - (m - k + 1)^2 - (m - l + 1)^2\right] \cdot C_{k,l}^2 \end{aligned} \tag{3.1.11}$$

where k and l $(k \neq l)$ are indices that run over all the positions for the two-holes and characterize the determinant for which the holes are located at position k and

l. The number of sites is taken as n. Similarly, for the bi-electronic term Z we have:

$$
\begin{aligned}
Z_{k,l} &= C_{k,l}^2 \langle \phi_{k,l} | \sum_i \sum_j \hat{x}_i \hat{x}_j | \phi_{k,l} \rangle \\
Z_{k,l} &= \left[-Y_{k,l} + (m-k+1)^2 + 2(m-k+1)(m-l+1) + (m-l+1)^2 \right] \cdot C_{k,l}^2 \\
Z_{k,l} &= \left[-Y_{k,l} + \left(2\frac{(n+1)}{2} - (k+l) \right)^2 \right] \cdot C_{k,l}^2 \qquad (3.1.12)
\end{aligned}
$$

therefore, the simplified form of the TPS for the two-hole case is:

$$
\begin{aligned}
TPS_{k,l} &= \sum_{k \neq l} (Y_{k,l} + Z_{k,l}) \\
TPS_{k,l} &= \sum_{k \neq l} \left[(n+1) - (k+l) \right]^2 \cdot C_{k,l}^2
\end{aligned}
$$

The above form of the TPS is much easier to manipulate than the previous one (Eq: 3.1.6) in terms of electron positions. It is important to note that the mono-electronic term Y is always positive whereas the bi-electronic term Z is almost always negative. It is the interplay between the two terms (Y, Z) that gives rise to the remarkable sensitivity to changes in electron distribution in the system, as we shall see in the section that follows.

It can be noticed immediately that the TPS will be zero for all determinants which are centrosymmetric. It would now be possible to derive similar formulae for three and more holes. In fact such a formula of the TPS in terms of the position of the holes turns out to be quite simply:

$$
\begin{aligned}
TPS &= \left\langle x_{holes}^2 \right\rangle_c \\
TPS &= \langle \psi | \sum_{ij} \hat{x}_{i,hole} \hat{x}_{j,hole} | \psi \rangle \\
TPS &= \sum_i (x_{i,hole} + x_{j,hole} + \cdots)^2 C_i^2
\end{aligned}
$$

3.1.3 Physical meaning of the TPS

Firstly, let us begin by noticing that the electronic dipole moment of a molecular system in state Φ_0 is given by:

$$d_x \propto \langle \Phi_0 | \hat{x} | \Phi_0 \rangle$$

and the x component of the quadrupole moment is given by:

$$Q_{xx} \propto \langle \Phi_0 | \sum_i \hat{x}_i \hat{x}_i | \Phi_0 \rangle$$

Therefore, we can see that the dipole moment, the quadrupole moment and the TPS are intricately related. Hence, it is not strange that TPS is able to distinguish between metals and insulators.

In a relatively recent review article by Resta [122], it was shown that the TPS can be written in terms of particle velocities ($\hat{v}_i$) as follows:

$$\begin{aligned} \langle r_i r_j \rangle_c &= \frac{1}{\hbar^2} \sum_{n \neq 0} \frac{\langle \psi_0 | \hat{v}_i | \psi_n \rangle \langle \psi_n | \hat{v}_j | \psi_0 \rangle}{(E_0 - E_n)^2} \\ &= \frac{1}{\hbar^2} \sum_{n \neq 0} \frac{\langle \psi_0 | \hat{v}_i | \psi_n \rangle \langle \psi_n | \hat{v}_j | \psi_0 \rangle}{\omega_{0n}^2} \end{aligned} \tag{3.1.13}$$

where $\omega_{0n} = (E_0 - E_n)/\hbar$. Meanwhile, the conductivity $\sigma(\omega)$ of a multi-electron system in the presence of an electric field of frequency ω is given by the Kubo formula and can also be written in terms of the velocities $\hat{v}_i$ as follows:

$$\sigma_{ij}(\omega) = \frac{ie^2}{\hbar L^3} \lim_{\eta \to 0+} \sum_{n \neq 0} \frac{1}{\omega_{0n}} \left(\frac{\langle \psi_0 | \hat{v}_i | \psi_n \rangle \langle \psi_n | \hat{v}_j | \psi_0 \rangle}{\omega - \omega_{0n} + i\eta} + \frac{\langle \psi_0 | \hat{v}_j | \psi_n \rangle \langle \psi_n | \hat{v}_i | \psi_0 \rangle}{\omega + \omega_{0n} + i\eta} \right) \tag{3.1.14}$$

One may notice the similarity between the formula for the TPS Eq: 3.1.13 and the Kubo conductivity Eq: 3.1.14. This expression for the conductivity given by Kubo allows us to compare the Localization tensor as defined in Eq: 3.1.13. Finally, looking the two equations Eq: 3.1.13 and Eq: 3.1.14, we have a direct relation between the Localization tensor and the conductivity:

$$\langle x_i x_j \rangle = \frac{\hbar L^3}{\pi e^2 N} \int_0^\infty \frac{d\omega}{\omega} \sigma_{ij}^+(\omega) \tag{3.1.15}$$

Therefore, although $\langle x_i x_j \rangle$ is a ground state property, the RHS of Eq: 3.1.15 concerns the response property of excited states. As stated by Resta himself:

Indeed, both equations ... (Eq: 3.1.15) look like the zero-temperature limit of a fluctuation dissipation theorem, several forms of which are known in statistical physics : in the lhs we have a groundstate fluctuation ... while the ingredient of the rhs is conductivity (dissipation).

Although, the analytical expressions presented above are adequate, it does not help us to gain sufficient qualitative interpretation of the physics measured by the TPS. In the following paragraphs, we will see how one can understand the TPS in terms of more intuitive tools.

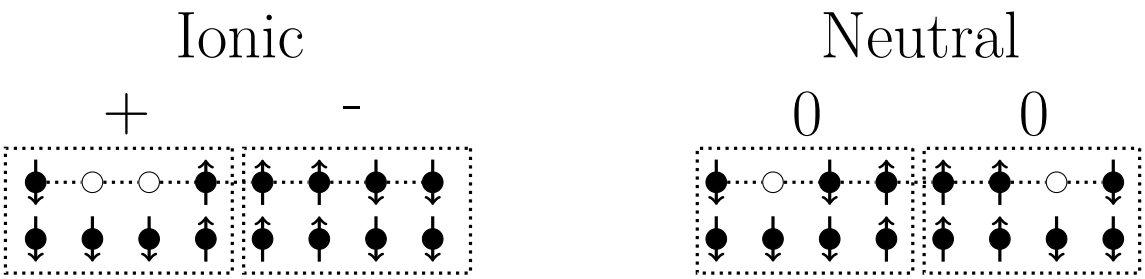

Figure 3.2: Definition of Ionic and Neutral determinants for the Double Exchange determinant space.

Take the DE Hamiltonian, which acts on a space made up of purely singly occupied determinants and holes. The "Ionic" determinants in this sense would then become difficult to define. Nevertheless, for values of J for which each hole has aligned a small ferromagnetic region while the ground state remains a low spin state, see Fig: 3.2, we can define "Ionic" and "Neutral" determinants such that two-holes occupy the same box, as shown above in Fig: 3.2.

Once we have classified the "Ionic" and "Neutral" determinants, we can then proceed to an analysis of the TPS in terms of this definition. Let us take a hypothetical wavefunction for the 8_2h system as follows:

$$|\Phi\rangle = \sum_{k \neq l} C_{k,l} \phi_{k,l}$$

where the indices k, l run over the various position of the two-holes (8_2h). Integrating over the spin space, there are in total 28 different position for the two-holes. Using now the formulae for TPS defined in the previous section, Eq: 3.1.11 and Eq: 3.1.12, we can find the expression for the TPS of such a general wavefunction as:

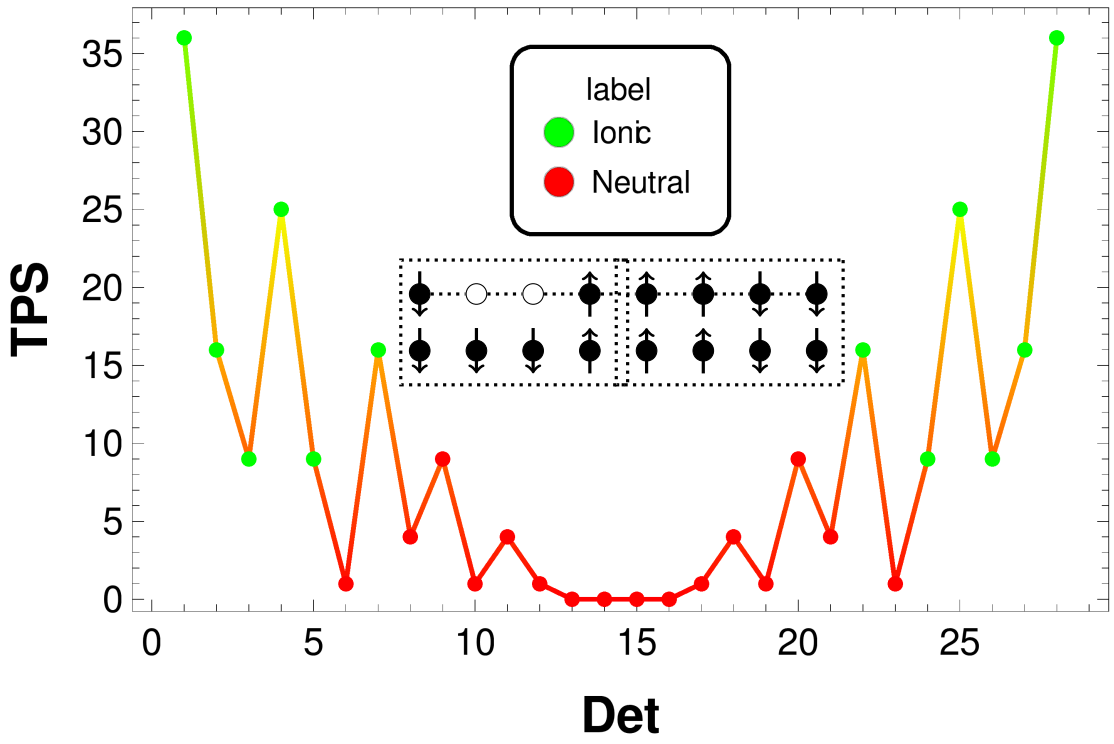

Figure 3.3: The TPS values for individual determinants of the 8_2h system, labeled by the position of holes only. The ionic and neutral determinants are labeled with green and red color respectively. As can be seen all ionic determinants have larger (or equal) TPS values compared to the neutral determinants.

$$\begin{aligned} TPS &= \sum_{k \neq l} \left(Y_{k,l} + Z_{k,l}\right) C_{k,l}^2 \\ &= \sum_{k \neq l} \left(\left((n+1) - (k+l)\right)^2\right) C_{k,l}^2 \\ &= \sum_{k \neq l} \left(TPS_{k,l}\right) C_{k,l}^2 \end{aligned}$$

Therefore, we have for each determinant k, l a contribution to the TPS which is given by the $TPS_{k,l}$. An important question is whether the contribution to the TPS ($TPS_{k,l}$) is the same for "Ionic" and "Neutral" determinants. In Fig: 3.3, we show this analysis, plotting the individual values of the TPS for the 28 determinants of the 8_2h system. The two types classes of determinants are marked with different colors, green for the "Ionic" and red for the "Neutral" determinants. It

can be seen clearly that the TPS is large for "Ionic" determinants and is small or zero for "Neutral" ones. **Thus it can be concluded that, quite simply, the TPS is an indicator of the ionic nature of an electronic wavefunction.** If the wavefunction Φ is dominated by ionic determinants (metallic character), the TPS will be large and vice versa. A more detailed comparison of the TPS and the weight of "Ionic" and "Neutral" determinants will be presented later in order to validate this idea.

In the following sections, we will show how the TPS allows one to draw rational conclusions about the amount of delocalization in the system as a function of J and K.

3.1.4 Applications

3.1.4.1 One-hole case

The evolution of the TPS with J (at $K = 0.8$) for all the states for the 5_1h system is reported in Fig: 3.4. The TPS of S_{max} state is constant whereas the TPS of the S_{min} state decreases with J. We observe that the TPS increases with the spin multiplicity of the states with S_{max} having the largest value. Therefore, when J increases, the TPS of the ground state decreases as its spin multiplicity decreases.

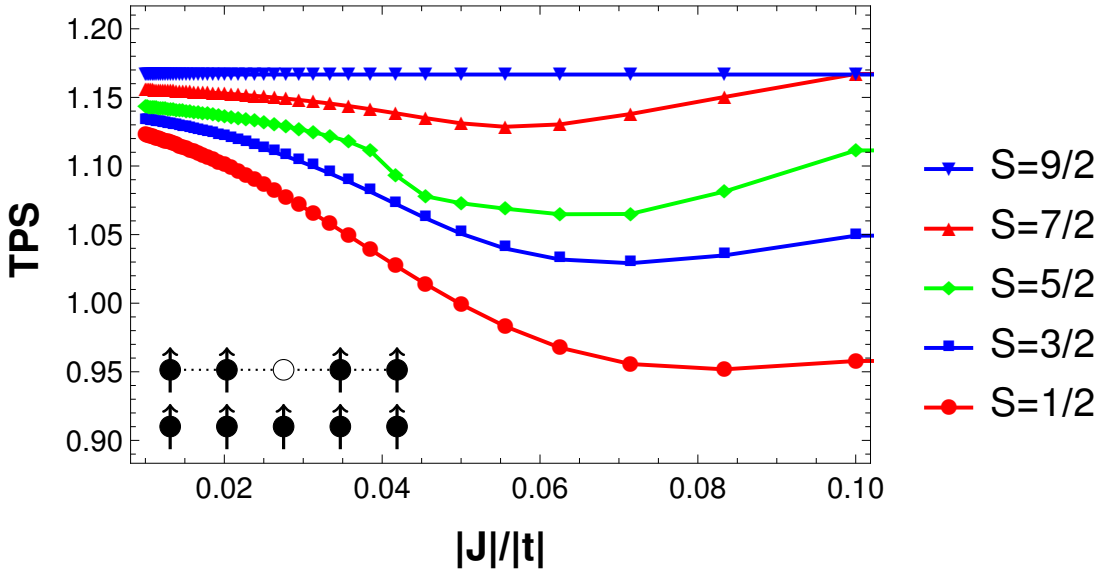

Figure 3.4: The TPS vs J for the 5_1h system for the fixed value of $K = 0.8$.

The variation of the TPS per site (TPS/N) with the size of the system for various values of J is shown in Fig: 3.5. The TPS/N does not show a monotonic increase for any values of J except for the $J = 0.0$ case, i.e. the S_{max} state (the black line), for which TPS/N shows a linear increase with N. In the definition of the TPS, Resta and Sorella demonstrated that the TPS **per site** (TPS/N) of a metallic state would diverge whereas it would tend towards zero for insulators. From the figure we see that only the S_{max} state or states close to S_{max} show divergence with N. Therefore, for the one-hole case, we conclude that the metallic nature of the system is dependent on J and the size of the system (N).

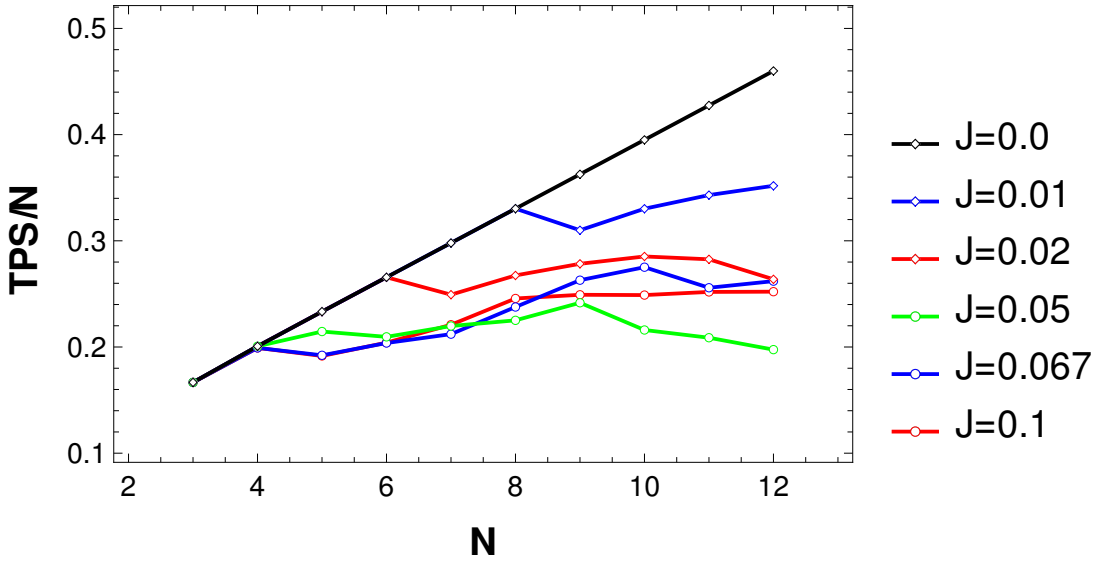

Figure 3.5: The TPS per site vs number of sites and for different values of J. The black line represents the analytic values obtained for the S_{max} state obtained from Eq: 3.1.10.

3.1.4.2 Two-hole case

The TPS plot for the 6_2h system is shown in Fig: 3.6. The TPS generally decreases with an increase in J for all spin subspaces. It is interesting to note the behavior at the limit ($J \to 0$). For system with a single hole, it appears that the TPS converges to the same value for all spin states, whereas for the two hole case, different spin states seem to converge to different values. Specifically, the amount of **delocalization in the high spin states** ($S = 5, S = 4$) **is much larger that that of a low spin states**.

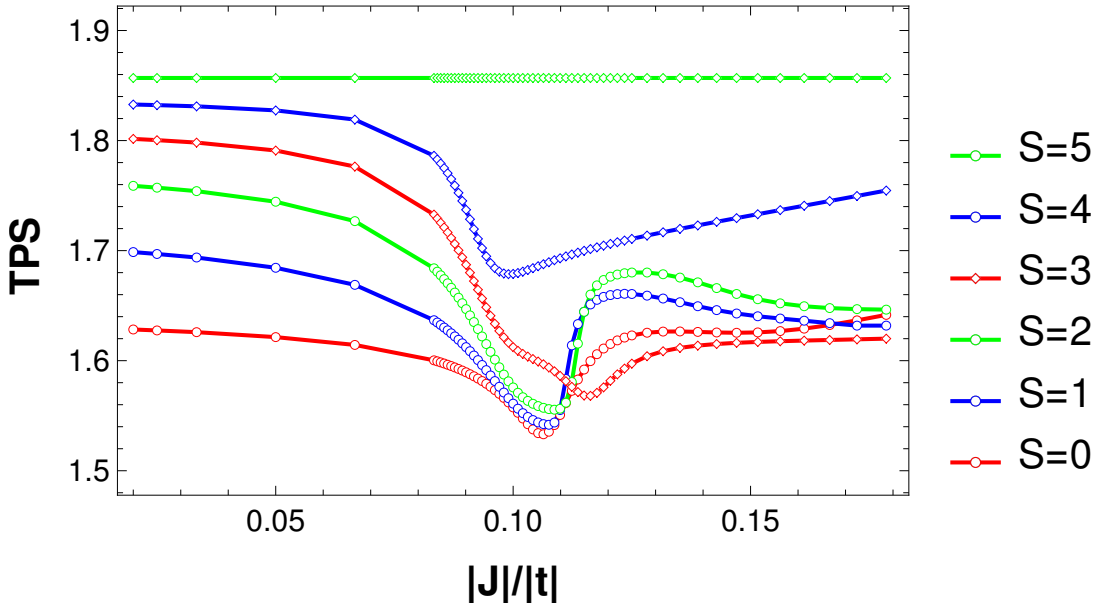

Figure 3.6: The TPS is shown for all six states of the 6_2h system.

3.1.4.3 Dependence of delocalization on doping

The TPS has been calculated for the ground state of the system with 12 sites and increasing number of holes in order to measure the effect of the delocalization on hole doping ratio. The values of $J = 0.1$ and $K = 0.8$ have been fixed. There is also an experimental work that shows the variation of the conductivity as a function of the doping ratio [2]. They study the conductivity of the $La_{1-x}Sr_xMnO_3$ 2D manganite for various values of the doping ratio x. This is a two dimensional doped double exchange system and therefore could be expected to follow similar tendencies as the 1D system studied here. The Fig: 3.7 shows a comparison of these experimental results with the TPS. Although the experimental work goes

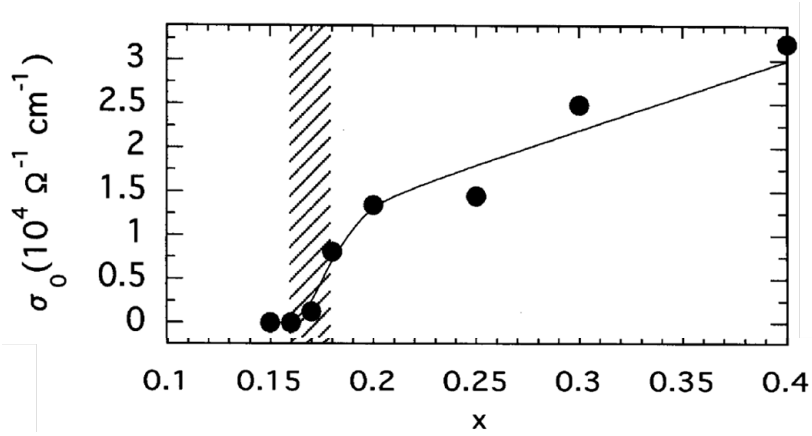

(a) Experimental results from Ref: [2], showing the conductivity for different doping ratios for the $La_{1-x}Sr_xMnO_3$ system.

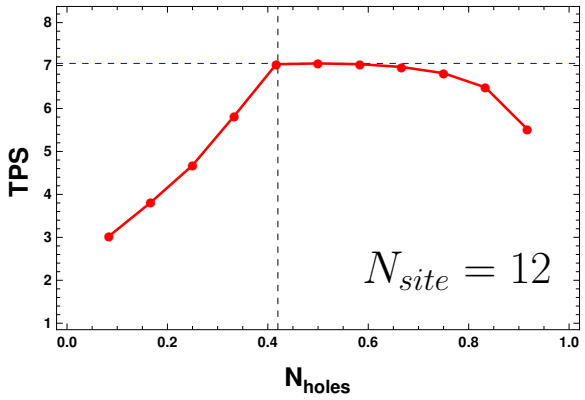

(b) The TPS as a function of the doping ration x for the 12 site system at $J = 0.1$ and $K = 0.8$.

Figure 3.7: The comparison of the experimental values of conductivity and the TPS, calculated for the 1D chain, with the doping ratio for a 12 site system.

only up until a doping ratio of $x = 0.4$, similar tendencies as the TPS are observed for the conductivity. The TPS increases up until a doping ratio of $x \approx 0.42$ and then decreases as the doping increases further and the experiment shows that the conductivity increases up until $x = 0.4$. Therefore, we expect that the qualitative physics represented by the TPS can be experimentally verified for specific systems.

3.1.5 Discussion on TPS

In order to understand the variations in the TPS, we have performed a comparison of the TPS for various systems with the S_{box} values. In the following two sections, we will demonstrate how the variations in the TPS can be used to predict critical points in the system.

3.1.5.1 TPS as an indication of an ordered phase

The critical points identified by the TPS tensor correspond to a drastic change in the electron distribution in the system. The TPS may be seen to be a response to the change in the nature of the wavefunction. Therefore a uniform size of the polaron would result in a constant TPS value whereas a change in the size of the polaron would show up as fluctuations in the TPS. A quantitative understanding of the type of change in the electron distribution is possible on a comparison of the TPS curves with the corresponding S_{box} values for a given system.

Firstly, we will compare the TPS and S_{box} plots for the system with $\frac{1}{3}$ doping. Consider the TPS values for the 6_2h and the 9_3h system, shown in Fig: 3.8 and Fig: 3.10. The changes in the TPS can be understood in the following manner:

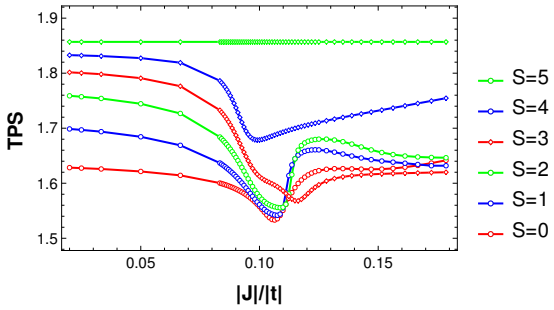

Figure 3.8: TPS as a function of J for the 6_2h system, the TPS is sensitive to critical points in the parameter space.

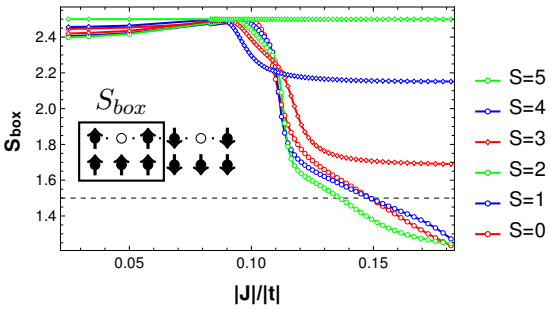

Figure 3.9: The figure shows the S_{box} values for all the spin states for various values of J for the 6_2h system. At about $J = 0.1|t|$, a single hole has aligned five spins inside the box.

- There is a maximum for both the systems at about $J \approx 0.12$, this maximum is explained in the next section 3.1.5.2.
- On further decreasing J, the configuration where each hole aligns five spins (3 sites) dominates. This increase in the extension of the polaron can be clearly seen in the S_{box} plots for 6_2h and 9_3h systems in Fig: 3.9 and Fig: 3.11 respectively.

- At this point where each hole aligns five spins (3 sites) and is localized in its own region, the TPS shows a very clear minimum. **This minimum in the TPS at about $J \approx 0.1$ for both systems corresponds to an order in the wavefunction where each hole has separately aligned five spins (3 sites) and is localized in its polaron.**

- Since the minimum occurs at almost the same point for both the systems i.e. at about $J \approx 0.1$, we can say that this ordered phase (five spin aligned) is not affected strongly by the size of the system.

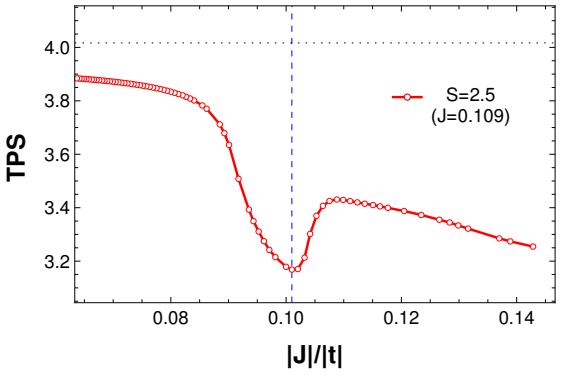

Figure 3.10: The dependence of the TPS on J for the 9_3h system shows two maximas corresponding to whether the hole has aligned three or five spins.

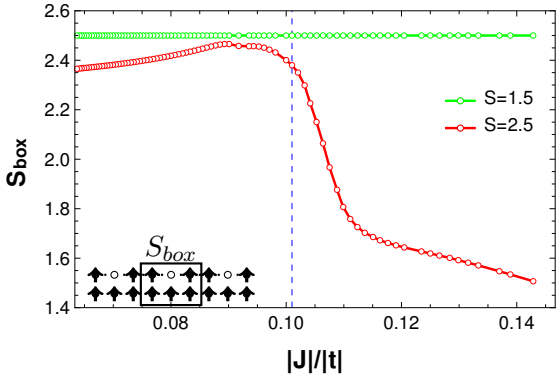

Figure 3.11: S_{box} for the 9_3h system where the hole has been fixed at the center.

Therefore, in conclusion, we find that for the two systems, the minimum of the TPS indicates an ordered phase. For the 6_2h and 9_3h system this order corresponds to the value of J at which a single hole aligns five spins (3 sites).

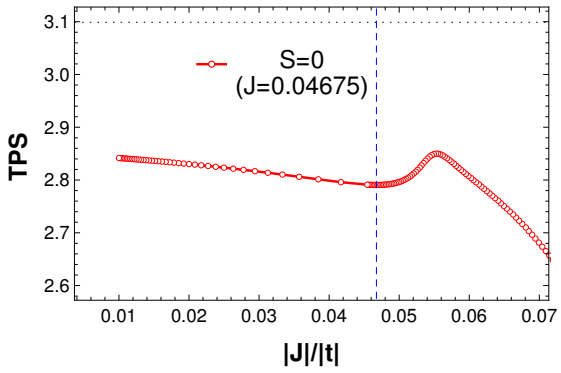

Figure 3.12: The TPS as a function of J for the $S = 0$ state of the 8_2h system, dotted line represents the value for the $S = 7$ state.

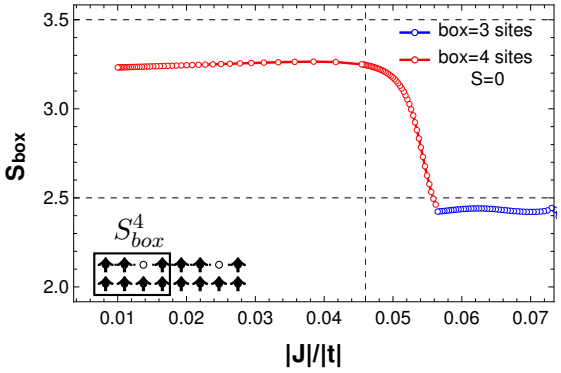

Figure 3.13: The S_{box} is calculated as a function of J with three and four sites in the box for the 8_2h system, all values correspond to the $S = 0$ spin state .

In order to find the value of J for which each hole aligns seven spins (4 sites), we have performed similar analysis for the 8_2h system. The TPS is plotted for the lowest $S = 0$ spin state at each value of J. The TPS curve shown in Fig: 3.12 clearly shows a minimum at $J \approx 0.05$ where S^4_{box} (box with 4 sites) has a maximum (Fig: 3.13). It is clear from the S_{box} plot for this value, the $S = 0$ state that the hole aligns seven spins (4 sites) at about $J \approx 0.05$. The minimum of the TPS also occurs very close to this value. Therefore, we conclude that similar to the 6_2h and 9_3h system, the critical point of the TPS for the 8_2h system corresponds to an ordered phase where a single hole aligns seven spins (4 sites). The above analysis for the 8_2h system validates our affirmation that **the minimum in the TPS corresponds to an ordered phase of the system.**

3.1.5.2 Double exchange vs Superexchange

The TPS plots for both the 6_2h and 9_3h systems show a maximum at about $J \approx 0.11$ for all states except the high spin states (e.g. $S = 5$ for the 6_2h). In this section, we will try to understand this local maximum.

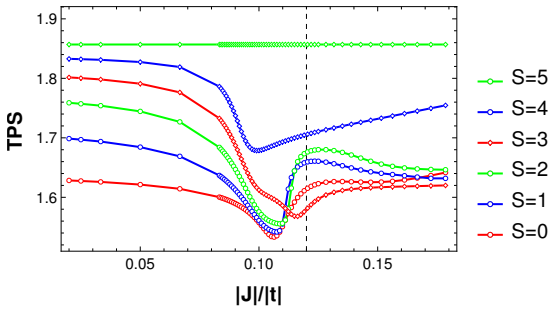

Figure 3.14: The TPS of 6_2h for the full range of J values.

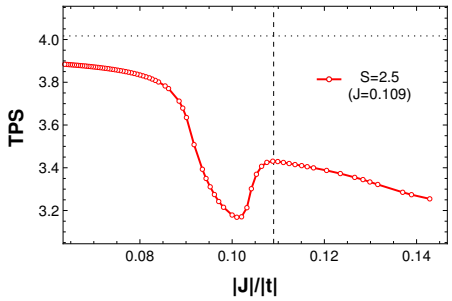

Figure 3.15: The TPS of 9_3h system. The dotted line is the TPS of the $S = 7.5$ state.

Take the 9_3h system as an example. For large values of J, the holes are located at the center (and the edges) of the system and do not have enough kinetic energy to align three spins (two sites). As we decrease the value of J by a small amount, the single hole is now able to align three spins (two sites). Initially, each of the polarons (of 2 sites) formed by the three holes will be aligned antiferromagnetically with each other. For sufficiently small values of J, these polarons will then be aligned parallel to each other in order to gain kinetic energy, this situation is shown in Fig: 3.16 on the right. There is another determinant where each hole has formed a polaron of five spins (3 sites) which are aligned antiferromagnetically with each other, this determinant is stabilized by J (i.e. SE). The two determinants are shown in the Fig: 3.16, these two are in competition with each other.

$$E \approx 2J + (6t) \qquad E \approx 3J + (4t)$$

Figure 3.16: The competition between aligning five spins (three sites) to three (two sites).

The competition can be explained as follows. For larger values of J, the determinant on the right (Fig: 3.16) dominates, i.e. the hole mobility is compromised in order to gain superexchange J. As J decreases, the determinant on the left of Fig: 3.16 dominates, where there is a loss of antiferromagnetic interaction J in favor of more kinetic energy of the holes (DE dominates). This is a typical case of

a competition between the DE mechanism which is trying to align as many spins as possible and the SE mechanism which is counteracting this effect. Indications of this competition can be clearly seen in the two TPS plots shown in Fig: 3.14 and Fig: 3.15. The small peak in the TPS value close to $J = 0.12$ for the 6_2h system and $J = 0.11$ for the 9_3h system correspond to the increase in mobility brought about by the configuration where each hole has aligned three spins which are aligned parallel to each other giving rise to a momentary increase in the hole spread. The subsequent decrease near the critical point at about $J = 0.1$ represents the case when the hole has aligned five spins and the polarons are antiferromagnetically aligned with each other, resulting in a decreased hole spread.

In summary, we state that the minima of the TPS correspond to the presence of an ordered phase in the wavefunction and has been corroborated by the S_{box} values. These critical points also enable us to pin point the value of J for which the hole has aligned five to seven spins. The ordered phases consequently have a reduced overall electron delocalization. Finally, we have also explained the maximum observed in the TPS just before this ordered phase. It is shown that the maximum is due to a competition between the DE and SE phenomenon. In the following section we will compare the entropy of the wavefunction with the TPS in order to verify whether that ordered phase leads to a decrease in total entropy of the system.

3.1.6 Density matrix analysis

In the paper by C. N. Yang [123] in the 60's, it was shown that extra-diagonal elements of the density matrices can be used to predict the critical properties (superfluid to metal transition) of a model system. We have used a similar analysis in order to extract information about the change in the nature of the states vs J (at $K = 0.8$). As a remark, we remind the reader that W. Kohn was aware of this work while writing his famous article on the "Theory of the Insulating State", he stated that although a density matrix analysis would serve as a distinction between the superfluid and a normal metallic state, there is no way to distinguish metals from insulators from this perspective.

In this section, we provide a comparison of the one-body and two-body density matrices with the TPS. It is shown that there is a correspondence between the TPS and the two-body reduced density matrix in terms of the critical points.

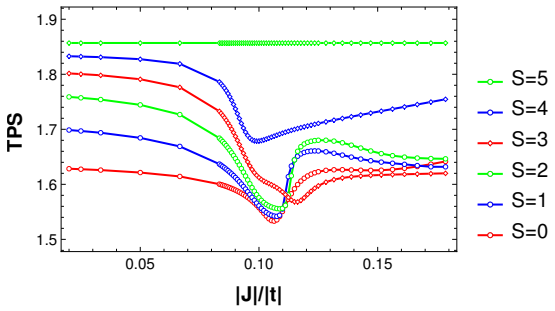

Figure 3.17: The TPS for the 6_2h system vs J.

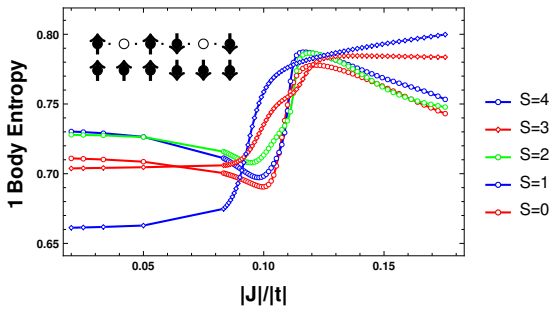

Figure 3.18: The one-body entropy with J. The one-body terms do not include the collective motion of the holes and hence do not represent correctly the TPS.

The one-body entropy is calculated for the whole system using the one body density matrix D. It is a matrix of size N_{elec} times N_{elec} and is calculated as follows:

$$\mathbf{D_{P,Q}} = \langle\psi| a_P^\dagger a_Q |\psi\rangle \tag{3.1.16}$$

And has the following property.

$$Tr\overline{\mathbf{D}} = \sum_p \langle\psi| \hat{N}_p |\psi\rangle = \langle\psi| \hat{N}_p |\psi\rangle = N \tag{3.1.17}$$

The diagonal elements of the one body density matrix give the probability of the holes occupying each site. In this sense, the one body density matrix does not show the correlated motion of the holes. A comparison of the one body density matrix with the TPS for the 6_1h system is shown in Fig: 3.18. Although, for

the one hole case, this would be sufficient, the two-hole case would require the two-body density matrix.

The two-body density matrix can be written in the atomic orbital basis as follows.

$$\mathbf{d_{P,Q,R,S}} = \langle\psi|\, a_P^\dagger a_Q^\dagger a_S a_R \,|\psi\rangle \tag{3.1.18}$$

Note that we have integrated over the electrons occupying the orbitals of type 2 because they do not contribute to the delocalization. This form of the two-body density matrix contains N^2 rows and N^2 columns and has the following permutation symmetry for the atomic indices [124].

$$\overline{d}_{P,Q,R,S} = -\overline{d}_{R,Q,P,S} = -\overline{d}_{P,S,R,Q} = \overline{d}_{R,S,P,Q} \tag{3.1.19}$$

This form of the density matrix can be simplified when limiting the indices to $P > Q, R > Q$, this also reduces the size of the matrix to $\frac{N\cdot(N-1)}{2}$ elements.

$$\overline{T}_{PQ,RS} = \langle\psi|\, a_P^\dagger a_Q^\dagger a_S a_R \,|\psi\rangle\,, P > Q, R > S \tag{3.1.20}$$

$$\overline{T}_{PQ,RS} = \overline{d}_{PQRS}, P > Q, R > S \tag{3.1.21}$$

This form makes it easy to compare with the one body density matrix where the trace gives the total number of particles in the system. The two body density matrix $\overline{T}_{PQ,RS}$ gives the total number of pairs of particles one can form i.e. $\frac{N\cdot(N-1)}{2}$. Take the example of the 6_2h system, there are six electrons in the type **1** orbitals which are mobile, the other six electrons occupying the type **2** orbitals can be thought of as being fixed. Thus, we have for the one body density matrix $(Tr\overline{\mathbf{D}}_{\mathbf{P,Q}})_{6\_2h} = 4$ and for the two-body density matrix $(Tr\overline{\mathbf{d}}_{\mathbf{PQ,RS}})_{6\_2h} = 6$.

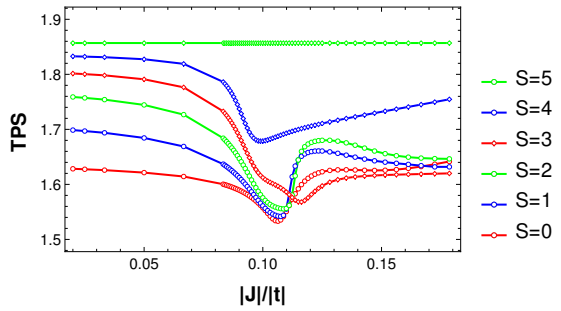

Figure 3.19: The TPS per spin state for the 6_2h system.

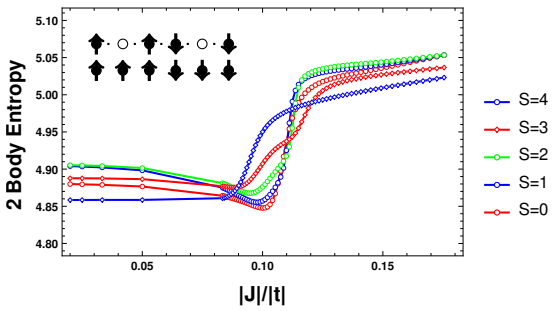

Figure 3.20: The two-body entropy with J.

The diagonal elements of the two-body density matrix give the probability of correlated position of the pair of holes. Note that in order to calculate the TPS, one also requires the probability of pair positions of the holes. Therefore, although there is of course no direct comparison of the TPS and the two-body density matrix, the critical values of the TPS should be reflected by the two-body density matrix. In order to compare the "entropy" is calculated from the two-body density matrix as follows:

$$S_{2body} = -\operatorname{Tr}(\rho \ln \rho)$$
$$S_{2body} = -\sum_i \lambda_i \ln \lambda_i$$

where ρ is the two-body density matrix and λ_i are its eigenvalues. The two-body entropy S_{2body} is compared to the TPS in Fig: 3.20 for the 6_1h system. We can see that the critical points for all spin states correspond well with the those of the TPS. It appears that although the S_{2body} has some information about the delocalization, it is not sufficient to conclusively distinguish metallic and insulating nature since the tendencies (at small J for e.g.) are not the same to that of the TPS for all spin states.

3.2 Magnetic field

The magnetic field is accounted for via the scalar Zeeman term of Eq: 3.2.1. The effect of the magnetic field, therefore, changes the energetic order of the spin subspaces according to their spin multiplicities. Although normally, the magnetic field couples the various spin states with each other, in the present study, the wavefunction of the various states remains unaffected by the inclusion of the Zeeman term, and it acts only on the diagonal of the Hamiltonian:

$$\begin{aligned} \hat{H}_{zee} &= \mu_{Bohr} g_s \hat{S} \cdot \hat{B} \\ \mu_{Bohr} &\approx 5.69 \cdot 10^{-5} eVT^{-1} \\ g_s &\approx 2.0 (L = 0, J = S) \end{aligned} \tag{3.2.1}$$

where $\hat{B}$ is given by the z component of the magnetic field $B.\hat{z}$ and $S \cdot B$ is then the z component of the spin operator i.e. $\hat{S}_z$. The Fig: 3.21, Fig 3.22 and Fig: 3.23 show the effect of the magnetic field on the TPS for the 6_2h, 9_3h and the 12_4h systems respectively.

3.2.1 Two holes

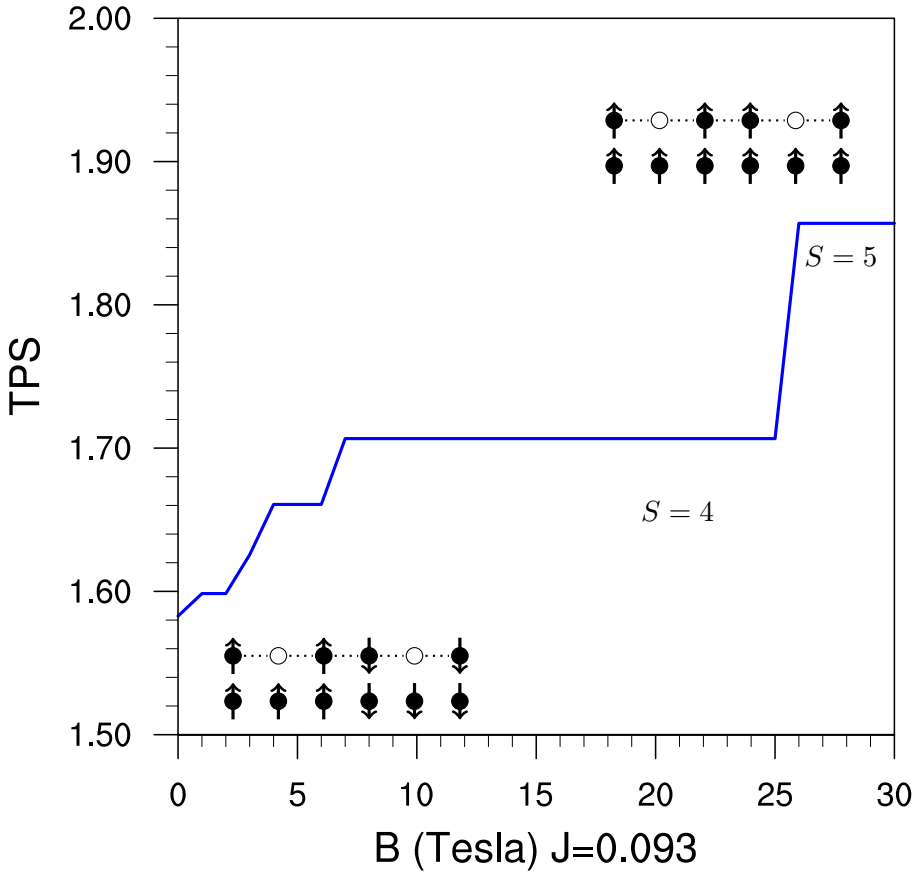

Figure 3.21: The effect of magnetic field on the 6_2h system at $K = 0.8$.

There are a total of six spin states in the 6_2h system, from $S = 0$ to the $S = 5$. The ground state goes from $S = 0$ to $S = 5$ uniformly with increasing field B strength. It appears that the first few states, from $S = 0$ to the $S = 3$, the TPS remains small and it is the $S = 4$ and $S = 5$ states are the ones which show a significant change in the TPS values. In other words, only the high spin states close to S_{max} are the ones responsible for the conduction while the states close to S_{min} are less metallic.

3.2.2 Three holes

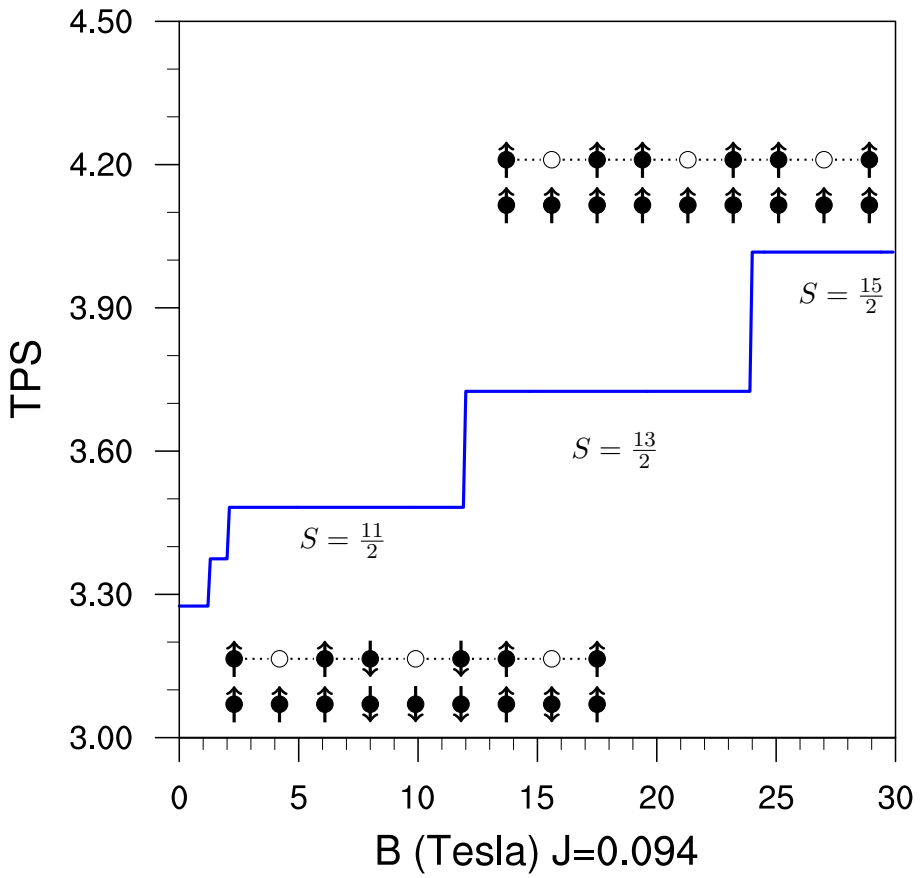

Figure 3.22: The TPS vs magnetic field plot for the 9_3h system at $K = 0.8$ and $J = 0.094$.

The three hole system (9_3h) shows similar behavior. Only three of the largest spin states $S = \frac{11}{2}$, $S = \frac{13}{2}$ and $S = \frac{15}{2}$ appear to be conducting while the rest of the states up to $S = \frac{9}{2}$ have a relatively small value of the TPS. The change in the TPS while going from $S = \frac{5}{2}$ to the $S = \frac{15}{2}$ state is larger by almost three times compared to the 6_1h system. This is a consequence of the increase in the size of the system. Since the TPS depends on the number of particles (holes or electrons), the change in the magnitude would be dependent on the system size and the number of holes.

3.2.3 Four holes

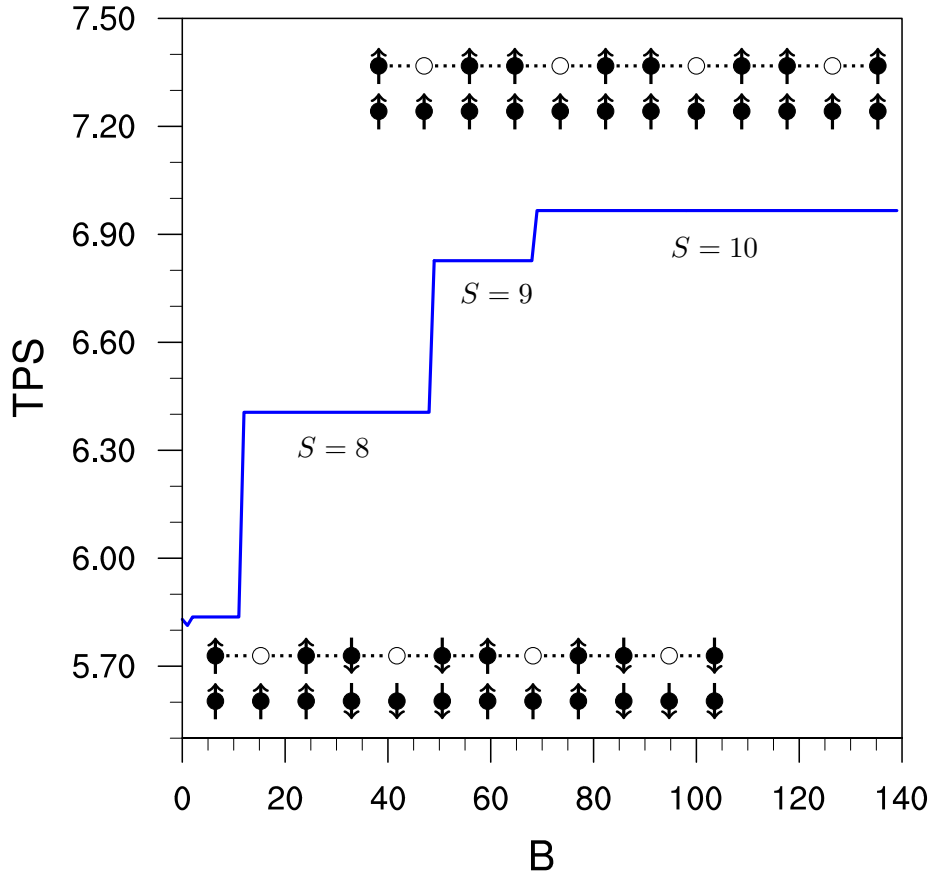

Figure 3.23: The 12_4h under the influence of a magnetic field at $J = 0.1$ and $K = 0.8\ eV$.

Finally, the four hole system also shows three of the largest spin states ($S = 8$, $S = 9$ and $S = 10$) with a conducting character. Extrapolating from these tendencies, we can postulate that as the system size increases and for a given doping ratio, the eventual transitions between the low and the high spin states would become continuous. This would mean that one need not excite the system to the $S = S_{max}$ state to observe an increase in conduction, an excited spin state close to S_{max} would be sufficient to show adequate change in electron delocalization compared to the S_{min} states. The experimental values for the magnetic field strengths for manganites has been observed to be about 5 Teslas [125] for the doping ration of $\frac{1}{3}$. Note that for all the three systems, the first transition into the conducting state (i.e. $S = 8$ in this case) occurs at sufficiently small values of B close to 10 Teslas. Therefore, it appears that, one only needs to compare the field strength for which

a **first major change** in the delocalization occurs.

3.3 Discussion

In this section we will analyze the effect of the magnetic field on the ground state physics of the system. The magnetic field changes the ground state from a low spin to that of a high spin state. Therefore, the resulting change in the properties of the system can be understood by looking at the physics governing the low spin and high spin states.

3.3.1 Ground state physics: DE to Heisenberg

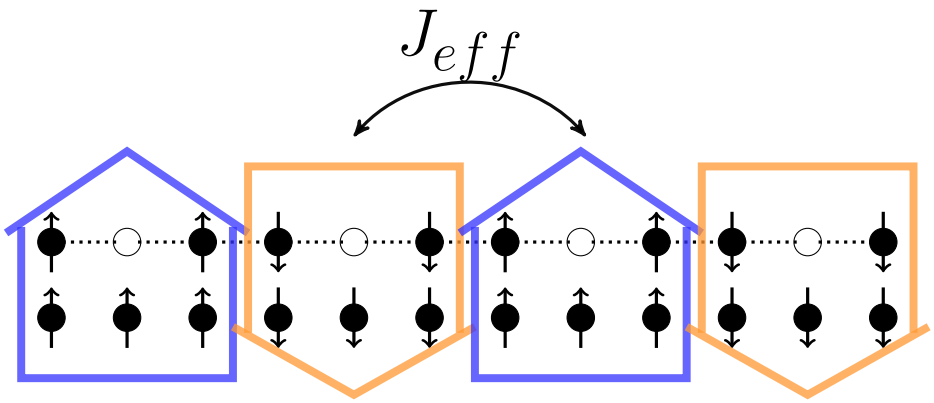

Figure 3.24: Schematic representation of the transition from DE to Heisenberg type Hamiltonian via the J_{eff} between $S = \frac{5}{2}$ spins.

A recent experimental study on 2D manganites by Ramirez *et al* presents a detailed analysis of the magnetic susceptibility [126]. In summary, they show that the ferromagnetic character is observed only close to the Curie temperature and that above this temperature, the magnetic susceptibility indicates an antiferromagnetic tendency for the system. Therefore, we make the hypothesis that the low spin states present an anti-ferromagnetic character along with the presence of a short range order.

A single hole aligns from five to seven spins for physical values of J and K as shown in the previous chapter 2.5. It was also shown that for values of J and K for which a single hole aligns five spins, the presence of a second hole does not decrease the number of spins aligned per hole. The interaction between the two ferromagnetic

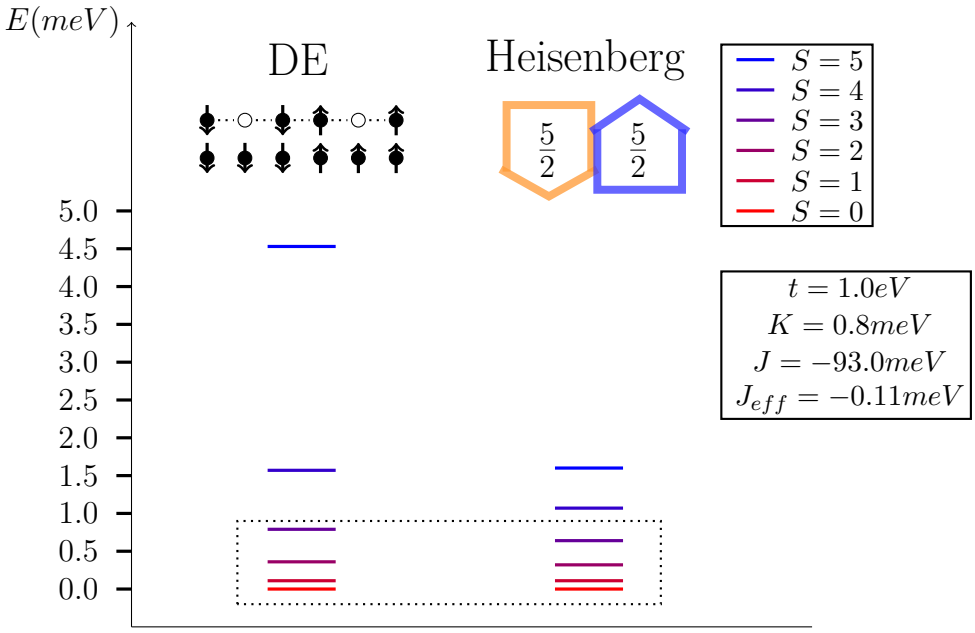

Figure 3.25: comparison of DE and Heisenberg spectra for 6_2h system.

polarons was shown to be antiferromagnetic in character. Therefore, it appears that the low spin states are dominated by an antiferromagnetic coupling between the polarons made up of $S = \frac{5}{2}$ spins. A comparison of the low energy spectrum of the DE system with six sites and two-holes (6_2h) with that of the Heisenberg model formed by two $S = \frac{5}{2}$ spins is shown schematically in Fig: 3.25. The low energy spectrum of 6_2h system shows surprising similarity to that of the Heisenberg system, although there is no *a priori* reason for this similarity. An analysis of the wavefunction for $J = 0.1$ and $K = 0.8$ (i.e. value for which one hole aligns five spins), is presented in Table: 3.1. The table also shows a comparison of the low energy spectrum of the 6_2h system with that of the Heisenberg Hamiltonian calculated using the effective exchange (J_{eff}), the J_{eff} was obtained from the lowest two spin states. As can be seen from the table, the ground state and lowest excited states are dominated by the configurations where the holes have formed their own FM clouds each aligning five spins (Fig: 3.24) ($S_{box} \approx 2.5$). The S_{box} value deviates as one looks at the higher spin states, for e.g. the $S = 4$ state has an S_{box} value of 2.30 whereas the $S = 0$ state has $S_{box} = 2.49$. The spectrum also significantly deviates from the Heisenberg one for the $S = 4$ and $S = 5$ states.
This shows that at least for the low lying states, for physical values of J and K, the physics of the DE model can be understood by an effective Heisenberg type AF interaction between $S = \frac{5}{2}$ spin polarons created by the individual holes.

	6_2h		
S	S_{box}	t-J-K	Heisenberg
0	2.49	0.00	0.00
1	2.47	0.17	0.17
2	2.44	0.54	0.52
3	2.39	1.09	1.04
4	2.30	1.85	1.74
5	2.50	4.53	2.60

Table 3.1: Comparison of DE and Heisenberg Energies in meV for the 6_2h system. All values are at $J = 0.1$ and $K = 0.8$ eV. The S_{box} values with three sites in the box are also shown.

	6_2h			9_3h			12_4h	
Spin(S)	t-J-K	Heisenberg	S	t-J-K	Heisenberg	S	t-J-K	Heisenberg
0	0.00	0.00	2.5	0.00	0.00	0	0.000	0.000
1	0.17	0.17	1.5	0.21	0.21	1	0.003	0.003
2	0.54	0.52	3.5	0.36	0.29	2	0.009	0.009
3	1.09	1.04	0.5	0.33	0.41	3	0.020	0.020
4	1.85	1.74	2.5	0.37	0.41	3	0.030	0.032
5	4.53	2.60	1.5	0.37	0.54	2	0.033	0.041
$J_{eff}(meV)$	0.174			0.083			0.006	

Table 3.2: Comparison of DE and Heisenberg Energies in meV. All values are at $J = 0.1$ and $K = 0.8$ eV. The spin(S) refers to the spin of the ground state.

Whereas, the high spin states, do not obey this physics. For the low spin states ($S = 0, S = 1$), there is no mixing between the two FM domains and almost 90 percent of the wavefunction consists of the holes localized in their respective FM regions. This would explain the low conductivity of the system just before the Curie temperature.

The comparison of the low energy spectrum for all the three systems i.e. 6_2h, 9_3h and 12_4h is shown in Table: 3.2. Only values of J have been taken for which each hole has aligned close to three spins which we have confirmed with the S_{box} values. The interaction between the $S = \frac{5}{2}$ spins has been taken to be J_{eff}. The J_{eff} values given in Table: 3.2 have been calculated in those cases using only the ground state and the first excited state as a first approximation. From the comparison of the spectrum for the three systems, we conclude that only few low lying

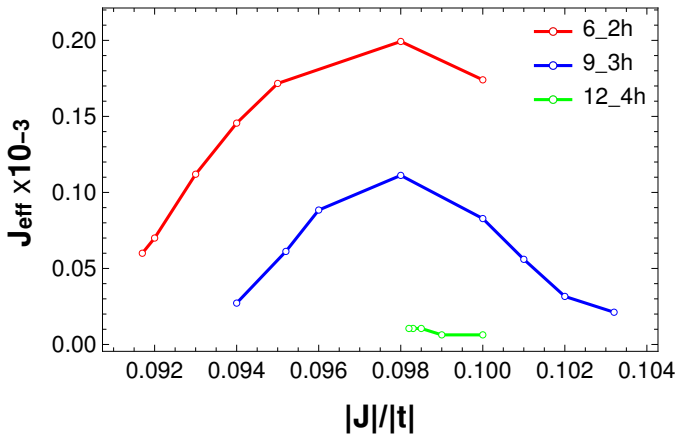

Figure 3.26: The variation of J_{eff} with J is shown for the 6_2h, 9_3h and the 12_4h system for a fixed value of $K = 0.8\ eV$.

spin states are adequately modeled by the Heisenberg picture. This is justified since only the low energy physics is expected to follow Heisenberg behavior and the high energy states will follow a different physics. Therefore, we cannot hope to represent the full spectrum with the Heisenberg model. Note that the low energy spectrum corresponds to that of the Heisenberg spectrum only for a small range of values of J which decreases as the system size increases. The J_{eff} values for the three systems have been calculated for various values of J and are reported in Fig: 3.26. The region for which the 12_4h system shows Heisenberg behavior along with the S_{box} value of $\frac{5}{2}$ is not as large as for the 6_2h and 9_3h systems. Therefore, only a few points have been plotted for the 12_4h system. The J_{eff} value has a maximum at about $J \approx 0.098$ and then decreases on either direction. This is due to the fact that for all the three systems, the S_{min} state is flanked on both directions of J by two different S_{min+1} states. Therefore, along both directions aways from $J \approx 0.098$, the energy difference between $S_{min} - S_{min+1}$ decreases leading to a decrease in J_{eff}. It is important to note that although on sufficiently increasing the value of J, we will again have a S_{min} state as the ground state, it will not have the proper S_{box} value, i.e. the holes will not have aligned five spins.

In conclusion, we have established that the physics of the low spin states follows the Heisenberg picture. Consequently, they are insulating in character. We have also calculated the J_{eff} (effective anti-ferromagnetic interaction) between the ferromagnetic polarons and shown that it can be used to model the low energy spectrum.

3.3.2 Excited state physics: Charge gap

Let us proceed now to an analysis of delocalization in the excited states. A measure of the electric current in linear systems is not exactly defined due to the open boundary conditions. The TPS is an approximate measure of the conductivity in the system. If we look at the determinants near the value of J for which each hole has aligned five spins ($J = 0.1$), we will have ferromagnetic regions each with one hole each, as shown earlier. At this point we can define the "ionic" and "neutral" determinants as shown in Figure below.

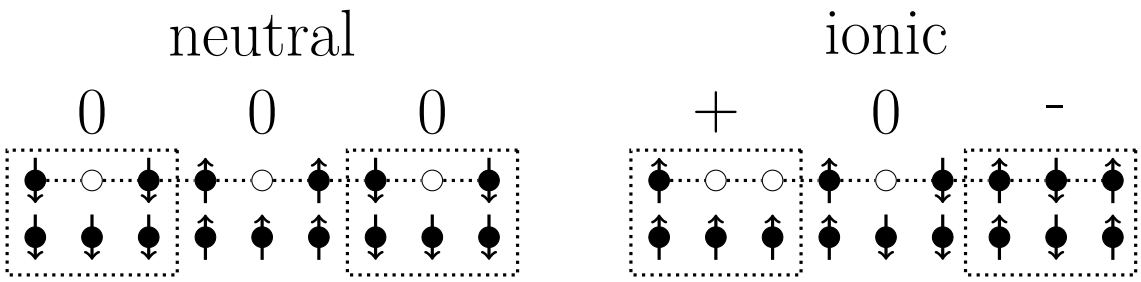

Figure 3.27: The two families of determinants with "ionic" and "non-ionic" character.

The figure Fig: 3.27 shows the two families that we have used to classify the determinants by the position of the hole. Looking at the weights of the two types of determinants in the wavefunction would then give a good idea of the changing nature of the state. The Fig: 3.28, 3.32 and 3.30 show such a study for the 6_2h, 9_3h and 8_2h systems respectively, where we have calculated the weight of the "ionic" type of determinants. The only problem is that the definition of the "Ionic" and "neutral" which would depends on the size of the box. Therefore, one needs to keep in mind that there is an inherent bias in this type of classification. Nonetheless, in this case it seems to be justified due to the fact that the size of the box corresponds with the physics of the system. Whereas for values of $J > 0.1$ for which the hole has aligned less than five spins, this definition would no longer be accurate.

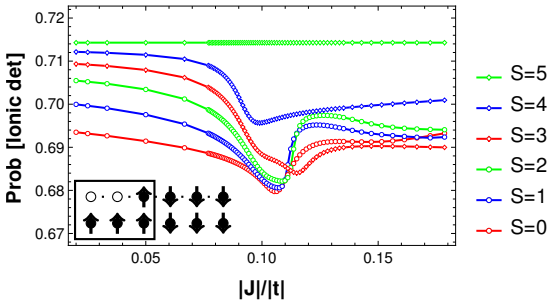

Figure 3.28: The weight of the ionic determinants for the 6_2h system. The inset shows the definition of ionic and neutral determinants.

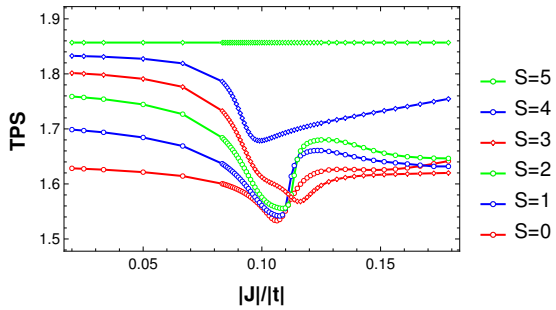

Figure 3.29: The weight of the non-ionic determinants for the 6_2h system.

This analysis would help to understand the nature of the conducting S_{max} and S_{max-1} states. The figures Fig: 3.28, 3.29 shows the comparison of the probability and the TPS for the 6_2h system, similarly Fig 3.30, 3.31 and Fig: 3.32, 3.33 shows this comparison for the 8_2h and 9_3h systems. In the inset of each figure we show the definitions we have used in order to separate the "ionic" and "neutral" determinants. In general the TPS shows a clear correspondence with the probability of the "ionic" determinants for all values of J and for all systems. The critical point at about $J \approx 0.1$ for the 6_2h and 9_3h systems and at $J \approx 0.05$ for 8_2h system, can also be seen for both the TPS and the probability plots. At this value there is a decrease in the weight of the ionic determinants in favor of the non-ionic ones signifying the order present in the wavefunction as shown in sec: 3.1.5.1. This leads to a decrease in the mobility of the holes and the net total charge ("ionic" determinants). This is also clearly reflected in a direct decrease in the TPS. Once the value of J permits a ferromagnetic coupling between the newly formed ferromagnetic regions (formed of five spins) each with a single hole, and the previous order is lost, the weight of the ionic determinants increases again and so does the TPS.

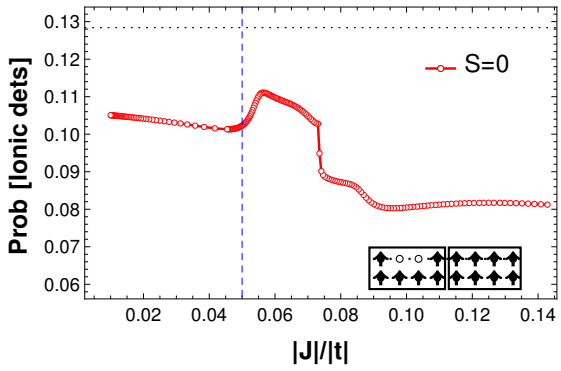

Figure 3.30: The probability of ionic determinants for the 8_2h system. The dotted line represents the probability for the $S_{max} = 7$ state. The inset shows the definition used for the ionic and neutral determinants.

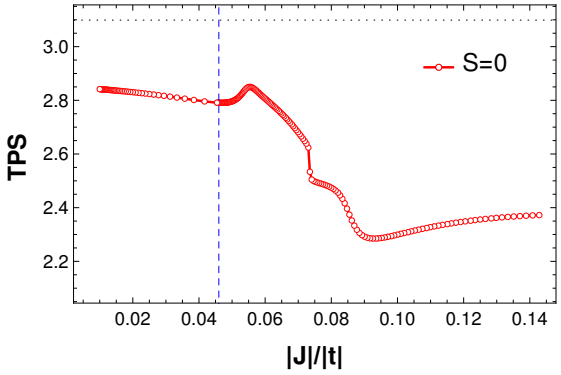

Figure 3.31: TPS for the same system 8_2h. The dotted line is the TPS for the $S = 7$ state.

The second important observation are the relative weights of the ionic determinants for the five spin states. Similar to the TPS, at all values of J, the ionic character of the wavefunction is larger for the larger spin states (i.e. $S = 5, S = 4$). This accounts for an increase in the metallic nature of the states with an increase in the spin. This analysis permits us to understand the contrasts in the characters of the insulating (e.g. $S = 0, S = 1, S = 3$) state with that of the conducting (e.g. $S = 4, S = 5$) states. It is postulated that the low lying states follow a Heisenberg physics resulting in an insulating behavior, whereas the excited states allow for an increased mobility of the charges leading to a metallic character.

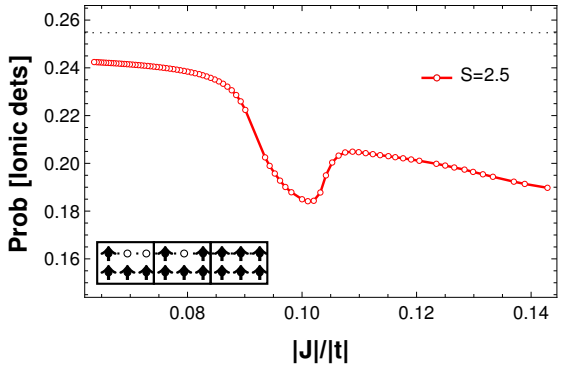

Figure 3.32: The probability of ionic determinants for the 9_3h system. The dotted line represents the probability for the $S_{max} = \frac{15}{2}$ state. The inset shows the definition used for ionic and neutral detrminants.

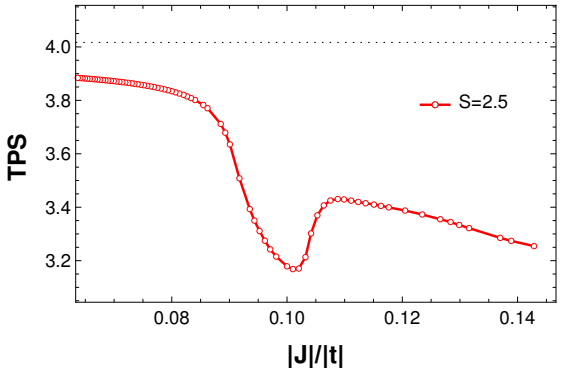

Figure 3.33: The TPS for the same system (9_3h) for comparison. The dotted line corresponds to the $S_{max} = \frac{15}{2}$ state.

In conclusion, since there is a clear correspondence of the probability of the

ionic determinants with the TPS, it appears that we have clearly identified the physics measured by the TPS. From the three pairs of figures Fig: 3.28, 3.29, and Fig: 3.30, 3.29 and Fig: 3.32, 3.33, we conclude that the increase in the delocalization is due to an increase in the "ionic" type of determinants.

3.4 Conclusion

The ordered phase in the double exchange model has been studied using exact diagonalization methods. The delocalization in the linear chain system was explained using the TPS value. Analytical derivation and numerical calculation was used to explain the origin of the increase in the delocalization. The S_{box} and the Total position spread tensor was used to quantify the size of the ferromagnetic "Islands". It was shown that critical values of the TPS indicates an ordered phase of the system. Using the S_{box} and the TPS value we identified the point where a single hole aligns three $J \approx 0.1$ and four sites $J \approx 0.05$.

In order to analyze the effect of magnetic field, the change in the TPS was studied as a function of the magnetic field. It was shown that the low spin states follow a Heisenberg physics. An effective Heisenberg type Hamiltonian has been shown to be able to describe the low energy spectrum for a specific region of the parameter space depending on the doping ration ($\frac{1}{4}$ to $\frac{1}{3}$). The effective exchange interaction J_{eff} has been extracted from the low energy spectrum showing the variation of this ordered phase with J. The physics of the high spin states has also been explained as a increase in the weight of the "ionic" type determinants which was corroborated with the TPS.
The increase in the delocalization in the system in the presence of the magnetic field was explained in the following manner:

- For systems in which the value of J is such that each hole has aligned a precise number of spins and the polarons are aligned antiferromagnetically, the ground state would have very low mobility due to the dominance of neutral determinants.
- On the application of a magnetic field, one can then increase the delocalization in the system by stabilizing the high spin states. The high spin states have a large delocalization as their wavefunction if dominated by ionic type determinants.

In this way we have a qualitative explanation of the mechanism of the change in the metallic/insulating nature on the application of a magnetic field.

Chapter 4

General conclusions

This work has been devoted to the study of double exchange systems from various theoretical approaches. The main conclusions are the followings:

- Organic molecules showing a Double Exchange phenomenon can be designed. The double exchange phenomenon is more difficult to produce in organic systems than in transition metal compounds. Despite the question of the stability of polyradical hydrocarbons which seems to be studied and controlled by experimentalists [127, 18, 128], the most problematic feature concerns the choice of the bridge. Due to the delocalized character of the magnetic orbitals their overlap may lead to strong covalent interactions. As a consequence, the pairing of the electrons belonging to the most overlapping orbitals prevents from entering the double exchange regime. Nevertheless, long-length bridges with appropriate connections to the magnetic units could be conceived on the basis of a rational analysis of the DFT results. The resulting compounds show a double exchange behavior with interactions of the same order of magnitude as those observed in transition metal compounds. One should however note that the local exchange integral K between the orbitals of the magnetic units is much lower than in transition metal ions and that, as a consequence, the Anderson Hasegawa model (which accounts explicitly for this integral) must be used to describe the magnetic property of these organic systems [36].

- From these molecular units, two-dimensional networks can be designed in which both magnetic and transport properties together with magnetoresistive effects could be expected. Such materials would be interesting organic alternatives in the domain of spintronics.

- Recent works have shown that when removing magnetic units from a graphene sheet, the remaining 2D material may exhibit particular magnetic properties such as ferro-, antiferro- and ferri-magnetism depending on the topology of

the extracted molecules [24, 129]. As experimentalists are gaining expertise with graphene [130, 131], an interesting perspective would be to conceive such materials based on the knowledge of the present work. While we have adopted a bottom-up approach, this would constitute a top-down counterpart.

- From a theoretical chemistry point of view, two different methods of extraction of the double exchange model interactions have been proposed. Due to the self-interaction error [132] Density Functional Theory broken symmetry solutions with a localized hole cannot be obtained. As these methods do not require the calculation of such solutions they are well-suited for DFT studies of DE compounds and one may hope that they could be useful to the quantum chemistry community.

- A second part of this work was devoted to a model study of finite size double exchange chains. Firstly, we studied the question of the number of spins aligned by a single hole. From a model study restricted to the most important t, K and J interactions, the range of values of these parameters for which a high-spin ground state occurs could be determined. This could be a guide for generating high-spin molecules from a double exchange mechanism.

- The emphasis of the work was on the effect of the Hund term K on the low energy spectrum. Contrary to traditional assumption of a large Hund coupling $K > 10|t|$ in usual model studies, it was shown that the $K \approx |t|$ range plays a crucial role in determining the low energy physics of the system.

- As we were also interested in collective effects in DE chains, we have developed tools of analysis to grasp the transport and magnetic properties of these systems. Indeed, we found that the spin multiplicity of the ground state was not a conclusive observable for quantifying the size of the ferromagnetic cloud as soon as the size of the system becomes large. In a first place the expectation value of the S^2 operator (S_{box}) in boxes of various sizes enables us to conclude that for a physical range of the DE parameters, a hole aligns the spins of three to four sites. We found that the amount of spins aligned is not too large depending on the size of the system and happens to be in good agreement with the observed DE properties of real doped ($\frac{1}{4}$ to $\frac{1}{3}$) materials. This shows that the size of the ferromagnetic cloud is essentially governed by local interactions and not affected by collective effects. As well the presence of a second hole does not qualitatively modify this result. A slight preference for the alignment of the spins of the fourth site was found for lower values of J in the presence of a second hole.

- The study of systems with several holes shows that the electronic structure of these chains is essentially governed by an antiferromagnetic arrangement of the ferromagnetic clouds. This result could rationalize the observed antiferromagnetic trend of the magnetic susceptibility at low temperatures in real compounds. It is worthwhile to notice that not only the ground state but also the lowest excited states can be described using a Heisenberg Hamiltonian involving effective spins (those of the ferromagnetic cloud) and effective magnetic couplings (J_{eff}).

- While transport properties cannot really be quantified in open-boundary compounds, the TPS was calculated for systems with one and more holes. A deep analysis of its physical meaning based on analytical derivations and numerical calculations shows that it quantifies the weight of the ionic component in the wavefunctions. Such information can therefore be used as an indicator of the delocalization of the holes.

- The behavior of the TPS as a function of J for physical values of K and t shows interesting features. While, as expected, it increases with the decrease of J (as we go to the Hückel limit), this behavior is not monotonous. An analysis combining the TPS values, the S_{box} values and the entropy shows that the drops in the TPS for peculiar values of J corresponds to specific spin orderings of the wavefunction. As J decreases, one observes successively that a single hole aligns the spins of more and more sites. At the critical value $J \approx 0.1|t|$, the nature of the wavefunction changes from an alignment of the spins of 2 sites to that of 3 sites, then at the values $J \approx 0.05$ an alignment of the spins of 4 sites is observed and so on. The TPS can therefore be used to determine critical values of the parameters for which spin orderings occur.

- As magnetoresistive effects occur in DE compounds we have finally studied the TPS as a function of an applied magnetic field for physical values of the DE parameters. Two important results were obtained. The first one is that one observes qualitative changes in the TPS for small values of the magnetic field. These values are nevertheless strongly depending on the size of the systems (as the spectrum is of course also strongly depending on the size of the system). The second important conclusion concerns the nature of the conducting state. As expected, the lowest states which obey a Heisenberg behavior do not show any significant changes in the TPS under magnetic field. Only the highest spin state (all spins are aligned) of this family of states conducts but unfortunately it is very high in energy and would require the application of too strong magnetic field. Conducting states of different nature than the low spin states, lie at reasonable energies. Their electronic structure show important ionic components (in terms of ionic boxes) which

to some extent gives a qualitative picture of a Mött-Hubbard transition for explaining the conduction in DE systems.

- Finally, this work has required the implementation of the DE model and the use of various algorithms of exact diagonalizations of sparse and large matrices. A massively parallel eigensolver was implemented for the double exchange Hamiltonian using the PETSc library. This code written in C++ and Fortran is also capable of treating more complicated topologies with different Hamiltonian models.

- Although much remains to be done in 1D systems, an interesting perspective would be the study of 2D systems. As the growth of the size of DE model matrix as a function of the size of the system is prohibitive, such a study could not be conducted in the context of this thesis. Other approaches have been used to study 2D systems. The advantages of exact diagonalizations over the methods applied to these systems is twofold: on the one hand it gives access to low-energy spectra i.e. ground state but also excited states, on the other hand it provides accurate wavefunctions from which deep analysis of the nature (electronic structure) of the various states can be performed.

Chapter 5

Article on mononuclear complex

Engineering the magnetic coupling at the molecule/electrode interface between self-assembled metal complexes and epitaxial ferrimagnetic iron oxide.

Victoria Campbell*[1], Monica Tonelli[1], Irene Cimatti[1], Jean-Baptiste Moussy[2], Ludovic Tortech[2,3], Yannick J. Dappe[2], Eric Rivière[1], Régis Guillot[1], Sophie Delprat[4], Richard Mattana[4], Pierre Seneor[4], Philippe Ohresser[5], Fadi Choueikani[5], Edwige Otero[5], Florian Koprowiak[6], Vijay Gopal Chilkuri[6], Nicolas Suaud[6], Nathalie Guihéry[6], Anouk Galtayries[7], Marie-Anne Arrio[8], Philippe Sainctavit[5,8], and Talal Mallah*[1]

*victoria.campbell@u-psud.fr and talal.mallah@u-psud.fr

[1]Institut de Chimie Moléculaire et des Matériaux d'Orsay, CNRS, Université Paris Sud 11, 91405 Orsay Cedex, France

[2]CEA-Saclay, IRAMIS, SPCSI, F-91191 Gif-sur-Yvette, France

[3]IPCM, UMR CNRS 7201, UPMC, Université Pierre et Marie Curie, F-75005 Paris, France

[4]Unité Mixte de Physique CNRS/Thales, 1 Avenue Auguste Fresnel, 91767 Palaiseau, France and Université Paris-Sud, 91405 Orsay, France

[5]Synchrotron SOLEIL, L'Orme des Merisiers Saint-Aubin—BP 48, Gif-sur-Yvette 91192, France

[6]Laboratoire de Chimie et Physique Quantiques, Universit´e de Toulouse III, 118, route de Narbonne, 31062 Toulouse, France

[7]Laboratoire de Physico-Chimie des Surfaces, CNRS-ENSCP (UMR 7045), Chimie ParisTech, 11 rue Pierre et Marie Curie, F-75005 Paris, France

[8]IMPMC-CNRS, Université Pierre et Marie Curie, F-75005 Paris, France

Abstract

Engineering and controlling the magnetic response of a molecular device is of paramount importance in spintronic applications. Here we show the self-assembly, structural orientation and magnetic coupling of two transition metal complexes that were chemically bound to a ferrimagnetic surface. We show that through a small, tunable modification we can modulate the magnetic behavior of our system. The molecules display magnetic anisotropy. Surface anchoring induced, for the cobalt(II)-containing complex ($CoPyipa_2$), blocking of its magnetization and hysteresis that was not observed in the isostructural nickel(II)-containing one ($NiPyipa_2$).

Theoretical calculations unraveled the nature of the magnetic coupling, and quantified the magnitude of the exchange interaction between the molecules and the surface. We found that $CoPyipa_2$ was strongly *ferromagnetically* coupled to the surface, while $NiPyipa_2$ was weakly *antiferromagnetically* coupled. These results highlight the importance of the synergistic effect that the electronic structure of a metal ion in conjunction with the nature of the organic spacer has on the exchange interaction at the molecule/electrode interface.

Introduction

With the quest to make electronic devices ever smaller, molecules have gained a place in the realm of not only traditional electronics, but also in spintronics. Molecular spintronics is a multidisciplinary field of research that unites the exceptional properties of molecules with the requirements of spin-based technology.[1,2] It has been shown that the magneto-resistance response of a molecular spintronic device hinges upon the interface between the ferromagnetic surface and the molecular layer.[3] Mastering the quality and the nature of this interface is of paramount importance for the construction of devices with reproducible responses.[3] A major challenge is to be able to control the structural orientation of the nanoscopic objects deposited on the ferromagnetic electrodes and to control the exchange coupling interaction between these objects and the electrode (the molecules/electrode interface).[4] Single magnetic molecules with designed geometry, architecture and electronic structure allow scientist to attain this goal.[5,6]

Recent endeavors towards molecular spintronics include (but are not limited to) the following examples. Mannini and co-workers demonstrated that the magnetic memory effect is retained at low temperature (< 1.0 K) when single molecule magnets (SMMs) are wired not only onto non-magnetic gold surfaces[7,8] but also onto magnetic surfaces commonly used as ferromagnetic electrodes in spintronic devices, such as the oxide lanthanum strontium manganite (LSMO) and metallic cobalt.[9] When ferromagnetic surfaces were employed, terbium(III) double-decker ($TbPc_2$) molecules organized with different orientations (parallel or perpendicular) depending on the surface employed and did not show significant magnetic interaction between the molecules and the electrode.[9] In alternative study, Rizzini *et al*. demonstrated that it is possible to induce exchange bias in

a small fraction of the $TbPc_2$ molecules adsorbed onto a manganese surface.[10] Another class of materials, paramagnetic porphyrin molecules (Mn-porphyrin and Fe-porphyrin) and phthalocyanine, are known to physically adsorb onto ferromagnetic Ni or Co surfaces and show surface induced magnetic ordering and hysteresis.[5,11-14]

Although these systems are promising, additional interface engineering is necessary to fully control and comprehend the nature of the interaction between the molecular layer and the ferromagnetic surface. In this paper, we demonstrate that it is possible to modulate the magnetic response of our system with a molecule that is engineered to control the magnetic interaction *via* the interface. Through a small tunable modification we can regulate the behavior of the system. More specifically, we investigate the structural orientation and the magnetic coupling of two self-assembled metal-containing complexes. The molecules synthesized display magnetic anisotropy and can be chemically tethered onto epitaxial Fe_3O_4 (111). Surface anchoring induced, in the paramagnetic cobalt(II)-containing complex ($CoPyipa_2$), a magnetic hysteresis at the Co-edge evidenced by X-ray magnetic circular dichroism (XMCD) studies. We did not observe hysteresis at the Ni-edge for the isostructural nickel(II)-containing complex ($NiPyipa_2$). First principle *ab initio* calculations indicated that $CoPyipa_2$ is *ferromagnetically* coupled with the surface, while $NiPyipa_2$ undergoes an *antiferromagnetic* exchange coupling with weaker magnitude. These results highlight the fundamental effect that the electronic structure of a metal ion in conjunction with the nature of the organic spacer has on the resulting molecule/electrode interaction.

Results and Discussion

When designing a versatile system that could be exploited in molecular spintronic applications such as spin filtering or spin transfer torque, we took into consideration two main factors. First, we wanted to construct a well-defined molecules/substrate interface by using *anchoring groups* as spacers that would graft reproducibly and in a controlled manner onto the oxide of choice to allow tuning of the molecule/electrode magnetic and electronic interactions. Second, these complexes must be air stable and more importantly thermodynamically

stable in solution in order to prevent possible reactions between the metal ion, belonging to the complex, and the surface.

Many different anchoring groups are known to graft to oxide surfaces such as phosphonates, carboxylates and methyl silanes.[15,16] Amongst them all, the phosphonic acid moiety was chosen because it is known to covalently tether to a variety of oxides (for example TiO_2, Ta_2O_5, LSMO, ZnO and Fe_3O_4),[17-19] is stable in a variety of solvents, in a large range of pH, and is insensitive to hydrolysis.[20-22]

The organic ligand and the related complexes were designed with three criteria in mind: (i) maximum thermodynamic stability, (ii) facile adjustment of the nature of the magnetic ion, and (iii) optimal orientation of the phosphonic acid groups that play the role of spacer units between the magnetic ion and the surfaces. This last criterion enables the tuning of the electronic communication between the surface and the magnetic complexes, which directly impacts the nature and the magnitude of their exchange coupling. The one pot reaction between 2-(aminoethyl)phosphonic acid (2 equiv.), 2-pyridinecarboxaldehyde (2 equiv.) and the corresponding hydrated $M^{II}(CH_3COO)_2$ salt (1 equiv.), using the metal ion M^{II} (Co^{II} or Ni^{II}) as a template, produced bisimine complexes Co- and $NiPyipa_2$ as the uniquely observed products (Figure 1, see SI for full characterization of the complexes). Single crystal X-ray analysis revealed that Co- and $NiPyipa_2$ are isostructural. In both complexes the metal center is bound to four nitrogen atoms and two oxygen atoms, leading to a distorted octahedral environment and molecular C_{2v} symmetry (Figure 1). As per design, both phosphonic acid moieties are oriented in the same direction.

The magnetic behavior of the complexes was studied by direct current (dc) magnetic susceptibility and magnetization measurements (Figures 1, S01, and S02) and by *ab initio* calculations that used the spin-orbit state interaction method (see SI for details).[23-25] The calculations and the experimental data are in good agreement and indicate the presence of an easy plane of magnetization for $CoPyipa_2$ and an easy axis for $NiPyipa_2$ (Figure 1e). We extracted the orientation of the magnetization axis from the *ab initio* calculations, and we found that the hard and easy axis of magnetization were perpendicular to the C_2 symmetry axis for $CoPyipa_2$, and $NiPyipa_2$, respectively.

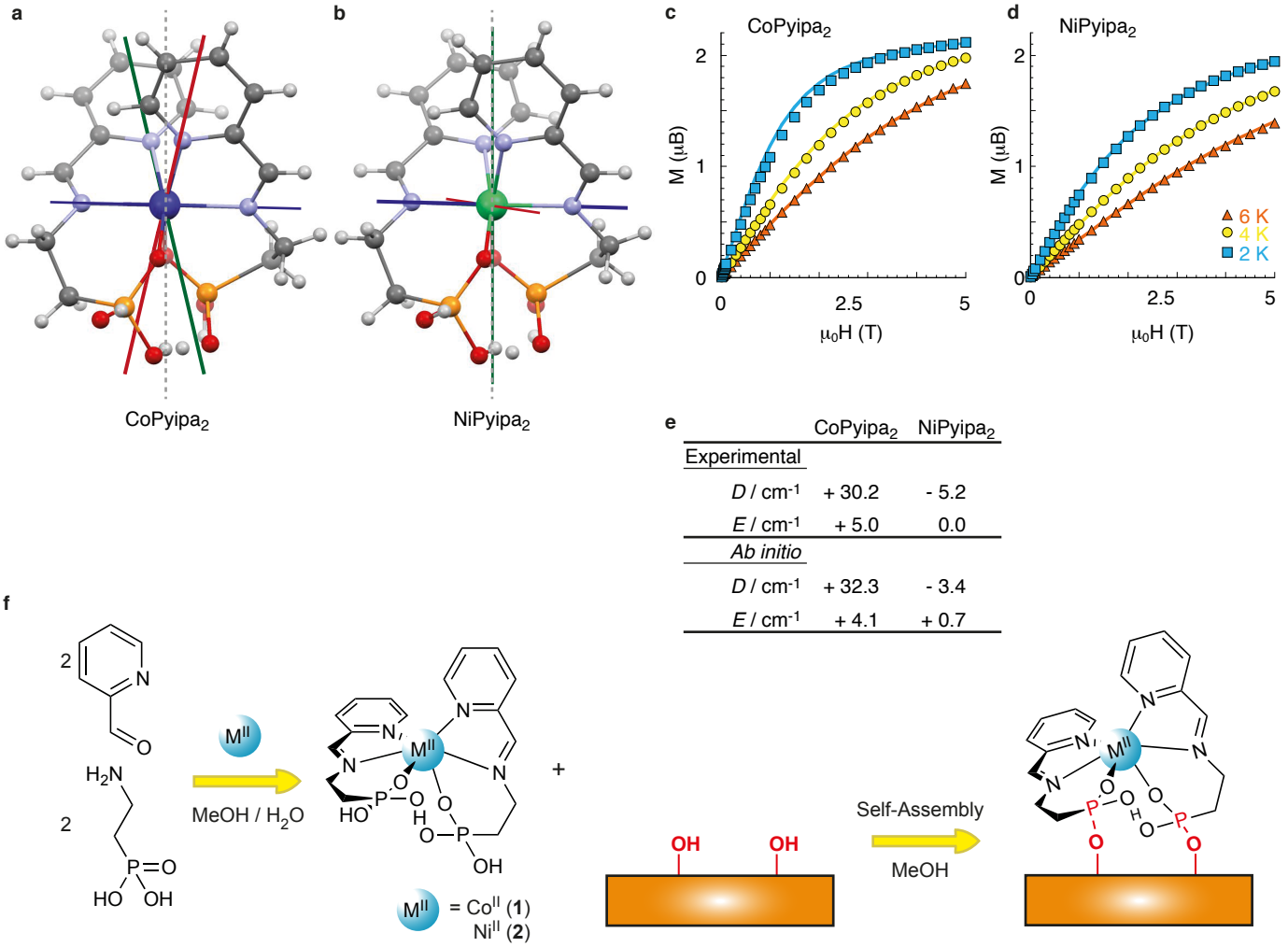

e	$CoPyipa_2$	$NiPyipa_2$
Experimental		
D / cm^{-1}	+ 30.2	- 5.2
E / cm^{-1}	+ 5.0	0.0
Ab initio		
D / cm^{-1}	+ 32.3	- 3.4
E / cm^{-1}	+ 4.1	+ 0.7

Figure 1. Complex Co- and $NiPyipa_2$. X-ray crystal structure of $CoPyipa_2$ (**a**) and $NiPyipa_2$ (**b**): C, grey; N, lilac; O, red; P, orange; H, white; Co, blue; Ni, green. The red, green and blue axes represent the x, y, z direction of the anisotropy tensor, respectively. The magnetization as a function of field plots for $CoPyipa_2$ (**c**) and $NiPyipa_2$ (**d**): solid lines correspond to the best fits; see SI for the parameter values. (**e**) Table of the experimental and calculated magnetization parameters reported in cm^{-1}: D, zero field splitting parameter; E, rhombic parameter **f**, Schematic representation of the synthesis of complex Co- and $NiPyipa_2$ followed by surface anchoring.

A monolayer of molecules (Co- or $NiPyipa_2$) on epitaxial Fe_3O_4 (111) was obtained by self-assembly from solution. Surface coverage was monitored by atomic force microscopy (AFM), X-ray photoelectron spectroscopy (XPS) and time-of-flight secondary ion mass spectrometry (ToF-SIMS) (Figures 2, and SI). XPS spectra indicated the presence of the 2s and 2p peaks from phosphorus (Figure S03). AFM data revealed homogenous coverage of the substrates (Figure 2b and S04) with the surface profile indicating a height of the

objects that is consistent with the complexes being deposited onto the surface (~ 1 nm). Positive and negative ToF-SIMS spectra (Figure S05 and S06) showed a variety of fragments confirming that the phosphonic acid moiety binds to the iron oxide *via* the oxygen (Fe-O-P$(OR)_2$). It is important to note that if the phosphonates were weakly bound to the iron oxide surface (i.e. hydrogen bonded), we would not expect complex fragments containing both iron and phosphonate to be present. Similar fragmentation was found in ToF-SIMS data of octadecylphosphoric acid on tantalum oxide surfaces.[19]

Since organophosphorous moieties may have different binding modes to the surface (mono-, bi- and tridentate), the preferential orientation of the molecules was determined by numerical simulations.[22] Determination of the equilibrium state and energy minimum of the system has been performed using density functional theory (DFT) molecular dynamics technique (FIREBALL).[26-29] In our calculations, we set the molecule onto a surface of Fe_3O_4 oriented along the (111) direction formed by octahedral (O_h) and tetrahedral (T_d) Fe ions bridged by oxo ligands.[30] We initially positioned the molecule in three different configurations (a physisorbed and two chemisorbed ones, see SI for details). The orientation of the molecule was chosen such that the anchoring phosphonate moieties pointed towards the surface with the different possible binding modes.[22] Since the physisorbed energy is not compatible with the experimental rinse cycles (the molecular layer is stable after this operation), we decided to directly simulate the anchoring of the molecule by substituting the surface oxygen atoms by the phosphonates one (this configuration is otherwise out of range of standard DFT optimization due to a strong potential barrier between the physisorbed and an anchored state). We proceeded to do a DFT molecular dynamic simulation at room temperature to reproduce the experimental conditions of molecular deposition on the surface, followed by a structural optimization at 0 K to determine the final configuration on the surface. This procedure gave a stable structure and the molecular adsorption energies of the three configurations (see SI).[31] Further magnetic optimization was performed on these structures in order to obtain an accurate description of the magnetic state of each molecule. The most stable orientation corresponds to the condition where the C_2 symmetry axis of the complexes is perpendicular to the surface as expected from the orientation of the oxygen phosphonate anchoring groups (Figure 2a); the two oxygen atoms belonging to the

two different phosphonates (phos) have replaced two oxygen atoms (bridging octahedral and tetrahedral Fe ions) belonging to the surface creating Fe–O_{phos} coordination bonds. This configuration leads to the molecules being linked to three Fe atoms, as highlighted in Figure 2a. For $NiPyipa_2$, the easy axis of magnetization is parallel to the surface, while for $CoPyipa_2$ the hard axis is parallel to the surface.

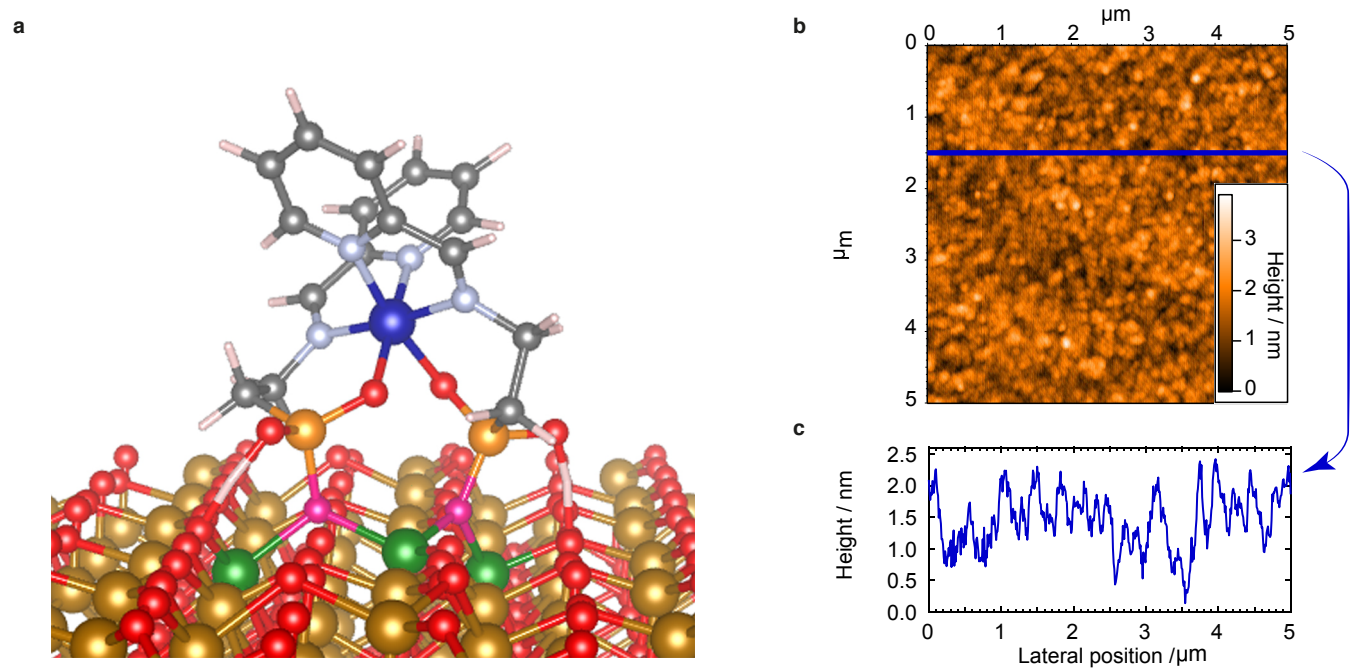

Figure 2. Monolayer of $CoPyipa_2$ on epitaxial Fe_3O_4. a, Schematic representation of the DFT minimized orientation of $CoPyipa_2$ anchored onto epitaxial Fe_3O_4: C, grey; N, lilac; O, red or magenta when bound to a phosphonate; P, orange; H, white; Co, blue; Ni, green; Fe, gold or green when bound to the molecule. **b**, AFM image of a monolayer of $CoPyipa_2$ anchored onto epitaxial Fe_3O_4. **c,** Surface profile of the monolayer of $CoPyipa_2$.

To attain the sensitivity required to probe a monolayer of molecules, element specific magnetic properties were investigated by recording the magnetic dichroic component of the X-ray absorption spectra (XAS) of the surface (Fe) and of the complexes (Co and Ni for Co- and $NiPyipa_2$, respectively) at the $L_{2,3}$ edges. Circular polarized X-rays were employed for two incidence angles ($\theta = 0°$ and 45°) between the sample normal and the X-ray propagation vector. All measurements were recorded at 2 K in the total yield electron mode with the magnetic field aligned parallel to the photon propagation vector.[7,32] The XAS spectra, and the resulting XMCD spectra (σ^--σ^+), at the iron, cobalt and nickel $L_{2,3}$ edges were acquired in the presence of a 6.5 T field employing the two circular polarizations (σ^+; σ^-). The XAS and XMCD spectra at the Fe $L_{2,3}$ edges of the

epitaxial Fe_3O_4 surface before and after molecule grafting are similar (Figure S07, and S08), and are comparable to those published in the literature,[33] demonstrating that the surface deposition method did not damage the substrates. The XAS and XMCD spectra at the Ni and the Co edges show a strong dichroic signal that is indicative of molecules deposited on the surface (Figure 3 and S09). The signals were compared with those recorded on a thick film of the same complexes deposited by drop casting. The spectra are similar, and confirmed that the electronic structure of the molecule is retained upon grafting (Figure S10). The shape of the XMCD signal at the Fe L_3 edge (Figure S07) corresponds to the situation where the magnetic moments of the octahedral Fe sites are aligned with the magnetic field (negative XMCD signal) and are antiparallel to those of the tetrahedral sites (positive XMCD signal), which correspond to an antiferromagnetic coupling between octahedral and tetrahedral sites.[33] The XMCD signal at the Co L_3 edge is aligned with the magnetic field (negative XMCD), therefore, it is aligned with the octahedral Fe sites. The identical scenario is true for Ni. It is not possible at this stage to conclude on the nature of the coupling between the magnetic molecules and the substrate from the XMCD measurements at 6.5 T and 2 K. For this task, we had to rely on theoretical calculations that are described at the end of the manuscript.

A sum rule analysis[34,35] was performed to extrapolate the values of the spin and orbital magnetic moments for Co and Ni and gave the following results. For Co^{II} the number of hole was taken to be $n_h = 3$, which results in an orbit magnetic moment $M_L = -\mu_B \langle L_Z \rangle = 0.29 \pm 0.03\ \mu_B$ and a spin magnetic moment $M_S = -g_0\mu_B \langle S_Z \rangle = 0.83 \pm 0.08\ \mu_B$, corresponding to a total magnetic moment $M = M_L + M_S = 1.12 \pm 0.11\ \mu_B$. For Ni^{II} the number of hole was taken to be $n_h = 2$, which results in an orbit magnetic moment $M_L = -\mu_B \langle L_Z \rangle = 0.18 \pm 0.02\ \mu_B$ and a spin magnetic moment $M_S = -g_0\mu_B \langle S_Z \rangle = 1.20 \pm 0.12\ \mu_B$, corresponding to a total magnetic moment $M = M_L + M_S = 1.38 \pm 0.14\ \mu_B$ (the error bars are estimated to 10 % and stem mainly from the normalization procedure and the background substraction). Interestingly the Co magnetic moment found corresponds to one third of the saturation magnetization of 3 μ_B for an isotropic $S = 3/2$ cobalt ion. This result confirms that the ground state of the Co^{II} ion is mainly built from $M_S = \pm 1/2$ with very small contributions from higher M_S ($\pm 3/2$) terms, exactly

what was found from the magnetization measurements analysis and confirmed by the *ab initio* calculations (see SI).

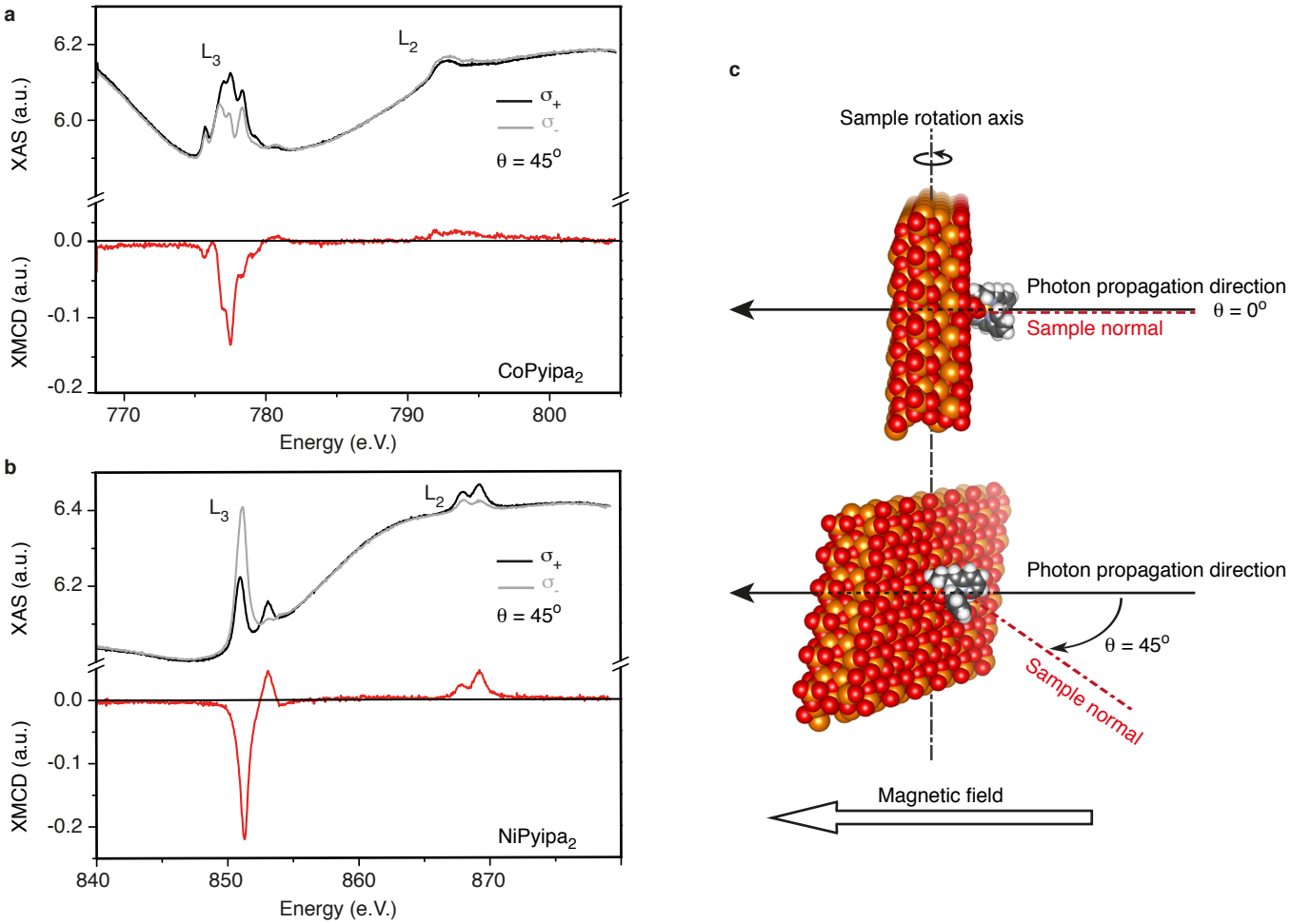

Figure 3. XAS/XMCD spectra of a monolayer of Co- and NiPyipa$_2$. a, Cobalt, and **b**, Nickel $L_{2,3}$ edges XAS (black and grey line) and XMCD (red lines) spectra recorded at T = 2 K, and θ = 45° using left (σ_+) and right hand (σ_-) circularly polarized light in 6.5 T field. **c**, Schematic representation of the measurement geometry.

To gain better insight on the nature of the interaction of Co- and NiPyipa$_2$ with the epitaxial Fe_3O_4 surface, we measured element-specific XMCD-detected hysteresis loops. The field-dependence Fe, Co and Ni L_3 XMCD intensity (multiplied by -1) at fixed photon energy and normalized are shown in Figure 4 for the geometry where the X-ray propagation vector is at 45° with the sample normal i.e. the substrate makes an angle of 45° with the applied magnetic field (Figure 3c). It was possible to see an opening of the hysteresis loop for CoPyipa$_2$ (Figure 4a), while no opening occurs when the magnetic field is perpendicular to the substrate (Figure S11a). To investigate the magnetic behavior of CoPyipa$_2$ isolated from the Fe_3O_4 surface, an ultrathin insulating

layer (1 nm of Al_2O_3) was deposited between the iron oxide surface and the molecules. No opening of the magnetization loop was seen for θ = 0 and 45°(Figure S12), which is the opposite situation in the absence of the non-magnetic, insulating layer. These data indicate that the magnetically isolated Co complexes have their hard magnetization axis parallel to the substrate as predicted from theoretical calculations (see above), and demonstrate that $CoPyipa_2$ is magnetically coupled to the surface switching the easy plane of magnetization of the Co complexes to an easy axis parallel to the substrate. No opening of the magnetization loop was seen for $NiPyipa_2$ (Figure 4b and S11b) highlighting the absence of (or the presence of very weak) magnetic coupling. We reasoned that the difference in coupling between $NiPyipa_2$ (absence of hysteresis) and $CoPyipa_2$ (presence of hysteresis) excludes dipole-dipole interactions between $CoPyipa_2$ and substrate, as such interactions would have resulted in the same behavior for the two molecules. The magnetic coupling between $CoPyipa_2$ and Fe_3O_4 is thus due to exchange.

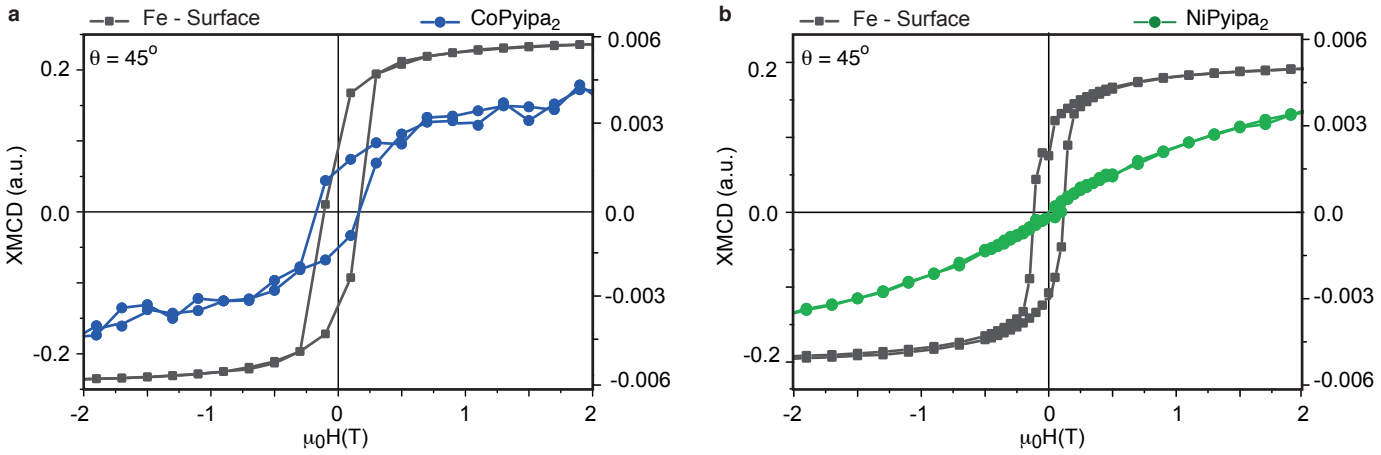

Figure 4. Element-specific field dependence of the magnetization of the Co atoms of $CoPyipa_2$, the Ni atoms of $NiPyipa_2$ and of the corresponding ferrimagnetic surface (Fe). Hysteresis curves (multiplied by -1) of the Co atoms (blue), Ni atoms (green) and Fe atoms (grey) obtained at the $L_{2,3}$ edges XMCD maxima at T = 2 K, and θ = 45°. (Monochromatized X-rays are set at the energy of the maximum absolute value of the XMCD signal (i.e. hν = 777.5 eV for Co, hν = 851 eV for Ni, and hν = 707 eV for Fe) then the external magnetic field is switched step by step from +6.5 T down to -6.5 T and back to +6.5 T. At each step the magnetic field is switched from left to right circular polarization to yield the element specific magnetization curves.

To elucidate the nature and relative magnitude of this exchange coupling, and the differences between the magnetic behavior of Co- and $NiPyipa_2$ when anchored to the surface, we carried out broken symmetry

calculations using the B3LYP functional of the GAUSSIAN 09 package (see SI for details).[36] We employed the extended basis sets: Valence Triple Zeta plus Polarization (VTZP) for Fe, Ni, Co and for the ligand atoms.[37-39] We used the results of the DFT molecular dynamic simulation described above, and considered the system composed of the three coupled Fe^{III} ions (S = 5/2) (Fe^{III}_{Oh}—Fe^{III}_{Td}–Fe^{III}_{Oh}, we assume that the surface Fe^{II} atoms were oxidized to Fe^{III})[40] surrounded by their coordinated oxygen atoms (from the surface) and the complexes either $CoPyipa_2$ (Co^{II}, S = 3/2) or $NiPyipa_2$ (Ni^{II}, S = 1). The Heisenberg Hamiltonian $\hat{H} = J_1(\hat{S}_A.\hat{S}_M + \hat{S}_C.\hat{S}_M) + J_2(\hat{S}_B.\hat{S}_M) + J_3(\hat{S}_A.\hat{S}_B + \hat{S}_B.\hat{S}_C)$ describes the low energy spectrum of the four spin centers: M = Ni^{II} or Co^{II}, $\hat{S}_B$ = the spin operator of the central tetracoordinated Fe^{III}_B ion, $\hat{S}_A$ and $\hat{S}_C$ = the spin operators of its hexacoordinated neighbors Fe^{III}_A and Fe^{III}_C, respectively (Figure 5a). The analytical energies of the various computed solutions are given in Figure 5. The Hamiltonian was chosen so that when the exchange parameters (J_i) are positive the coupling is antiferromagnetic.

First, we calculated the surface coupling in the absence of Co- or $NiPyipa_2$ ($J_1 = J_2 = 0$). As expected for an epitaxial Fe_3O_4 (111) surface, we found that the surface Fe^{III} have an antiferromagnetic coupling (J_3 = 52 cm^{-1}). The ferromagnetic solution was 1321 cm^{-1} higher in energy than the antiferromagnetic one. Second, we computed the energies in the presence of Co- or $NiPyipa_2$. The four possible coupling solutions are depicted in Figure 5b. The geometries were optimized and were quasi-identical for both complexes for the different solutions (Figure 5c).

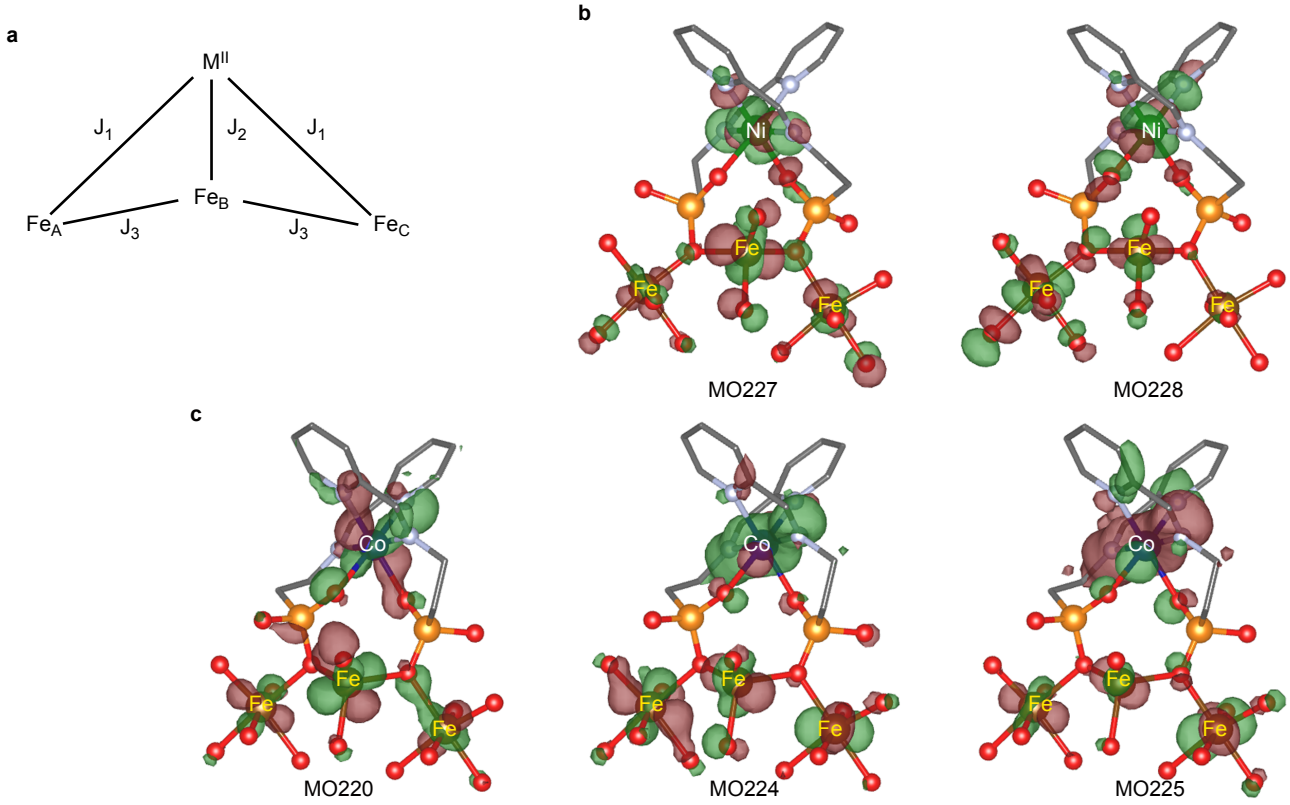

Figure 5. a, Interaction topology between the $MPyipa_2$ (M = Ni or Co) and the surface Fe ions. Optimized geometry of the singly occupied magnetic orbitals for $NiPyipa_2$ (**b**) and $CoPyipa_2$ (**c**). Positive (red) and negative (green) isosurfaces for the high spin solution. C, grey; N, lilac; O, red; P, orange; Co, blue; Ni, green; Fe, dark orange; hydrogen atoms were omitted for clarity. The MO labels are in ascending energy levels.

By computing the energies of the different solutions based on the coupling scheme depicted in Figure 5a, we find that the coupling between the Ni^{II} (or Co^{II}) ions and the surface is independent from the nature (ferromagnetic or antiferromagnetic) of the exchange coupling within the substrate (see SI for details). From the energy differences between the various solutions we obtained $J_1 = 18$ cm^{-1}, $J_2 = -2$ cm^{-1}, $J_3 = -40$ cm^{-1} for $NiPyipa_2$, and $J_1 = -54$ cm^{-1}, $J_2 = -49$ cm^{-1}; $J_3 = -47$ cm^{-1} for $CoPyipa_2$. This translates into a *weakly antiferromagnetic* exchange coupling between the $NiPyipa_2$ and the surface and a *strongly ferromagnetic* coupling for $CoPyipa_2$..

The opposite nature of the exchange interaction can be explained by the difference in the molecular orbitals (MO) depicted in Figure 5. None of the singly occupied molecular orbitals (SOMOs) of $CoPyipa_2$ have a strong overlap with the Fe^{III} SOMOs through the bridging oxygen ligands (see MOs number 220, 224 and 225 in Figure 5). The most important physical factor contributing to the exchange coupling of $CoPyipa_2$ with the surface is brought by the direct exchange integrals between all the magnetic SOMOs, which are always

ferromagnetic.[41,42] On the contrary, one of the two SOMOs of $NiPyipa_2$ (MO number 228, Figure 5) exhibits an extended delocalization tail on the oxygen atom bridging the complex to the surface through the phosphonic acid anchoring group. The overlap between this $NiPyipa_2$ SOMO and the Fe^{III} one brings a large kinetic contribution (antiferromagnetic) to the exchange coupling that compensates and overcomes the ferromagnetic contribution and leads to an overall antiferromagnetic interaction.[41,42] The difference between the nature of the couplings is also corroborated by the shorter M^{II}/spacer/surface distance for $NiPyipa_2$ than for $CoPyipa_2$, strengthening the antiferromagnetic superexchange mechanism. It is important to note that the absolute numerical values of J_i have to be considered with caution due to the approximations made in the calculations. The much stronger ferromagnetic coupling of the Co^{II} center with the surface compared to the Ni^{II} center explains the opening (or lack there of) of the magnetic hysteresis for $CoPyipa_2$ (or $NiPyipa_2$) when deposited onto the ferrimagnetic surface. XMCD measurements at lower temperatures (XMCD below 1 K is not accessible on the DEIMOS line) would likely provide further indications on the nature of the magnetic coupling in the $NiPyipa_2$ system. [7,8]

Conclusions

In conclusion, we have shown that by *molecular design*, we can chemically anchor metal-containing molecules to a magnetic iron oxide electrode and we can finely control the molecule/electrode interface structure. The coupling between the magnetic molecules and Fe_3O_4 is due to exchange and not to dipole-dipole interactions. The electronic structure of the metal ion has a paramount importance on the nature of the coupling: $CoPyipa_2$ undergoes a strong ferromagnetic coupling with the substrate while the structurally analogous $NiPyipa_2$ is weakly antiferromagnetically coupled. We can, therefore, envision that controlling the molecule/substrate exchange interaction would allow tuning the spin current (sign of the magnetoeresistance) at the interface and eventually lead to using such current to switch the magnetization of single anisotropic molecules in molecule-based spintronic devices.

Methods

This section describes general synthetic methods for Co- and $NiPyipa_2$ synthesis and self-assembly on epitaxial Fe_3O_4 (111) only; a detailed experimental section is provided in the Supplementary Methods.

($MPyipa_2$). A round bottom flask was charged with 2-aminoethylphosphonic acid (2 equiv.), 2-pyridinecarboxaldehyde (2 equiv.), $M(CH_3COO)_2{\cdot}4\ H_2O$ (1 equiv.), MeOH (4 mL) and demineralized H_2O (4 mL). The reaction mixture was heated at reflux for 3 hours. The solvent was evaporated and a red product was obtained. The product was purified by vapor diffusion of Et_2O into a MeOH solution of $MPyipa_2$ ($CoPyipa_2$: *m* = 109.5 mg; yield = 74%; $NiPyipa_2$: *m* = 98.6 mg; yield = 67%).

Monolayer preparation: The monolayers were prepared by immersion of the Fe_3O_4 substrates into 10 mL of a freshly filtered 0.5 mM solution of either $CoPyipa_2$ or $NiPyipa_2$ dissolved in the desired solvent. After 3 days of immersion the substrates were removed from the solution and rinsed thoroughly with neat solvent. All the functionalization experiments were carried out at room temperature.

Acknowledgements

This work is supported by a public grant overseen by the French National Research Agency (ANR) as part of the "Investissements d'Avenir" program "Labex NanoSaclay" (reference: ANR-10-LABX-0035). We acknowledge SOLEIL for provision of synchrotron radiation facilities. This work was performed using HPC resources from CALMIP (Grant 2015-1517).

Author Contribution

V.E.C., M.T., J.B.M., and T.M. planned and conceived the experiments and study. M.T. and I.C. synthesized and characterized the molecules. J.B.M. provided the surfaces. R.G. collected and analyzed the single crystal X-ray data. M.T., E.R., V.E.C., and T.M. executed the magnetic characterization. L.T., M.T., and I.C. took the AFM images. Y.J.D. performed the DFT molecular simulations. V.E.C., M.T., T.M., E.O., P.O, P.S., M.A.A., R.M., P.S. and S.D. collected and analyzed the XMCD data. N.G., V.G.C., F.K, and N.S performed the *ab initio* calculations on the isolated molecules and the molecules on the surface. A.G., and V.E.C. collected the

Tof-SMIs data. All authors participated in the discussion. V.E.C. wrote the paper with contributions form all authors.

Additional information

Supplementary information and compound characterization accompany this manuscript. Correspondance and request for materials should be addressed to V.E.C. and T.M.

Competing financial interest

The authors declare no competing financial interests.

References

1 Bogani, L. & Wernsdorfer, W. Molecular spintronics using single-molecule magnets. *Nat. Mater.* **7**, 179-186, (2008).
2 Sanvito, S. Molecular spintronics. *Chem. Soc. Rev.* **40**, 3336, (2011).
3 Barraud, C. *et al.* Unravelling the role of the interface for spin injection into organic semiconductors. *Nat. Phys.* **6**, 615-620, (2010).
4 Blouzon, C., Ott, F., Tortech, L., Fichou, D. & Moussy, J. B. Anti-ferromagnetic coupling in hybrid magnetic tunnel junctions mediated by monomolecular layers of α-sexithiophene. *Appl. Phys. Lett.* **103**, 042417, (2013).
5 Wende, H. *et al.* Substrate-induced magnetic ordering and switching of iron porphyrin molecules. *Nat. Mater.* **6**, 516-520, (2007).
6 Schmaus, S. *et al.* Giant magnetoresistance through a single molecule. *Nat. Nanotech.* **6**, 185-189, (2011).
7 Mannini, M. *et al.* Magnetic memory of a single-molecule quantum magnet wired to a gold surface. *Nat. Mater.* **8**, 194-197, (2009).
8 Mannini, M. *et al.* Quantum tunnelling of the magnetization in a monolayer of oriented single-molecule magnets. *Nature* **468**, 417-421, (2010).
9 Malavolti, L. *et al.* Magnetism of $TbPc_2$ SMMs on ferromagnetic electrodes used in organic spintronics. *Chem. Commun.* **49**, 11506, (2013).
10 Lodi Rizzini, A. *et al.* Exchange Biasing Single Molecule Magnets: Coupling of $TbPc_2$ to Antiferromagnetic Layers. *Nano Letters* **12**, 5703-5707, (2012).
11 Scheybal, A. *et al.* Induced magnetic ordering in a molecular monolayer. *Chem. Phys. Lett.* **411**, 214-220, (2005).
12 Annese, E., Casolari, F., Fujii, J. & Rossi, G. Interface magnetic coupling of Fe-phthalocyanine layers on a ferromagnetic surface. *Phys. Rev. B* **87**, 054420, (2013).
13 Auwärter, W., Écija, D., Klappenberger, F. & Barth, J. V. Porphyrins at interfaces. *Nat. Chem.* **7**, 105-120, (2015).
14 Rizzini, A. L. *et al.* Coupling of single, double, and triple-decker metal-phthalocyanine complexes to ferromagnetic and antiferromagnetic substrates. *Surf. Sci.* **630**, 361-374, (2014).
15 Gooding, J. J. & Ciampi, S. The molecular level modification of surfaces: from self-assembled monolayers to complex molecular assemblies. *Chem. Soc. Rev.* **40**, 2704, (2011).
16 Bauer, T. *et al.* Phosphonate- and Carboxylate-Based Self-Assembled Monolayers for Organic Devices: A Theoretical Study of Surface Binding on Aluminum Oxide with Experimental Support. *ACS Appl. Mater. Inter.* **5**, 6073-6080, (2013).
17 White, M. A., Johnson, J. A., Koberstein, J. T. & Turro, N. J. Toward the syntheses of universal ligands for metal oxide surfaces: Controlling surface functionality through click chemistry. *J. Am. Chem. Soc.* **128**, 11356-11357, (2006).
18 Tatay, S. *et al.* Self-assembled monolayer-functionalized half-metallic manganite for molecular spintronics. *Acs Nano* **6**, 8753-8757, (2012).
19 Textor, M. *et al.* Structural Chemistry of Self-Assembled Monolayers of Octadecylphosphoric Acid on Tantalum Oxide Surfaces. *Langmuir* **16**, 3257-3271, (2000).
20 Queffélec, C., Petit, M., Janvier, P., Knight, D. A. & Bujoli, B. Surface Modification Using Phosphonic Acids and Esters. *Chem. Rev.* **112**, 3777-3807, (2012).
21 Gagnon, K. J., Perry, H. P. & Clearfield, A. Conventional and Unconventional Metal–Organic Frameworks Based on Phosphonate Ligands: MOFs and UMOFs. *Chem. Rev.* **112**, 1034-1054, (2012).
22 Mutin, P. H., Guerrero, G. & Vioux, A. Hybrid materials from organophosphorus coupling molecules. *J. Mater. Chem.* **15**, 3761, (2005).
23 Roos, B. O. & Malmqvist, P.-A. Relativistic quantum chemistry: the multiconfigurational approach. *Phys. Chem. Chem. Phys.* **6**, 2919-2927, (2004).
24 Karlstroem, G. *et al.* MOLCAS: a program package for computational chemistry. *Comput. Mater. Sci.* **28**, 222-239, (2003).

25 Malmqvist, P. A., Roos, B. O. & Schimmelpfennig, B. The restricted active space (RAS) state interaction approach with spin-orbit coupling. *Chem. Phys. Lett.* **357**, 230-240, (2002).
26 Lewis, J. P. *et al.* Advances and applications in the FIREBALL ab initio tight-binding molecular-dynamics formalism. *Phys. Status Solidi B* **248**, 1989–2007, (2011).
27 Basanta, M. A., Dappe, Y. J., Jelínek, P. & Ortega, J. Optimized atomic-like orbitals for first-principles tight-binding molecular dynamics. *Comput. Mater. Sci.* **39**, 759-766, (2007).
28 Harris, J. Simplified Method for Calculating the Energy of Weakly Interacting Fragments. *Phys. Rev. B* **31**, 1770-1779, (1985).
29 Jelínek, P., Wang, H., Lewis, J., Sankey, O. & Ortega, J. Multicenter approach to the exchange-correlation interactions in ab initio tight-binding methods. *Phys. Rev. B* **71**, 235101, (2005).
30 Pentcheva, R. *et al.* Jahn-Teller Stabilization of a "Polar" Metal Oxide Surface:Fe_3O_4 (001). *Phys. Rev. Lett.* **94**, 126101, (2005).
31 Schull, G., Dappe, Y. J., González, C. s., Bulou, H. & Berndt, R. Charge Injection through Single and Double Carbon Bonds. *Nano Letters* **11**, 3142-3146, (2011).
32 Nakajima, R., Stohr, J. & Idzerda, Y. U. Electron-yield saturation effects in L-edge x-ray magnetic circular dichroism spectra of Fe, Co, and Ni. *Phys. Rev. B* **59**, 6421, (1999).
33 Carvallo, C. *et al.* Biogenic vs. abiogenic magnetite nanoparticles: A XMCD study. *Am. Mineral.* **93**, 880-885, (2008).
34 Carra, P., Thole, B. T., Altarelli, M. & Wang, X. X-ray circular dichroism and local magnetic fields. *Phys. Rev. Lett.* **70**, 694-697, (1993).
35 Thole, B. T., Carra, P., Sette, F. & van der Laan, G. X-ray circular dichroism as a probe of orbital magnetization. *Phys. Rev. Lett.* **68**, 1943-1946, (1992).
36 Gaussian 09 (Revision C.01) (Gaussian, Inc., Pittsburgh, PA, 2003).
37 Wachters, A. J. H. Gaussian Basis Set for Molecular Wavefunctions Containing Third‐Row Atoms. *J. Chem. Phys.* **52**, 1033, (1970).
38 Hay, P. J. Gaussian basis sets for molecular calculations. The representation of 3d orbitals in transition‐metal atoms. *J. Chem. Phys.* **66**, 4377, (1977).
39 Raghavachari, K. & Trucks, G. W. Highly correlated systems. Excitation energies of first row transition metals Sc–Cu. *J. Chem. Phys.* **91**, 1062, (1989).
40 Kaya, S., Ogasawara, H. & Nilsson, A. Determination of the surface electronic structure of Fe3O4(1 1 1) by soft X-ray spectroscopy. *Catal. Today* **240, Part B**, 184-189, (2015).
41 Malrieu, J. P. Cancellations Occurring in the Calculation of Transition Energies by a Perturbation Development of Configuration Interaction Matrices. *J. Chem. Phys.* **47**, 4555, (1967).
42 Anderson, P. W. New Approach to the Theory of Superexchange Interactions. *Phys. Rev. Lett.* **115**, 2-13, (1959).

Engineering the magnetic coupling at the molecule/electrode interface between self-assembled metal complexes and epitaxial ferrimagnetic iron oxide.

Victoria Campbell*[1], Monica Tonelli[1], Irene Cimatti[1], Jean-Baptiste Moussy[2], Ludovic Tortech[2,3], Yannick J. Dappe[2], Eric Rivière[1], Régis Guillot[1], Sophie Delprat[4], Richard Mattana[4], Pierre Seneor[4], Philippe Ohresser[5], Fadi Choueikani[5], Edwige Otero[5], Florian Koprowiak[6], Vijay Gopal Chilkuri[6], Nicolas Suaud[6], Nathalie Guihéry[6], Anouk Galtayries[7], Marie-Anne Arrio[8], Philippe Sainctavit[5,8], and Talal Mallah*[1]

*victoria.campbell@u-psud.fr and talal.mallah@u-psud.fr

[1]Institut de Chimie Moléculaire et des Matériaux d'Orsay, CNRS, Université Paris Sud 11, 91405 Orsay Cedex, France

[2]CEA-Saclay, IRAMIS, SPCSI, F-91191 Gif-sur-Yvette, France

[3]IPCM, UMR CNRS 7201, UPMC, Université Pierre et Marie Curie, F-75005 Paris, France

[4]Unité Mixte de Physique CNRS/Thales, 1 Avenue Auguste Fresnel, 91767 Palaiseau, France and Université Paris-Sud, 91405 Orsay, France

[5]Synchrotron SOLEIL, L'Orme des Merisiers Saint-Aubin—BP 48, Gif-sur-Yvette 91192, France

[6]Laboratoire de Chimie et Physique Quantiques, Universit´e de Toulouse III, 118, route de Narbonne, 31062 Toulouse, France

[7]Laboratoire de Physico-Chimie des Surfaces, CNRS-ENSCP (UMR 7045), Chimie ParisTech, 11 rue Pierre et Marie Curie, F-75005 Paris, France

[8]IMPMC-CNRS, Université Pierre et Marie Curie, F-75005 Paris, France

Methods

Epitaxial Fe_3O_4(111) thin films were grown by molecular beam epitaxy on α-Al_2O_3 (0001) according to literature procedures.[1]

Unless otherwise stated, all reagents were purchased from Aldrich or TCI and used without further purification. Electrospray ionization mass spectrometry (ESI-MS) spectra were recorded on a Thermo Scientific 2009 mass spectrometer. IR spectra were recorded on a Bruker TENSOR-27 Fourier transform infrared (FT-IR)

spectrometer equipped with an attenuated total reflectance (ATR crystal diamond/ZnSe) sample holder in the 4000 - 500 cm^{-1} range. Elemental analysis was taken on a Thermo Scientific Flash analyzer.

Cobalt(II) bis-2-[(Pyridin-2-ylmetylene)amino]ethyl phosphonic acid ($CoPyipa_2$). A round bottom flask was charged with 2-aminoethylphosphonic acid (77.8 mg, 0.622 mmol), 2-pyridinecarboxaldehyde (58 μL, 0.610 mmol), $Co(CH_3COO)_2 \cdot 4\ H_2O$ (75 mg, 0.301 mmol), MeOH (4 mL) and demineralized H_2O (4 mL). The reaction mixture was heated at reflux for 3 hours. The solvent was evaporated and a red product was obtained. The product was purified by vapor diffusion of Et_2O into a MeOH solution of $CoPyipa_2$ (*m* = 109.5 mg; yield = 74%). IR (ν/cm^{-1}): 3317 (br), 2946 (br), 2888 (br), 2529 (br), 2162 (s), 1981 (br), 1780 (m), 1660 (s), 1626 (m), 1589 (m), 1571 (m), 1469 (br), 1446 (s), 1366 (br), 1352 (br), 1286 (s), 1226 (s), 1156 (s), 1104 (m), 1091 (m), 1051 (m), 1033 (m), 1010 (s), 988 (s), 962 (m), 937 (s), 897 (s), 875 (s), 813 (m), 785 (m), 744 (m), 707 (br), 662 (s), 634 (m). ESI-MS: *m/z* 486.03 ($[CoPyipa_2]^+$). Elem anal. Calcd for $C_{16}H_{24}N_4O_8P_2Co$: C, 36.87; H, 4.64; N, 10.75. Found: C, 36.80; H, 4.82; N, 10.73.

Nickel(II) bis-2-[(Pyridin-2-ylmetylene)amino]ethyl phosphonic acid ($NiPyipa_2$). A round bottom flask was charged with 2-aminoethylphosphonic acid (85.0 mg, 0.680 mmol), 2-pyridinecarboxaldehyde (64 μL, 0.673 mmol), $Ni(CH_3COO)_2 \cdot 4\ H_2O$ (80 mg, 0.321 mmol), MeOH (4 mL) and demineralized H_2O (4 mL). The reaction mixture was heated at reflux for 3 hours. The solvent was evaporated and a red product was obtained. The product was purified by vapor diffusion of Et_2O into a MeOH solution of $NiPyipa_2$ (*m* = 98.6 mg; yield = 67%). IR (ν/cm^{-1}): 3317 (br), 2946 (br), 2888 (br), 2529 (br), 2162 (s), 1981 (br), 1780 (m), 1660 (s), 1626 (m), 1589 (m), 1571 (m), 1469 (br), 1446 (s), 1366 (br), 1352 (br), 1286 (s), 1226 (s), 1156 (s), 1104 (m), 1091 (m), 1051 (m), 1033 (m), 1010 (s), 988 (s), 962 (m), 937 (s), 897 (s), 875 (s), 813 (m), 785 (m), 744 (m), 707 (br), 662 (s), 634 (m). ESI-MS: *m/z* 485.04 ($[NiPyipa_2]^+$). Elem anal. Calcd for $C_{16}H_{28}N_4O_{10}P_2Ni$: C, 34.50; H, 5.07; N, 10.06. Found: C, 34.37; H, 4.54; N, 10.02.

Single Crystal X-ray Diffraction Studies. X-ray diffraction data were collected by using a Kappa X8 APPEX II Bruker diffractometer with graphite-monochromated $Mo_{K\alpha}$ radiation (λ = 0.71073 Å). Crystals were mounted on a CryoLoop (Hampton Research) with Paratone-N (Hampton Research) as cryoprotectant and then

flashfrozen in a nitrogen-gas stream at 100 K. The temperature of the crystal was maintained at the selected value (100K) by means of a 700 series Cryostream cooling device to within an accuracy of ±1 K. The data were corrected for Lorentz polarization, and absorption effects. The structures were solved by direct methods using SHELXS-97[2] and refined against F^2 by full-matrix least-squares techniques using SHELXL-97[3] with anisotropic displacement parameters for all non-hydrogen atoms. Hydrogen atoms were located on a difference Fourier map and introduced into the calculations as a riding model with isotropic thermal parameters. All calculations were performed by using the Crystal Structure crystallographic software package WINGX.[4] CCDC-1049643 and CCDC-1049644 contain the supplementary crystallographic data for $NiPyipa_2$ and $CoPyipa_2$, respectively. These data can be obtained free of charge from the Cambridge Crystallographic Data Centre via www.ccdc.cam.ac.uk/data_request/cif.

Table S1. Crystallographic data for complex $CoPyipa_2$ and $NiPyipa_2$.

Compound	**$CoPyipa_2$**	**$NiPyipa_2$**
Formula	$C_{16}CoH_{20}N_4O_6P_2$,	$C_{16}H_{20}N_4NiO_6P_2$,
fw	485.23	484.99
Crystal size / mm^3	0.11 x 0.07 x 0.04	0.24 x 0.06 x 0.01
Crystal system	monoclinic	monoclinic
Space group	*C 2/c*	*C 2/c*
a, Å	26.3780(13)	25.9071(8)
b, Å	9.0590(4)	9.1614(3)
c, Å	16.5517(7)	16.4713(4)
α, °	90	90
β, °	102.2860(10)	100.9560(10)
γ, °	90	90
Cell volume, $Å^3$	3864.6(3)	3838.1(2)
Z	8	8
T, K	100(1)	100(1)
F_{000}	1992	2000
μ / mm^{-1}	1.097	1.221
θ range / °	1.58 – 30.51	1.60 – 30.51
Refl. collected	29 403	29 473
Refl. unique	5 844	5 540
R_{int}	0.0616	0.0340
GOF	1.031	1.036
Refl. obs. ($I>2\sigma(I)$)	3 926	4 321
Parameters	676	266
wR_2 (all data)	0.1299	0.1401
R value ($I>2\sigma(I)$)	0.0524	0.0540
Largest diff. peak and hole (e-.$Å^{-3}$)	-0.967; 1.996	-1.268 ; 1.642

Magnetic Measurements. The magnetic susceptibility measurements were obtained using a Quantum Design SQUID magnetometer MPMS-XL7 operating between 1.8 and 300 K for dc-applied fields ranging from -5 to 5 T. Dc analysis was performed on polycrystalline samples of Co- and $NiPyipa_2$ (17.61 mg and 17.31 mg, respectively) wrapped in eicosan under a field between 0.1 and 1 T and between 1.8 and 300 K. The $\chi_M T$ = f(T) curve for $NiPyipa_2$ shows a Curie-law behavior between 300 and 50 K (ground state with no first order orbital momentum $^3A_{2g}$) and then decreases indicating the presence of a zero-field splitting (ZFS) within the S = 1 state (Figure S01). While, for $CoPyipa_2$ a steady decrease is observed from room temperature down to 75 K and then more rapidly, in line with a ground state with a non completely quenched orbital momentum as expected for slightly distorted octahedral for Co^{II} complexes.[5] The data for Co- and $NiPyipa_2$ were fitted by a full

diagonalization of the energy matrices considering many orientations of the magnetic field. The best fits lead to the following parameters: D_{Ni} = – 5.2 cm^{-1}, E_{Ni} = 0, g_{Ni} = 2.22, R (agreement factor) = $2x10^{-5}$, D_{Co} = + 30.2 cm^{-1}, E_{Co} = 5.0 cm^{-1}, g_{Co} = 2.3, R = $5x10^{-4}$. *D* and *E* are the axial and the rhombic ZFS parameters, and g is the Lande factor of the spin Hamiltonian $H = g\mu_B\mathbf{H}\bullet\mathbf{S} + D[S_z^2 - S(S+1)/3] + E(S_x^2 - S_y^2)$. These parameters are related to the **D** tensor matrix elements by $2E = |D_{xx} - D_{yy}|$ and $D = 3D_{zz}/3$.

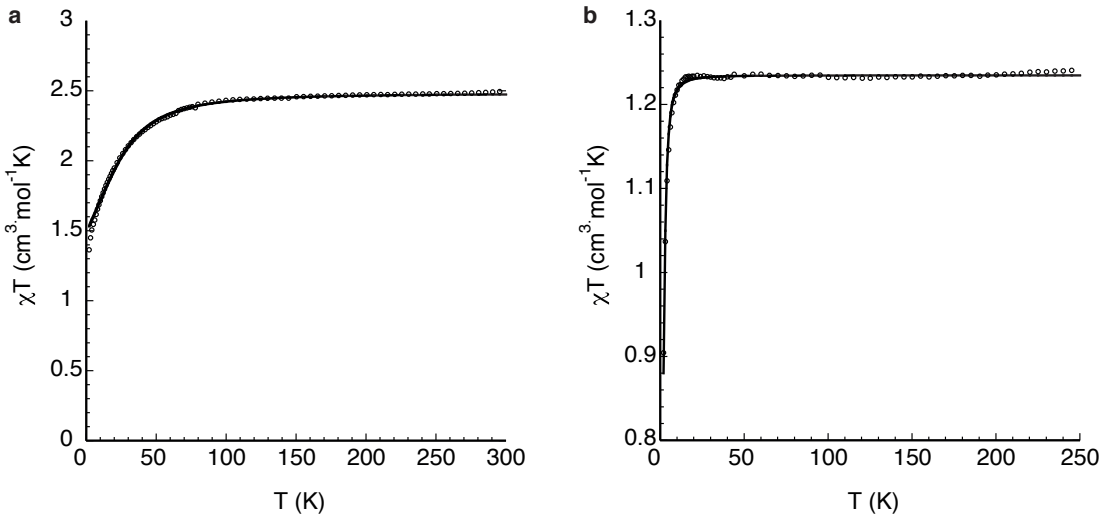

Figure S01. $\chi_M T$ = f(T) curve for $CoPyipa_2$ (a) and $NiPyipa_2$ (b). Solid line corresponds to the best fit.

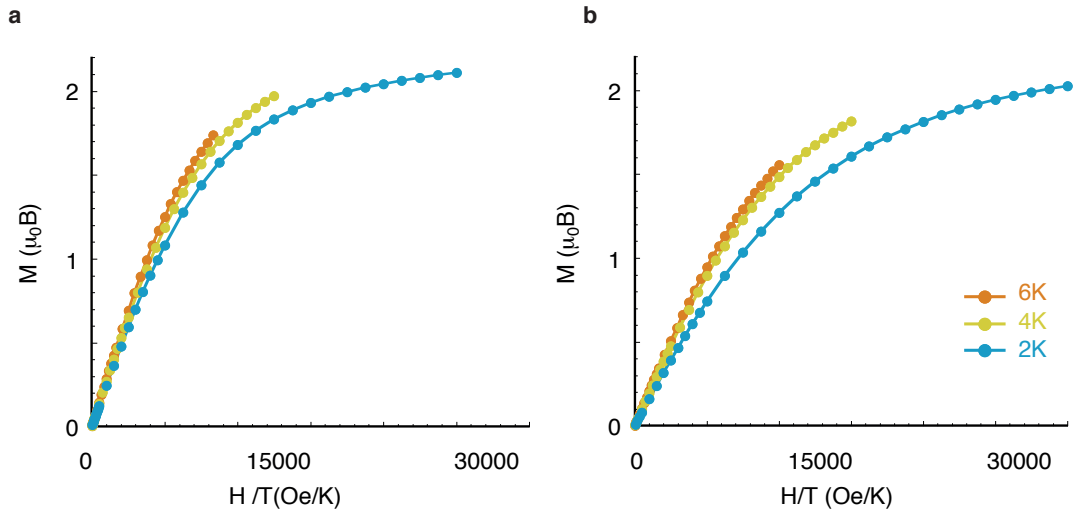

Figure S02. Reduced magnetization plots (M = f(μ_0H/T) for $CoPyipa_2$ (a) and $NiPyipa_2$ (b).

***Ab initio* calculations**. *Ab initio* calculations using the spin-orbit state interaction (SOSI) method, which treats the spin-orbit coupling (SOC)[6,7] in the wave function theory (WFT)- based framework (implemented in the

MOLCAS code[8]) permits the calculation of the ZFS parameters from first principles and the determination of the orientation of the main axes of the anisotropy tensor according to a well-established method, which is known to provide accurate results.[9-15] The calculations, in very good agreement with experimental data, lead to D_{Ni} = -3.4 cm^{-1} and E_{Ni} = 0.7 cm^{-1}, which corresponds to a weak separation between the ground $M_S = \pm 1$ (not degenerate because $E \neq 0$ for a non Kramers sub-levels) and the excited $M_S = 0$ of 3.4 cm^{-1}. The easy axis of magnetization was found to be perpendicular to the C_2 symmetry axis of the molecule and makes an angle of 10° with the N_{amine}-Ni-N_{amine} direction. For $CoPyipa_2$, the calculation gives D_{Co} = + 32.3 cm^{-1} and E_{Co} = 4.1 cm^{-1}, which corresponds to a large energy separation between the ground $M_S = \pm 1/2$ and the excited $M_S = \pm 3/2$ sub-levels of 64.6 cm^{-1} (= 2|D|).

X-ray photoelectron spectroscopy was carried out using monochromatized Al K alpha1 X-rays (hv = 1486.6 eV), a hemispherical analyzer, and a channel plate detector. The spectrometer was calibrated at the Au 4f core level at a binding energy of 84 eV. Spectra were recorded at a takeoff angle of 90°. The pass energy was set to 160 eV for survey and 20 eV for core level, giving an energy resolution of 0.38 eV.

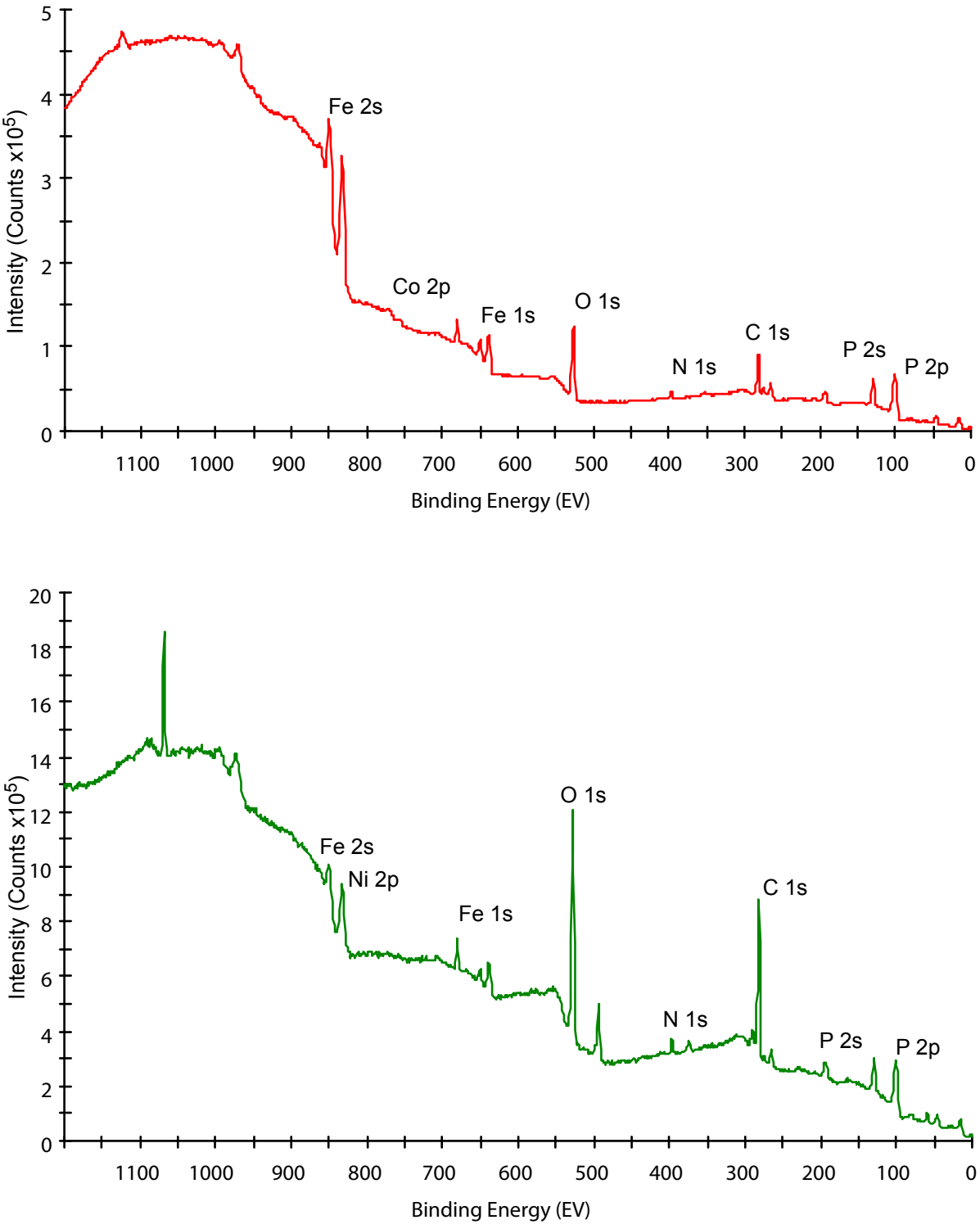

Figure S03. XPS of: top, $CoPyipa_2$; bottom, $NiPyipa_2$.

Atomic Force Microscopy:

AFM images were recorded using a Pico-LE microscope (Molecular Imaging-Agilent Technologies) in contact mode. AFM tips were Si-coated with Pt/Ir alloy with a stiffness in between 0.1 N/m and 0.3 N/m. The tip radius was given at 20 nm.

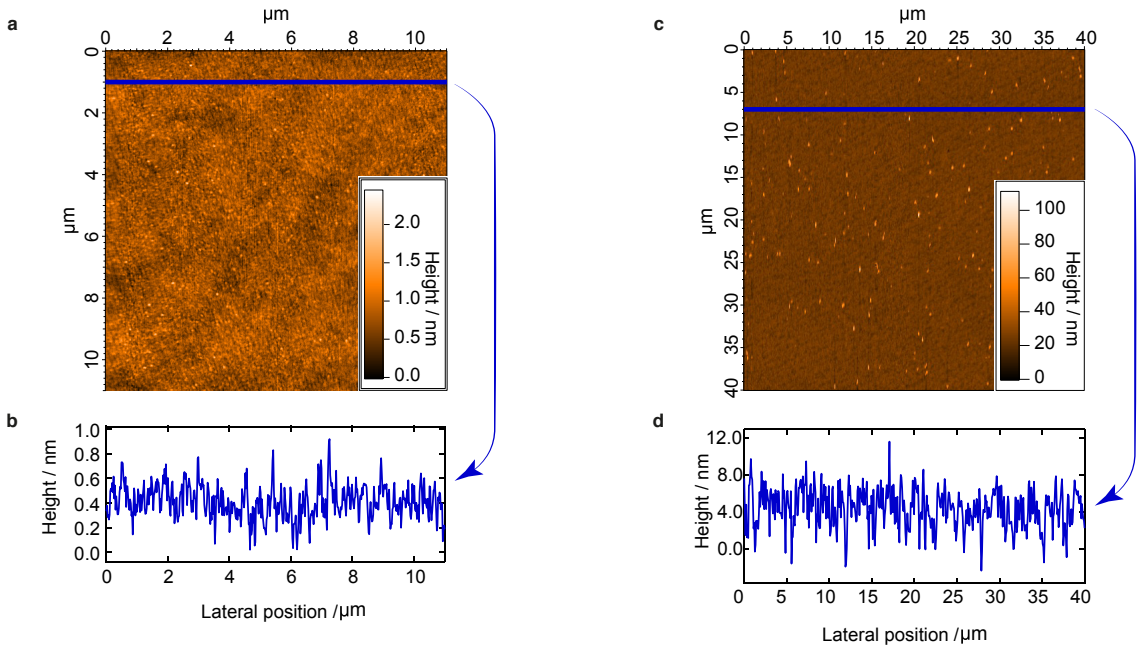

Figure S04. AFM images. a, Fe_3O_4; **b**, surface profile of Fe_3O_4 as indicated by the blue line; **c** monolayer of $NiPyipa_2$; **d**, surface profile of $NiPyipa_2$ as indicated by the blue line.

Time-of-flight secondary ion mass spectrometry (Tof-SIMS): Time-of-flight secondary ion mass spectrometry data were acquired using a TOF.SIMS V spectrometer (ION-TOF GmbH, Muenster, Germany). The analysis chamber was maintained at less than 5 10^{-7} Pa under operational conditions. The total primary ion flux was less than 1012 ions cm^{-2} ensuring static conditions. A pulsed 25 keV Bi^+ primary ion source at a current of 1.3 pA (high current bunched mode), rastered over a scan area of 100 mm 100 mm was used as the analysis beam. ToF-SIMS depth profiles were measured with the instrument working in the dual-beam mode. The sputtering was performed using a 0.5 keV (30nA) or 2 keV (80 nA) Cs^+ ion beam, rastered over an area of 300 mm 300 mm. Both ion beams were impinging the sample surface forming a 45° angle with the surface normal and were aligned in such a way that the analyzed ions were taken from the center of the sputtered crater. Data acquisition and processing analyses were performed using the commercial IonSpec program. The exact

mass values of at least five known species, from H^-, C^-, C^-_2, C^-_3, and Cl^-, were used for calibration of the data acquired in the negative ion mode, in which the best information was obtained with regard to our oxidized systems. The mass resolution, M/ΔM, was >10 000 for the low mass range (<100).

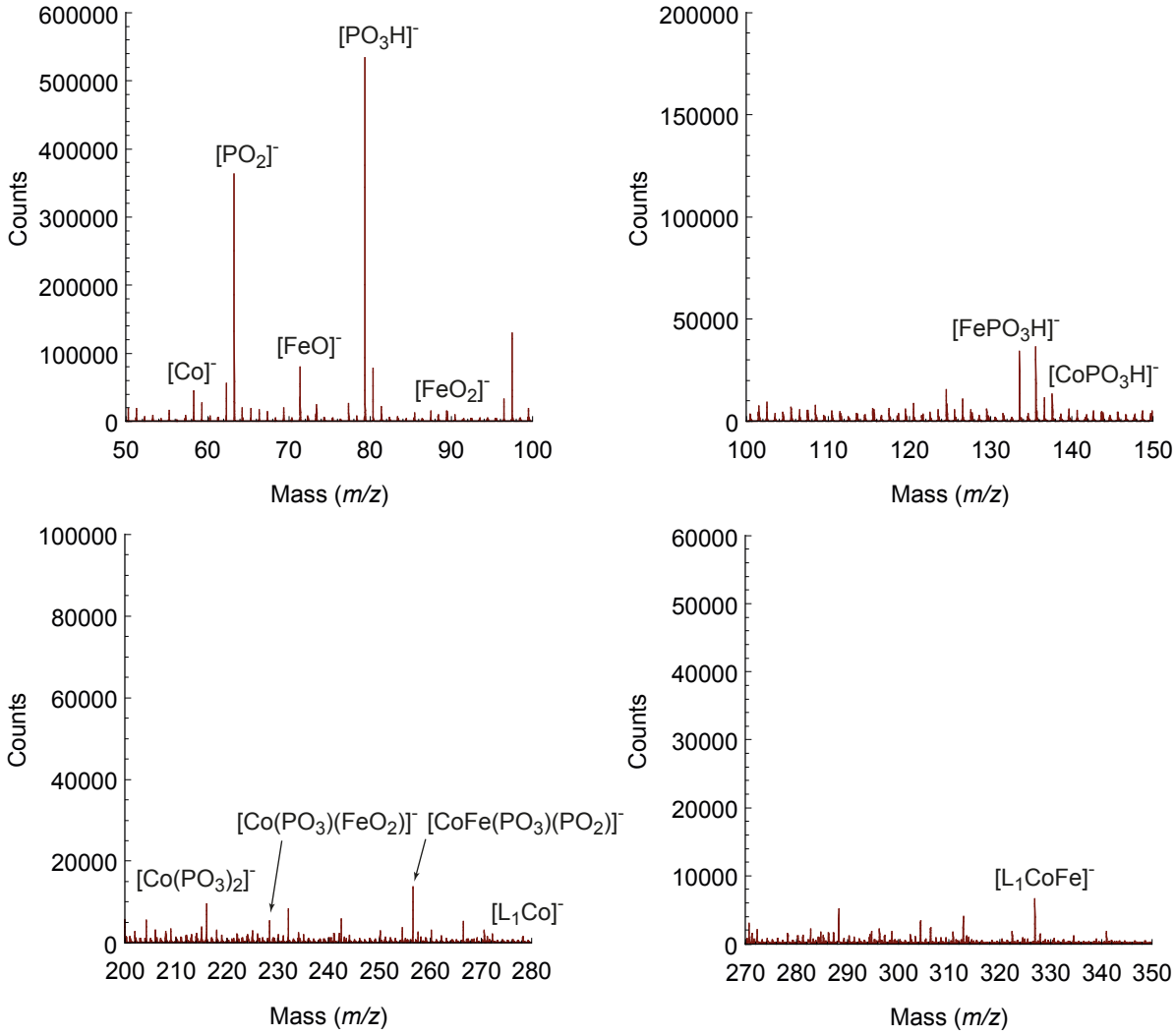

Figure S05. Tof-SIMS spectra of $CoPyipa_2$ on epitaxial $F_3O_4(111)$.

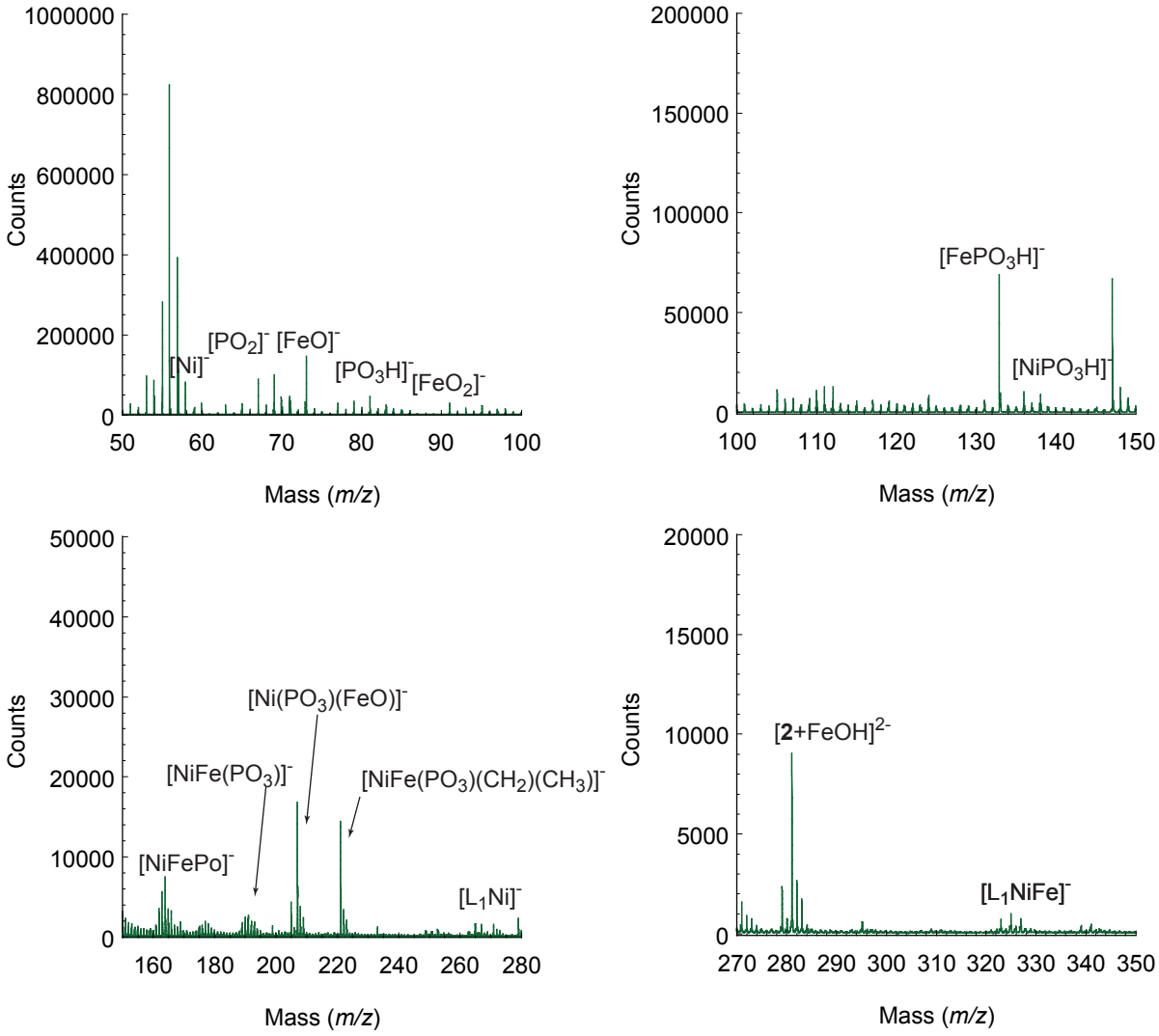

Figure S06. Tof-SIMS spectra of $NiPyipa_2$ on epitaxial $F_3O_4(111)$.

Density Functional Theory – Geometrical optimization: The FIREBALL package uses a localized optimized minimal basis set[16] and the self-consistency is achieved over the occupation numbers through the Harris functional.[17] The LDA exchange-correlation energy is calculated using the efficient multi center weighted exchange correlation density approximation (McWEDA).[18]

In our calculations, we have considered an 8 ML slab of 4 x 4 unit cells of Fe_3O_4 oriented along the (111) direction and two *k*-points. We have set the molecule in three different initial configurations, namely a physisorbed configuration and two chemisorbed configurations, considering the anchoring of the molecule with two equivalent or non-equivalent oxygen atoms of the surface. Then, we have proceeded to a DFT molecular

dynamic simulation at room temperature to reproduce the experimental conditions of molecular deposition on the surface, followed by a structural optimization at 0K to determine the final configuration on the surface. This well-established procedure[19] gives us a stable structure in the three configurations, as well as the molecular adsorption energies:

Physisorption: -2.51 eV/molecule

Chemisorption (non equivalent O): -8.14 eV/molecule

Chemisorption (equivalent O): -10.11 eV/molecule

The latter configuration seems to be the most stable, defining the molecular orientation observed in the experiments and more importantly the site where the molecules are linked to the Fe surface atoms.

XAS/ XMCD studies: The XAS/XMCD studies at the Fe, Co and Ni $L_{2,3}$ edges were carried out at the DEIMOS beam line, SOLEIL Synchrotron (Gif-sur-Yvette, France).[20,21] To ensure optimal detection sensitivity, the absorption spectra were measured in the Total Electron Yield mode. We used low density photons to avoid radiation damages to the samples. XMCD spectra were obtained from circularly polarized absorption spectra at 2 K under an applied magnetic filed of 6.5 T parallel to the X-ray propagation vector. The XMCD-detected hysteresis loops were obtained at 2 K with the magnetic field sweeping (-6.5 to 6.5 T) parallel to the X-ray propagation vector.

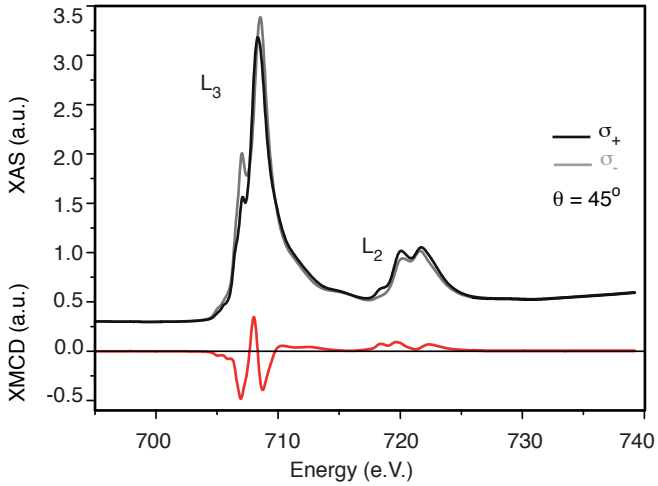

Figure S07. XAS/XMCD of epitaxial Fe_3O_4(111). Iron $L_{2,3}$ edge XAS and XMCD spectra recorded at T = 2 K, and θ = 45° using left (σ_+) and right hand (σ_-) circularly polarized light in 6.5 T field.

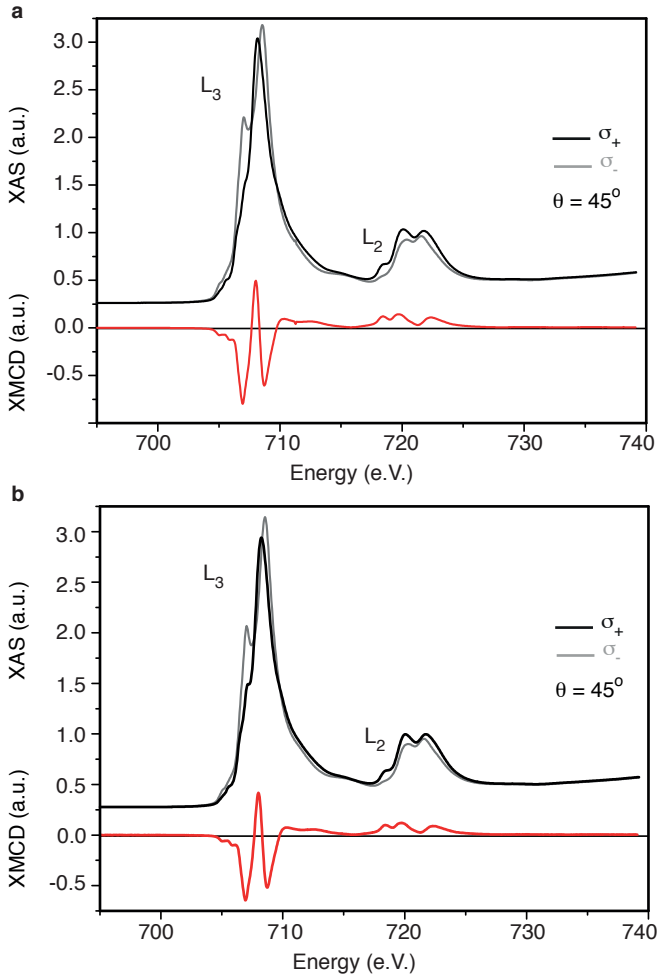

Figure S08. XAS/XMCD of epitaxial F_3O_4(111). Iron $L_{2,3}$ edge XAS and XMCD spectra recorded at T = 2 K, and θ = 45° using left (σ_+) and right hand (σ_-) circularly polarized light in 6.5 T field. **a** $CoPyipa_2$ monolayer was deposited onto the Fe_3O_4; **b** $NiPyipa_2$ monolayer was deposited onto the Fe_3O_4.

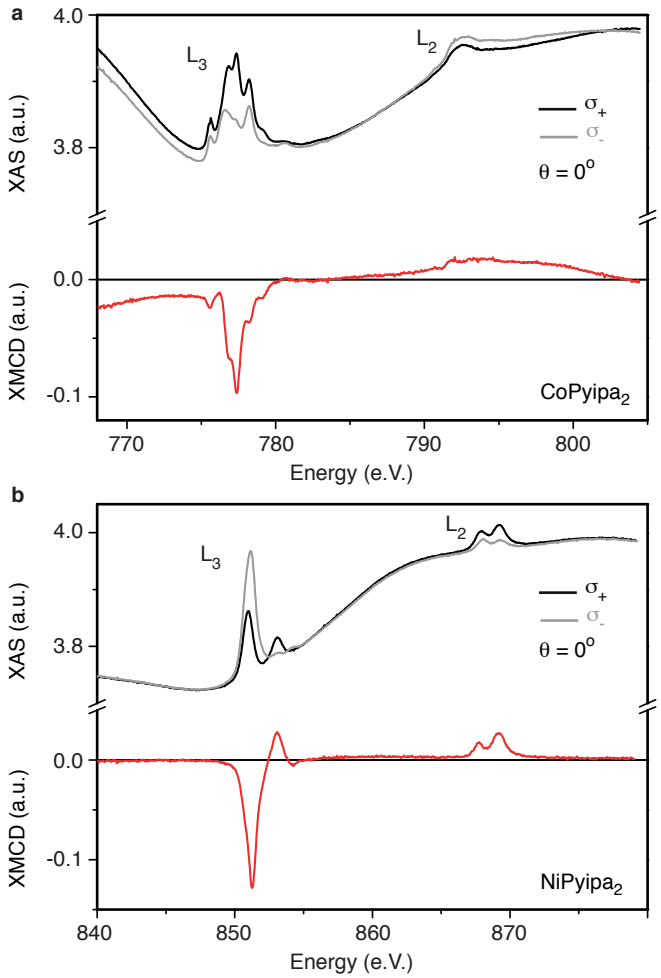

Figure S09. XAS/XMCD of $CoPyipa_2$ **and** $NiPyipa_2$**. a**, Cobalt $L_{2,3}$ edge XAS and XMCD spectra recorded at T = 2 K, and θ = 0° using left (σ_+) and right hand (σ_-) circularly polarized light in 6.5 T field. **b**, Nickel $L_{2,3}$ edge XAS and XMCD spectra recorded at T = 2 K, and θ = 0° using left (σ_+) and right hand (σ_-) circularly polarized light in 6.5 T field. Note that the non-flat background for the XMCD in figure S09a comes from the XMCD signal of the Fe $L_{2,3}$ edges and can be removed by recording the XMCD on a pure Fe_3O_4 surface in the energy range of the Co $L_{2,3}$ edges. This is what has been done to obtain Figures S10.

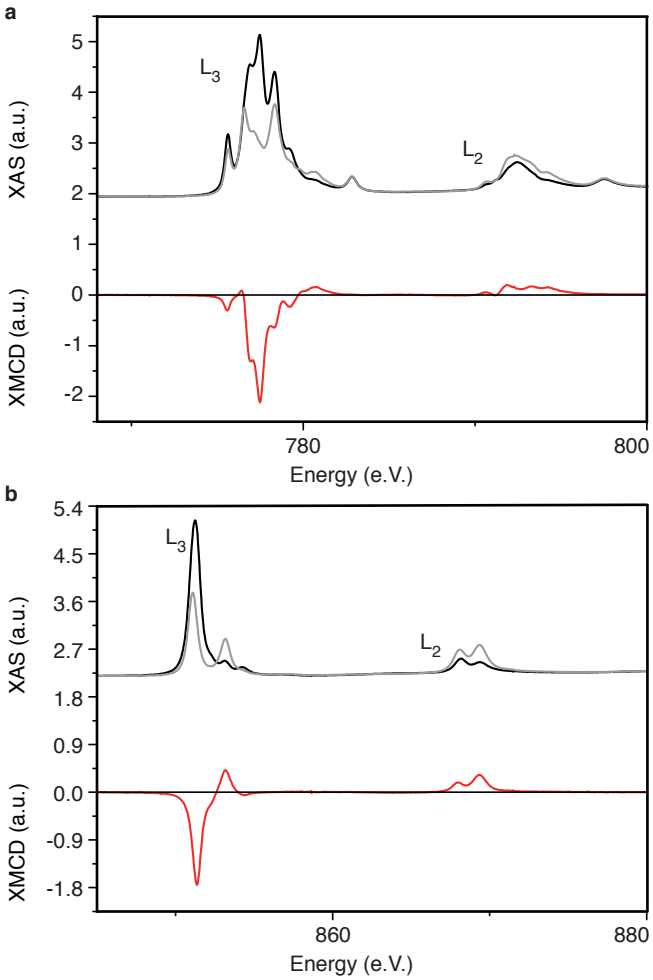

Figure S10. XAS/XMCD of bulk $CoPyipa_2$ **and** $NiPyipa_2$**. a**, Cobalt $L_{2,3}$ edge XAS and XMCD spectra recorded at T = 2 K, and θ = 45° using left (σ_+) and right hand (σ_-) circularly polarized light in 6.5 T field. **b**, Nickel $L_{2,3}$ edge XAS and XMCD spectra recorded at T = 2 K, and θ = 45° using left (σ_+) and right hand (σ_-) circularly polarized light in 6.5 T field.

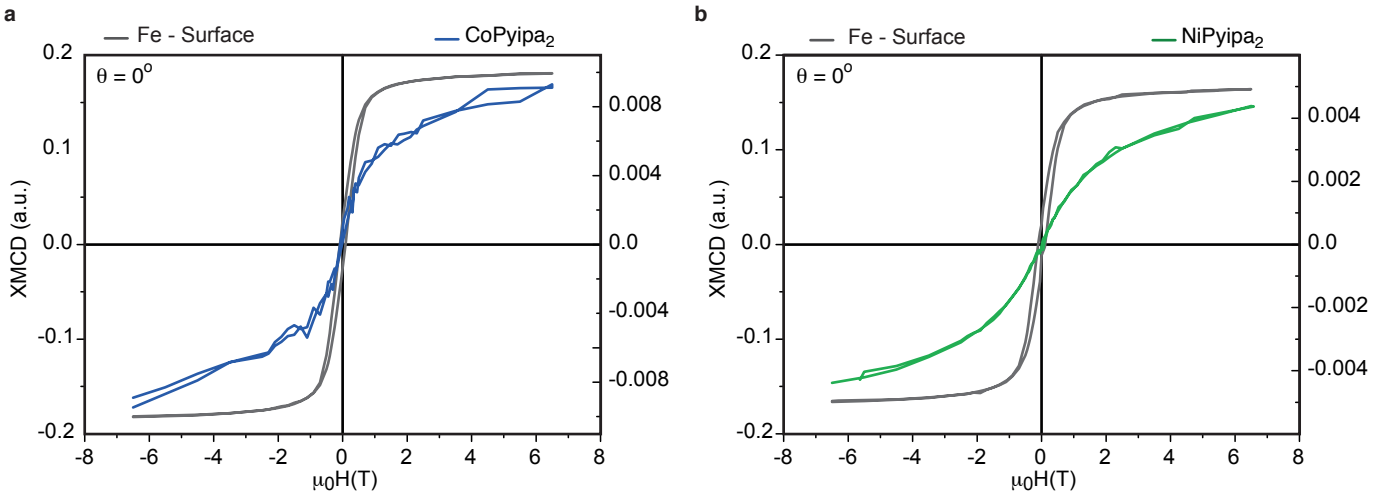

Figure S11. Element-specific field dependence of the magnetization of the Co atoms of CoPyipa$_2$, the Ni atoms of NiPyipa$_2$ and of the ferrimagnetic surface (Fe). Hysteresis curves (multiplied by -1) of the Co atoms (blue), Ni atoms (green) and Fe atoms (grey) obtained at the $L_{2,3}$ edges XMCD maxima at T = 2 K, and θ = 0°. (Monochromatized X-rays are set at the energy of the maximum absolute value of the XMCD signal (i.e. hν = 777.5 eV for Co, hν = 851 eV for Ni, and hν = 707 eV for Fe) then the external magnetic field is switched step by step from +6.5 T down to -6.5 T and back to +6.5 T. At each step the magnetic field is switched from left to right circular polarization to yield the element specific magnetization curves.

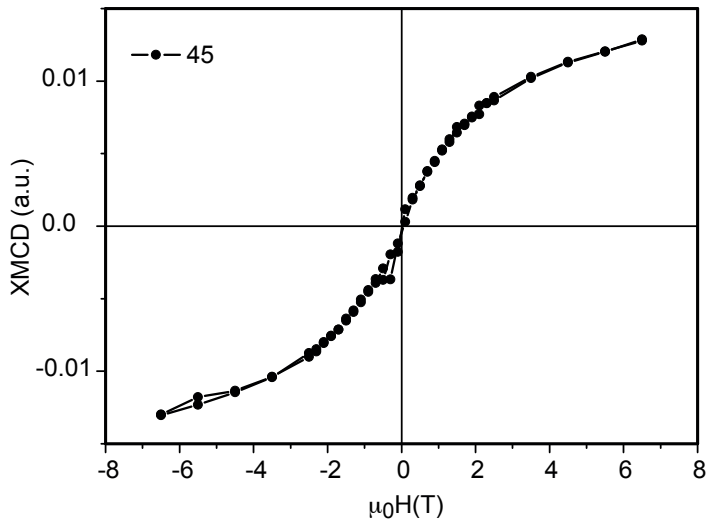

Figure S12. Element-specific field dependence of the magnetization of the Co atoms of CoPyipa$_2$ on the ferrimagnetic surface (Fe) separated by an Al_2O_3 insulating layer. Hysteresis curves (multiplied by -1) of the Co atoms obtained at the $L_{2,3}$ edges XMCD maxima at T = 2 K, θ = 45°. (Monochromatized X-rays are set at the energy of the maximum absolute value of the XMCD signal (i.e. hν = 777.5 eV for Co) then the external magnetic field is switched step by step from +6.5 T down to -6.5 T and back to +6.5 T. At each step the magnetic field is switched from left to right circular polarization to yield the element specific magnetization curves.

Density Functional Theory – calculation of the magnetic coupling between the molecules the surface:

These calculations have been performed using the B3LYP functional of the GAUSSIAN 09 package.[22,23] First, the structure of each complex anchored to the surface was optimized. The effect of the surface onto the complex was modeled as follows: a piece containing three Fe^{III} centers and the coordinated O atoms (see Figure 5) was cut into the structure that was predetermined by the molecular dynamics technique. The external oxo anions were protonated. It is important to note that even if the surface model is approximated, it is exactly the same for both complexes. The structure of the model surface was frozen and the structure of the whole complex was optimized for the M_s = 18/2 ($CoPyipa_2$) or M_s = 17/2 ($NiPyipa_2$) solution corresponding to a ferromagnetic coupling between the three Fe^{III} and the Co^{II} or Ni^{II} metal centers. Very small spin contamination is observed: for $CoPyipa_2$, S = 9.03, compared to an expected value of S = 9.00 without spin contamination; for $NiPyipa_2$, S = 8.52 *vs* an expected value of S = 8.50. For both complexes, the spin density of the central the Fe^{III} centers are almost the same and independent of the M_s values. A substantial spin density delocalization toward the O atoms bound to the Fe centers is observed in both cases (as usual in metal oxides).[24-28] The Co^{II} and Ni^{II} ions have spin densities of 1.33 and 0.86, respectively. A non-negligible delocalization of the spin density on the coordination sphere atoms was observed: -0.06 for Co^{II} and +0.05 for Ni^{II}. Unexpectedly, the coordination sphere of $NiPyipa_2$ is slightly smaller than that of $CoPyipa_2$ as can be seen from the differences in bond distances: Ni-N distances are between 2.03Å and 2.15Å (average 2.10Å); Ni-O distances are 2.03Å and 2.08Å; Co-N distances are between 2.05Å and 2.19Å (average 2.14Å); Co-O distances are 2.09Å and 2.24Å. The distance from the metal center to the closest Fe^{III} ion is shorter by 0.5 Å for Ni $Pyipa_2$ than that of Co $Pyipa_2$ (4.27Å *vs.* 4.77Å). Second, the solution corresponding to a ferromagnetic coupling between the Fe^{III} centers and an antiferromagnetic coupling with the Co^{II} and Ni^{II} ions was computed (M_s = 12/2 and M_s = 13/2 for Co- and $NiPyipa_2$, respectively). As expected, the spin contamination of these solutions is larger but it remain small: S = 6.28 (exp. 6.00) for $CoPyipa_2$; S = 6.67 (exp. 6.50) for $NiPyipa_2$. The spin densities on the iron centers are almost the same as in the high spin solution (variations of less than 0.02); that of Co^{II} and Ni^{II} are -1.40 and -0.87, respectively. The delocalization on the coordination sphere atoms is -0.24 for Co^{II} and -0.21 for Ni^{II}.

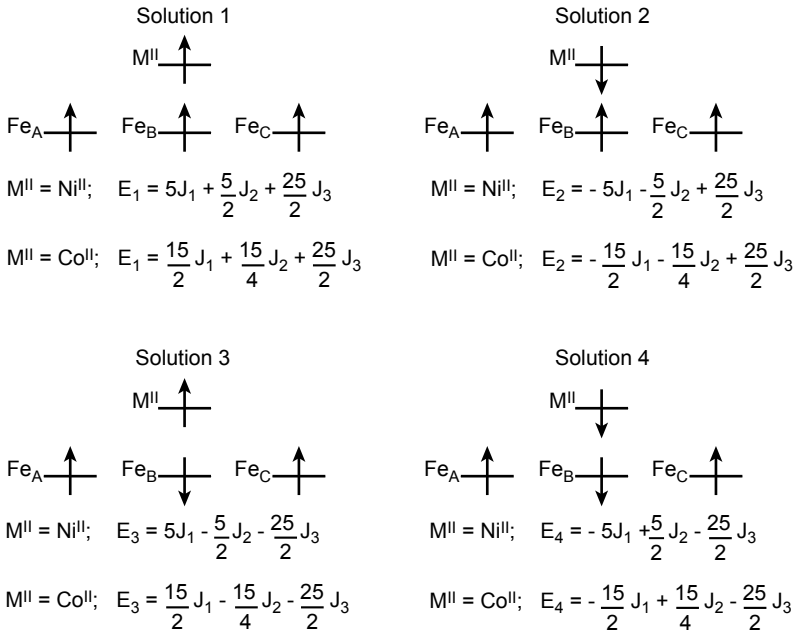

Figure S13. DFT broken symmetry solutions and their analytical energies as functions of the magnetic exchange coupling parameters J_1, J_2 and J_3. Solutions 1 and 2 correspond to the situation when the surface Fe^{III} ions are *ferromagnetically* coupled and the M^{II} ions are ferro- and antiferromagnetically coupled to them, respectively; solutions 3 and 4 correspond to the situation when the surface Fe^{III} ions are *antiferromagnetically* coupled and the M^{II} ions are ferro- and antiferromagnetically coupled to them, respectively. Although solutions 1 and 2 (ferromagnetic coupling between Fe ions of the surface) are lower in energy than solutions 3 and 4 (antiferromagnetic coupling between Fe ions of the surface), the coupling between the complexes and the substrate is independent from the nature of the coupling within the substrate because equations $E_1 - E_2$ and $E_3 - E_4$ are a function of J_1 and J_2 only

References

1 Ramos, A. V. *et al.* Magnetotransport properties of Fe3O4 epitaxial thin films: Thickness effects driven by antiphase boundaries. *J. Appl. Phys.* **100**, 103902, (2006).
2 SHELXS-97, Program for Crystal Structure Solution, University of Göttingen (Göttingen, Germany, 1997).
3 SHELXL-97, Program for the refinement of crystal structures from diffraction data, University of Göttingen (Göttingen, Germany, 1997).
4 Farrugia, L. J. *J. Appl. Crystallogr.*, 837-838, (1999).
5 Kahn, O. *Molecular magnetism*. (VCH, 1993).
6 Malmqvist, P. A., Roos, B. O. & Schimmelpfennig, B. The restricted active space (RAS) state interaction approach with spin-orbit coupling. *Chem. Phys. Lett.* **357**, 230-240, (2002).
7 Roos, B. O. & Malmqvist, P.-A. Relativistic quantum chemistry: the multiconfigurational approach. *Phys. Chem. Chem. Phys.* **6**, 2919-2927, (2004).
8 Karlstroem, G. *et al.* MOLCAS: a program package for computational chemistry. *Comput. Mater. Sci.* **28**, 222-239, (2003).
9 Ruamps, R. *et al.* Giant Ising-Type Magnetic Anisotropy in Trigonal Bipyramidal Ni(II) Complexes: Experiment and Theory. *J. Am. Chem. Soc.* **135**, 3017-3026, (2013).
10 Maurice, R., Graaf, C. d. & Guihéry, N. Theoretical determination of spin Hamiltonians with isotropic and anisotropic magnetic interactions in transition metal and lanthanide complexes. *Phys. Chem. Chem. Phys.* **15**, 18784, (2013).
11 Ruamps, R. *et al.* Origin of the Magnetic Anisotropy in Heptacoordinate Ni^{II} and Co^{II} Complexes. *Chem. -Eur. J.* **19**, 950-956, (2012).
12 Batchelor, L. J. *et al.* Pentanuclear cyanide-bridged complexes based on highly anisotropic Co(II) seven-coordinate building blocks: synthesis, structure, and magnetic behavior. *Inorg. Chem.* **50**, 12045-12052, (2011).
13 Maurice, R., Guihéry, N., Bastardis, R. & Graaf, C. d. Rigorous Extraction of the Anisotropic Multispin Hamiltonian in Bimetallic Complexes from the Exact Electronic Hamiltonian. *J. Chem. Theory Comput.* **6**, 55-65, (2010).

14 Maurice, R., de Graaf, C. & Guihéry, N. Magnetic anisotropy in binuclear complexes in the weak-exchange limit: From the multispin to the giant-spin Hamiltonian. *Phys. Rev. B* **81**, 214427, (2010).
15 Maurice, R. *et al.* Universal Theoretical Approach to Extract Anisotropic Spin Hamiltonians. *J. Chem. Theory Comput.* **5**, 2977-2984, (2009).
16 Basanta, M. A., Dappe, Y. J., Jelínek, P. & Ortega, J. Optimized atomic-like orbitals for first-principles tight-binding molecular dynamics. *Comput. Mater. Sci.* **39**, 759-766, (2007).
17 Harris, J. Simplified Method for Calculating the Energy of Weakly Interacting Fragments. *Phys. Rev. B* **31**, 1770-1779, (1985).
18 Jelínek, P., Wang, H., Lewis, J., Sankey, O. & Ortega, J. Multicenter approach to the exchange-correlation interactions in ab initio tight-binding methods. *Phys. Rev. B* **71**, 235101, (2005).
19 Schull, G., Dappe, Y. J., González, C. s., Bulou, H. & Berndt, R. Charge Injection through Single and Double Carbon Bonds. *Nano Letters* **11**, 3142-3146, (2011).
20 Henke, B. L., Liesegang, J. & Smith, S. D. Soft-x-ray-induced secondary-electron emission from semiconductors and insulators: Models and measurements. *Phys. Rev. B* **19**, 3004-3021, (1979).
21 Ohresser, P. *et al.* DEIMOS: A beamline dedicated to dichroism measurements in the 350–2500 eV energy range. *Rev. Sci. Instrum.* **85**, 013106, (2014).
22 Gaussian 03 (Revision B.05) (Gaussian, Inc., Pittsburgh, PA, 2003).
23 Gaussian 09 (Revision C.01) (Gaussian, Inc., Pittsburgh, PA, 2003).
24 Gellé, A., Munzarová, M. L., Lepetit, M.-B. & Illas, F. Role of dynamical polarization of the ligand-to-metal charge transfer excitations in *ab initio* determination of effective exchange parameters. *Phys. Rev. B* **68**, 125103, (2003).
25 Labèguerie, P. *et al.* Is it possible to determine rigorous magnetic Hamiltonians in spin s=1 systems from density functional theory calculations? *J. Chem. Phys.* **129**, 154110, (2008).
26 Calzado, C. J. On the Controversial Fitting of Susceptibility Curves of Ferromagnetic CuII Cubanes: Insights from Theoretical Calculations. *Chem.-Eur. J.* **19**, 1254-1261, (2013).
27 Malrieu, J. P., Caballol, R., Calzado, C. J., de Graaf, C. & Guihéry, N. Magnetic Interactions in Molecules and Highly Correlated Materials: Physical Content, Analytical Derivation, and Rigorous Extraction of Magnetic Hamiltonians. *Chem. Rev.* **114**, 429-492, (2014).
28 Noh, J., Osman, O. I., Aziz, S. G., Winget, P. & Bredas, J.-L. A density functional theory investigation of the electronic structure and spin moments of magnetite. *Sci. Tech. Adv. Mater.* **15**, 044202, (2014).

References

[1] P. Dai, J. Hu, and E. Dagotto, Nature Physics **8**, 709 (2012). 1

[2] Y. Tokura and Y. Tomioka, Journal of Magnetism and Magnetic Materials **200**, 1 (1999), 00813. 1, 91, 92

[3] E. Dagotto, T. Hotta, and A. Moreo, Phys. Rep. **344**, 1 (2001). 1, 39, 76

[4] E. Dagotto, Reviews of Modern Physics **66**, 763 (1994). 1

[5] M. T. Lemaire, Pure and Applied Chemistry **83**, 141 (2010). 1, 5, 36

[6] B. Bechlars *et al.*, Nature Chemistry **2**, 362 (2010). 1, 36

[7] M.-C. Dul *et al.*, Journal of the American Chemical Society **131**, 14614 (2009). 1, 5, 36

[8] E. M. Zueva *et al.*, Dalton Trans. **43**, 11269 (2014). 1, 36

[9] S. Jin, Metals and Materials **5**, 533 (1999). 1, 36

[10] D. Gatteschi, R. Sessoli, and J. Villain, *Molecular nanomagnets* (Oxford University Press, 2006). 5

[11] A. Soncini, T. Mallah, and L. F. Chibotaru, Journal of the American Chemical Society **132**, 8106 (2010). 5, 36

[12] S. Drüeke *et al.*, Journal of the Chemical Society, Chemical Communications , 59 (1989). 5

[13] X.-Q. Ding *et al.*, The Journal of Chemical Physics **92**, 178 (1990). 5

[14] L. Sacconi, C. Mealli, and D. Gatteschi, Inorganic Chemistry **13**, 1985 (1974). 5

[15] D. Gatteschi, C. Mealli, and L. Sacconi, Journal of the American Chemical Society **95**, 2736 (1973). 5

[16] A. Bencini, D. Gatteschi, and L. Sacconi, Inorganic Chemistry **17**, 2670 (1978). 5

[17] A. Rajca, Chemical reviews **94**, 871 (1994). 6

[18] A. Rajca, S. Rajca, and J. Wongsriratanakul, Journal of the American Chemical Society **121**, 6308 (1999). 6, 113

[19] A. Rajca, J. Wongsriratanakul, and S. Rajca, Science **294**, 1503 (2001). 6

[20] A. Rajca, J. Wongsriratanakul, and S. Rajca, Journal of the American Chemical Society **126**, 6608 (2004). 6

[21] A. Rajca, J. Wongsriratanakul, S. Rajca, and R. L. Cerny, Chemistry (Weinheim an Der Bergstrasse, Germany) **10**, 3144 (2004). 6

[22] M. Lofthagen, R. VernonClark, K. K. Baldridge, and J. S. Siegel, The Journal of Organic Chemistry **57**, 61 (1992). 6

[23] B. W. Laursen *et al.*, Journal of the American Chemical Society **120**, 12255 (1998). 6

[24] G. Trinquier, N. Suaud, and J.-P. Malrieu, Chemistry (Weinheim an Der Bergstrasse, Germany) **16**, 8762 (2010). 6, 114

[25] G. Trinquier, N. Suaud, N. Guihéry, and J.-P. Malrieu, Chemphyschem: A European Journal of Chemical Physics and Physical Chemistry **12**, 3020 (2011). 6

[26] E. Clar and D. G. Stewart, Journal of the American Chemical Society **75**, 2667 (1953). 6

[27] E. Clar and D. G. Stewart, Journal of the American Chemical Society **76**, 3504 (1954). 6

[28] J. Inoue *et al.*, Journal of the American Chemical Society **123**, 12702 (2001). 6

[29] D. A. Shultz and R. K. Kumar, Journal of the American Chemical Society **123**, 6431 (2001). 6

[30] T. Soda *et al.*, Chemical Physics Letters **319**, 223 (2000). 6

[31] C. Boilleau, N. Suaud, R. Bastardis, N. Guihéry, and J. P. Malrieu, Theoretical Chemistry Accounts **126**, 231 (2009). 6

[32] C. Zener, Phys. Rev. **82**, 403 (1951). 9

[33] J.-J. Girerd, The Journal of Chemical Physics **79**, 1766 (1983). 9

[34] V. Papaefthymiou, J. J. Girerd, I. Moura, J. J. G. Moura, and E. Muenck, J. Am. Chem. Soc. **109**, 4703 (1987). 9

[35] K. K. S. J.-J. Girerd, V. Papaefthymiou and E. Munck, Pure Appl. Chem. **61**, 805 (1989). 9

[36] P. W. Anderson and H. Hasegawa, Phys. Rev. **100**, 675 (1955). 9, 113

[37] D. Taratiel and N. Guihéry, The Journal of Chemical Physics **121**, 7127 (2004), 00009. 9

[38] N. Guihéry, Theoretical Chemistry Accounts **116**, 576 (2006). 9

[39] L. M. C. Beltran and J. R. Long, Accounts of Chemical Research **38**, 325 (2005). 36

[40] G. Jonker and J. V. Santen, Physica **16**, 337 (1950). 36

[41] G. Jonker and J. V. Santen, Physica **19**, 120 (1953). 36

[42] J. Darriet and L. P. Regnault, Solid State Commun. **86**, 409 (1993). 37

[43] B. Batlogg, S.-W. Cheong, and L. W. Rupp Jr., Physica B **194–196, Part 1**, 173 (1994). 37

[44] N. Guihery and J. P. Malrieu, J. Chem. Phys **119**, 8956 (2003). 37

[45] T. Ito *et al.*, Phys. Rev. B **64**, 060401 (2001). 37, 38, 52

[46] J. F. DiTusa *et al.*, Physical Review Letters **73**, 1857 (1994), 00148. 37

[47] K. Tsutsui, W. Koshibae, and S. Maekawa, Physical Review B **59**, 9729 (1999). 37

[48] C. S. Nelson *et al.*, X-ray Scattering Studies of Correlated Polarons in La0.7Ca0.3Mno3, in *Vibronic Interactions: Jahn-Teller Effect in Crystals and Molecules*, edited by M. D. Kaplan and G. O. Zimmerman, , NATO Science Series No. 39, pp. 209–213, Springer Netherlands, 2001. 37

[49] R. Bastardis, N. Guihéry, and C. de Graaf, Physical Review B **74**, 014432 (2006), 00010. 37

[50] Z. Hu *et al.*, The European Physical Journal B - Condensed Matter and Complex Systems **26**, 449 (2002). 37

[51] P. Sippel *et al.*, The European Physical Journal B **85**, 1 (2012). 38

[52] N. Nasani, D. Ramasamy, I. Antunes, B. Singh, and D. P. Fagg, Journal of Alloys and Compounds **620**, 91 (2015). 38

[53] F. Tedoldi *et al.*, Journal of Applied Physics **83**, 6605 (1998), 00000. 38

[54] J. M. Tranquada, D. J. Buttrey, V. Sachan, and J. E. Lorenzo, Physical Review Letters **73**, 1003 (1994). 38

[55] H. Yoshizawa *et al.*, Physical Review B **61**, R854 (2000). 38

[56] T. Mizokawa and A. Fujimori, Physical Review Letters **80**, 1320 (1998). 38

[57] G. Xu *et al.*, Science **289**, 419 (2000). 39

[58] J. V. Alvarez and C. Gros, Physical Review B **66**, 094403 (2002), 00029. 39

[59] T. L. van den Berg, P. Lombardo, R. O. Kuzian, and R. Hayn, Physical Review B **86**, 235114 (2012). 39

[60] C. D. Batista, A. A. Aligia, and J. Eroles, EPL **43**, 71 (1998). 39

[61] Y. A. Izyumov and Y. N. Skryabin, Phys.-Usp. **44**, 109 (2001). 39

[62] E. Dagotto, J. Riera, A. Sandvik, and A. Moreo, Phys. Rev. Lett. **76**, 1731 (1996). 39

[63] A. L. Malvezzi, S. Yunoki, and E. Dagotto, Physical Review B **59**, 7033 (1999). 39

[64] O. Navarro, E. Vallejo, and M. Avignon, International Journal of Modern Physics B **26**, 1250048 (2012). 40

[65] B. Ammon and M. Imada, Phys. Rev. Lett. **85**, 1056 (2000). 40

[66] B. Ammon and M. Imada, Journal of the Physical Society of Japan **69**, 1946 (2000), 00003. 40, 50

[67] C. D. Batista, J. Eroles, M. Avignon, and B. Alascio, Physical Review B **58**, R14689 (1998), 00033. 40, 41

[68] D. J. Garcia *et al.*, Physical Review B **65**, 134444 (2002). 40, 47, 50

[69] A. L. Malvezzi and E. Dagotto, Phys. Rev. B **63**, 140409 (2001). 40, 75

[70] S. Costamagna and J. A. Riera, Physical Review B **77**, 045302 (2008), 00002. 40

[71] S. Costamagna and J. A. Riera, Physical Review B **77**, 235103 (2008), 00007. 40

[72] A. Koga, N. Kawakami, and M. Sigrist, Physica B: Condensed Matter **312–313**, 606 (2002), 00000. 40

[73] K. Kubo, Journal of the Physical Society of Japan **51**, 782 (1982). 40

[74] Y. Nagaoka, Solid State Communications **3**, 409 (1965). 40

[75] H. Tasaki, Physical Review B **40**, 9192 (1989). 40

[76] J. Riera, K. Hallberg, and E. Dagotto, Physical Review Letters **79**, 713 (1997). 41

[77] A. Edmonds, Unitary symmetry in theories of elementary particles: The reduction of products of representations of the groups u (3) and su (3), in *Proceedings of the Royal Society of London A: Mathematical, Physical and Engineering Sciences* Vol. 268, pp. 567–579, The Royal Society, 1962. 43

[78] M. Rashid, Il Nuovo Cimento Series 10 **26**, 118 (1962). 43

[79] C. A. Lamas, S. Capponi, and P. Pujol, Physical Review B **84**, 115125 (2011), 00003. 47, 50

[80] E. Wang *et al.*, Intel math kernel library, in *High-Performance Computing on the Intel® Xeon Phi*, pp. 167–188, Springer, 2014. 47

[81] D. R. S. Martin, D. C. Reinsch, and J. H. Wilkinson, Numerische Mathematik **11**, 181 (1968). 47

[82] H. Bowdler, R. S. Martin, D. C. Reinsch, and D. J. H. Wilkinson, Numerische Mathematik **11**, 293 (1968). 47

[83] R.-K. Nesbet, The Journal of Chemical Physics **43**, 311 (1965). 48

[84] I. Shavitt, C. Bender, A. Pipano, and R. Hosteny, Journal of Computational Physics **11**, 90 (1973). 48

[85] E. R. Davidson, Journal of Computational Physics **17**, 87 (1975). 48

[86] C. Lanczos, Journal of Research of the National Bureau of Standards **45** (1950). 48

[87] C. Campos and J. E. Roman, Numer. Algorithms **60**, 279 (2012). 48

[88] W. E. Arnoldi, Quarterly of Applied Mathematics **9**, 17 (1951). 48

[89] G. Stewart, SIAM Journal on Matrix Analysis and Applications **23**, 601 (2002). 48

[90] G. Stewart, SIAM Journal on Matrix Analysis and Applications **24**, 599 (2002). 48

[91] V. Hernandez, J. E. Roman, and V. Vidal, ACM Trans. Math. Software **31**, 351 (2005). 49

[92] V. Hernandez, J. E. Roman, and V. Vidal, Lecture Notes in Computer Science **2565**, 377 (2003). 49

[93] J. E. Roman, C. Campos, E. Romero, and A. Tomas, D. Sistemes Informàtics i Computació, Universitat Politècnica de València Report No. DSIC-II/24/02 - Revision 3.6, 2015 (unpublished). 49

[94] S. Yamada, T. Imamura, and M. Machida, 16.447 TFlops and 159-Billion-dimensional Exact-diagonalization for Trapped Fermion- Hubbard Model on the Earth Simulator, in *Supercomputing, 2005. Proceedings of the ACM/IEEE SC 2005 Conference*, pp. 44–44, 2005. 49

[95] S. Balay *et al.*, PETSc Web page, http://www.mcs.anl.gov/petsc, 2015. 49

[96] S. Balay *et al.*, Argonne National Laboratory Report No. ANL-95/11 - Revision 3.6, 2015 (unpublished). 49

[97] S. Balay, W. D. Gropp, L. C. McInnes, and B. F. Smith, Efficient management of parallelism in object oriented numerical software libraries, in *Modern Software Tools in Scientific Computing*, edited by E. Arge, A. M. Bruaset, and H. P. Langtangen, pp. 163–202, Birkhäuser Press, 1997. 49

[98] vijay gopal Chilkuri, N. Guihery, N. Suaud, and A. Scemama, Deham: First public beta, http://dx.doi.org/10.5281/zenodo.20450, 2015. 49

[99] B. Ammon and M. Imada, Journal of the Physical Society of Japan **70**, 547 (2001), 00008. 50

[100] S. K. Pati, S. Ramasesha, and D. Sen, Phys. Rev. B **55**, 8894 (1997). 50

[101] S. R. White and D. J. Scalapino, Physical Review B **55**, 6504 (1997). 50

[102] F. Verstraete, V. Murg, and J. I. Cirac, Advances in Physics **57**, 143 (2008). 50

[103] B. Bauer *et al.*, Journal of Statistical Mechanics: Theory and Experiment **2011**, P05001 (2011). 50

[104] F. Jin, Z. Xu, H. Ying, and B. Zheng, Journal of Physics: Condensed Matter **17**, 5541 (2005), 00000. 50

[105] J. Das *et al.*, Physical Review B **69**, 144404 (2004). 50

[106] M. Matsumoto and H. Takayama, Progress of Theoretical Physics Supplement **159**, 412 (2005), 00000. 50

[107] E. Dagotto, A. Moreo, F. Ortolani, D. Poilblanc, and J. Riera, Physical Review B **45**, 10741 (1992), 00249. 51

[108] S. Sorella *et al.*, Physical Review Letters **88**, 117002 (2002). 51

[109] F. Mezzacapo, Physical Review B **83**, 115111 (2011). 51

[110] D. Zaslavsky and V. G. Chilkuri, Interp2d, `https://github.com/diazona/interp2d`, 2015. 53

[111] S. R. White, I. Affleck, and D. J. Scalapino, Physical Review B **65**, 165122 (2002). 65

[112] S. Costamagna, C. J. Gazza, M. E. Torio, and J. A. Riera, Physical Review B **74**, 195103 (2006). 65

[113] C. Schuster and P. Brune, physica status solidi (b) **241**, 2043 (2004). 65

[114] G. Bedürftig, B. Brendel, H. Frahm, and R. M. Noack, Physical Review B **58**, 10225 (1998). 65

[115] W. Kohn, Physical Review **133**, A171 (1964). 77

[116] R. Resta and S. Sorella, Physical Review Letters **82**, 370 (1999). 77

[117] G. L. Bendazzoli, M. El Khatib, S. Evangelisti, and T. Leininger, Journal of Computational Chemistry **35**, 802 (2014). 77

[118] G. L. Bendazzoli, S. Evangelisti, and A. Monari, International Journal of Quantum Chemistry **112**, 653 (2012). 77

[119] G. L. Bendazzoli, S. Evangelisti, A. Monari, and R. Resta, The Journal of Chemical Physics **133**, 064703 (2010). 77

[120] M. El Khatib, T. Leininger, G. L. Bendazzoli, and S. Evangelisti, Chemical Physics Letters **591**, 58 (2014). 77

[121] M. E. Khatib *et al.*, The Journal of Chemical Physics **142**, 094113 (2015). 77

[122] R. Resta, The European Physical Journal B **79**, 121 (2011). 85

[123] C. N. Yang, Reviews of Modern Physics **34**, 694 (1962). 98

[124] T. Helgaker, P. Jorgensen, and J. Olsen, *Molecular electronic-structure theory* (John Wiley & Sons, 2014). 99

[125] D. Kumar, J. Sankar, J. Narayan, R. K. Singh, and A. K. Majumdar, Phys. Rev. B **65**, 094407 (2002). 104

[126] F. E. N. Ramirez, E. Francisquini, and J. A. Souza, J. Alloys Compd. **571**, 21 (2013). 105

[127] A. Rajca and S. Utamapanya, Journal of the American Chemical Society **115**, 10688 (1993). 113

[128] S. Rajca, A. Rajca, J. Wongsriratanakul, P. Butler, and S.-m. Choi, Journal of the American Chemical Society **126**, 6972 (2004). 113

[129] G. Trinquier and J.-P. Malrieu, Chemistry: A European Journal **21**, 814 (2015). 114

[130] K. S. Novoselov *et al.*, Science **306**, 666 (2004). 114

[131] K. S. Novoselov *et al.*, Proceedings of the National Academy of Sciences of the United States of America **102**, 10451 (2005). 114

[132] J. P. Perdew and A. Zunger, Physical Review B **23**, 5048 (1981). 114